Dissertation

Submitted to the
Combined Faculty of Natural Sciences and Mathematics
of Heidelberg University, Germany
for the degree of
Doctor of Natural Sciences

Put forward by
Fleur Versteegen
born in Zutphen.
Oral examination: 30.10.2019

Quantum Gravity:
From continuous to discrete

Referees:
Assoc. Prof. Dr. Astrid Eichhorn
Prof. Dr. Björn-Malte Schäfer

Abstract

The consistent definition of a quantum gravity theory has to overcome several obstacles. Here we take important steps in the development of three approaches to quantum gravity. By utilising matter fields as mediators from ultraviolet to infrared energies, we study a coupling between asymptotically-safe quantum gravity and the hypercharge. The resulting symmetry enhancement allows for a possible ultraviolet completion of the joined system, predicting the infrared value of the hypercharge within estimated systematic errors, thereby increasing the predictive power of the model. Additionally, previous studies suggest that Kähler-Dirac fermions on Euclidean dynamical triangulations do not spontaneously break chiral symmetry. Here we develop computational tools accounting for the back reaction of fermions on the lattice. If extended studies support the evidence that chiral symmetry remains intact, then the model passes an important observational viability test. Lastly, we provide procedures allowing for the extraction of geometrical and topological properties from a causal set. Specifically, we build a spatial distance function which can be used to construct dimensional estimators for the Hausdorff and spectral dimension. In agreement with other quantum-gravity approaches, the latter exhibits a form of dimensional reduction at high energies on account of the inherent non-localness of causal sets.

Abstract

Die konsistente Definition einer Theorie der Quantengravitation muss mehrere Hindernisse überwinden. Hier nehmen wir wichtige Schritte in der Entwicklung von drei Ansätzen der Quantengravitation. Durch das Verwenden von Materiefeldern als Mediator von ultraviolett zu infrarot Energien, untersuchen wir eine Kopplung zwischen asymptotisch sicherer Quantengravitation und der Hyperladung. Die entstehende verstärkte Symmetrie ermöglicht eine Ultraviolett Vervollständigung des kombinierten Systems, welches den Infrarotwert der Hyperladung innerhalb geschätzter systematischer Fehler vorhersagt, und somit die Voraussagekraft des Modells erhöht. Zusätzlich legen frühere Untersuchungen nahe, dass Kähler-Dirac Fermionen in euklidischen dynamischen Triangulationen nicht zu spontaner Brechung von chiraler Symmetrie führen. Hier entwickeln wir computergestützte Methoden, welche die Rückkopplung von Fermionen auf das Gitter berücksichtigen. Wenn ausgedehntere Untersuchungen den Hinweis unterstützen, dass die chirale Symmetrie ungebrochen bleibt, besteht das Modell einen wichtigen phänomenologischen Test bezüglich seiner Realisierbarkeit. Zuletzt stellen wir Verfahren vor, welche es ermöglichen geometrische und topologische Eigenschaften aus einer kausalen Menge zu gewinnen. Im Speziellen konstruieren wir eine Funktion für den räumlichen Abstand, welche die Konstruktion von Schätzwerten für die Hausdorff und spektrale Dimension ermöglichen. In Übereinstimmung mit anderen Ansätzen der Quantengravitation weist Letztere eine Art der dimensionalen Reduzierung bei hohen Energien auf, welche die inhärente Nichtlokalität kausaler Mengen widerspiegelt.

The results in Chpt. 2.1.4 are based on the work [1], in collaboration with Astrid Eichhorn. In addition, Chpt. 3.3.3, 3.3.4 and Chpt. 3.3.5 are a result of the work performed in [2] and [3], in collaboration with Astrid Eichhorn and Sumati Surya. Chpt. 2.2.6.2 is based on unpublished work with Jack Laiho and Judah Unmuth-Yockey and in Chpt. 4 and Chpt. 5 I will present an argument based on the work [4], which was performed in collaboration with Senerath de Alwis, Astrid Eichhorn, Aaron Held, Jan Pawlowski and Marc Schiffer.

Contents

Chapter 1

Introduction

For centuries past scientists have been pushing technological and intellectual boundaries further and further to obtain a more complete picture of nature. In the case of physics, the formulation of quantum mechanics (QM) in the early 1900s opened an, at the time, unexplored world of possibilities. Around the same time, Einstein attempted to explain the validity of Maxwell's (field) theory of electrodynamics by postulating a constant speed of light and introducing the principles of relativity, leading to his theory of special relativity (SRT). A natural next step at the time was to combine the quantum nature of microscopic physics with the field-theoretic high velocity description of SRT. Reconciling the two frameworks into a quantum theory of fields (QFT) turned out to be highly non-trivial and it took several decades to develop the methods necessary to deal with several technical difficulties. Half-way through the last century, renormalisation techniques finally led to a theory of quantum electrodynamics (QED) consistent with experiment [5, 6, 7].

Over the second half of the 20^{th} century, three of the fundamental forces together with all known elementary particles were combined into the Standard Model of particle physics [8, 9, 10]. The Standard Model describes elementary physics and has provided a large set of predictions, which have been verified extensively [11, 12, 13, 14] for reviews see for instance [15, 16]. Nevertheless, it cannot be the full story. The failure to explain the expansion of the universe [17, 18, 19, 20] and the fact that dark matter particles [21] are not incorporated in the Standard Model are just two of the vexing flaws of the Standard Model. Here we will focus on a different short-coming, namely the exclusion of the fourth fundamental force of nature: Gravity. Unlike the weak -and strong force, gravity works over long distances and its existence has been known much longer than that of the weak -and strong force. Despite many attempts, unifying gravity and the Standard Model into a framework which includes all four fundamental forces and can be extended up to arbitrarily high energy scales, has not been successful to date. Even the less ambitious goal of finding a description of gravity alone which can be extended up to arbitrarily high energies has proven highly non-trivial, as we will see in the following sections.

1.1 General relativity

Prior to the development of QFT, came Einsteins field equations of General Relativity, first presented in 1915 and published in 1916 [22]. Einsteins field equations provide a link between the geometry of spacetime and the matter (radiation) living on this spacetime, showing a dynamical interplay between the two. An important technical development came from Riemann [23], who generalised the concepts of Euclidean geometries and paved the way for a Lorentzian description.

Provided with the (pseudo-) Riemannian framework, the non-linear field equations of general relativity in $d = 4$ spacetime dimensions are

$$R_{\mu\nu} - \frac{1}{2} R\, g_{\mu\nu} + \Lambda g_{\mu\nu} = \frac{8\pi\, G_N}{c^4}\, T_{\mu\nu}. \tag{1.1}$$

Here $R_{\mu\nu}$ is the Ricci curvature tensor and carries information on how the volume of an object changes as it moves through spacetime, in absence of external forces (i.e., along geodesics). The Ricci scalar is obtained by taking the trace, $R = g^{\mu\nu} R_{\mu\nu}$, and roughly specifies how much the volume of a ball evaluated at some spacetime point deviates from its Euclidean version. The metric field, $g_{\mu\nu}$, represents the dynamical degrees of freedom of spacetime itself. It carries information on the causal structure of spacetime and provides a length scale. The accelerated expansion of the universe is encoded in a non-zero cosmological constant, Λ, often thought of as the energy density of spacetime. The smallness of the observed value for Λ today [24], requires a precise fine-tuning of initial values which was dubbed the cosmological constant problem [25][1]. On the right-hand side of the Einstein equations, we find the stress energy tensor $T_{\mu\nu}$ which captures all matter degrees of freedom. Usually the left-hand side of Eq. (1.1) is thought of as the pure-gravity part of the Einstein equations whereas the right-hand side summarises the matter contributions.

Despite its complexity, there exist several analytic solutions to the equation above. Under the assumption that spacetime is isotropic, the metric is represented by a symmetric tensor, leading to a reduction in the degrees of freedom of $g_{\mu\nu}$ (and consequently the number of equations to solve) from 16 to 10. In the simplest case we omit the cosmological constant and consider a vacuum, i.e., i.e., $\Lambda = 0$ and $T_{\mu\nu} = 0$. Taking the trace of Eq. (1.1) by multiplying through with the inverse metric, $g^{\mu\nu}$, gives rise to the vacuum Einstein equations: $R_{\mu\nu} = 0$ and $R = 0$. It can be checked that the flat spacetime (Minkowski) metric, $\eta_{\mu\nu} = \mathrm{diag}(-1, 1, 1, 1)$, trivially satisfies this equation. A more interesting solution was developed by Schwarzschild [26], shortly after Einstein published his theory of general relativity, and describes the spacetime outside a spherically symmetric, static mass distribution

$$ds^2 = -\left(1 - \frac{R_s}{r}\right) dt^2 + \left(1 - \frac{R_s}{r}\right)^{-1} dr^2 + r^2\, d\Omega, \tag{1.2}$$

with $d\Omega = d\theta^2 + \sin\theta^2 d\phi^2$ the two-sphere. A prominent example of an object producing such a spherically symmetric gravitational field is a static, electrically neutral black hole, with Schwarzschild radius R_S, parametrising the coordinate distance from the centre of the black hole ($r = 0$) to

[1] Let us note that, since the smallness of Λ is not a prediction of any sorts, the term "problem" can be interpreted as a comment on the aesthetics of the theory rather than its fundamental properties.

its *event horizon*. The apparent singularity at the horizon, $r = R_S$, in Eq. (1.2) is a coordinate singularity and can be removed by switching to a more suitable coordinate frame. The horizon of the black hole is a causal boundary separating events "within" the black hole from those outside, in the sense that any event taking place at $r_1 < R_S$ cannot influence an event at $r_2 > R_S$ (where r_1, r_2 are defined in a suitable coordinate frame). In a generalised coordinate frame, one finds that the "in" of the black hole is separated from the "out" by an interchange of the radial and temporal coordinates at the horizon. In other words, the direction of time for an observer on an ingoing trajectory points *towards* the point $r = 0$ the moment the horizon is crossed and hence, there exist no trajectories that cross the horizon from the inside. In that sense, any trajectory crossing the horizon is a one-way "street", with a predetermined destination at the centre of the black-hole. Note that also for any two events within the horizon, $r_1 < r_2 < R_S$, the event at r_2 cannot influence the event at r_1.

There is, however, a second singular point in Eq. (1.2) found at $r = 0$, which cannot be removed through a coordinate transformation. In particular, to investigate whether a singularity is "physical" or not, we can look at the behaviour of curvature invariants at points where we might expect a singularity to occur. Since the Schwarzschild solution is a vacuum solution to the Einstein equations, we know that $R_{\mu\nu}$ and R vanish identically. However, the Riemann tensor[2], $R_{\mu\alpha\nu\beta}$, does not vanish and we can calculate the curvature invariant known as the Kretschmann scalar

$$R^{\mu\alpha\nu\beta}R_{\mu\alpha\nu\beta} = 12\frac{R_S^2}{r^6}. \tag{1.3}$$

The expression above is indeed perfectly regular at $r = R_S$, confirming that the horizon is not a real singularity, but it does diverge at the centre of the black-hole, $r = 0$. In general, physical singularities such as diverging curvature invariants are interpreted as a breakdown of the theoretical description rather than representing physical phenomena. Since the singularity corresponds to an infinitesimally small point, one can in principle approach the region close to the singularity to arbitrarily small length scales. In particular, to reach $r = 0$ one would need to enter the Planckian regime, ℓ_{Pl}, where quantum gravitational effects are thought to become relevant. The break-down of GR is then often viewed as a signal for the need of a theory of quantum gravity. Note that the more general treatment of rotating, uncharged black holes (Kerr black holes), non-rotating, charged black holes (Reissner-Nordström black holes) and rotating, charged black holes (Kerr-Newman) are all found to have a singularity at $r = 0$.

An alternative explanation of the singular behaviour at $r = 0$, might be that GR itself is faulty and that a modified theory of gravity could remove the (semi-classical) singularities. GR has withstood many experimental tests [27, 28, 29, 30, 31] and any modified gravitational theory would have to respect the same experimental bounds. Since gravity is a relatively weak force, most tests of GR take place at astrophysical or even cosmological scales. An important set of constraints come from so-called Parametrised Post-Newtonian (PPN) tests [32, 29, 33, 34], which aim to test weak-field gravity at small scales. In weak-field gravity one expands the metric in small

[2]Heuristically, the Riemann tensor carries information on how the shape and volume of an object change as the object moves along a geodesic. Its trace, $R_{\mu\nu} = g^{\alpha\beta}R_{\mu\alpha\nu\beta}$ vanishes in vacuum, signalling that the volume of an object remains constant along a geodesic. Its shape, however, may still be altered (as is encoded in the contribution of the Weyl tensor to $R_{\mu\alpha\nu\beta}$).

fluctuations around a flat background, where the strength of the fluctuations is measured in terms of normalised velocities $\sim v^2/c^2$, such that the limit where the speed-of-light becomes infinite, $c \to \infty$, corresponds to Newtonian gravity. This formalism gives rise to a set of parameters which can be explicitly compared to experiment. For example, γ, represents the sensitivity of (spatial) curvature to stationary massive objects. An important constraint on γ comes from the radio waves transmitted by the Cassini space probe, which were found to undergo a measurable frequency shift due to the deformation of space-time around the sun [35].

In addition to weak-field tests, there have been recent developments in testing the strong-field regime of GR. LIGO observations have successfully confirmed the existence of gravitational waves generated by binary-merger systems of black-holes and neutron stars [36, 37] and has led to an extensive testing ground of GR [38] in both the weak-field (far away from the binary) as well as the strong-field regime (close to the binary).

Next to the LIGO-Virgo collaboration, the Event Horizon Telescope (EHT) has managed to capture the very first image of the black hole M87* [39, 40, 41, 42, 43, 44]. Since light cannot escape from a black hole, it is by definition not possible to detect a black hole through direct radiation[3], the idea is then to use the absence of emission to "see" the black hole. In particular, the strong gravitational field around a black hole bends background emissions of the black hole, resulting in a high luminosity ring bordering the shadow of the black hole.

1.2 Electroweak

Electromagnetism is another long-range force which, due to its macroscopic properties, has been known to mankind in one form or another for a long time. Unlike gravity, electromagnetism is described by the Standard Model of particles. In particular, the electroweak sector of the Standard Model consists of the symmetry group $SU(2) \times U(1)_Y$ and represents the unification of electromagnetism with the weak force at energies above the electroweak scale $M_{EW} \approx 246$ GeV. The group $SU(2)$ is generated by three vector bosons whereas the Abelian gauge group $U(1)_Y$ is represented by only one generator: the hypercharge. Below the electroweak scale, it becomes energetically favourable for the system to select a vacuum state which no longer respects the $SU(2) \times U(1)_Y$ symmetry, i.e., the symmetry is spontaneously broken. This is known as the Higgs mechanism [48, 49]. The resulting state will still contain a $U(1)$ symmetry, but rather than the hypercharge, the produced $U(1)_{em}$ now corresponds to the photon known from electromagnetism.

The low-energy behaviour of QED has been compared with experiment extensively and no inconsistencies between theory and observation were found, signalling that the theory of QED performs well at low energies. High energy tests involving the resonance of the Z boson have been performed [50]. In addition, the fine-structure constant, α, can be extracted from light atoms, see [51] for an extensive review. Tests that provide high accuracy involve the measurements of the anomalous magnetic moment of the muon [52, 53] and electron [54, 55]. In the absence of QED,

[3] A black hole does in fact emit thermal radiation, so called Hawking radiation (see Chpt. 3 for a brief discussion), but the Hawking temperature is too low to be detected directly. There are proposals to experimentally test Hawking radiation equivalents in analogue gravity, see for instance [45, 46] and for reviews on analogue gravity [47].

the magnetic moment of the electron and muon are predicted to be equal to 2. As one increases the energy, a cloud of virtual photons screen the charge and the magnetic moment becomes anomalous. The correction terms induced by the virtual photons can be calculated through a series expansion in terms of α and hence, allow for a comparison between experiment and theory. See [56] for an extensive review on the muon anomalous magnetic moment.

Despite the aforementioned high precision with which QED has been tested at low energies, attempts to extend the theory up to arbitrarily high scales have been unsuccessful and lead to a divergence in physical quantities, as first noted in [57]. Intuitively the effect originates from quantum fluctuations in the form of virtual particle-antiparticle pairs, which screen the central charge. Resolving the charge at smaller distances corresponds to an increase in energy. Since the charge carried by the particle-antiparticle pairs increases with energy, this zooming in on the central charge is directly translated into an increase in the effective, measured charge. One can then imagine that there will be an energy scale at which the central charge tends to infinity. Note that heuristically the nature of the problem is very similar to the divergence of curvature invariants near the centre of black-holes: zeroing in beyond certain length scales causes a blow-up in physical quantities.

Since we are probing energies above M_{EW}, it is really the electroweak hypercharge which causes a breakdown. There are strong indications that the Landau pole carries over to the electroweak sector of the Standard Model [58, 59, 60, 61, 62, 63, 64, 65, 66, 67], signalling that we are in fact not dealing with a fundamental theory and the question becomes what needs to be added or altered to resolve this issue. Before speculating about possible solutions, let us briefly discuss how this breakdown at high energies comes about.

To analyse this in more detail, we can study the behaviour of the hypercharge, $g_Y(k)$, as a function of the scale, k, where we define our theory. This information is encoded in the *beta function* of the charge, which tells us how $g_Y(k)$ changes with k. Typically, the value of $g_Y(k)$ is fixed at some scale k_0 by performing a measurement: $g_{Y,r} = g_Y(k_0)$ which can be thought of as fixing an initial value. This procedure yields the *renormalised* coupling $g_{Y,r}$.

To leading order, the beta function, β_{g_Y}, is given by

$$\beta_{g_Y} = k\frac{\partial g_Y(k)}{\partial k} = \beta_0 g_Y^3(k) + \mathcal{O}\left(g_Y^5(k)\right), \tag{1.4}$$

with β_0 a constant, typically depending on the matter content taken into account. Solving this equation for $g_Y(k)$ gives the desired expression for the hypercharge as a function of the momentum scale

$$g_Y^2(k) = \frac{g_{Y,r}^2}{1 - 2\beta_0\, g_{Y,r}^2 \ln\frac{k}{k_0}}. \tag{1.5}$$

Here $g_{Y,r}$ is the renormalised coupling, k_0 the reference scale, β_0 the 1-loop coefficient and k the scale up to where our theory is defined. As can be seen from Eq. (1.5), in the case that $g_{Y,r}^2 > 0$, the charge $g_Y(k)$ diverges at $k \to k_0 \exp\frac{1}{2\beta_0\, g_{Y,r}}$ and hence, the theory contains a Landau pole, cf.,

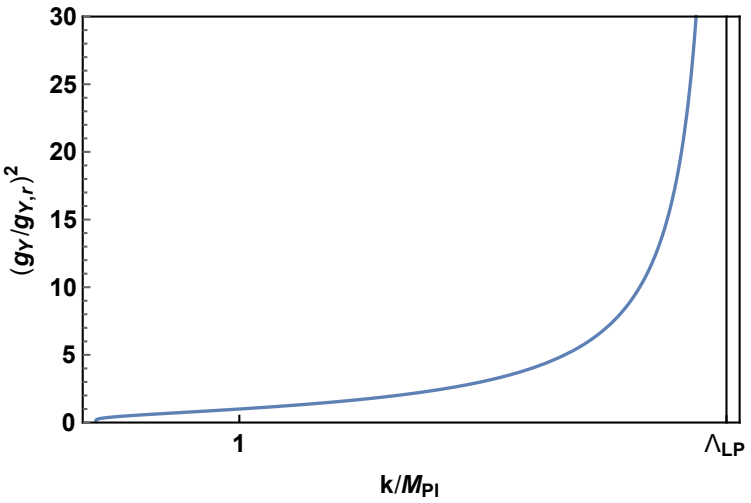

Figure 1.1: The hypercharge coupling g_Y^2 runs into a Landau pole at large scales, Λ_{LP}, signalling a breakdown of the theory.

Fig. 1.1. Turning the argument around and solving for $g_{Y,r}$, we instead end up with

$$g_{Y,r}^2 = \frac{g_Y^2(k)}{1 + 2\beta_0\, g_Y^2(k) \ln \frac{k}{k_0}}, \tag{1.6}$$

from which we can deduce that in the limit $k \to \infty$, while keeping $g_Y^2(k)$ fixed, the renormalised coupling $g_{Y,r}^2$ tends to zero. This would mean that interactions are switched off in the infrared and the theory becomes trivial [68, 69]l, cf. Eq. (1.5).

If instead we would find that in the limit $k \to \infty$, the coupling g_Y reaches some finite value g_Y^*, then one could avoid the triviality problem and interactions would remain present at all scales. However, so far no evidence suggesting $g_Y \to g_Y^*$ when $k \to \infty$ has been found [66, 67, 70, 71, 52]. Since the Landau pole occurs at energies well beyond the Planck scale, the general consensus is indeed that we are dealing with the low-energy limit of a more fundamental theory which takes over around the Planck scale. One proposal resolving this breakdown will be discussed in more detail in Chpt. 2.1.4, and indeed involves the inclusion of quantum gravitational degrees of freedom. In particular, we find evidence that the coupling of an Abelian gauge field to asymptotically safe gravity, approaches a fixed value.

Since the Landau pole occurs well beyond the Planck scale, $\Lambda_{LP} \approx 10^{41}$ GeV [72], its existence plays in practice no role at experimentally observable energies. The triviality problem is then a theoretical problem with no known (currently accessible) experimental consequences, i.e., the microscopic physics does not leave any signatures on macroscopic physics. It is, however, a shortcoming of the theory and renders the Standard Model to be an effective theory, valid only up to certain energy scales. This motivates the search for a more fundamental theory to which the Standard Model is a low-energy limit. In particular, it could be that the fundamental parameters of nature are not those included in the Standard Model, leading to the intriguing scenario where the number of free parameters can be reduced and hence, predictivity enhanced.

1.3 Motivation

Experiments testing the robustness of classical GR will continue to develop in the future and it might be that eventually GR will fail to reproduce observations. So far, however, it has passed every test. Under the assumption that, until proven otherwise, GR indeed provides the "correct" description of classical gravity, it can still not be the complete picture. In particular, since GR breaks down at Planckian curvature scales, it merely provides us with an effective description and should be replaced with a fundamental, UV-complete theory.

When probing high energies, the matter content of the universe will enter the quantum regime such that the right-hand side of the Einstein equations Eq. (1.1), must be replaced by an expectation value

$$G_{\mu\nu} = \frac{8\pi G_N}{c^4}\langle T_{\mu\nu}\rangle, \tag{1.7}$$

where we defined the Einstein tensor $G_{\mu\nu} \equiv R_{\mu\nu} - \frac{1}{2}g_{\mu\nu}R$ and set the cosmological constant term to zero. Settings which consider a scenario where quantum matter propagates on a classical background go under the name *semi-classical* gravity and have been explored, see for instance [73] for a review. However, these type of theories face fundamental issues such as the inability to form semi-classical interactions or reconstruct the conservation laws the classical matter fields should satisfy. It then appears natural to quantise the mediating field as well, i.e., spacetime itself, leading to a theory of quantum gravity.

In terms of the fundamental constants, $(1/c, G_N, \hbar)$, one can characterise SRT in terms of the speed of light alone: $(1/c, 0, 0)$ whereas the non-relativistic description of gravity, i.e., Newtonian gravity, has: $(0, G_N, 0)$. The combination of these two into a single framework yields GR: $(1/c, G_N, 0)$. A natural extension of GR incorporates the reduced Planck constant, $\hbar$, describing a theory which, in addition to gravitational and relativistic properties, features quantum mechanical characteristics as well. We can use these three dimensionful constants to build a length scale

$$\ell_{Pl} = \sqrt{\frac{\hbar G_N}{c^3}}. \tag{1.8}$$

The expression above is known as the Planck length and represents the fundamental length scale where gravity, relativity and quantum physics all become relevant. Plugging in the numbers for the three constants, we find that $\ell_{Pl} \approx 10^{-35}m$. Or, equivalently, the Planck mass $M_{Pl} = \sqrt{\frac{\hbar c}{G_N}} \approx 10^{19}$ GeV/c^2 indicating that quantum fluctuations of gravity will become relevant at an energy of approximately $E_{Pl} = 10^{19}$GeV. It is then evident that a description of GR which is valid beyond the Planck scale, will necessarily require a treatment of quantum fluctuations.

This theory of quantum gravity has been sought after for decades without conclusive success, the main reason being that the standard formalism employed to construct the quantum version of a classical theory breaks down for gravity. We will look at this in more detail in Sect: 1.3.1. The heuristic explanation is that the high-energy limit of macroscopic gravity (in the form of GR), cannot be constructed consistently, i.e., without diverging physical quantities.

A major obstacle in finding a theory of quantum gravity is the comparison between theory and experiment. Even if we consistently write down a theoretical model for gravity which is valid at all energies and reduces to GR at low energies (or some modified form of GR, consistent with experimental bounds), quantum gravity is expected to become relevant around Planckian energy scales, indicating that an energy of approximately 10^{19} GeV is necessary to probe the regime of quantum gravity. The highest energies available through human-made experiments can be found at CERNs Large Hadron Collider (LHC), and reach up to $\sim 10^4$ GeV, leaving a staggering energy gap of about $\sim 10^{15}$ to be bridged before direct tests of quantum gravity become possible. Since we cannot go "up", we could instead try to bring quantum gravity "down" to experimentally observable energies. Given a model of quantum gravity, one could search for effects that latched on to physical quantities at high energies and propagate through in the low-energy limit.

Inspired by the notion that gravity and matter are dynamically linked in classical GR, cf. Eq. (1.1), a possible testing ground lies in the coupling of matter degrees of freedom to (quantum) gravitational ones. Ideally, one could search for possible low-energy modifications/violations induced by a coupling between matter and gravity to exclude/confirm specific models. For example, if a coupling between quantum gravity and fermionic matter leads to a spontaneous breaking of chiral symmetry, then one would have fermions bound states with Planckian masses. This is exactly what was observed in early studies involving a lattice quantisation of gravity [74, 75], but more recent constructs show no evidence of chiral symmetry breaking for lattice models [76] or continuum settings [77, 78], see Chpt. 2.2.6. Of course most approaches to quantum gravity are dealing with technical issues which already makes it challenging to investigate the low-energy limit of quantum gravity alone (which is generally believed to limit to classical GR). One might then wonder how the additional bells and whistles that come with the inclusion of matter are supposed to make things better. However, rather than viewing these additions as complications, they might prove to bring additional structures, rendering the "gravity + matter" scenarios less daunting than pure gravity. A prominent example comes from the asymptotic-safety scenario [25], where the influence of asymptotically safe quantum gravity on matter models can be investigated through the running of coupling constants , see [79, 80] for reviews. One can then extract observable quantities, such as the low-energy value of a coupling, and confirm whether or not this value is consistent within the parameters of the model, cf. Chpt. 2. In particular, we will see there are scenarios where the low-energy values of the matter couplings become a *prediction* of the theory in gravity-inclusive settings, Chpt. 2.1.4. In addition, since it is clear that the universe is not empty, it is not *a priori* apparent that a consistent theory of pure-gravity exists or, in case it does, can be generalised to gravity-matter settings.

Since the extraction of possible quantum-gravity imprints on observable low-energy quantities is typically not a clear-cut procedure, other methods of cross-checking are desirable. In particular, if not experimentally, then perhaps theoretical tests across different approaches will be able to provide useful insights. Preferably, one would define a set of quantum-gravity observables and compare the properties of these observables across different approaches. Unfortunately, there exists no obvious way of defining such a set of observables, in part due to the diffeomorphism invariance of GR which, in most approaches, is carried over to the quantum regime. The challenge is then not only the construction of observables that are invariant under coordinate transformation, but

these observables need to be "quantum" in addition, i.e., we need diffeomorphism-invariant, quantum observables. Steps towards the construction of such an observable have been made in, e.g., the Causal Dynamical Triangulations approach to quantum gravity [81, 82]. In addition, several approaches not included in this thesis conjecture the existence of scale symmetry at high energies. For example, spin foams [83, 84] group field theory [85] and matrix/tensor models [86, 87, 88, 89], see [90] for an overview on the existing approaches to quantum gravity. The existence of scale invariance typically signals universality and allows for the extraction of critical exponents which, in turn, potentially allow for a comparison between different approaches.

1.3.1 Perturbative breakdown

Before embarking on the task of finding a theory of quantum gravity, we will shortly summarise why gravity does not adhere to the standard quantisation procedures. For a more detailed account, see for instance [91, 92]. Naively, one would take the classical action and perform a perturbative expansion of the generating functional for small couplings to calculate quantum corrections in the form of loop diagrams. Classically, the gravitational action is given by the Einstein-Hilbert action

$$S = \frac{1}{16\pi G_N} \int d^d x \sqrt{-g}\, R, \tag{1.9}$$

with R the Ricci scalar and we set the cosmological constant to zero for now. Since the Newton coupling is dimensionful when $d \neq 2$, i.e., $[G] = 2 - d$, one-loop corrections of the from $G\mu^{d-2}$, with μ an ultraviolet cutoff, are expected to appear. This comes about in the following way: every propagator comes with powers of momenta $P \propto p^{-2}$ and each vertex $V \propto p^2$ due to the two derivatives of the metric hidden in R. Then, for a diagram with one loop and n vertices and propagators, there will be a momentum integral $\int^\mu d^d p\, (PV)^n \propto \mu^d$ since the combination $PV \propto 1$. If we now add an internal line and corresponding vertices (resulting in an additional loop), then this corresponds to adding a momentum integral $\int^\mu d^d p\, P(PV)^2 \propto \mu^{d-2}$. The problem is that these terms result in run-away behaviour in the limit where μ is removed. In particular, using that the number of loops L in a diagram is related to the propagators and vertices as $L = P - V + 1$, the superficial degree of divergence in d dimensions is

$$\mathbf{D} = 2 + (d-2)L, \tag{1.10}$$

where L counts the number of loops in a given diagram. Hence, when $d > 2$, the divergences grow with each loop-order, leading to a divergent perturbation series. It can be shown that at one-loop, the induced divergences are proportional to R^2, $R_{\mu\nu}R^{\mu\nu}$ and $R_{\mu\nu\rho\sigma}R^{\mu\nu\rho\sigma}$ meaning that removing these divergences requires a counterterm of the same form. The issue is that these terms are not of the form Eq. (1.9) and can therefore not straightforwardly be included. It turns out, however, that one-loop is special, since on-shell we have $R_{\mu\nu} = R = 0$ for pure gravity, and hence, the equations of motion can be used to remove the divergences proportional to $R_{\mu\nu}$ and R. The only remaining term is then $R_{\mu\nu\rho\sigma}R^{\mu\nu\rho\sigma}$. However, in $d = 4$ the sum of the three curvature-squared terms form a total derivative and hence, a topological invariant (Gauss-Bonnet theorem)

$$E = R_{\mu\nu\rho\sigma}R^{\mu\nu\rho\sigma} - 4R_{\mu\nu}R^{\mu\nu} + R^2. \tag{1.11}$$

We can use this to rewrite the remaining term $\propto R_{\mu\nu\rho\sigma}R^{\mu\nu\rho\sigma}$ in terms of the other curvature-squared terms, resulting in a vanishing on-shell contribution. This argument no longer goes through under the inclusion of matter [93, 94, 95], since the equations of motion now take the form $R_{\mu\nu} = 8\pi G\left(T_{\mu\nu} - \frac{1}{2}g_{\mu\nu}T\right)$, with $T_{\mu\nu}$ the energy momentum tensor.

Furthermore, it can be shown that for higher-order loop expansions it is no longer possible to remove the divergences. In particular, already at two-loop level, the so-called Goroff-Sagnotti counterterm [96, 97]

$$\Gamma^{(2)}_{GS} \sim \frac{1}{d-4}\hbar^2 G_N \int d^4x\sqrt{g}R^{\rho\sigma}_{\mu\nu}R^{\kappa\lambda}_{\rho\sigma}R^{\mu\nu}_{\kappa\lambda}, \tag{1.12}$$

was shown not to vanish (on-shell or otherwise), confirming the (perturbatively) non-renormalisability of gravity.

Since the problem arises due to the fact that PV is dimensionless (i.e., $\sqrt{G_N}\,p$ is a dimensionless combination) in $d = 4$ and can therefore appear at any order in the loop expansion. We can circumvent this problem by modifying the action to include a quadratic curvature term, such that the propagator goes as $P \propto p^{-4}$. This, in turn, leads to a degree of divergence $\mathbf{D} = 4 + (d-4)L$, signalling that R^2-gravity is perturbatively renormalisable in $d = 4$ [98, 99]. The problem now is that the inclusion of an R^2 term induces additional poles in the propagator,

$$P \propto \frac{1}{p^4 + ak^2}, \tag{1.13}$$

leading to ghosts that appear to be physical particles which, in turn, spoil perturbative unitarity. It would then seem that in order to obtain perturbative renormalisability, one has to give up on unitarity.

A common misconception is that GR and QFT are incompatible, on account of the perturbative non-renormalisability of gravity. However, there are no inconsistencies in an effective field theoretic treatment of perturbative quantum gravity sufficiently far below the Planck scale.

1.3.2 Gravity as an effective field theory

At energies below the Planck scale, $q < M_{Pl}$, couplings to gravity are in general severely suppressed due to the weak coupling of gravity. This can be easily seen by realising that in a loop expansion all contributing higher order operators come with additional factors of G_N, due to the presence of additional propagators. Then, since $G_N \sim 1/M_{Pl}^2$, higher order contributions are suppressed by factors of $\left(\frac{q}{M_{Pl}}\right)^c$, where $c > 2$ already for the 1-loop counterterms. As long as the couplings of the corresponding terms are reasonably small (order one) and we probe energies below the Planck scale, only a finite number of counterterms need to be included to construct a perturbative, quantum effective description of gravity [100, 101, 102]. In these settings it is then for example possible to determine leading order quantum gravity corrections to the gravitational interaction between two heavy masses. These considerations are only valid at energy scales significantly below the Planck scale, since around the Planck scale the couplings are no longer small enough to admit

a perturbative expansion. It should be noted that in such an effective framework the coefficients of the counterterms need to be set by experiment and it is not straightforward to find experimental quantities that allow us to probe the tiny corrections needed to fix the coefficients.

1.4 Properties of quantum gravity

The apparent impossibility of reconciling the notions of QFT with those of GR has led to a large variety of candidate theories, each of which attempts to capture one or multiple characteristics a theory of QG might possess. Roughly these approaches can be grouped into one of two categories; those that try to stay close to the known frameworks of QFT and GR and try to modify one or the other and those that completely abandon the idea that physics beyond the Planck scale should admit a similar description to physics below the Planck scale. Theories falling in the first category would for example be Loop Quantum Gravity, the attempt to build a background independent QFT see [103, 104] for reviews, or the asymptotic-safety scenario for gravity, where a non-perturbative treatment of gravity (either through functional or lattice methods) provides evidence that G_N and Λ reach a scale invariant regime at high energies and thereby might allow for a UV completion of gravity. The second category contains, for example, Causal Set Theory [105], cf. Chpt. 3, which completely abandons any notion of continuum field theory and instead proposes that fundamentally spacetime consists of discrete "atoms", and the causal relations between these atoms in addition to the total number of atoms should be enough to extract all known physics. Another theory that belongs in this second category is String Theory, in which a two-dimensional surface rather than a one-dimensional world line evolves through spacetime, see [106, 107, 108] for reviews.

In any of these approaches, one would like to make sense of the object

$$Z = \int \mathcal{D}[g] e^{\frac{i}{\hbar} S[g]}, \tag{1.14}$$

which is at best a collection of ingredients at this point. To be well-defined, we need to specify each of the "ingredients" that make up Z. The measure $\mathcal{D}[g]$, in general tells us which type of metrics (spacetimes) should be taken into account and typically requires some form of regularisation in order to avoid divergences. Furthermore, it is not clear whether the integration over metrics should be supplemented by a sum over topologies. The fundamental action $S[g]$ will describe the dynamics of the theory in the high-energy regime and it might very well be that a consistent theory of quantum gravity needs to necessarily be accompanied by matter degrees of freedom to make sense. In that case we would need an action, $S[g, \Phi]$, which takes into account some form of matter contributions, Φ, and corresponding measure terms $\mathcal{D}\Phi$ need to be specified and regularised. Additionally, there might be boundary terms in the action that need to be taken into account. In general, different approaches can be distinguished based on their list of ingredients. However, for technical reasons it is often necessary to make certain approximations/simplifications. A prominent example of such a simplification is the assumption that one can start out from a "Euclideanised" version of Eq. (1.14), where all metrics g have a Euclidean signature, and perform a Wick rotation to Lorentzian signature by analytically continuing the time coordinate $t \to it$. Such a prescription does not carry over straightforwardly to spacetimes admitting non-zero curvature effects, since

one often cannot define a natural time coordinate [109, 110]. The assumption underlying the Euclidean definition of quantum gravity is that Euclidean and Lorentzian quantum gravity lie in the same universality class, i.e., low-energy physics is not sensitive to the sign of the metric at high energies. Whether this is indeed the case remains to be seen, but it should be noted that Euclidean (Riemannian) manifolds satisfy certain properties that do not have a Lorentzian counterpart. For example, it can be proven that every smooth manifold admits a Euclidean metric but this does not carry over to Lorentzian metrics[4] [111] p. 149. Intuitively then, it might be that a Euclidean theory of quantum gravity will limit to a Lorentzian version under particular assumptions. As we will see in Chpt. 2.2, the split between Euclidean and Causal dynamical triangulations was exactly motivated by such a consideration. Alternatively, one might pose no restrictions at all on the metrics taken into account and instead demand that the dynamics contained in $S[g]$ is sufficient to select only those metrics that are phenomenologically viable.

Apart from the lack of experimental data and the perturbative non-renormalisability of gravity, a major challenge every theory of quantum gravity needs to face is that of diffeomorphism invariance at low energies. Since classical GR admits a completely coordinate-independent description, most approaches demand some form of background independence. There is of course the possibility that coordinate independence is a symmetry which emerges as part of the low-energy limit, rather than being part of the fundamental theory. In that case the corresponding high-energy theory would be required to describe the mechanism responsible for such an increase in symmetry. Leaving this option be, there is still the question of how to obtain a truly background independent UV-complete theory. In a field-theoretic setting, the most natural implementation would be to never specify a specific background configuration. Of course this makes it technically difficult to do computations and a better way to go might be to restore the broken symmetries through a specific formalism such as the Ward identities. For those approaches using discrete methods, recognising what exactly is meant by a coordinate frame is often more subtle but usually refers to the assignment of labels to discrete building blocks. The dynamics of these discrete formulations should then be formulated in a relabelling invariant way. In some approaches, such as Causal Set quantum gravity, one does not "just" demand an independence under coordinate transformations, but additionally puts very few restrictions on the topology and geometry that are expected to contribute to the fundamental theory. For example, the dimension of spacetime and the number of "holes" a spacetime might possess are left free.

The rest of this thesis is structured in the following way. In Chpt. 2 the asymptotic safety scenario for gravity will be introduced and applied to a model involving the Abelian hypercharge and gravity in Chpt. 2.1.4 using functional methods. A lattice treatment of gravity will follow in the Chpt. 2.2, where the effects of fermions will be studied in Chpt. 2.2.6. In the final section we will move away from the concepts of asymptotic safety and (continuum/discrete) field theories and focus on causal set theory Chpt. 3. Starting from a spatial distance function in Chpt. 3.3.3, dimensional estimators for the Hausdorff dimension, Chpt. 3.3.4 and spectral dimension, Chpt. 3.3.5 will be developed. We will conclude in Chpt. 4 and give an outlook for possible future work in Chpt. 5

[4] The simplest example is the n-dimensional sphere S^n, which readily admits a Euclidean metric for any n but can only be equipped with a Lorentzian metric for n odd and $n \geq 3$.

Chapter 2

Asymptotically safe quantum gravity

Rather than giving up entirely on a QFT description of quantum gravity, one can argue that the perturbative breakdown of gravity simply signals the need for a non-perturbative framework. Here we will explore the possibility where gravity becomes asymptotically safe in the UV. As a starting point, we provide a general introduction to the continuum setting, which can be explored by means of functional methods detailed in Chpt. 2.1.1.3. After a short discussion on pure-gravity, Chpt. 2.1.2 and general matter-gravity models Chpt. 2.1.3, we will refocus in detail on the Abelian hypercharge coupled to asymptotically safe quantum gravity, Chpt. 2.1.4.

2.1 Asymptotic-safety scenario

Asymptotic safety, as originally proposed by Weinberg, [112], provides a mechanism which allows for a theory to be extended up to arbitrary high energies, without requiring for couplings to be power-counting renormalisable. The basic idea is that if all dimensionless counterparts of the essential couplings of a theory, i.e., those couplings which cannot be removed through a field redefinition, approach a fixed value. If this is the case, then the theory is *asymptotically safe* and all observables of the theory will be finite. In the simplest case, all the couplings attain a constant zero value, resulting in a non-interacting theory. An example of such an *asymptotically free* theory is QCD, where the strong coupling asymptotically approaches a free fixed point at high energies, and hence, renders the theory non-interacting. Asymptotic safety generalises this concept and conjectures that at least one of the couplings in the theory approaches a non-zero value at the fixed point, resulting in an asymptotically interacting theory. For reviews on asymptotic safety see [113, 114, 115, 116, 117, 118, 80, 119] and for an introduction to quantum scale symmetry [120].

If, however, there exists a fixed point such that the gravitational coupling approaches scale invariance around the Planck scale, then gravity can be renormalised non-perturbatively. This scenario was dubbed the *asymptotic-safety scenario*. One of the strengths of asymptotically safe gravity is that it does not demand the inclusion of any new physical degrees of freedom, rather, it proposes the existence of an additional symmetry in the fundamental theory. The presence of this *scale* symmetry is signalled by the observation that the couplings of the theory cease to run, and

hence, become independent of the scale at which they are probed. Intuitively then, scale invariance in gravity implies that once the scale invariant regime has been reached, zooming in on spacetime will no longer change the description of spacetime itself. The fundamental structure of spacetime can then be thought of as fractal-like.

To be more precise, a fixed point in the space of all couplings, g_i^*, is characterised by the simultaneous vanishing of all beta functions. That is

$$\beta_{g_i} \mid_{g_i=g_i^*} = k\,\partial_k\, g_i(k) \mid_{g_i=g_i^*} = 0, \tag{2.1}$$

with $g_i(k)$ the dimensionless couplings, i.e., $g_i(k) = \bar{g}_i(k)\, k^{-d_{\bar{g}_i}}$, where $\bar{g}_i(k)$ is the dimensionful coupling with canonical mass-dimension $d_{\bar{g}_i}$. Since the vanishing of the beta function in Eq. (2.1) indicates all dimensionless couplings reach scale invariance at the fixed point, the dimensionful couplings necessarily need to scale with their canonical mass dimension i.e., $\bar{g}_i(k) \propto k^{d_{\bar{g}_i}}$. The reason for choosing the dimensionless couplings in Eq. (2.1) is motivated by demanding that divergences at finite values of k should not enter any physical quantities, i.e., we are interested in the change of the couplings relative to the cut-off. Weinberg argued for this in the following way [112]: For a physical process $P = k^D f(E_{phys}/k, X, g(k))$, where D is the dimensionality of the process, E_{phys} the physical energy scale characteristic for the process under consideration and X summarises all other dimensionless physical variables. Any physical process can not depend on the renormalisation point k, where the couplings are defined. We are then free to associate $k = E_{phys}$, such that $P = E_{phys}^D f(1, X, g(E_{phys}))$ and hence, as we increase the energy, the physical process depends only on the behaviour of the dimensionless couplings times the factor E_{phys}^D.

The couplings g_i can be used to find a critical hypersurface of renormalisation trajectories emanating from the fixed point in the UV towards the IR, cf. Fig. 3.8. If we reverse the flow such that we flow from the IR to the UV, then the dimensionality of the hypersurface is defined as the number of directions in coupling space which are attracted towards the fixed point. These directions are called relevant or UV-attractive and signal a departure from scale invariance since trajectories guided by these directions can end in a selection of IR values despite originating from the same fixed point. To select the unique, phenomenologically relevant trajectory of these couplings one needs to experimentally determine the value they take on in the IR. As each relevant coupling requires a measurement, a theory is said to be *predictive* if its infinite space of couplings admits a finite number of relevant directions and hence, the dimension of the UV hypersurface is finite. Conversely, irrelevant or UV-repulsive directions are characterised by the exact opposite behaviour, i.e., they start off the critical hypersurface in the UV and are pulled towards the fixed point in the IR (IR-attractive directions), thus yielding a unique value of the couplings at low energies without the necessity of performing a measurement. A non-interacting or Gaussian fixed point has the property that all couplings vanish at the fixed point, i.e., $g_i^* = 0$ in Eq. (2.1). Perturbation theory works for a theory admitting such a fixed point since all higher order couplings (i.e., higher order in their canonical scaling) are irrelevant and thus all trajectories starting in the UV will be pushed towards zero in the IR. As a result the physics predicted by such a theory is fully determined by its relevant and marginally relevant couplings.

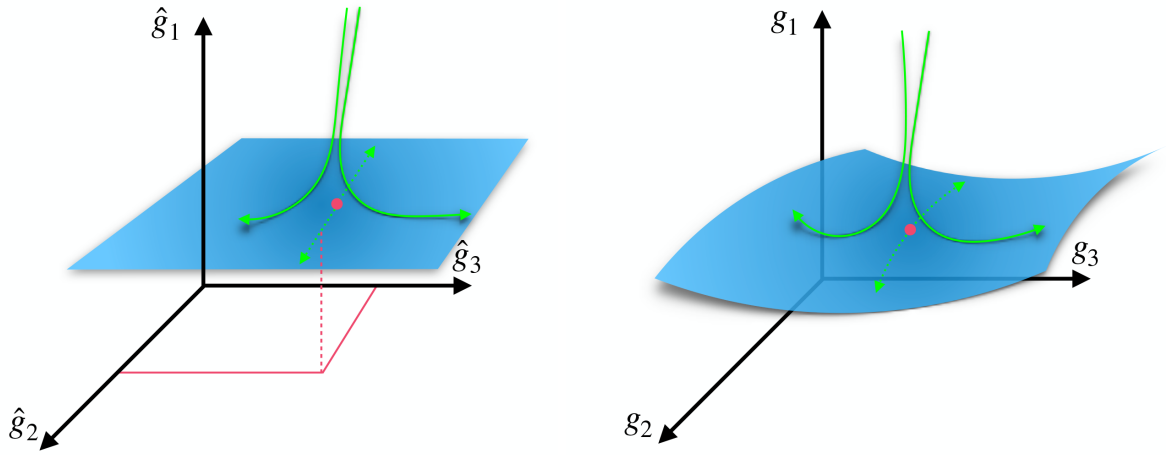

Figure 2.1: Left: In the case where the couplings line up exactly with the eigen-directions around the fixed-point (magenta dot), the relevant couplings $\hat{g}_2$, $\hat{g}_3$ span the critical hypersurface (blue plane) whereas the irrelevant coupling $\hat{g}_1$ is perpendicular to the critical hypersurface. The solid green trajectories are pulled towards the hypersurface along the irrelevant (IR attractive) direction as the momentum scale is lowered, resulting in a prediction of the IR value for $\hat{g}_1$ (i.e., the intersection of the plane with the vertical, $\hat{g}_1$ axis). In contrast, the dotted green trajectories emanate from the UV fixed point and constitute IR repulsive trajectories. Projecting a specific point of the trajectories onto the $\hat{g}_2$, $\hat{g}_3$ plane (pink, dashed line) yields different IR values for the relevant (IR repulsive) couplings. Right: The UV critical hypersurface will typically exhibit curvature in the original basis g_1, g_2, g_3, resulting in couplings that do not exactly line up with the linearised eigen-directions around the fixed-point.

To explicitly illustrate the concepts of irrelevant and relevant directions, consider the linearised flow of a set of couplings close to the fixed point

$$\beta_{g_i} = \sum_j \frac{\partial \beta_{g_i}}{\partial g_j}\bigg|_{\mathbf{g}=\mathbf{g}^*} (g_j - g_j^*) + \mathcal{O}(g_j - g_j^*)^2, \tag{2.2}$$

where $\mathbf{g}^* = (g_1^*, g_2^*, \dots)$ holds the fixed point values of all couplings. Recognising the Jacobi matrix[1] $\mathbf{M}_{i\,j} = \frac{\partial \beta_{g_i}}{\partial g_j}$ the solution can be written as

$$g_i(k) = g_i^* + \sum_I C_I V_i^I \left(\frac{k}{k_0}\right)^{-\theta_I}, \tag{2.3}$$

[1] Note that the fixed-point can be recognised as a critical point of the differentiable function β_{g_i} by observing that the rank of its Jacobian $\mathbf{M}$ is not maximal. In other words, at the critical point, the number of independent columns of $\mathbf{M}$ is less than at some point in its neighbourhood.

in terms of the components of the eigenvectors V^I and eigenvalues $-\theta_I{}^2$ of the Jacobi matrix

$$\begin{aligned}\sum_j \mathbf{M}_{i\,j}\, V_j^I &= -\theta_I V_i^I \\ \Rightarrow \theta_I &= -\left.\frac{\partial \beta_{g_i}}{\partial g_j}\right|_{\mathbf{g}=\mathbf{g}^*}.\end{aligned} \tag{2.4}$$

Here C_I are integration constants and k_0 refers to a fixed reference scale. Despite the fact that $\mathbf{M}$ has real entries it is usually not symmetric, which can result in imaginary eigenvalues $-\theta_I$. Close to the fixed-point, the imaginary part of the critical exponents induces a spiralling type of behaviour, but does not convey any information on whether the flow points towards or away from the fixed-point. The sign of the real part of θ_I does carry that information and in the following we shall study Eq. (2.3) in more detail to extract whether a coupling is relevant or irrelevant.

In general, the couplings do not line up with the eigenvectors V^I of the Jacobi matrix and the solution, Eq. (2.3), for a coupling $g_i(k)$ will be a mixture of several directions. Let us then rotate to a basis for the couplings $\hat{g}_i(k)$ where the Jacobi matrix becomes diagonal, cf. Fig. 3.8 left panel. In this case, the couplings do line up with V^I, and the solution simplifies to

$$\hat{g}_i(k) = \hat{g}_i^* + \hat{C}_i V_i^i \left(\frac{k}{k_0}\right)^{-\hat{\theta}_i}. \tag{2.5}$$

For those critical exponents with a negative real part $\mathrm{Re}\,\hat{\theta}_I < 0$, we observe that if we start close to the fixed point in the UV and lower k, the coupling $\hat{g}_i(k)$ remains close to its fixed point value independently of $\hat{C}_I$ (i.e., the second term on the right-hand side of Eq. (2.3) decreases when lowering k). The IR values of these couplings are therefore a prediction of the theory and these couplings are therefore irrelevant. In contrast, when $\mathrm{Re}\,\hat{\theta}_I > 0$, lowering k drives the coupling away from its fixed point value and the exact values of the coefficients C_I' become important in the extraction of $\hat{g}_i(k)$ (i.e., in this case the second term on the right-hand side of Eq. (2.3) increases when lowering k). These coefficients need to be fixed by experiment to obtain the IR value of the coupling and hence, they are relevant. Conversely, one can study Eq. (2.3) in the UV limit $k \to \infty$. In order for the coupling to obtain its fixed-point value $\hat{g}_i(k) \to \hat{g}_i^*$, the exact value of $\hat{C}_I$ is not of importance when $\mathrm{Re}\,\hat{\theta}_I > 0$, whereas one necessarily needs to have $\hat{C}_I = 0$ for all I corresponding to a negative value of $\mathrm{Re}\,\hat{\theta}_I < 0$.

For a coupling with canonical mass dimension $d_{\bar{g}_i}$, we can write

$$\beta_{g_i} = -d_{\bar{g}_i}\, g_i(k) + f_i(\mathbf{g}) g_i^2(k), \tag{2.6}$$

where we summarised all higher order quantum contributions in $f_i(\mathbf{g})$. Close to the Gaussian fixed point, the term $f_i(\mathbf{g})$ will be small, and hence, the set of couplings with a positive canonical mass dimension will represent the relevant directions. At an interacting fixed point, the second term in Eq. (2.6) can form a significant contribution, making the question of whether a coupling is relevant or irrelevant more subtle.

[2] We point out that the sign of $\theta_I = -\mathrm{eig}\,\mathbf{M}_{i\,j}$ is purely conventional.

Extracting the critical exponent

$$\theta_I = d_{\bar{g}_i} - f_i(\mathbf{g}^*). \tag{2.7}$$

We see then that when $f(\mathbf{g}^*) > d_{\bar{g}_i} > 0$, higher order terms can flip the sign of θ_I and turn a relevant direction into an irrelevant one, thus increasing the predictivity of a theory[3]. Physically the critical exponents carry information on the rate with which a fixed point is approached along a certain direction. Note that in the case where one switches to the diagonal basis, $\hat{g}_i$ the scaling will no longer be with the canonical mass dimension, but rather with some anomalous dimension $\eta_i = d_{\bar{g}_i} - \Delta_i$. Since a non-diagonal Jacobi in general occurs whenever interaction terms are present, the anomalous dimension vanishes at the free fixed-point (i.e., when interactions are switched off) and is taken to be small in the case of perturbation theory, where the couplings themselves are small.

Note that the existence of an interacting fixed point demands that the collective contribution of the quantum fluctuations captured by f_i in Eq. (2.7) have to contribute with a sign that is opposite to the canonical term. Keeping in mind that ultimately we are interested in gravity, an important question is exactly how non-perturbative gravity needs to be for an interacting fixed point to exist, see [121] for a preliminary analyses.

Let us briefly recap the concepts described so far and how they will be employed in what follows. The dynamics of theories which become asymptotically free or asymptotically safe in the UV is governed by scale invariance, i.e., the dimensionless couplings of the theory asymptotically attain a constant value as they approach the fixed point. For a finite number of relevant directions, one can formulate a well-defined theory, valid at all momentum scales[4], where the relevance/irrelevance of couplings is determined by their critical exponents at the fixed point Eq. (2.4). At an asymptotically safe fixed point, at least one (dimensionless) coupling takes on a non-zero value, resulting in an interacting theory at high energies. If all couplings take on a zero value, then the theory becomes completely non-interacting and we are in the asymptotically free setting. Since the concepts of asymptotic safety are particularly useful in a non-perturbative setting (i.e., where couplings might not take on small values), we will apply them to gravity and search for a fixed point in coupling space where one may define a theory of quantum gravity.

We will see in the following that to extract the flow of couplings and search for possible fixed points in the space of couplings, one may resort to different "tool-boxes", i.e., sets of tools which can be used to safely treat the unphysical divergences of a theory. Here we start with the continuum (functional) renormalisation group methods in Chpt. 2.1.1, and apply them to gravity and matter models in subsequent sections. In Chpt. 2.2, we will employ lattice-gravity methods to regularise our theory.

[3]Note that the converse is true as well, an irrelevant direction can become relevant, which in turn decreases predictivity.

[4]Let us place the disclaimer that the possibility of new physics setting in at arbitrarily high scales can never be disproven and introduces a new scale into the theory, which could spoil scale symmetry. However, as long as there are no observational indications or theoretical inconsistencies signalling new physics, there is *a priori* no motivation to embark on such a search for new physics.

2.1.1 The renormalisation group

As we saw in the previous section, the search for asymptotic safety can be conveniently described in terms of stationary points of the beta functions. The Wilsonian renormalisation group [122, 123, 124, 125] is particularly well-tailored to this description.

2.1.1.1 Basic concepts

The key point can be summarised as follows: given a theory which is well-behaved up to a certain momentum scale, we introduce a cut-off, μ, which has the job of taming UV divergences occurring above this energy scale. In general any theory we hope to extend to arbitrarily high energies needs this type of regularisation since a priori fluctuations can occur without any restriction on their length scale. Small length scales (a.k.a., high energy -or fast-modes) in particular cause observable quantities, which should be finite, to blow up if not treated carefully, see Chpt. 1.3.1.

Let us then associate the renormalisation group (RG) scale k with a UV cut-off which restricts the energy that can run through a loop in perturbation theory and more generally imposes a restriction on the measure of a functional integral. This restriction then unavoidably introduced a new scale into the theory and as it was put in by hand, it should not appear in any physical quantity we might be interested in. If we let $O(\mathbf{g}(k), E_{phys})_k$ be such a quantity of interest, depending on the couplings $\mathbf{g}$ and some physical energy scale E_{phys}, then we should be able to change the cut-off without spoiling the effective description at energies far below k. That is

$$O(\mathbf{g}(k), E_{phys})_k = O(\mathbf{g}(k'), E_{phys})_{k'}, \tag{2.8}$$

where the change in the couplings $\mathbf{g}$ as a function of the energy scale will be exactly encoded in the beta functions. The equation above implicitly tells us that we need to integrate out the physical degrees of freedom over the momentum shell between k and k', which can be interpreted as a type of coarse graining procedure. Furthermore, since k is an arbitrary scale, we are free to identify $k = E_{phys}$ such that the effective description only includes modes at or below the physical energy scale of the process.

Preferably one would like to iterate the momentum shell integration and study the behaviour of the couplings under this change of scale (i.e., the beta-functions). If the couplings approach a constant value under these transformations, then a fixed point in the space of couplings has been reached. Its existence signals universality in the sense that all theories defined on a renormalised trajectory describe the same physics on energy scales below the scale at which the physics is defined. In other words, different coarse graining/renormalisation schemes might find different positions of the fixed point, but the rate with which the fixed point is approached should be the same. If this is the case, then one can ensure that macroscopic physics does not depend on the specifics of microscopic physics.

It typically happens that integrating out momentum shells induces new terms paired with new couplings. If these new terms tend to zero as more modes are integrated out, then these are exactly the irrelevant couplings. In the case they do not, they are relevant and one needs to revisit the

theory by including these couplings from the start. This type of behaviour naturally occurs in the vicinity of a free fixed-point, where the couplings are small and any higher-order terms that are generated are rapidly driven towards zero.

In this setting the advantage of perturbative theories is that one can include counterterms which cancel the infinities that were originally there in absence of the momentum cut-off. Usually it is then possible to prove that the cut-off can be taken to infinity without re-introducing any divergences (hence, one can take a continuum limit). It is then possible to obtain the microscopic, bare action. For non-perturbative theories this is in general not the case. Gravity is a prominent example where the prescription above fails in the perturbative setting since at each loop order a new counter term appears which cannot be absorbed by the terms that were already present and hence, needs to be added to the bare action (Chpt. 1.3.1). Furthermore, these terms become important around the Planck scale where we can no longer do expansions around small values of the coupling.

It should be noted that not all perturbatively renormalisable theories admit a removal of the UV cut-off. In particular, QED cannot be extended up to arbitrarily high energies despite being perturbatively renormalisable. In this case then, the persistence of the divergencies are caused by the non-fundamental nature of the theory.

Before setting up a non-perturbative framework, let us first derive some of the quantities that play an important role in the perturbative setting [126, 127, 128, 129].

2.1.1.2 Technical tools

In general, for a real scalar field[5] in the presence of a source J, we can derive all physical properties from the correlation functions generated by the functional

$$Z[J] = \int_\Lambda \mathcal{D}\Phi \, e^{-S[\Phi]+J\cdot\Phi}, \tag{2.9}$$

where we introduced the short-hand $J \cdot \Phi = \int d^dx \, \Phi(x) \, J(x)$. In standard QFT, the source term works as a form of control parameter, allowing for the extraction of n-point correlation functions and usually set to zero at the end of the calculation. Keeping the source term, we find the correlation functions in presence of J

$$\langle \Phi(x_1), ..., \, \Phi(x_n) \rangle_J = \frac{1}{Z[J]} \int \mathcal{D}\Phi \, \Phi(x_1) \cdots \Phi(x_n) e^{-S[\Phi]+\Phi\cdot J}. \tag{2.10}$$

Preferably, we would like to have an object which straightforwardly allows the computation of these correlation functions and does not carry any additional, superfluous information. A convenient choice is the generator of one-particle irreducible correlation functions, or the *effective action* Γ

$$\Gamma[\varphi] = \sup_J (J \cdot \varphi - W[J]), \tag{2.11}$$

[5]The discussion below can be generalised to any matter content.

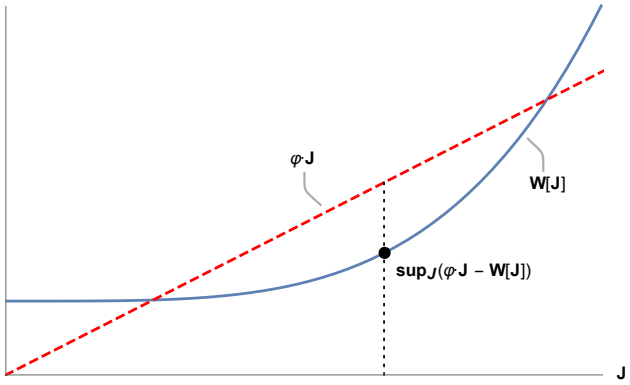

Figure 2.2: The line $\varphi \cdot J$ (red, dashed) is tangent to the functional $W[J]$ (blue, solid) at the point specified by $\sup_J(J \cdot \varphi - W[J])$. Rather than considering the entire functional $W[J]$, the Legendre transform ensures that given φ, we select the the unique point on $W[J]$ where $\varphi = \delta W/\delta J$ holds.

where

$$W[J] \equiv \log Z[J] = \log \int \mathcal{D}\Phi \, e^{-S[\Phi]+J\cdot\Phi}, \tag{2.12}$$

is the Schwinger functional.

In perturbation theory we would now go on to express $\Gamma[\varphi]$ in terms of the bare action $S[\varphi]$ and higher order contributions summarised as $\Gamma_l[\varphi]$ where l indicates the l^{th} loop-order. In particular, we would find

$$\Gamma[\varphi] = S[\varphi] + \Gamma_l[\varphi] = S[\varphi] - \log \int_\mu \mathcal{D}\Phi \, e^{-S[\Phi+\varphi]+\int_x \frac{\delta\Gamma[\varphi]}{\delta\varphi(x)}\Phi(x)}, \tag{2.13}$$

where we sent $\Phi \to \varphi + \Phi$ and interpret φ as the classical or background field while Φ will play the role of the fluctuation field. The crucial difference with non-perturbative methods is now that for a perturbatively renormalisable theory, we can expand around $\Phi = 0$ (i.e., we take the fluctuations to be small) and systematically remove infinities that occur at high energies by redefining couplings, masses and wave-function normalisations as a function of the momentum scale. In a perturbative setting this dependence on the momentum scale can be written as a perturbative series in the couplings and one can consistently counter any divergencies such that the removal of the UV cut-off $\Lambda \to \infty$ is safe. For a non-perturbative theory this breaks down simply because such a perturbative series is not well defined up to arbitrarily high energies and one needs to counter more and more terms as the energy increases.

2.1.1.3 Functional methods

It is nevertheless possible to generalise the methods described above to a non-perturbative setting. To do so, we cast it in a mathematical framework known as the functional renormalisation group (FRG) which has the benefit that it is not restricted to perturbative settings. For reviews see for instance [130, 131, 132, 133, 134, 135, 136, 137, 138, 139].

Since we do not a priori know what the bare action of our theory will look like and whether we can express the effective action, Γ, as an expansion around S_{bare}, we would like to define an object Γ_k which captures the physical properties of a theory depending on some momentum-shell k. This object should allow us to connect the bare, microscopic quantities defined at $k \to \mu$ with μ a UV cut-off (which we would like to send to infinity in the full theory) to their full effective form at $k \to 0$. This object Γ_k, is called the *average effective action* and it interpolates between the bare action $\Gamma_{k\to\mu} \sim S_{bare}$ and the full effective action $\Gamma_{k\to 0} = \Gamma$. It turns out we can obtain an object displaying this type of behaviour by adding a term to the generating functional of the form

$$\Delta S_k[\Phi] = \frac{1}{2}\int \frac{d^d q}{(2\pi)^d}\Phi(-q)R_k(q)\Phi(q), \tag{2.14}$$

such that

$$e^{W_k[J]} = Z_k[J] = \int_\mu \mathcal{D}\Phi e^{-S[\Phi]-\Delta S_k[\Phi]+J\cdot\Phi}. \tag{2.15}$$

Here R_k is called the *regulator* of the theory and ΔS_k has a mass-like form which depends on the momentum. We can derive certain properties of R_k by requiring the properties listed above for Γ_k to be satisfied. First off, in the IR we want the regulator to regularise our theory and thus,

$$\lim_{q^2/k^2\to 0} R_k(q) > 0, \tag{2.16}$$

needs to hold. As we lower the momentum scale $k \to 0$ we should recover the full effective action, without regulator

$$\lim_{k^2/q^2\to 0} R_k(q) = 0. \tag{2.17}$$

Lastly, the microscopic action is obtained as $k \to \mu$ in the limit where the ultraviolet cut-off is removed

$$\lim_{k\to\mu\to\infty} R_k(q) \to \infty, \tag{2.18}$$

assuring that the generating functional is dominated by the stationary point of the action. Note that indeed the $\mu \to \infty$ limit can be taken because the theory runs into the fixed point at infinity and on account of universality, physics cannot depend on the cutoff μ.

Without diving into the technical details, we can study how W_k changes as a function of the momentum scale k by taking its derivative

$$\partial_t W_k = k\partial_k W_k = -\frac{1}{2}\int_q \partial_t R_k(q)G_k - \partial_t \Delta S_k[\varphi], \tag{2.19}$$

where G_k is the connected propagator

$$G_k(q) = \frac{\delta W_k}{\delta J \delta J}(q) \tag{2.20}$$

and $\varphi(q) = \langle\Phi(q)\rangle = \frac{\delta W_k[J]}{\delta J(q)}$. We then define the average effective action as the modified Legendre transform such that

$$\Gamma_k[\varphi] = \sup_J(J\cdot\varphi - W_k[J]) - \Delta S_k[\varphi], \tag{2.21}$$

and the quantum equation of motion generalises to

$$J(x) = \frac{\delta \Gamma_k[\varphi]}{\delta \varphi(x)} + (R_k \varphi)(x). \tag{2.22}$$

The dependence of Γ_k on the scale can then be investigated through its scale derivative, which can be expressed as

$$\partial_t \Gamma_k[\varphi] = \frac{1}{2} \mathrm{Tr} \left[\left(\Gamma_k^{(2)}[\varphi] + R_k \right)^{-1} \partial_t R_k \right], \tag{2.23}$$

where $\Gamma_k^{(2)} = \frac{\delta \Gamma_k}{\delta \varphi \delta \varphi}$. This equation is known as the *flow equation* [130], see also [131]. Even though it has a one-loop structure (due to the trace on the right-hand side) the flow equation above is exact, in the sense that the propagator appearing on the right-hand side is the full propagator and in principle all terms allowed by the symmetries of the theory are taken into account in Γ_k. The regulator term R_k takes care of the IR regularisation of the theory, whereas $\partial_t R_k$ assures UV regularisation, cf., Fig. 2.3. At the same time the peak of $\partial_t R_k$ selects those modes q^2 close to k^2. An example is the optimised regulator [140, 141], which is optimised with respect to stability and convergence of the flow for bosonic fields

$$R_k(q^2) = k^2 \left(1 - \frac{q^2}{k^2} \right) \theta \left(1 - \frac{q^2}{k^2} \right), \tag{2.24}$$

where $\theta(x)$ is the Heaviside step function. Let us note that the regulator breaks diffeomorphism invariance and to recover background independence one should take into account the modified Ward-identities [142, 132, 143, 144, 145, 146].

Note that in the case of perturbation theory, one expands the average effective action around the bare action $\Gamma_k = S + \hbar \Gamma_k^{\text{1-loop}} + \mathcal{O}(\hbar^2)$ and, hence, to 1-loop we can set $\Gamma_k^{(2)} = S^{(2)}$ such that

$$\begin{aligned} \partial_t \Gamma_k^{\text{1-loop}} &= \frac{1}{2} \partial_t \mathrm{Tr} \log \left(S^{(2)} + R_k \right) \\ &\text{and} \\ \Gamma_k^{\text{1-loop}} &= S + \frac{1}{2} \mathrm{Tr} \log S^{(2)} + \text{const.} \end{aligned} \tag{2.25}$$

If we expand Eq. (2.13) up to 1-loop (lowest order around $\Phi = 0$), we would recover the last line of the expression above. In a perturbatively renormalisable theory we would then be able to integrate down to the IR and obtain the full effective action, Γ, whereas the non-perturbative setting requires the momentum-shell type of integration provided by the regulator. The difference between the two methods is then exactly the "step-by-step" procedure of integrating out the momentum dependence employed here.

The FRG methods described here have been employed to a diverse collection of models, from high-energy physics [147, 148, 149, 150, 151] to condensed matter models. For example, the Wilson-Fisher fixed point [152] has been studied [153, 154, 155] as have the non-linear sigma model [156, 157, 158] and the Gross-Neveu model [159].

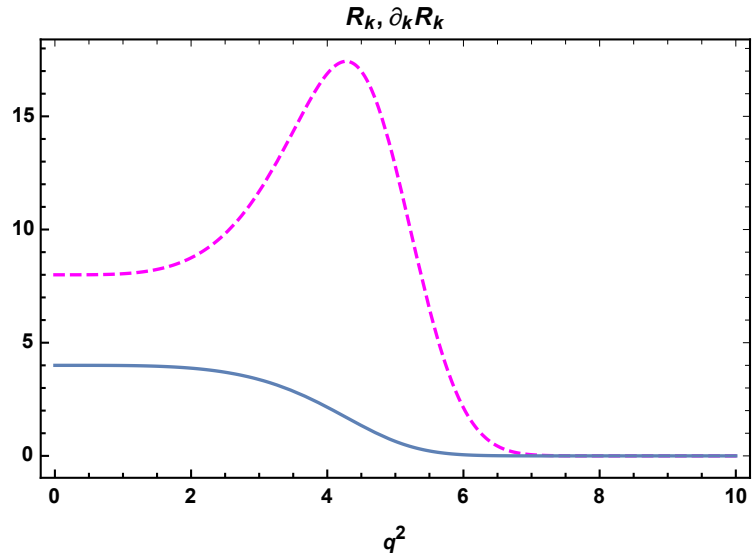

Figure 2.3: The regulator $R_k(q^2) = \frac{2k^2}{e^{(q^2/k^2)^4}+1}$ (solid, blue line), assures regularisation of the IR modes, whereas its derivative $\partial_t R_k$ (dashed, magenta line) takes care of the regularisation of UV modes and peaks around $q^2 = k^2$ (here $k^2 = 4$), selecting modes close to k^2.

Despite Eq. (2.23) being formally exact, it should be emphasised that in practice one needs to approximate the infinite number of terms that are allowed by the symmetries. Here we will focus on a selection procedure based on the canonical dimension of operators, which can be motivated by recalling that the beta function of a coupling, g_i, has the form

$$\beta_{g_i} = -d_{\bar{g}_i}\, g_i(k) + f_i(\mathbf{g}) g_i^2(k), \tag{2.26}$$

and, hence, the leading contribution to the critical exponents around the fixed point is proportional to the canonical dimension

$$\theta_I = d_{\bar{g}_i} - f_i(\mathbf{g}^*). \tag{2.27}$$

One would then expect that irrelevant operators ($\theta_I < 0$) with a large canonical dimension will remain irrelevant at the fixed point and hence, neglecting them in a first approximation should yield reliable results. This expectation only holds under the assumption that quantum fluctuations do not scale up faster than linear with the canonical dimension, which seems a reasonable restriction but needs to be verified explicitly. In the case of gravity this has been tested explicitly for several higher order, irrelevant terms, as we will see in Chpt. 2.1.2. As mentioned before, the critical exponents contain information on the *rate* with which the fixed point is approached along a certain direction such that in the absence of quantum fluctuations, we obtain classical scaling (if we would reintroduce $\hbar$ then f_i would obtain an $\hbar$ dependence such that $\lim_{\hbar\to 0} f_i \to 0$). The fixed point values themselves might then be scheme dependent, but if the rate with which they are approached would be as well then this would indicate that at some energy scale k along a given RG trajectory, a different "amount" of physics has been integrated out and hence, two distinct schemes would yield different effective descriptions. Furthermore, we may try to draw a lesson from statistical physics, where the critical exponents tell us how physical quantities scale as a second-order phase

transition is approached. In certain settings, this scaling can be measured, signalling that they must be universal quantities. Intuitively then, we expect universality to be encoded in the set of critical exponents.

In what follows we will employ the concepts and tools described above to gravity settings. Of particular interesting will be gravity-matter scenarios which will be treated in detail in Chpt. 2.1.4.

2.1.2 Pure-gravity models

Now that we have set up the tools necessary to search for scale invariance, we can ask if there is indeed evidence indicating that gravity is asymptotically safe. A first application of the FRG applied to gravity was explored in [160], where the running of the Newton coupling and the cosmological constant in Einstein-Hilbert gravity were considered

$$\begin{aligned}\Gamma_k = &-\frac{1}{16\pi G_N}\int d^4x\,\sqrt{g}(R-2\bar{\Lambda})\\ &+\frac{1}{32\pi G_N\,\alpha}\int d^4x\,\sqrt{\bar{g}}\bar{g}^{\mu\nu}\left(\bar{D}^\kappa h_{\mu\kappa}-\frac{1+\beta}{4}\bar{D}_\mu h\right)\left(\bar{D}^\lambda h_{\nu\lambda}-\frac{1+\beta}{4}\bar{D}_\nu h\right)\\ &-\sqrt{2}\int d^4x\,\sqrt{\bar{g}}\bar{c}_\mu\left(\bar{g}^{\mu\rho}\bar{D}^\kappa g_{\rho\nu}D_\kappa+\bar{g}^{\mu\rho}\bar{D}^\kappa g_{\kappa\nu}D_\rho-\frac{1+\beta}{2}\bar{D}^\mu D_\nu\right)c^\nu.\end{aligned} \tag{2.28}$$

Here the second line represents a gauge fixing with gauge parameters α, β and the third line the Faddeev-Popov operator. Furthermore, the metric is split in a background and fluctuation field

$$g_{\mu\nu}=\bar{g}_{\mu\nu}+h_{\mu\nu}, \tag{2.29}$$

where the background is chosen to be a spherical one (a d-sphere), such that it becomes more straightforward to project on the gravity couplings. The dimensionless couplings $G=G_Nk^2$ and $\Lambda=\bar{\Lambda}/k^2$ are found to be relevant directions [161, 162, 163] and hence, their IR values need to be fixed by experiment. In particular, the beta functions are found to be [118]

$$\begin{aligned}\beta_G &= 2G-\frac{11}{3\pi}G^2,\\ \beta_\Lambda &= -2\Lambda+\frac{G}{2\pi}+\frac{4}{3\pi}G\Lambda.\end{aligned} \tag{2.30}$$

Using canonical scaling as a guiding principle for enlarging theory space, the next operators to include are the canonically marginal, higher-order curvature terms R^2 and $R_{\mu\nu}R^{\mu\nu}$, which are found to provide a third relevant direction [164]. The inclusion of canonically irrelevant operators R^i, $i\geq 3$ does not generate new relevant directions, confirming the expectation that canonically irrelevant operators remain irrelevant [164, 165, 166, 167, 168, 169]. In particular, the inclusion of the Goroff-Sagnotti counter term which spoils perturbative quantum gravity, does not introduce any inconsistencies here [169]. For calculations respecting background independence by calculating the fluctuation field propagator see [170, 171, 172, 173] and for the bi-metric truncation [174, 175, 176, 177]. The observation that the number of relevant directions appears to remain finite is encouraging, since only these need to be fixed by performing a measurement and thus the predictivity of a theory is encoded by the finiteness of the set of relevant directions.

2.1.3 Matter-gravity models

Ultimately, we set out to find a description of nature consistent with observation. The structure of spacetime itself is only one feature of such a model and a crucial next step involves the inclusion of matter degrees of freedom. In particular, both gravity and matter degrees of freedom have to be present on experimentally accessible scales and need to be consistent with observation. Under the assumption that no new degrees of freedom present themselves at scales between the Standard Model and Planck scale, we may assume that below the Planck scale, where gravity becomes weak, Standard Model interactions attain their usual (perturbative) running as they flow down to the IR. In such a setting, one can potentially connect quantum-gravity to Standard Model physics through the flow of matter couplings. For this to work, the couplings need to have a "slow" running below the Planck scale, as otherwise the microscopic imprints of quantum-gravity will be washed out at low energies. Marginal and perturbatively relevant couplings are then particularly good candidates for this mechanism to work.

Here we give a brief summary of the extensive literature exploring the impact of asymptotically-safe quantum-gravity on matter. In the next section, Chpt. 2.1.4, we will focus specifically on a coupling between the Abelian hypercharge and asymptotically-safe quantum gravity and study its implications in detail.

For all marginal couplings, g_M, of the Standard Model, it was found that the gravitational contribution to the beta functions are linear in the marginal couplings, i.e.,

$$\beta_M \sim \#_g g^3 - \#_G G\, g, \tag{2.31}$$

where a large set of FRG studies indicate that $\#_G \geq 0$ [178, 1, 179, 180, 181, 182, 183, 184, 185, 186, 77, 187, 188, 78, 189, 79, 190]. For non-Abelian gauge theories, such as QCD, the pure-matter contribution to the beta function generates asymptotic freedom at high energies, i.e., $\#_g < 0$. We see then that the sign of the gravity contribution is in the same direction and hence, quantum-gravity fluctuations are compatible with asymptotic freedom in the UV.

In the case of Abelian couplings, the sign $\#_g > 0$. This case was illustrated in Eq. (1.4), where the positive sign of the beta function was exactly the type of structure that led to a breakdown of the theory at high energies. The gravity contribution to the beta function of Abelian functions will then work in the opposite direction of the matter contribution in Eq. (2.31), indicating that a balancing between matter and quantum fluctuations could give rise to an interacting fixed-point, if quantum fluctuations are large enough to compensate the positive sign of $\#_g$ [180, 181, 1]. An important question is how large the quantum fluctuations need to be for an interacting fixed-point to exist, i.e., how non-perturbative is gravity in this scenario. We will discuss this setting in detail Chpt. 2.1.4.

Additionally, an important question is how matter impacts the gravitational sector. In particular, whether the presence of matter degrees of freedom could potentially lead to a vanishing of the interacting fixed point. The minimal coupling of Standard Model matter to asymptotically-safe quantum-gravity contributes at order G^2 to the beta functions Eq. (2.30), in the absence of self-interactions of the matter fields, see for example [191]. In this setting, the gravitational beta

functions, β_G and β_Λ, are supplemented by matter terms of the form

$$\begin{aligned}\beta_G &= 2G + \frac{G^2}{6\pi}\left(2N_D + N_S - 4N_V\right) - \frac{G^2}{6\pi}\left(14 + \frac{6}{1-2\Lambda} + \frac{9}{(1-2\Lambda)^2}\right),\\ \beta_\Lambda &= -2\Lambda + \frac{G}{4\pi}\left(N_S - 4N_D + 2N_V\right) + \frac{G\Lambda}{6\pi}\left(2N_D + N_S - 4N_V\right)\\ &\quad - \frac{3}{2\pi}G - \frac{7}{3\pi}G\Lambda - \frac{3G}{4\pi(1-2\Lambda)^2} + \frac{7G}{4\pi(1-2\Lambda)},\end{aligned} \tag{2.32}$$

where N_S, N_D, N_V indicate the number of scalars, Dirac fermions and vector (gauge) bosons and the gravitational contribution was taken to be Einstein-Hilbert. Furthermore, we used the perturbative approximation, where contributions of the anomalous dimensions can be ignored. Of particular importance are the pre-factors multiplying N_S, N_D, N_V, since they contribute to β_G as $\sim \#_i N_i\, G^2$ and have the potential to destroy the existence of an interacting fixed-point in the gravity sector when too many matter fields are present. Extensive studies indicate that the signs agree with those in Eq. (2.32), i.e., the scalars and fermions generate a screening contribution $\#_S > 0$ [191, 192, 193, 194, 195, 196, 197, 198], and $\#_D > 0$ [191, 193, 198] while the contributions of the gauge bosons to G is anti-screening $\#_V < 0$ [191, 121, 197, 196, 199]. When the number of matter fields is increased only slightly beyond the number of fields present in the Standard Model, the fixed point persists. The fate of the theory is currently undecided for a significant increase in the matter fields, as an extension of the truncation seems to be necessary for a consistent treatment [193, 198].

Encouraged by the qualitative study performed here, we will analyse the running of the Abelian hypercharge coupling, in the presence of asymptotically-safe quantum-gravity, and search for possible UV-completions of the Abelian coupling.

2.1.4 Abelian hypercharge revisited

With the tools developed throughout the previous sections, we now come back to the triviality problem haunting Abelian gauge theories. In particular, we will study scalar QED and the running of the Abelian gauge coupling to connect with the only Abelian coupling present in the Standard Model: the hypercharge coupling. We saw that in a perturbative setting, the only scenario in which the Landau pole vanishes renders the theory trivial, see Chpt. 1.2, [57]. Non-perturbative approaches to the triviality problem confirm these results [66, 67, 70, 71, 52], suggesting that the Landau-pole is not an artefact of technical limitations but rather hints towards a break-down of the theory at high energies. Since scalar QED performs remarkably well below the Planck scale [52, 50, 53, 54, 55], a possible way out is that the Standard Model as we observe it today appears as the low energy limit of some theory of quantum gravity. In this section we investigate the possibility of gravity becoming asymptotically safe beyond the Planck scale and ask how this might affect the triviality problem, following the work of [180, 181]. In particular, we study whether quantum gravity fluctuations can counter the positive sign of the matter contributions to the beta function (along the lines of Eq. (2.6)) and, hence, remove the Landau-pole. In this setting there are two possible resolutions to the Landau pole problem one can explore. The first one drives the Abelian

gauge coupling towards zero (asymptotic freedom) whereas the second one induces a fixed point for the coupling with a finite, non-zero, value (asymptotic safety). If, in addition to reaching an asymptotically safe fixed point, the coupling becomes IR attractive (irrelevant), then its IR value becomes a prediction of the theory and, hence, we have achieved the scenario detailed in Chpt. 2.1 and reduced the number of free parameters of the theory. Let us emphasise that no "new physics" in the sense of new degrees of freedom is conjectured and hence, a reduction in free parameters is not just a replacement of one set of degrees of freedom by another (presently unobserved) set but truly a reduction in the total number of experimental observations one needs to perform to fix the model. This is arguably one of the most important strengths of the model.

Here we will focus on scalar QED, following closely the work in [1]. The matter sector of the theory consists of an Abelian gauge field and a complex scalar while the gravity contributions come from an Einstein-Hilbert term

$$\begin{aligned}\Gamma_k = &-\frac{1}{16\pi\, G_N}\int d^4x\,\sqrt{g}(R-2\bar{\Lambda})\\ &+\frac{1}{32\pi\alpha\, G_N}\int d^4x\,\sqrt{\bar{g}}\bar{g}^{\mu\nu}\left(\bar{D}^\sigma h_{\sigma\mu}-\frac{1+\beta}{4}\bar{D}_\mu h\right)\cdot\left(\bar{D}^\lambda h_{\lambda\mu}-\frac{1+\beta}{4}\bar{D}_\mu h\right)\\ &+\frac{Z_A}{4}\int d^4x\,\sqrt{g}g^{\mu\nu}g^{\sigma\lambda}F_{\mu\sigma}F_{\nu\lambda}+\frac{1}{\xi}\int d^4x\,\sqrt{\bar{g}}(\bar{g}^{\mu\nu}\bar{D}_\mu A_\nu)^2\\ &+Z_\phi\int d^4x\,\sqrt{g}g^{\mu\nu}\left(\partial_\mu+i\bar{\rho}A_\mu\right)\phi^\dagger\left(\partial_\nu-i\bar{\rho}A_\nu\right)\phi.\end{aligned} \tag{2.33}$$

The coupling between the matter and gravitational sector is a minimal one, induced by the fluctuations of the metric volume factor $\sqrt{g}$, metric contractions of the $U(1)$ kinetic term $\sqrt{g}g^{\mu\nu}g^{\sigma\lambda}$ and the scalar kinetic term $\sqrt{g}g^{\mu\nu}$. Here the metric is split in a background and fluctuation field $g_{\mu\nu}=\bar{g}_{\mu\nu}+h_{\mu\nu}$. Since the fluctuations $h_{\mu\nu}$ are not restricted to be small we can set $\bar{g}_{\mu\nu}=\delta_{\mu\nu}$ without loss of generality. In addition, we will see that this choice of background allows for a simple extraction of the running coupling ρ from the gauge kinetic term. The covariant derivative $\bar{D}_\mu$ represents the covariant derivative in terms of the background metric $\bar{g}_{\mu\nu}$ (since we chose a flat background, the covariant derivative reduces to the usual partial derivative). The first and second line hold the gravitational contributions: An Einstein-Hilbert and gauge fixing term with α, β the gauge-fixing parameters. On the third line are the kinetic and gauge fixing terms of the Abelian gauge field A_μ, with ξ the gauge parameter. Finally, the last line is the kinetic term of the complex scalar field ϕ with $\bar{\rho}$ the Abelian gauge coupling.

From here on we will adopt the dimensionless notation where $G=G_Nk^2$, $\Lambda=\bar{\Lambda}k^{-2}$ and work under the restriction that only $\bar{\rho}$ is allowed to run, such that the induced Faddeev-Popov ghost contributions to the gauge-fixing terms can be ignored. If we had let the gravitational couplings run, then the $U(1)$ gauge-fixing term would have influenced the running of the background couplings of the gravity sector [191, 184]. The action as it is right now contains kinetic terms for A_μ and ϕ but the kinetic term for the fluctuation field $h_{\mu\nu}$ has not been explicitly written down. It can be obtained by expanding the Einstein-Hilbert term (first line) to second order in h and rescale the fluctuations by a factor $\sqrt{16\pi G_N}$ such that $h_{\mu\nu}$ has canonical mass dimension 1 and we include a renormalisation Z_h for the metric field.

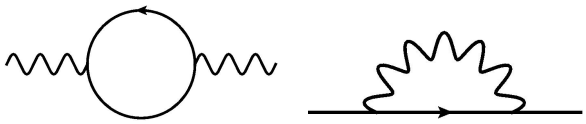

Figure 2.4: Left: Diagram contributing to the flow of the anomalous dimension η_A. Right: Diagram contributing to the flow of η_ϕ. The wavy lines denote the Abelian gauge field and the solid lines are the scalar fields.

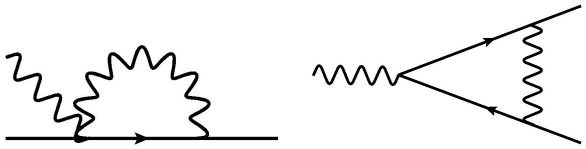

Figure 2.5: The pure-matter contribution to the running of the three-point vertex is generated by two diagrams. The $\partial_t R_k$ is inserted on each internal line in turn, to render the total contribution UV finite. The total contribution is then a sum over such regulator-inserted diagrams.

In principle the coupling ρ can be extracted from three different terms. The four-vertex $\bar{\rho}^2\phi\phi^\dagger A^2$, the three-vertex $\bar{\rho}(\partial\phi)\phi^\dagger A$ (or $\bar{\rho}(\partial\phi^\dagger)\phi A$) and lastly we could choose to rescale the gauge field $A_\mu \to \frac{A_\mu}{\rho}$ such that the coupling appears in the propagator of the $U(1)$ coupling [181] . We should be able to determine the running of ρ from either of these terms on grounds of gauge invariance, but since we explicitly break gauge invariance through a regulator term, it is not obvious that this will indeed be the case. For this reason, we distinguish explicitly between ρ_3 and ρ_4^2, the running of the three -and four-vertex, normalised such that

$$\rho_3 = \frac{\bar{\rho}_3}{Z_\phi\sqrt{Z_A}}, \quad \rho_4^2 = \frac{\bar{\rho}_4^2}{Z_\phi Z_A}. \tag{2.34}$$

From the anomalous scaling above we immediately find the following contributions to the beta functions

$$\begin{aligned}
\beta_{\rho_3} &= \partial_t\rho_3 = \frac{\bar{\rho}_3}{Z_\phi\sqrt{Z_A}}\cdot\left(-\frac{1}{Z_\phi}\partial_t Z_\phi - \frac{1}{2Z_A}\partial_t Z_A\right) + \frac{(\partial_t\bar{\rho}_3)}{Z_\phi\sqrt{Z_A}} \approx \rho_3\left(\eta_\phi + \frac{1}{2}\eta_A\right), \\
\beta_{\rho_4} &= \partial_t\rho_4 = \frac{\bar{\rho}_4}{\sqrt{Z_\phi}\sqrt{Z_A}}\cdot\left(-\frac{1}{2Z_\phi}\partial_t Z_\phi - \frac{1}{2Z_A}\partial_t Z_A\right) + \frac{(\partial_t\bar{\rho}_4)}{\sqrt{Z_\phi}\sqrt{Z_A}} \approx \rho_4\left(\frac{1}{2}\eta_\phi + \frac{1}{2}\eta_A\right),
\end{aligned} \tag{2.35}$$

where we introduced the anomalous dimensions

$$\eta_\phi \equiv -\partial_t \ln Z_\phi, \quad \eta_A \equiv -\partial_t \ln Z_A, \tag{2.36}$$

which encode the departure from (classical) canonical scaling of the fields themselves. Note that the far right-side of Eq. (2.35) neglects contributions generated by the three-point and four-point vertices (the terms that go as $\partial_t\bar{\rho}_3$ and $\partial_t\bar{\rho}_4$).

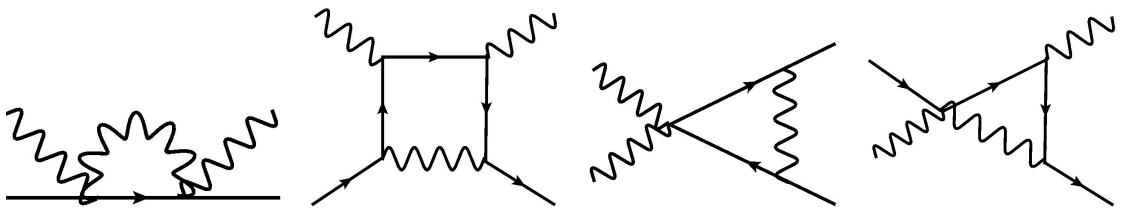

Figure 2.6: We show the four diagrams that contribute to the running of the four-point vertex.

We may then use the flow equation Eq. (2.23) to study the flow of ρ_3 and ρ_4 and choose a regulator of the form Eq. (2.24), i.e.,

$$R_k(p^2) = Z\,k^2\left(1-\frac{p^2}{k^2}\right)\theta\left(1-\frac{p^2}{k^2}\right). \tag{2.37}$$

The derivative of the regulator $\partial_t R_k$ regulates the UV modes, and should therefore be inserted on the internal lines of contributing diagrams. For example, the contribution from the diagram on the left in Fig. 2.5 is a sum over the two versions one obtains when inserting the regulator on either one of the two internal lines. In general then, for a diagram with n_i internal lines, one has n_i versions of the diagram that need to be summed over to obtain the full contribution. The expansion of Γ_k in terms of vertices with a certain number of external legs (here three or four), receives contributions at all orders in the momenta, q_μ, of those legs. Then, for ρ_3, we want to project on the vertex $\sim A_\mu\phi\phi^\dagger$

$$\partial_t = -\left(\frac{2}{3q^2}q_1^\nu P_{\nu\sigma}(q_1-q_2)\cdot\frac{\delta^3}{\delta A_\sigma(q_1-q_2)\delta\phi^\dagger(q_2)\delta\phi(q_1)}\partial_t\gamma_k\right)\Big|_{q=0,A=\phi^\dagger=\phi=0}, \tag{2.38}$$

where the transverse projector $P_{\mu\nu}(q)$ can be found in App. A Eq. (A.2) and projects the photon on its transverse, physical component. We then multiply through with the external and the configuration of the external momenta q^μ in Eq. (A.3) and Eq. (A.3) for the three -and four vertex respectively.

At one-loop perturbation theory the gauge dependence of the matter sector does not vanish unless the anomalous dimensions above are taken into account, cf. Fig. 2.4. In addition to η_A and η_ϕ, the flow of ρ_3 and ρ_4 receive contributions from two and four matter diagrams respectively, cf. Fig. 2.5 and Fig. 2.6, yielding

$$\begin{aligned}
\beta_{\rho_3} &= \rho_3\left(\eta_\phi+\frac{\eta_A}{2}\right)+\frac{3+\xi}{96\pi^2}\left((6-\eta_A)+(6-\eta_\phi)\right)\rho_3-\frac{\xi}{96\pi^2}\left((8-\eta_A)+(16-2\eta_\phi)\right)\rho_3^3,\\
\beta_{\rho_4} &= \rho_4\left(\frac{\eta_A}{2}+\frac{\eta_\phi}{2}\right)+\frac{3+\xi}{192\pi^2}\rho_4^3\left((6-\eta_A)+(6-\eta_\phi)\right)\\
&\quad+\xi\left(-\frac{8-\eta_A+16-2\eta_\phi}{192\pi^2}\cdot\frac{3\rho_3^2\rho_4}{2}+\frac{10-\eta_A+30-3\eta_\phi}{640\pi^2}\frac{\rho_3^4}{\rho_4}\right).
\end{aligned} \tag{2.39}$$

The expression above appears gauge dependent at first glance. However, ξ drops out upon identifying $\rho_3=\rho_4=\rho$ and calculating perturbative one-loop forms for the anomalous dimensions.

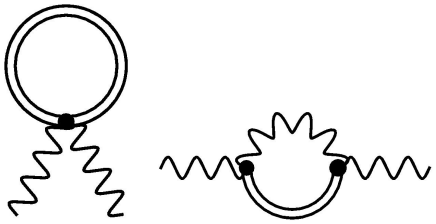

Figure 2.7: Gravity contributions to the anomalous dimension η_A. Here double lines denote metric fluctuations and wavy lines gauge bosons.

Specifically, the anomalous dimensions are of the form

$$\begin{aligned}\eta_\phi &= -\frac{3(12+\eta_\phi+\eta_A)-\xi(12+2\eta_\phi-\eta_A)}{96\pi^2}\rho_3^2,\\ \eta_A &= \frac{1}{24\pi^2}\rho_3^2.\end{aligned} \tag{2.40}$$

One can solve these equations for η_ϕ and η_A, which for the scalar anomalous dimension will result in an expression $\eta_\phi \sim \#_1\rho_3^2 + \#_2\rho_3^4$. The second term goes as ρ_3^4 and will contribute to the beta function at order ρ_3^5 in the coupling, indicating that it will be suppressed when ρ_3 is small. In the perturbative approximation we neglect these contributions and rather than treating Eq. (2.39) as a system of equations, we set all factors η_ϕ and η_A on the right-hand side to zero

$$\begin{aligned}\eta_\phi \mid_{pert} &= -\frac{3-\xi}{8\pi^2}\rho^2,\\ \eta_A \mid_{pert} &= \frac{1}{24\pi^2}\rho^2.\end{aligned} \tag{2.41}$$

In this approximation, we find for the beta functions

$$\beta_{\rho_3} = \beta_{\rho_4} = \frac{\eta_A}{2}\rho = \frac{1}{48\pi^2}\rho^3, \tag{2.42}$$

which is exactly the result we get from reading off the running from the kinetic term of the gauge field (i.e., from $\rho^2 = \bar{\rho}^2/Z_A$). This confirms that universality of 1-loop perturbation theory holds between different schemes.

Solving the equation above for ρ we indeed recover

$$\rho^2(k) = \frac{\rho_0^2}{1-\frac{\rho_0^2}{24\pi^2}\ln\frac{k}{k_0}}, \tag{2.43}$$

which is of the same form as Eq. (1.5) and renders (scalar) QED UV-incomplete.

So far we have confirmed the perturbative result using FRG techniques, but not included any gravitational contributions. As an approximation we can take the perturbative matter result

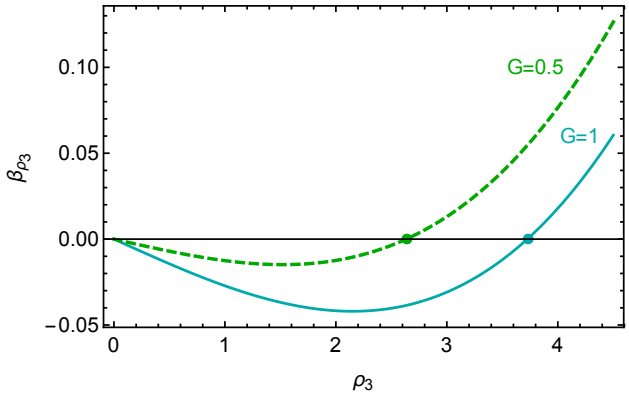

Figure 2.8: We show the beta function for ρ_3 in the TT approximation. The coupling ρ_3 constitutes a relevant direction at the free fixed point and an irrelevant direction at the interacting fixed point. We see that lowering the gravitational contribution shifts the interacting fixed point towards the free fixed point. In the limit where the gravitational fluctuations are switched off, the two fixed points will be merged and we lose asymptotic safety.

Eq. (2.42) and add gravitational modifications induced by the transverse-traceless metric mode $h^{TT}_{\mu\nu}$, satisfying $\bar{D}^\nu h^{TT}_{\mu\nu} = 0$ and $h^{\mu\ TT}_{\mu} = 0$. In general, the graviton can be split into four modes: $(h^{TT}_{\mu\nu}, \xi_\mu, s, w)$, where ξ_μ is traceless, s is transverse and a fourth mode, w is neither. The TT-mode is a rank-2 tensor and corresponds to the spin-2 part of the graviton. Since it is gauge independent, it is often taken as the dominant degree of freedom and used as a first approximation to the full graviton. The projector employed to select the TT-mode can be found in Eq. (A.1) App. A

As a consequence of the transverse-traceless approximation, we only find gravity contributions to the anomalous dimensions η_A, cf. Fig 2.7, which may be understood as consequence of the gauge-independence of η_A. The beta function then becomes

$$\beta^{TT}_\rho = \frac{\eta_A}{2}\rho = \frac{1}{48\pi^2}\rho^3 - G\,\rho\,\frac{5}{36\pi}\left(\frac{8}{1-2\Lambda} + \frac{8-\eta_h}{(1-2\Lambda)^2}\right). \tag{2.44}$$

Here $G > 0$, $\Lambda < 1/2$ and $\eta_h < 16(1-\Lambda)$ yielding an asymptotically free fixed point ($\rho = 0$) and an asymptotically safe one for

$$\rho_* = \sqrt{\frac{20\pi}{3}G}\,\frac{\sqrt{16(1-\Lambda)-\eta_h}}{1-2\Lambda}. \tag{2.45}$$

If we rewrite the equation above as

$$\beta^{TT}_\rho = \frac{1}{48\pi^2}\rho(\rho^2 - \rho_*^2), \tag{2.46}$$

and solve for $\rho(k)$ as in the pure matter case, we obtain

$$\rho^2(k) = \frac{\rho_*^2}{1 + \left(\frac{k}{k_0}\right)^{\frac{\rho_*^2}{24\pi^2}}\left(\frac{\rho_*^2}{\rho_0^2} - 1\right)}, \tag{2.47}$$

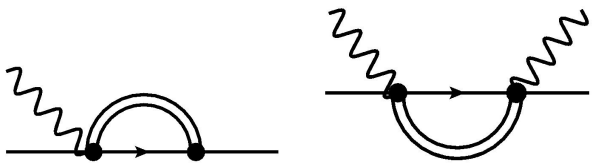

Figure 2.9: Left: The only diagram containing metric fluctuations that contributes to β_{ρ_3}. Right: The only diagram containing metric fluctuations that contributes to β_{ρ_4}.

where we defined $\rho_0 \equiv \rho(k_0)$. Indeed, we find that for $k_0 \to \infty$ the coupling is driven to its fixed point value. Moreover, if we start out from ρ_*^2, keep k_0 fixed at a finite value, while lowering k, the positive power of $\left(\frac{k}{k_0}\right)^{\rho_*^2/24\pi^2}$ ensures that ρ^2 stays close to ρ_*^2, i.e., the coupling ρ is irrelevant at the interacting fixed point, cf. Fig. 2.8. Note that a negative power would have rendered ρ relevant since in that case lowering k would drive the coupling away from its fixed point value and, hence, one would require a measurement to uniquely fix the value of ρ in the IR. Alternatively, one could argue that since the free fixed-point is UV attractive (IR repulsive), the interacting fixed-point is necessarily UV repulsive (IR attractive). This is simply a consequence of the fact that for the flow to cross zero twice, it needs to go through a local maximum or minimum and hence, the derivative with respect to the coupling along the flow approaches the zeros with opposite sign. Since the critical exponent is read off at the zeros of the beta function, it needs to flip sign when switching between the fixed-points. Note that this only holds as long as the flow is continuous, i.e., there is no pole separating the two fixed-points from each other.

Turning on the full gravity contribution induces a dependence of the flow on the gravity as well as the matter gauge parameters. The full beta functions are then given by

$$\begin{aligned}
\beta_{\rho_3} &= -\frac{34+3\eta_A+3\eta_\phi+\xi(12-4\eta_\phi)}{96\pi^2}\,\rho_3^3 + (3+\xi)\,\frac{12-\eta_\phi-\eta_A}{96\pi^2}\,\rho_3\,\rho_4^2 \\
&\quad + \frac{G}{96\pi\,(1-2\Lambda)}\left[2A\,(8-\eta_\phi)+B\,(8-\eta_A)+\frac{2A\,(8-\eta_h)+B\,(4-\eta_h)}{1-2\Lambda}\right]\rho_3, \\
\beta_{\rho_4} &= (3+\xi)\,\frac{12-\eta_\phi-\eta_A}{192\pi^2}\,\rho_4^3 - \frac{1}{192\pi^2}(\xi\,(24-\frac{\eta_A}{2}-5\eta_\phi)+32+3\eta_A+3\eta_\phi)\,\rho_3^2\,\rho_4 \\
&\quad + \xi\,\frac{40-\eta_A-3\eta_\phi}{640\pi^2}\,\frac{\rho_3^4}{\rho_4} \\
&\quad + \frac{G}{96\pi(1-2\Lambda)}\left[A\,(8-\eta_\phi)+B\,(8-\eta_A)+\frac{A\,(8-\eta_h)+B\,(4-\eta_h)}{1-2\Lambda}\right]\rho_4,
\end{aligned}$$

where A and B depend on the cosmological constant Λ and the graviton gauge parameters α, β, see Eq. (A.3), App. A. The diagrams containing contributions from metric fluctuations are shown in Fig. 2.9

We saw before that in the pure-matter setting the gauge independence translated directly into $\beta_{\rho_3} = \beta_{\rho_4} = (\eta_A/2)\rho$, i.e., we could read off the running of the gauge coupling in three different ways. Demanding that the same holds for the full gravity setting uniquely selects the gauge $\alpha =$

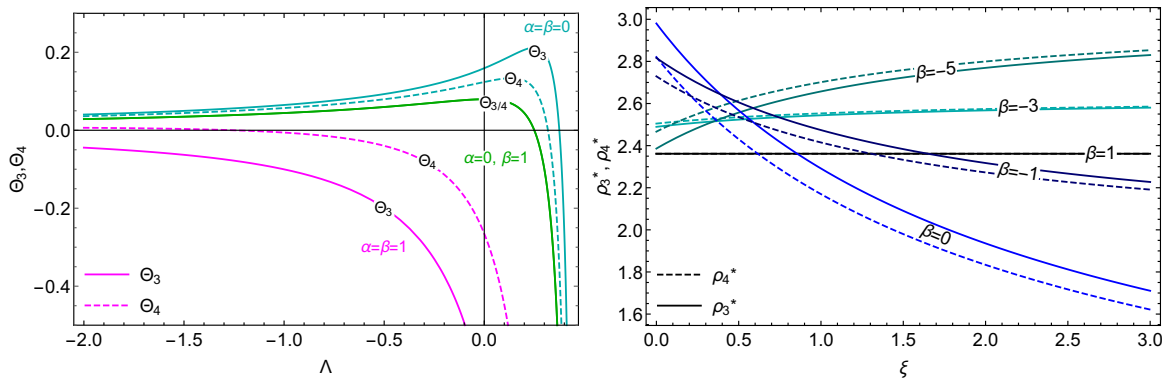

Figure 2.10: Left: We show the dependence of the critical exponents at the free fixed-point, read off from the 3 -vertex (solid lines) and 4-vertex (dashed lines) as a function of Λ. We set $G = 1$ and choose $\xi = 0$ for all gauges except $\alpha = 0$, $\beta = 1$ where the ξ dependence drops out. Right: The fixed point-values ρ_3^* (solid line) and ρ_4^* (dashed line) as a function of the Abelian gauge parameter ξ. We show different lines of constant β and find that the lines ρ_3^* and ρ_4^* in general do not overlap except when $\beta = 1$, where the fixed-point value agree and become independent of ξ. In all cases we set $G = 1$, $\Lambda = 0$, $\alpha = 0$.

0, $\beta = 1$ while the dependence on ξ drops out altogether. Note that in the Einstein-Hilbert truncation it can be shown that according to the principle of minimal sensitivity, this specific choice of gauge approaches an extremum of the critical exponents in [200], providing further indications that this choice of gauge might be preferred. Before studying the system in this particular gauge, we will analyse how the gauge dependence influences certain properties of the system, and how this motivates the particular gauge used here. In particular, we can study the critical exponents

$$\theta_{3,4} \equiv -\frac{\partial\, \beta_{\rho 3,4}}{\partial\, \rho_{3,4}}\Big|_{\rho_{3,4}=\rho^*_{3,4}}, \tag{2.48}$$

at the free fixed point, $\rho_3^* = \rho_4^* = 0$, as a function of Λ, see the left panel of Fig. 2.10. As expected, the critical exponents in all gauge choices diverge as we approach the pole located at $\Lambda = 1/2$ and approach zero for Λ negative and large. Since all gravity contributions come with factors of $1/(1-2\Lambda)^n$ with $n = 1, 2$ this is exactly the regime where gravity becomes suppressed, until finally, in the limit $\Lambda \to -\infty$, the gravity contribution, and with it the asymptotically free fixed-point, disappears. For those gauge choices corresponding to $\alpha = 0$, the critical exponents remain positive in the full range of allowed values for Λ, whereas $\alpha = \beta = 1$ leads to a negative value for θ_3 (loss of asymptotic freedom) and a positive value of θ_4 at sufficiently large and negative Λ. Although the lines for θ_3 and θ_4 get closer and closer the further away one moves from the pole, the lines never lie on top of each other with the exception of $\alpha = 0$, $\beta = 1$. In addition to the gravity gauge parameters, we study the dependence of the interacting fixed-point values ρ_3^* and ρ_4^* on the matter gauge parameter ξ, see the right panel of Fig. 2.10. Here as well, the gauge $\alpha = 0$, $\beta = 1$ is the unique gauge for which the lines coincide. Moreover, for all other gauge choices there is a clear ξ dependence present in the fixed-point values.

For the remainder of this section we will then select the gauge $\alpha = 0$, $\beta = 1$. For this particular

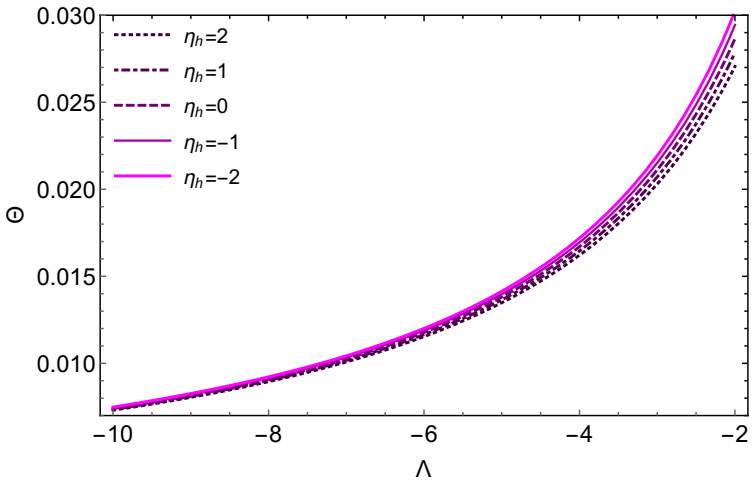

Figure 2.11: The value of the critical exponent for negative values of Λ only shows minor deviations for different choices of $\eta_h = -2, -1, 0, 1, 2$.

choice, the parameters A and B in Eq. (2.48) simplify to $A = 0$, $B = 6$ such that the full beta function becomes

$$\beta_\rho = \frac{1}{48\pi^2}\rho^3 - G\,\rho\,\frac{4(1-4\Lambda)+\eta_h}{16\pi^2(1-2\Lambda)^2}, \tag{2.49}$$

which is of a similar form as Eq. (2.44). Similarly to the TT setting, we find both a Gaussian and an interacting fixed point with ρ being relevant at the former and irrelevant for the latter. We can confirm this by explicitly calculating the critical exponents

$$\theta_{\rho_*} \equiv -\frac{\partial\beta_\rho}{\partial_\rho}\,|_{\rho=\rho_*} = -G\,\frac{4(1-4\Lambda)+\eta_h}{8\pi^2(1-2\Lambda)^2}, \tag{2.50}$$

and we necessarily find $\theta_0 = -\theta_{\rho_*}/2$ at the free fixed point[6]. As mentioned above, when the flow of a coupling is continuous and has two zeros then one of them must be approached from above and the other from below and hence, one always ends up with an attractor-repulser combination.

To obtain a rough indication of the stability of our result under extensions of the truncation, we can study the sensitivity of the critical exponent to changes in η_h. In particular, we find that for $\Lambda \ll 0$, lines of constant η_h only cause a modest difference in θ, see Fig. 2.11. It appears then that extensions of the truncation which alter the anomalous dimensions, η_h, do not change the qualitative analyses performed above.

In terms of Standard Model physics, we would like to implement the procedure above to the $U(1)$ hypercharge coupling. Note that in this case there will be two additional vertices from which we could read of the Abelian gauge coupling; a photon-fermion-antifermion vertex and a photon-photon-fermion-antifermion vertex. Since these terms will not generate additional diagrams

[6]Note that this is simply a consequence of the form of the beta function since $\frac{\partial\beta_\rho}{\partial\rho} = \frac{\partial}{\partial\rho}\#\rho(\rho^2-\rho_*^2) = \#(3\rho^2-\rho_*^2)$ and hence, evaluating at the free fixed point $\theta_0 = -\#\rho_*^2$ and at the interacting fixed point $\theta_{\rho_*} = 2\#\rho_*^2$.

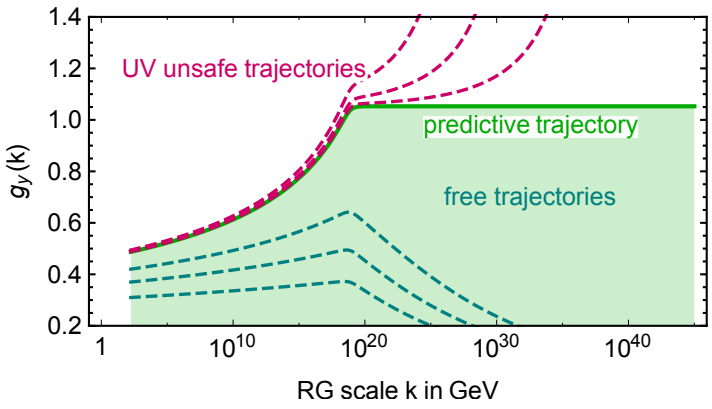

Figure 2.12: The running g_Y coupling is irrelevant at the interacting fixed point, leading to an upper bound on the IR values of the hypercharge coupling within our scenario.

contributing to ρ_3 and ρ_4 above, we can apply the analyses above to the hypercharge coupling. We then find a balancing of the beta-function between the 1-loop perturbative result and quantum fluctuations

$$\beta_{g_Y} = \frac{1}{16\pi^2}\frac{41}{6}g_Y^3 - f_g g_Y, \tag{2.51}$$

where the pre-factor of the pure matter contribution ($\sim g_Y^3$) now includes fermionic contributions. The factor f_g summarises the quantum-gravity contributions and would correspond to the second term on the right-hand side of Eq. (2.44). The interacting fixed point in terms of f_g is then simply

$$g_Y^* = 4\pi\sqrt{\frac{6}{41}\,f_g}, \tag{2.52}$$

inducing an irrelevant direction in the coupling g_Y at the fixed point. Since irrelevant directions yield predictions, we can integrate down to the IR along the renormalisation group trajectory to obtain a prediction for the value of the $U(1)$ coupling. Moreover, since "switching off" gravity will result in a Landau pole in g_Y, we can place an upper bound on the IR value of the g_Y for which a UV completion exists, Fig. 2.12. Specifically, starting out from the UV hypersurface around the Gaussian fixed point, the flow towards the IR yields a range of low-energy values which can be reached whereas the interacting fixed point selects just one IR value and restricts the set of IR values reachable from the free fixed-point from above. Turning the argument around, there is a range of IR values which can be followed towards the UV Gaussian fixed point and result in a non-interacting theory, whereas only one unique trajectory, starting from $g_{Y\,IR}^c$, will end in the UV interacting fixed point. Starting out from an IR value above this critical value will result in a trajectory which "overshoots" the UV-fixed point and drives the coupling into the Landau pole.

To identify g_Y with the coupling ρ above, we assume that the gauge dependence of the full system (i.e., including fermionic interactions) is such that the gauge $\alpha = 0$, $\beta = 1$ remain preferred.

Then f_g is simply the second term on the right-hand side of Eq. (2.49) with η_h set to zero, yielding

$$\beta_{g_Y} = \frac{1}{16\pi^2}\frac{41}{6}g_Y^3 - \frac{1-4\Lambda}{4\pi(1-2\Lambda)^2}Gg_Y. \tag{2.53}$$

The value of the interacting fixed point then clearly depends on the exact values of G, Λ at their interacting fixed-point. Since different values of G^* and Λ^* alters the range of allowed IR values for g_Y, the scenario described here sets first steps into the direction of testing quantum gravity in the IR through matter degrees of freedom. This bridging of scales between UV and IR physics is a huge advantage of the Renormalisation Group and illustrates how it could be a powerful tool in the search for a theory of quantum gravity.

Since the $\Lambda \ll 0$ regime we are currently considering corresponds to weakly-coupled gravity, any effects induced by quantum gravity on the running of g_Y are suppressed. For example, taking into account induced photon self-interactions through an F^4 type of term, as was done in [181], only yields contributions that are sub-leading with respect to the main gravity contribution. In addition, since the coupling between the matter and gravitational sector is a minimal one, interactions between matter and gauge fields will only appear in the anomalous dimensions of the included matter fields. The matter and gauge anomalous dimensions only contribute at higher-order and, hence, the beta functions for G and Λ are taken to only receive contributions from minimally coupled matter. The back-reaction of g_Y onto the flow of gravitational sector is then assumed to be negligible and we use [191] to parametrise the dependence of the flow of G and Λ on matter degrees of freedom, i.e., β_G and β_Λ are given by Eq. (2.32). Plugging in the number of Standard Model fields, $N_S = 4$, $N_D = 45/2$, $N_V = 12$ and searching for simultaneous zeros in β_G, β_Λ, β_{g_Y} yields the fixed-point values

$$G^* = 2.73,\ \Lambda^* = -3.76,\ g_Y^* = 1.05. \tag{2.54}$$

Using these values as a set of initial conditions at the Planck scale, we use the beta function for g_Y, Eq. (2.53), to flow down (with the dimensionful coupling) to lower energies and read off the IR value of g_Y at the electroweak scale

$$g_{Y\,IR}^c = 0.487. \tag{2.55}$$

The value above is a *prediction* of the interacting fixed-point found in the current setup and compared to the measured, experimental value of $g_{Y\,IR}^{exp} = 0.358$ we are off by about 35%. In [191], a systematic error up to 60% in the fixed-point values of Λ and G, induced by the choice or regulator, was estimated. Our results then fall within the bounds of this error, indicating that the fixed point studied here is viable. In addition, it is not unlikely that an extension of the truncation will reduce the error. The simplest extensions would involve additional terms within the pure-gravity or/and the pure-matter sector. The next gravitational terms would be R^2 and $R^{\mu\nu}R_{\mu\nu}$ whereas the additional matter-only contributions would be of the form $(F)^4$, or alternatively, a second Abelian field B_μ playing the role of a "dark photon" may be introduced. In particular, one could allow for non-minimal couplings between the gravitational and matter sector by including terms that explicitly couple the Ricci tensor to the matter sector, i.e., terms of the form $\sim \sigma R^{\mu\nu}g^{\kappa\omega}F_{\mu\kappa}F_{\nu\omega}$. Similar couplings were performed involving interactions between $R^{\mu\nu}$ and scalar-field derivatives [201] and fermion derivatives [202]. In both cases it was found that the contribution of σ to the

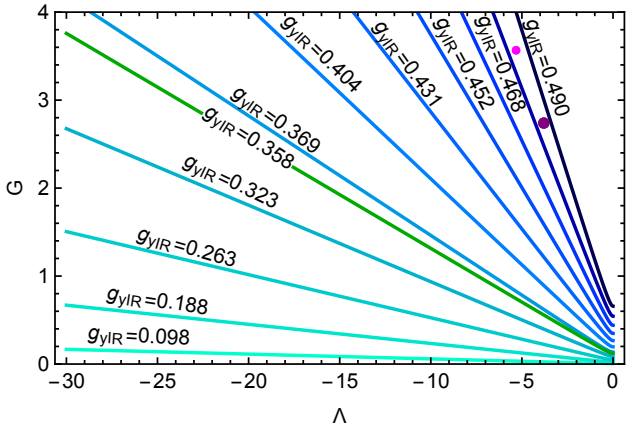

Figure 2.13: For fixed infrared values of the hypercharge coupling g_Y, we find that the gravitational couplings G and Λ trace out different lines of compatible values. The green line represents the experimental value $g_{Y\,IR}^{exp} = 0.358$, whereas the purple and smaller magenta dots are the predictions given by the fixed point values of G, Λ and g_Y for Standard Model content without and with three Weyl fermions necessary for the production of neutrino masses.

flow is sub-leading and it would be interesting to see if this prevails in the Abelian hypercharge setting studied here.

Furthermore, if we "only" demand a UV-complete theory, then the free fixed-point is viable as well and since $g_{Y\,IR}^{c}$ provides an upper bound on the IR values reachable from this free fixed-point, the experimental value $g_{Y\,IR}^{exp} < g_{Y\,IR}^{c}$ is compatible with the analyses provided. Note that the trajectories starting from the free and interacting fixed point cannot cross on their way to the IR since this would require a flip in the sign of the critical exponents. The exact value of the fixed points are in general scheme dependent but the critical exponents should be universal quantities. Of course the critical exponents will be scheme dependent as long as we work within a truncation but if this dependence does not flip the sign of quantum fluctuations, one would expect that qualitatively the situation remains the same. To explicitly test this, an extension of the truncation should be implemented to search for convergence in the fixed point values and critical exponents.

In summary, we have studied a possible solution to the triviality problem of the Abelian gauge sector of the Standard Model by including gravitational degrees of freedom. In particular, we studied a combined model of scalar QED weakly-coupled to asymptotically safe Einstein-Hilbert gravity and found two possible solutions to the triviality problem. The first solution renders the hypercharge coupling, g_Y, asymptotically free and allows for a range of IR values of g_Y, including the experimentally observed value. In addition, there is scenario where g_Y reaches perturbative asymptotic safety in the UV, resulting in an interacting theory which is not only UV-complete but provides a prediction of the IR value of g_Y. As illustrated in Fig. 2.12, the asymptotically safe trajectory places an upper-bound on the allowed range of IR values. For IR values up till the upper-bound $g_{Y\,IR}^{c}$, the hypercharge coupling will not run into the Landau pole at high energies, rendering the theory UV-complete. The prediction for $g_{Y\,IR}$ lies within the estimated systematic

error bounds, suggesting that, if under extensions of the truncation, g_Y remains asymptotically safe, the Abelian gauge sector of the Standard Model is not only UV-complete, but the free parameter previously associated with the IR value of g_Y can be fixed without the necessity of performing a measurement. We see then that indeed, the anti-screening contribution of asymptotically safe gravity coupled to matter can lead to a sign flip in the corresponding matter beta-functions and hence, enhance predictivity in gravity-matter models.

It is interesting that the perturbative fixed-point regime of G and Λ for which all three couplings reach the interacting fixed point is the same as the regime where asymptotically safe gravity yields a fixed point in the Higgs quartic and top Yukawa coupling which predicts masses close to the experimental value [178]. The near-perturbative nature of the fixed point studied here carries over to other settings For further discussion on the near-perturbative nature of asymptotically safe gravity see [121]. Furthermore, the findings of the work above have been used to extract a prediction for the fine-structure constant in the context of GUT theories [203].

2.2 Asymptotic safety on the lattice

In the previous section we have discussed the asymptotic-safety scenario in detail and, recognising the non-perturbative nature of gravity, explicit calculations were performed using the functional renormalisation group. Next to the FRG, lattice techniques have proven to be another powerful non-perturbative tool and have led to high-precision predictions in, for instance, QCD, see [204, 15] for reviews. In lattice formulations the lattice itself introduces a short distance (UV) cut-off through the lattice spacing, a and thus functions as a regulator. Since the lattice only functions as a regularisation (i.e., the lattice itself is not physical), continuum physics is recovered in the limit that the cut-off is removed, $a \to 0$. In general such a limit leads to diverging quantities, similar to divergences in QFT that present themselves in the $1/a \to \infty$ limit. To obtain finite physical quantities, one searches for trajectories along which the physics (i.e., a set of observables) remains constant and follows these quantities in the direction of decreasing a. A fixed point on the lattice then corresponds to a point in theory space where the lattice spacing, a, drops out of the expressions for physical quantities such that one can safely send $a \to 0$. Typically, the system exhibits this behaviour in the vicinity of second-order phase transitions, where correlation lengths diverge and hence, signal sensitivity to interactions across the lattice. We can interpret this as the onset of a scale-invariant regime, since physical quantities become independent of the scale a. Note that in principle such a critical point can be of higher-order, as long as the phase transition is continuous such that correlation lengths diverge (first-order phase transitions generically do not come with diverging correlation lengths). Since the type of long-range behaviour associated with diverging correlation lengths washes out the microscopic dependencies of macroscopic physics, a diverging correlation length is also desirable from a universality perspective.

In most lattice formulations the lattice itself is treated as a static space (-time) background the physics of interest "lives" *on*. However, since quantum gravity is a theory *of* spacetime, the lattice itself needs to be dynamical and represents the degrees of freedom of the theory. It is exactly the discrete nature of the lattice which ensures a finite number of degrees of freedom, in contrast to the continuum. This procedure is similar to the renormalisation group methods discussed before, where at finite values of k one is assured to only include a finite number of degrees of freedom. In the limit $k \to \infty$ one includes fluctuations of arbitrarily high momenta and hence, an infinite number of degrees of freedom. One of the proposals for such a lattice formulation,[7]of gravity is *Dynamical Triangulations* (DT) [206, 207] see [208] for an extensive review and [209] for an early review of lattice approaches to quantum gravity. The theory is founded on a Euclidean formulation of the path integral and its regularisation scheme inspired by Regge calculus [210]. More details on Regge calculus will be given in Chpt. 2.2.1, but it is based on the idea that a d-dimensional manifold can be constructed out of d-dimensional building blocks. The simplest building blocks one can obtain are simplices, the d-dimensional generalisations of triangles, and the resulting manifold is a simplicial or triangulated manifold[8]. Since two triangulations of the same manifold can differ in connectivity, the dynamics of the theory is exactly encoded by summing over all such triangulations, where different triangulations receive different "weights". This sum over different triangulations is

[7] For earlier proposals of lattice quantum gravity see for instance [205].

[8] If $d \leq 3$ then a simplicial manifold is automatically piecewise linear, but for higher dimensions this is not automatically satisfied [211, 212].

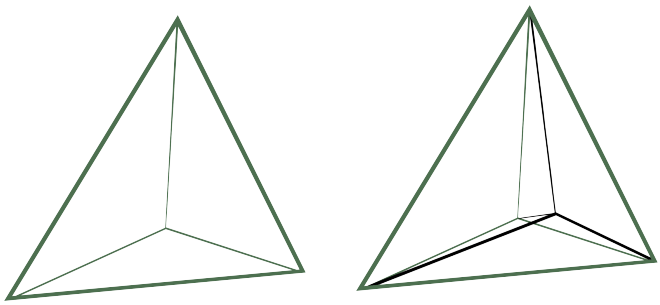

Figure 2.14: Illustration of the 3 and 4-dimensional building blocks.

then the discrete analogue of the integration over different metrics in the continuum path-integral. The Regge calculus framework proposed to perform the (Euclidean) path integral as a sum over all piecewise linear manifolds, equipped with fixed triangulations but variable edge lengths. Instead of varying the length of the edges, the dynamics of the DT approach lies in the sum over all possible triangulations of a manifold while keeping the edge length fixed [213, 214, 215, 216].

One of the major successes of DT is the fact that in two dimensions one can actually take the continuum limit and show its equivalence to two-dimensional Euclidean quantum gravity, in the form of Liouville gravity, as we will briefly discuss in Chpt. 2.2.3. It is not clear whether Regge calculus shares this feature and consequently, whether DT and Regge calculus are equivalent.

2.2.1 Regge calculus

Inspired by the need for a coordinate-free description of GR, Regge developed a framework which successfully reproduces the (classical) Einstein-Hilbert action without introducing a coordinate frame, but rather through a triangulation of spacetime [210, 217, 218] see [219] for a review and for recent developments in numerical relativity [220, 221, 222, 223]. Since Regge calculus was originally developed for the purposes of classical gravity, we will adapt the classical concepts to the quantum regime.

To be precise, we search for a coordinate-independent discretisation of the "Euclideanised" version of Eq. (1.14)

$$Z_E = \int \mathcal{D}[g_E]\, e^{-S_E[g_E]}, \tag{2.56}$$

where we now integrate over the space of Euclidean metrics, and weigh each configuration with a Euclidean action. Assuming the Einstein-Hilbert action provides a microscopic description of spacetime, we find two terms which need to be accounted for: A volume term $\int_{\mathcal{M}} d^d x \sqrt{|g|}$ and the curvature term $\int_{\mathcal{M}} d^d x \sqrt{|g|}\, R$, with $\mathcal{M}$ the manifold under consideration. Defining s_d to be a

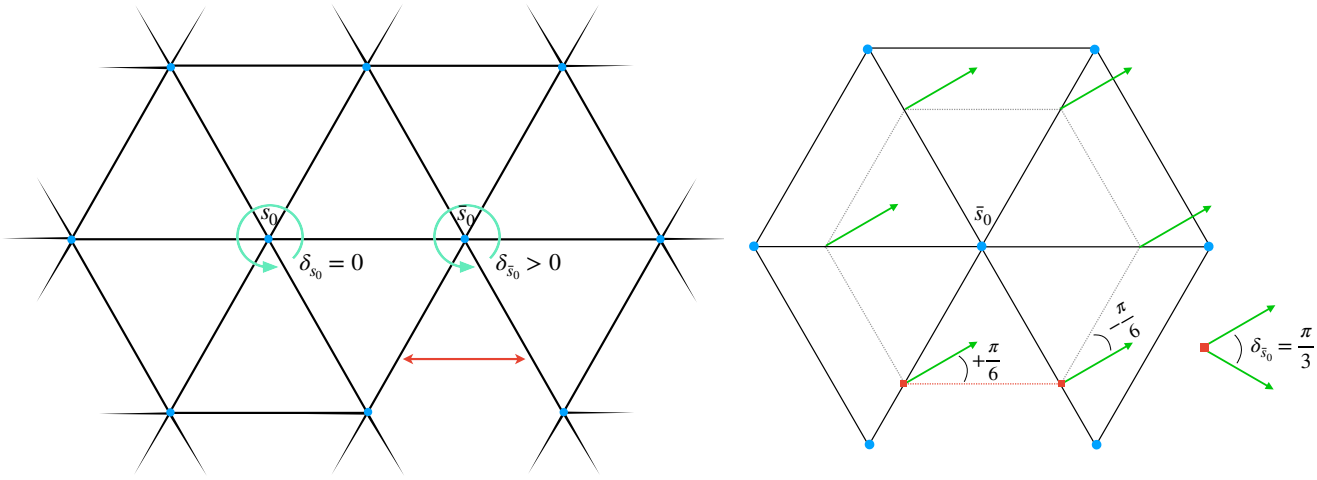

Figure 2.15: Illustration of the deficit angle in a two-dimensional triangulation. Left: The vertex s_0 is shared by six equilateral triangles and hence, the deficit angle vanishes. The deficit angle of $\bar{s}_0$ is larger than zero since this vertex is only shared by five triangles. gluing the edges indicated by the red arrow, will "bend" the 2-dimensional surface into a triangulated cone. Right: Parallel transporting a vector (green arrow) along a path enclosing $\bar{s}_0$ (dotted grey lines) results in a deficit angle upon identification of the edges, i.e., the red squares are glued on top of each other. There is a notion of extrinsic (i.e., embedding dependent) curvature on the edges.

d-dimensional simplex, the volume term is straightforwardly discretised as

$$\int_{\mathcal{M}} d^d x \sqrt{|g|} \to \sum_{s_d} V_{s_d}. \tag{2.57}$$

The discretised curvature term [210, 224], is intuitively simplest to understand in two dimensions. Heuristically R measures a "departure" from flat spacetime. In two dimensions, a simplicial manifold may be constructed by gluing triangles along their edges in such a way that the topology of the manifold is preserved, i.e., the gluing rules are topology preserving (see Chpt. 2.2.7 for more details). Since all triangles are by definition equilateral, each internal angle of such a triangle is $\pi/3$. A triangulation of flat spacetime then corresponds to a gluing of triangles such that the *deficit angle* θ_{s_0} around each hinge (vertex) is exactly 2π. In other words, each vertex needs to belong to six distinct triangles, c.f., Fig. 2.15.

This can be easily generalised to higher dimensions. Since the d-dimensional simplices s_d are flat by construction and no (intrinsic) curvature is introduced on the $(d-1)$-dimensional faces [9] (the edges in Fig. 2.15)

$$\delta_{s_{d-2}} = 2\pi - \sum_{s_d} \theta_{s_d}(s_{d-2}), \tag{2.58}$$

[9] Curvature centred on the faces would require more than two faces to be glued together. Such a gluing would induce a change in topology, which will not allowed for reasons motivated in Chpt. 2.2.2.

where the curvature resides on the $(d-2)$-dimensional simplex [10].

The discretised Einstein-Hilbert-action can then be written as

$$S_R = \frac{1}{8\pi G_N}\left[\sum_{s_{d-2}} V_{s_{d-2}}\,\delta_{s_{d-2}} - \bar{\Lambda}\sum_{s_d} V_{s_d}\right], \tag{2.59}$$

and has been dubbed the Regge action.

To account for the quantum dynamics of the theory, we will have to specify what happens to the measure term in Eq. (2.56). As a result of the classical purpose for which Regge calculus was originally developed, the general formalism tries to mimic the continuum as close as possible. The dynamics is then encoded in the variation of edge lengths, l_e, and a standard choice for the measure is

$$\mathcal{D}[g] \to \prod_e \frac{dl_e^2}{l_e^\beta}, \tag{2.60}$$

where the product is over all edges e. However, it is not clear whether this measure captures the dynamics correctly.

There are two prominent worries raised towards Regge calculus. The first one is that fixing the connectivity while varying the edge length does not necessarily guarantee that the entire space of metrics is explored [206]. Although this cannot be proven, there has been no success in any dimension in finding a continuous phase-transition where one might take a continuum limit in pure-gravity [225, 226, 227]. Additionally, one might expect an over-counting of equivalent lattices without some type of gauge-fixing term and associated Faddeev-Popov determinant, but in two dimensions this introduces non-local terms, complicating any form of analysis [228].

As a result of the aforementioned concerns, a departure from Regge calculus in favour of dynamical triangulations occurred. This model as well, has been abandoned and replaced with modified versions, cf. Chpt. 2.2.4 and Chpt. 2.2.5.

2.2.2 Dynamical triangulations

Switching to the dynamical triangulations (DT) framework [213, 214, 215, 216, 206, 207] has the advantage that, since the edge length is held fixed, now the volume of each d-simplex is a fixed quantity. In addition, the sum over the curvature term (first term in the brackets of Eq. (2.59)) can be performed exactly, yielding a simplified form of the Regge action

$$S_R = \kappa_d\, N_d - \kappa_{d-2}\, N_{d-2}. \tag{2.61}$$

[10] Intuitively this can be understood as a remnant of the formulation of the Riemann tensor in terms of the non-commutativity of the second covariant derivative. Specifically, to parallel transport a vector around a loop requires two tangent vectors. Then, in two-dimensions, the infinitesimal loop will enclose a point (0-dimensional object), whereas in three dimensions an additional direction is available and thus, a loop will enclose a line (1-dimensional object).

Here N_d and N_{d-2} represent the total number of d -and $(d-2)$-dimensional simplices respectively and the dimensionless couplings κ_d and κ_{d-2} are defined in terms of the bare cosmological and gravitational constant $\bar{\Lambda}$ and G_N as

$$\begin{aligned} \kappa_d &= \bar{\Lambda}\, V_{s_d} + \frac{d}{2}(d+1)\,\frac{\arccos 1/d}{16\pi G_N}\, V_{s_{d-2}}, \\ \kappa_{d-2} &= \frac{V_{s_{d-2}}}{8\pi G_N}. \end{aligned} \tag{2.62}$$

Note that for any action involving only the total number of sub-simplices N_i, the action Eq. (2.61) is of the most general form for a four dimensional manifold without boundaries [206] [11].

Following [229], Chpt. 1.2., the quantisation of DT utilises the *Euclidean* path integral formalism where, in its discrete form the partition function can be written as a sum over triangulated manifolds rather than an integral over geometries

$$Z_E(\kappa_d,\, \kappa_{d-2}) = \sum_{\mathcal{T}} \frac{1}{A(\mathcal{T})}\, e^{-S_R}. \tag{2.63}$$

If a manifold has additional symmetries, this can render two triangulations to be equivalent. To correct for possible over-counting, we divide by the number of equivalent triangulations, $A(\mathcal{T})$. The sum over different triangulations can be interpreted as a sum over different manifolds, in the same spirit as the summation over gauge orbits in gauge theories. The idea is then that the sum over triangulations corresponds to summing over equivalence classes of metrics and as we take the continuum limit, the dependence on different parameterisations should drop out. Despite the coordinate-independent formulation of DT, the introduction of a background structure involving a fixed lattice spacing makes it unclear whether or not the diffeomorphism invariance is broken explicitly at fixed a, and one of the challenges of the program is to ensure its recovery in the continuum.

Furthermore, if we choose to fix N_d, i.e., the total volume of the universe is held fixed, then

$$\begin{aligned} Z_E(\kappa_d,\, \kappa_{d-2}) &= \sum_{N_d} e^{-\kappa_d\, N_d}\, Z(\kappa_{d-2}, N_d), \\ \text{with } Z(\kappa_{d-2}, N_d) &\equiv \sum_{\mathcal{T}_{N_d}} \frac{1}{A(\mathcal{T})}\, e^{\kappa_{d-2}\, N_{d-2}}, \end{aligned} \tag{2.64}$$

where $\mathcal{T}_{N_d}$ are now simplicial manifolds of fixed volume. It is clear that the quantity $Z(\kappa_{d-2}, N_d)$ will not introduce any divergences since there are only finitely many values of N_{d-2} for a fixed total volume. However, if $Z(\kappa_{d-2}, N_d)$ has a faster than exponential growth, then the sum with respect to N_d will be divergent without further restrictions. In two dimensions it can be proven [230] that fixing the topology to that of a 2-sphere assures convergence of Eq. (2.64) and the expectation is

[11] Basically the dependence on all sub-simplices of uneven dimensionality s_1, s_3, ..., s_{d-1}, for d even, can be removed through linear relations that hold between faces of the i-dimensional sub-simplices. The Euler characteristic $\chi\,(d) = \sum_{i=0}^{d} (-1)^i\, N_i$ can then be used to remove the dependence on N_0.

that this should generalise to three and four dimensions [231, 232]. Note that $Z_E(\kappa_d, \kappa_{d-2})$ and $Z(\kappa_{d-2}, N_d)$ can be thought of as the grand canonical and canonical partition function, respectively.

At this point let us take a step back and remember that the triangulations are merely a tool, to be ultimately removed in the form of a continuum limit. It seems reasonable that continuum physics will present itself for large volumes. Assuming the large-volume limit of $Z(\kappa_{d-2}, N_d)$ takes the form [12]

$$Z(\kappa_{d-2}, N_d) \sim N_d^{\gamma-3} e^{\kappa_d^c N_d} (1 + \mathcal{O}(1/N_d)), \tag{2.65}$$

with $\gamma = \gamma(\kappa_2)$ the susceptibility exponent[13]and $\kappa_d^c = \kappa_d^c(\kappa_{d-2})$ is the (suggestively named) critical line. Plugging this expression back into Eq. (2.64), we see that for a fixed number of building blocks N_d, the partition function grows as $Z_E \sim \exp N_d(\kappa_d^c - \kappa_d)$ and, hence, as long as $\kappa_d > \kappa_d^c$ the partition function will converge.

The line $\kappa_d^c(\kappa_{d_2})$ separates the system in two phases. In one of those phases $\kappa_d < \kappa_d^c$, the partition function diverges and it is not clear how to assign a physical meaning to such an ill-defined partition function. In contrast, for $\kappa_d > \kappa_d^c$, the partition function converges and we may extract physical quantities of the system as we tune κ_d to its critical value.

For this purpose we approach the critical line from above, and find that to leading order the partition function behaves as

$$Z_E(\kappa_{d-2}, \kappa_d \to \kappa_d^c) \sim (\kappa_d - \kappa_d^c)^{2-\gamma}. \tag{2.66}$$

Now that we have an expression for the behaviour of Z_E close to the critical line, we can start analysing the physical properties of the system. One particularly interesting property is the *physical* volume of the lattice, $\langle V \rangle = a^d \langle N_d \rangle$, which is conjugate to the (renormalised) cosmological constant $\langle V \rangle \sim \Lambda^{-1}$.

We can extract the lattice volume close to the critical line as

$$\langle N_d \rangle = -\frac{\partial \ln Z(\kappa_{d-2},\, \kappa_d \to \kappa_d^c)}{\partial \kappa_d} \sim \frac{\gamma - 2}{\kappa_d - \kappa_d^c}, \tag{2.67}$$

and see that it diverges on the critical line $\kappa_d \to \kappa_d^c$. Demanding that the physical volume of the system is finite as we approach the critical line, will force the lattice spacing, a, to zero as to counter the infinity in the coupling κ_d.

Evaluating the physical volume close to the phase transition, we readily obtain

$$\langle V \rangle \sim a^d \frac{\gamma - 2}{\kappa_d - \kappa_d^c} = \frac{1}{\Lambda}. \tag{2.68}$$

For the physical volume to become independent of the lattice spacing, we necessarily need

$$\kappa_d \sim \kappa_d^c(\kappa_{d-2}) + a^d \Lambda, \tag{2.69}$$

[12] It can be shown that this is indeed the case when $d = 2$, see for instance [233].

[13] The susceptibility associated with fluctuations of the volume is defined as $\chi_V(\kappa_{d-2}, \kappa_d) = -\frac{d^2 \ln Z(\kappa_{d-2}, \kappa_d)}{d\, \kappa_d^2}$, which goes as $\chi_V(\kappa_{d-2}, \kappa_d) \sim \frac{1}{(\kappa_d - \kappa_d^c(\kappa_{d-2}))^{\gamma(\kappa_{d-2})}}$ close to the critical line under the assumption that $\gamma_{\kappa_{d-2}} < 2$ [234, 233].

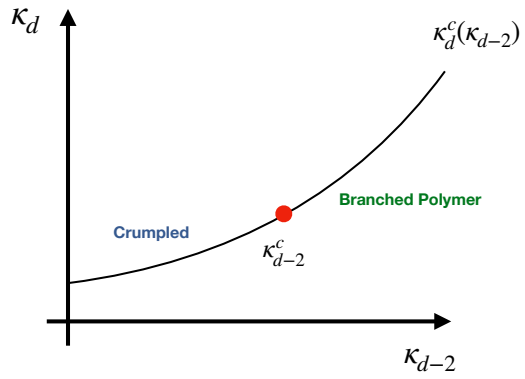

Figure 2.16: Phase diagram of 3 -and 4-dimensional dynamical triangulations [247].

and consequently, we can write the *renormalised* cosmological constant as

$$\Lambda \sim \frac{\kappa_d - \kappa_d^c(\kappa_{d-2})}{a^d}. \tag{2.70}$$

We see then that indeed, as we approach the critical line, $\kappa_d \to \kappa_d^c$, we may take the continuum limit, $a \to 0$, to obtain a constant physical volume.

Fine-tuning the coupling κ_d alone turns out to be enough to obtain a well-defined continuum limit in two dimensions [235, 236, 237, 238], see Chpt. 2.2.3. Furthermore, in the special case of $d = 2$, one can map the triangulations to the dual lattice and describe the model in terms of $N \times N$ matrix models [239]. Here it is possible to take the continuum limit by means of a double-scaling limit [240], where in addition to tuning to the phase transition, one takes the $N \to \infty$ limit. In this case it is the topological fluctuations which render physical quantities finite as the double scaling limit is taken, and thus a sum over topologies needs to be included in the path-integral.

For $d > 2$, however, the situation changes since κ_{d-2} might have to be tuned to some critical value, yielding a critical point rather than a critical line in the (κ_{d-2}, κ_d) plane. Whether a continuum limit exists in these dimensions has been investigated for a manifold with boundary [241] and without[206, 242, 243, 244, 245, 246]. A conclusive answer remains to be found but the general consensus is that the original DT model has two phases, separated by a first-order phase transition, cf. 2.16. In 4-dimensions, one finds a crumpled (collapsed) phase for $\kappa_2 < \kappa_2^c$ and an elongated (branched polymer) one for $\kappa_2 > \kappa_2^c$ in the infinite volume limit.

2.2.3 Two dimensions

As shown in previous sections, a naive dimensional analysis of the Newton coupling, $[G] = 2 - d$ in d-dimensions, leads to the conclusion that gravity is perturbatively non-renormalisable for $d > 2$. However, in two dimensions the Einstein-Hilbert action is a topological invariant, i.e., the topology of spacetime alone is enough to fully specify Einstein-Hilbert gravity. This can most easily be seen when counting the degrees of freedom of the Riemann curvature tensor.

In d-dimensions $R_{\alpha\beta\gamma\sigma}$ has $\frac{d^2}{12}(d^2-1)$ degrees of freedom. Setting $d=2$, we find that $R_{\alpha\beta\gamma\sigma}$ has just one degree of freedom, which necessarily has to correspond to its trace R. Preserving the symmetries and index structure of the Riemann tensor, it is immediately clear that

$$R_{\alpha\beta\gamma\sigma} = \frac{R}{2}(g_{\alpha\gamma}g_{\beta\sigma} - g_{\beta\gamma}g_{\alpha\sigma}), \tag{2.71}$$

in two dimensions. And hence, the Einstein tensor

$$\begin{aligned} G_{\mu\nu} &\equiv R_{\mu\nu} - \frac{1}{2}g_{\mu\nu}\,R \\ &= \frac{R}{2}\left(g^{\alpha\gamma}\left(g_{\alpha\gamma}g_{\mu\nu} - g_{\mu\gamma}g_{\alpha\nu}\right) - g_{\mu\nu}\right) \\ &= 0, \end{aligned} \tag{2.72}$$

vanishes identically and independently of the geometry under consideration.

A somewhat different route to the same result comes from the realisation that $\int d^2x\sqrt{g}\,R$ is a total derivative (in the absence of boundary terms) and corresponds in two dimensions to the Euler characteristic of the manifold, $\chi = 2-2g$, with g the number of handles, determined from topology alone. This implies that as soon as the topology has been fixed, there is no freedom left in G, leaving $\kappa_2 \sim \Lambda$ as the only tuneable parameter of the model.

Since the continuum limit can be taken in 2-dimensional DT, a central question is what this continuum limit corresponds to, i.e., what are the physical properties. As it turns out, the observed system exhibits behaviour which does not seem to resemble the observable universe. Specifically, the occurrence of so called "baby universes" [234, 248], results in a Hausdorff dimension $d_H = 4$ [14]. A baby universe, in two dimensions, is generated when a sub-triangulation splits off from the main simplicial manifold, in such a way that its boundary is given by a loop of three edges on the main triangulation. The issue is that these constructions receive a dominating contribution in the path-integral and consequently the continuum limit is a 2-dimensional manifold with at each point a 2-dimensional sub-manifold (baby universe) attached to it, resulting in an effective dimension $d_H = 4$. Such a manifold does not resemble the observable universe and is therefore regarded as unphysical.

In the continuum, two dimensional Euclidean quantum gravity coupled to conformal, bosonic matter, can be written as [249, 239]

$$Z = \int \mathcal{D}[g]\mathcal{D}_g[X]e^{-S_M(X,g)-S^{(2)}_{EH}}, \tag{2.73}$$

where the two-dimensional Einstein-Hilbert action can be expressed in terms of the bare cosmological constant alone

$$S^{(2)}_{EH} = \frac{\bar{\Lambda}}{2\pi}\int d^2x\sqrt{g}, \tag{2.74}$$

[14] The Hausdorff dimension is defined through the (leading-order) scaling of the volume of a ball with its radius i.e., $V_B(r) \propto r^{d_H}$ defines the Hausdorff dimension d_H. See Chpt. 3.3.4

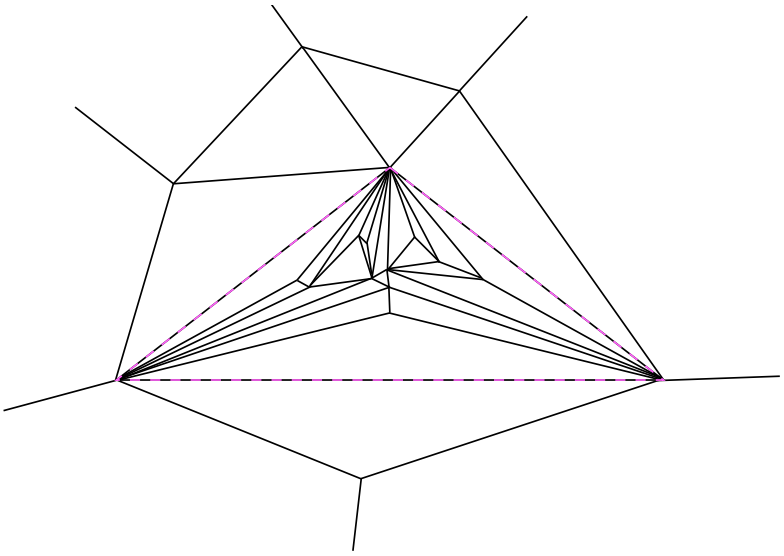

Figure 2.17: Illustration of a baby universe, glued to the main triangulation along the dashed magenta-black triangle. The fractal-like structure results in an effective dimension $d_H = 4$.

and the matter action of a bosonic field X is given by the Polyakov action [250]

$$S_M(X, g) = \frac{1}{8\pi} \int d^2x \sqrt{g} g^{\mu\nu} \partial_\mu X \partial_\nu X. \tag{2.75}$$

The matter action itself is invariant under conformal rescaling of the metric $g_{\mu\nu} = e^{\phi} \bar{g}_{\mu\nu}$, but the measure term, $\mathcal{D}_g[X]$, is not and gives rise to an additional term

$$S_L(\phi, \bar{g}_{\mu\nu}) = \frac{1}{4} \int d^2x \sqrt{\bar{g}} \left(\bar{g}^{\mu\nu} \partial_\mu \phi \partial_\nu \phi + 2\phi \bar{R} + 16\lambda\, e^{\phi} \right), \tag{2.76}$$

called the Liouville action with ϕ the conformal factor.

The key point is that from these models we can derive the critical exponent γ_{str} (string susceptibility) by studying the behaviour of Z for fixed, large areas A [239]

$$Z(A) \sim A^{(\gamma_{str}-2)\frac{\chi}{2}-1}. \tag{2.77}$$

Here the string susceptibility is

$$\gamma_{str} = \frac{1}{12}(c - 1 - \sqrt{(c-1)(c-25)}), \tag{2.78}$$

with c the central charge such that $c = 1$ corresponds to a free boson. Since we are currently interested in the pure-gravity case, we have $c = 0$ and, hence, $\gamma = \gamma_{str} = -\frac{1}{2}$. Comparing with Eq. (2.65), we see that for $\chi = 2$ (topological sphere), the string susceptibility coincides with

the susceptibility exponent $\gamma_{str} = \gamma$. In addition, the Hausdorff dimension can be extracted as a function of the central charge

$$d_H = 2\frac{\sqrt{25-c}+\sqrt{49-c}}{\sqrt{25-c}+\sqrt{1-c}}. \tag{2.79}$$

Plugging in $c = 0$ gives a Hausdorff dimension of $d_H = 4$, which agrees with the results found in DT and establishes an equivalence between two dimensional DT and Liouville quantum-gravity.

As we saw, the DT formulation described so far does not appear to yield a well-defined continuum limit for $d > 2$, let alone a continuum limit in which one recovers the observed universe. It seems then that a successful lattice description of quantum-gravity necessitates an alteration of the model described so far. Here we will discuss the two main proposals for alternatives to DT.

2.2.4 Causal Dynamical Triangulations

The first proposal for an "upgrade" was motivated by the realisation that the set of geometries one sums over might be inconsistent. In particular, it was proposed to restrict the summation to triangulations with an appropriate causal structure. The implementation of this restriction alters both the fundamental building blocks (simplices) as well as the gluing rules and goes under the name Causal Dynamical Triangulations (CDT) [251, 252, 253], for reviews see e.g., [254, 255, 256, 257]. In particular, the simplices are defined to have a Lorentzian signature, resulting in edges which are either time-like, $\ell_t^2 = -\alpha a^2$ with $\alpha > 0$ or space-like, $\ell_s^2 = a^2$, see Fig. 2.18. Gluing is then only allowed along edges of the same type and the same length. Additionally, spacetime is "sliced" at equal time intervals Δt, introducing a global time. For each triangle between the slices t_i and t_{i+1}, its space-like edge either belongs to the spatial boundary at t_i or t_{i+1} [15] and we have thus introduced a foliation on the triangulated manifold. Consequently, next to restricting the global topology, the sum over histories now involves only those particular geometries which allow a triangulation as described above and hence, possess a preferred proper-time direction. The idea is that the foliation does not correspond to a particular choice of gauge since the definition of proper time is independent of a choice of coordinates. We see then that, although conceptually different, it can be argued that CDT is a sub-class of DT, in the sense that the (simplicial) geometries thought to make up the quantum-gravity theory space are a very special sub-class of those included in DT.

In two dimensions it is possible to solve the model exactly and obtain a continuum limit for the Euclidean version of CDT, which can then be analytically continued to its Lorentzian analogue by rotating α to negative values. The resulting theory can be shown to share properties with 2-dimensional pure gravity in the proper time gauge [258], i.e., we associate the height of a cylinder with the time coordinate x^0, perpendicular to spatial coordinate x^1 which traces out a cycle, then the proper time gauge [259, 260] fixes $g_{00} = 1$, $g_{01} = g_{10} = 0$. Moreover, the theory turns out to be unitary [252]. It should be noted, however, that there is an ambiguity on how to perform the analytic continuation in $d = 2$. In two dimensions, it can be shown that rotating from Lorentzian

[15] Since one now has different types of edges, simplices with different orientations can be distinguished as different building blocks in the following way. In d-dimensions each building-block has a $(d-1-k)$ sub-simplex at time slice t and a k sub-simplex at time slice $t+1$, where $k = 0, \ldots, d-1$. Consequently, for $d = 4$ one now has four types of building blocks: $(3,0)$, $(2,1)$, $(1,2)$, $(0,3)$.

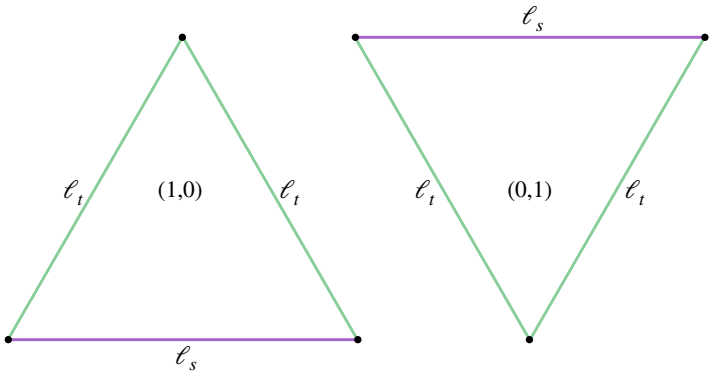

Figure 2.18: In $d = 1 + 1$ dimensions, the CDT model has two building blocks, which we label as type (a, b) with a and b the dimension of the sub-simplex glued to the t-slice and $(t + 1)$-slice, respectively. Here the triangle on the left is then of type $(1, 0)$ and the triangle on the right has type $(0, 1)$. Each triangle has one spacelike edge (purple) and two timelike edges (green).

to Euclidean metrics is equivalent to analytically continuing the cosmological constant Λ, since

$$\int dx\, dt \sqrt{|g|} \to i \int dx\, dt_E \sqrt{|g_E|}, \tag{2.80}$$

with g_E and and t_E the Euclidean metrics and time. One can then take the continuum limit in the Euclidean setting, but has two choices for the rotation back to a Lorentzian signature. Specifically, analytically continuing the two-loop propagator between two time slices by sending $T \to -iT$ does not seem to result in a unitary theory [251], whereas the continuation $\Lambda \to -i\Lambda$ does. This was resolved by the observation that the analytic continuation should be performed in terms of $a_t \to -ia_t$ and since the propagator contains terms proportional to $\sqrt{a_t a_s \Lambda}$, an analytical continuation in terms of Λ was concluded to be the correct choice. Already in [261, 262], it was argued that the analytical continuation through a square root type of term (here $\sqrt{\Lambda}$) should be handled with care and might requires the inclusion of Lorentzian, Euclidean and (when $d > 4$) mixed signature configurations [262]. However, this ambiguity in how to perform the Wick rotation is lifted for $d > 2$ and it can be shown that CDT satisfies reflection positivity in higher dimension [252] (the Euclidean version of unitarity). This suggests that CDT will provide a unitary theory in the continuum limit, after a Wick rotation has been performed.

In addition, calculations in $d = 2$ show that the CDT model does not have an anomalous fractal dimension [251], i.e., the average spatial volume $\langle N_s \rangle$, can be shown to scale as $1/\sqrt{\Lambda}$ rather than $1/\Lambda^{3/4}$, which was obtained from DT models.

In $d = 4$ dimensions, the CDT equivalent of the Regge action, Eq. (2.61), is found to be

$$S_{CDT} = -(\kappa_0 + 6\Delta)N_0 + \kappa_4(N_4^{(3,0)} + N_4^{(2,1)}) + \Delta(2N_4^{(3,0)} + N_4^{(2,1)}), \tag{2.81}$$

where κ_0, κ_4 and Δ depend on $\bar{\Lambda}$, G_N^{-1} and α. In particular, Δ measures the asymmetry between the spacelike and timelike edges such that setting $\Delta = 0$ yields $\alpha = 1$ and hence, $S_{CDT}|_{\Delta=0} = -\kappa_0 N_0 + \kappa_4 N_4$. Note that the Euler characteristic $\chi = \sum_{i=1}^{d}(-1)^i N_i$ allows us to express N_0 and N_2 in terms of each other and N_4 (all dependencies on sub-simplices of uneven dimensionality can be removed) and hence, we can re-express κ_0 in terms of κ_2.

2.2.4.1 Phase diagram of Causal Dynamical Triangulations

Extensive exploration of the phase structure of CDT quantum-gravity has uncovered a rich phase diagram [263, 264], cf. Fig: 2.19. The A-phase is characterised by a spatial volume which exhibits irregular fluctuations between different time slices and does not seem to resemble the physical universe. In the B-phase all 4-simplices are "squeezed" into a minimal number of time slices, such that the spatial volume of the universe is collapsed into a short time span. We see that this phase occurs when the asymmetry between space and time is small. The C-phase occurs for $\Delta > 0$, indicating that there is an asymmetry between time and space and can be split into two sub-phases. The bifurcation phase C_b and the de Sitter phase C_{dS}, which was only identified relatively recently. In C_b the spatial volume expands and contracts in sequences of two times steps, such that at t_i and t_{i+2} the spatial volume is minimal and reaches its maximum at t_{i+1}. This "bouncing"-type of behaviour repeats itself indefinitely. In the de Sitter phase, C_{dS}, the time evolution of the spatial volume exhibits a volume-profile similar to that of Euclidean de Sitter spacetime. The $B - C_b$ phase transition was found to be second order, whereas the $A - C_{dS}$ phase is first-order [265, 266, 267, 268]. The C_b phase is relatively new but evidence points in the direction of a second order phase transition at the line $C_b - C_{dS}$ [269].

Furthermore, the effective dimension of spacetime can be estimated by setting up a random walk on the triangulations and measuring the probability for a random walker to return to its starting point. The scaling of the return probability with the diffusion time then yields an estimation of the effective dimension of spacetime, called the *spectral dimension*, d_s (see Chpt. 3.3.5 for a detailed description of such a setup in Causal Set Theory). For the C_b phase such an effective dimension of spacetime was found to be large and possible infinite, i.e., $d_s \to \infty$. In the C_{dS} phase, however, the effective dimension is consistent with the topological dimension, hence, $d_s = 4$ [264, 270, 271].

In summary, the CDT formulation of quantum-gravity supplements the original DT model with a causality condition, equivalent to the introduction of a time foliation on the triangulated manifold. Motivated by the Lorentzian signature of spacetime, the hope is that this restriction of the configuration space to metrics consistent with the causality condition, will remove unphysical contributions to the path-integral. Explorations of the phase diagram of CDT show evidence of the existence of a Euclidean de Sitter type phase, which has an effective dimension consistent with 4 and appears to exhibit a second order phase transition between the C_{dS} and C_b phase. The existence of such a second order phase transition is crucial, since at the phase transition, correlation lengths diverge and one may take the continuum limit by sending the lattice spacing to zero. Further explorations will have to show whether or not the continuum limit indeed results in a description of the universe consistent with observations. In particular, the anisotropy between time and space suggest a connection between CDT and continuum Horava-Lifshitz theory [272, 273]. Ideas in this

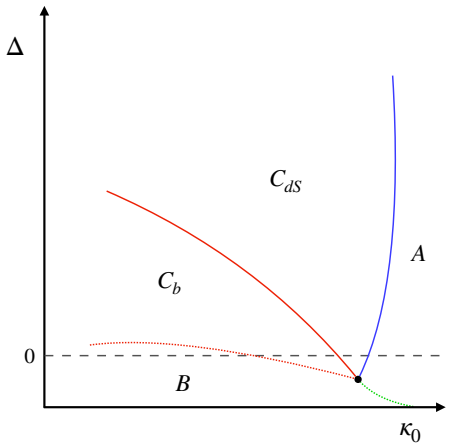

Figure 2.19: We show an illustration of the phase diagram of 4-dimensional CDT quantum-gravity.

direction have been investigated [265, 274], it was argued, however, that since CDT only sums over configurations consistent with the foliation, the diffeomorphism symmetry is not broken as it was not present to begin with [257]. In addition, it was shown in three dimensional CDT that even without imposing an external foliation, the desired causal structure of spacetime can be obtained through a specific set of local gluing rules and reproduces the de Sitter-like phase [275, 276].

Since CDT can be viewed as a particular subclass of DT, it is not unthinkable that the two lie in the same universality class, i.e., describe the same macroscopic physics in the continuum limit. If this is indeed the case, then one should be able to recover a similar de Sitter-like phase through a Euclidean description. It is clear that the original DT model does not exhibit such a phase but one might wonder if there is a modified Eulidean DT model which does. In the next section we will discuss exactly such a scenario.

2.2.5 Euclidean Dynamical Triangulations

An alternative proposal to save DT came from the realisation that the measure (i.e., the fine lattice spacing) might break diffeomorphism invariance and that one should perhaps use a form of fine-tuning mechanism to restore the broken symmetries. This led to the introduction of a non-trivial measure term [277, 278] and later [279]. The inclusion of such a term led to the discovery of a seemingly distinct region in the phase diagram which received the name "crinkled" region. Upon further study, the crinkled region turned out to be connected to the collapsed phase by a cross-over rather than a phase transition [280, 281]. More recent work, however, suggests that a proper fine-tuning leads to results that are in better agreement with continuum physics [282].

Specifically, for $d = 4$ we find for Eq. 2.61 that

$$\begin{aligned}\kappa_2 &= \frac{\sqrt{3}a^2}{16G_0},\\ \kappa_4 &= \frac{a^2}{16\pi G_0}\,5\sqrt{3}\arccos\left(\frac{1}{4}\right) + \frac{\sqrt{5}}{96}\frac{a^4\bar{\Lambda}}{8\pi G_N}.\end{aligned} \tag{2.82}$$

Including the measure term, the partition function Eq. 2.63 can be written as

$$Z_E(\Lambda,\kappa) = \sum_{\mathcal{T}} \frac{1}{C_{\mathcal{T}}} \left[\prod_{j=1}^{N_2} \mathcal{O}(t_j)^{\beta}\right] e^{-S_{ER}}, \tag{2.83}$$

where $\mathcal{O}(t_j)$ counts the number of four-simplices to which triangle j belongs (the *order* of triangle j) and introduces a non-uniform weight since the measure term explicitly assigns different weights to different triangulations based on the order of their triangles. The continuum analogue of the measure term would be $\prod_x \sqrt{g}^{\beta}$. Original work in DT excluded such a non-trivial measure term since in two dimensions the continuum limit exists and can be performed independently of the choice for β (except for large, negative values where one crosses from the Liouville phase into the collapsed/crumpled phase) [283]. In more recent work [279, 281, 282] it has been argued that since the setting $d = 2$ is special, one might expect that the successful recovery of continuum physics in higher dimensions (where gravity *is* dynamical) does require this inclusion. Consequently, we upgrade β to be a free parameter, which might have to be tuned to different values depending on the lattice spacing. Note that when $\beta = 0$ one recovers the original DT model.

To distinguish the program including the measure term from the original DT model and its causal counterpart, CDT, it has been dubbed Euclidean Dynamical Triangulations (EDT). Other than the inclusion of this measure term, the EDT model is equivalent to DT, i.e., the topology is held fixed, as is the edge length, and the gluing occurs along the $(d-1)$-dimensional simplices.

The addition of the measure term has been considered in a different context. Already early on, the interplay between matter and gravity was explored on the lattice. In particular, when gauge fields were first added to the lattice this resulted in a significant back-reaction of matter on the geometry [284]. It was then shown that most of the contributions could actually be captured in an ultra-local measure term [278] of the form Eq. (2.83) and finally [285] found that there are no significant matter contributions on the lattice when one places the gauge field on the dual lattice to begin with, suggesting that the measure term functions as a sort of Jacobian. On grounds of universality, adding gauge fields to the lattice or its dual should be equivalent and hence, the apparent discrepancy should vanish in the continuum limit. Whether or not this is the case remains to be seen.

Alternatively, it has been proposed to interpret the measure term as a generalised higher-order curvature term [280]. Intuitively this is clear since Eq. (2.58) can be rewritten as

$$\delta_{s_{d-2}} = 2\pi - \mathcal{O}(s_{d-2})\theta_{s_d}, \tag{2.84}$$

where $\theta_{s_d} = \arccos 1/d$ and in $d = 4$ the simplex s_{d-2} is a triangle. Arguably, the most natural way to construct higher order curvature terms is by simply including terms of the form $(\delta_{s_{d-2}})^k$. The

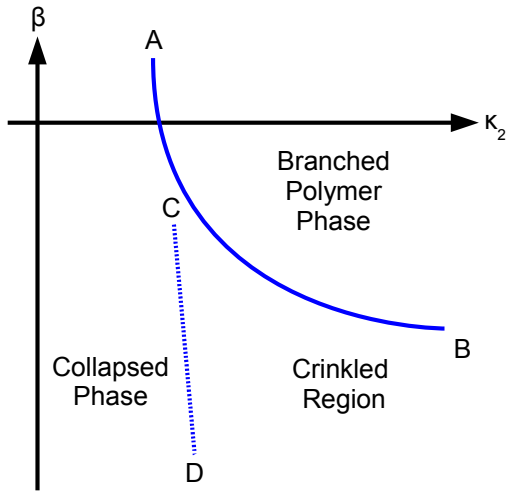

Figure 2.20: The phase diagram of EDT as presented in [281].

inclusion of an R^2-like term of this type led to the surprising result that the expectation value of the curvature does not vanish as one tunes towards the critical point [286]. That is, in the limit $a \to 0$, while keeping the volume finite, the curvature is larger than zero. This implies that the resulting configurations bear no resemblance to flat spacetime and led to the conclusion that either flat spacetime cannot be constructed from building-blocks when an R^2-like term is included or that the performed analyses are to naive and perhaps a different scaling relation should be used. In hindsight it is no surprise that continuum-like physics was not recovered since the critical line used for tuning is really a first-order phase transition.

2.2.5.0.1 Phase diagram of Euclidean Dynamical Triangulations

To study the validity of the EDT model we explore various properties of its phase structure [279, 281, 282]. We tune the parameter κ_4 to its critical value, such that an infinite-volume limit can be taken which yields a phase diagram described in terms of κ_2 and β, cf. Fig. 2.20.

The line AB represents a first-order phase transition between the branched polymer phase and the collapsed (crumpled) phase. This phase was already observed in the original DT model (i.e., for $\beta = 0$), see Fig. 2.16. In the collapsed phase a large number of simplices share the same vertices, resulting in a high connectivity and large curvature. This phase is characterised by an infinite Hausdorff dimension, d_H and very large spectral dimension d_s. In contrast, the branched polymer phase has the structure of a highly branched tree, where the branchings can be of any size. Spacetime appears to be fractal in this phase as it has $d_H = 2$ and $d_s = 4/3$. The crinkled region is separated from the collapsed phase by a cross-over, CD, rather than a phase-transition, and shares features of both phase C and D. For large volumes, the Hausdorff and spectral dimension resemble

those of the collapsed phase, indicating that the crinkled region might be a finite-size effect.

So far, none of the phases described above seem reasonable candidates for continuum spacetime as we observe it. However, as one moves closer to the first-order phase transition line AB, the Hausdorff dimension seems to approach four. The question is then whether a proper tuning of β could nevertheless result in a critical point with a second-order phase transition. First steps in this direction show that approaching AB from the left (collapsed phase) and lowering β while adjusting κ_2 softens the phase transition (i.e., the phase transition becomes less discontinuous) which might indicate that the line AB ends in a second-order phase transition in the limit $\beta \to -1$, $\kappa_2 \to \infty$. Moreover, the volume profile of the geometries resemble that of Euclidean de Sitter space better and better as one tunes towards $\beta \to -1$, $\kappa_2 \to \infty$. This is an important finding as it signals agreement with the CDT results [268] and possible signals that EDT and CDT could lie in the same universality class.

Under the assumption that such a critical point exists, one can distinguish between two scenarios: If the phase transition occurs for finite values of both β and κ_2, then this would imply that one can approach the fixed point from several directions and the tuning of β to compensate for diffeomorphism breaking is not necessary. Note that it could still be that a trajectory can be removed on physical grounds, e.g., if they lead to a clear breaking of diffeomorphism invariance. However, if the critical point occurs for finite β but infinite κ_2, then this suggest one has to tune the parameters to a trajectory which stays close to the first-order transition line. Since a large number of trajectories would correspond to a large number of relevant directions, a lower number of trajectories would be the preferred scenario on grounds of predictivity. Extended explorations of the phase diagram are expected to provide further insights in the viability of EDT. An important test is provided by the consistency of the model under inclusion of matter degrees of freedom and in the following section we will focus specifically on the inclusion of fermionic matter.

2.2.6 Lattice fermions

In the previous section, we saw that the coupling between asymptotically safe gravity and matter degrees of freedom can leave its signature on the IR behaviour of matter couplings. Since an important advantage of the lattice approach over the continuum FRG techniques is that there is no need to truncate the action, a comparison between EDT and FRG results in asymptotic safety can possibly provide an important cross-check.

2.2.6.1 Quenched formulation

Work involving the addition of scalar [287] and gauge degrees of freedom [288, 278] to the dynamical lattice have been performed in the past. Fermions on the other hand, have proven to be more difficult. In [76] the first steps studying the effects of the lattice on Kähler-Dirac fermions were set. Here we will shortly review this work and comment on ongoing work in the direction of the unquenched setting, i.e., the steps necessary to include the effects of matter on the dynamical triangulations.

Kähler-Dirac fermions readily admit a description in terms of geometric objects rather than requiring the introduction additional degrees of freedom, making it particularly suitable for the lattice setting [289, 290]. To be more precise, we first consider the continuum version of the Kähler-Dirac operator, which can be obtained from the Euclidean Laplace operator written in terms of exterior derivatives

$$\Delta = (d - \delta)^2 = -(d\delta + \delta d), \tag{2.85}$$

where we wrote $d^\dagger = \delta$ and used $d^2 = \delta^2 = 0$. Since intuitively the exterior derivative applied to an object yields the co-boundary of that object, its adjoint, δ, provides the boundary. The equation $\delta^2 = 0$ tells us then that the "boundary-of-the-boundary" vanishes, and similarly for $d^2 = 0$ and the co-boundary.

We then define the Kähler-Dirac operator

$$K = d - \delta, \tag{2.86}$$

such that

$$KK^\dagger = -(d - \delta)^2 = -\Delta. \tag{2.87}$$

This leads to the Kähler-Dirac equation for a field ω with mass m_0 as

$$(K - m_0)\,\omega = 0. \tag{2.88}$$

Here ω does not correspond to a field in the usual sense, but rather to a series of differential forms. To obtain a well-defined operation of K on ω we write

$$\omega = A + A_\mu dx^\mu + \frac{1}{2} A_{\mu\nu} dx^\mu \wedge dx^\nu + ... \tag{2.89}$$

If we wish to successfully describe fermions, then we need to relate Eq. (2.88) to the standard Dirac equation. On dimensional grounds this corresponds to generalising the ordinary Dirac spinor Ψ to be a four dimensional square matrix, i.e.,

$$\Psi = A + A_\mu \gamma^\mu + \frac{1}{2} A_{\mu\nu} \gamma^\mu \gamma^n u + ... \tag{2.90}$$

Here γ^μ are the standard gamma matrices and generate the Clifford algebra of (flat) spacetime. From the decomposition above, we can then deduce that Ψ contains four copies of the standard Dirac spinor, one for each column of Ψ, such that

$$(\gamma^\mu \partial_\mu + m_0)\Psi = 0, \tag{2.91}$$

represents four copies of the standard Dirac equation. If defined in this way, it can be shown that the action of Eq. (2.88) on ω is equivalent to the action of $\gamma^\mu \partial_\mu$ on Ψ [291, 290]. Note that since Eq. (2.91) only holds in flat spacetime, whereas the Kähler-Dirac operator is well-defined in curved setting as well, the equivalence between Eq. (2.91) and Eq. (2.88) is only present in the absence of curvature. The idea of incorporating Kähler-Dirac fermions in lattice theories is not new, but the particular dynamical setting we are concerned with here introduces additional subtleties that need to be taken into account.

Following [76] in both notation and procedure, we may discretise the continuum operators above by defining their operation on discrete building blocks. If we let $\overline{d}$ denote the discrete co-boundary operator, then $\overline{\delta} = \overline{d}^T$ is the discrete boundary operator. The operation of the boundary operator on a d-dimensional simplex, decomposes the simplex into the $(d-1)$-dimensional building blocks that make up its boundary. Each $(d-1)$-dimensional boundary simplex contributes with a certain sign, depending on its orientation within the d-dimensional simplex. If the lattice is combinatorial, then each d-simplex can be uniquely identified based on its set of vertices, $[v_0, ..., v_d]$ and its boundary consists of $(d+1)$ boundary simplices of dimensions $(d-1)$. As an example, consider a triangle, T, composed of the vertices $T \equiv [0, 1, 2]$. Its boundary is given by the three edges $E_0 \equiv [1, 2]$, $E_1 \equiv [0, 2]$, $E_2 \equiv [0, 1]$ which can be extracted from T by removing one of its vertices at a time. The boundary operator does exactly this and additionally orientates the edges in such a way that the operation $\overline{\delta}^2 T = 0$ is satisfied.

For a d-simplex we then have

$$\overline{\delta}_d \, [v_0, ..., v_d] = \sum_{i=0}^{d} (-1)^i [v_0, ..., v_d] \setminus [v_i], \tag{2.92}$$

where, with slight abuse of notation, $[v_0, ..., v_d] \setminus [v_i]$ indicates the removal of the i^{th} vertex from the list. In the case of our simple example above

$$\begin{aligned} \overline{\delta}_2 \, T = \overline{\delta}_2 \, [0, 1, 2] &= +[1, 2] - [0, 2] + [0, 1] \\ &= +E_0 - E_1 + E_2, \end{aligned} \tag{2.93}$$

and applying the boundary operator twice

$$\begin{aligned} \overline{\delta}_1 \, (\overline{\delta}_2 \, T) &= +\overline{\delta}_1 \, E_0 - \overline{\delta}_1 \, E_1 + \overline{\delta}_1 \, E_2 \\ &= +[2] - [1] - [2] + [0] + [1] - [0] \\ &= \emptyset, \end{aligned} \tag{2.94}$$

vanishes as it should. Note that the ordering of the vertices in the different sub-simplices is crucial here, i.e., if we had defined one of the edges as $E_1' \equiv [2, 0]$ then the double application of the boundary operator would not have vanished. Since the labelling, and in particular the order in which we store the vertices of an object, carries no physical meaning whatsoever, we are free to order the vertices however we like. The co-boundary operator, $\overline{d}$, acts on the simplices in the exact opposite way, i.e., acting with $\overline{d}_1$ on the edge E_1 would produce a list set of triangles, with T among them.

In order for the construction above to work, the lattice needs to be oriented. In particular, consider two neighbouring d-simplices, sharing one $(d-1)$-simplex. The orientation of the $(d-1)$-simplex within the two d-simplices needs to be opposite, e.g., the vertex $v_0 \equiv [0]$ above, is shared by E_1 and E_2 and has a $(-)$ orientation in E_1 and a $(+)$ orientation in E_2, guaranteeing that $\overline{\delta}^2 \, T = 0$.

Now that the operation of the boundary and co-boundary operator is clear, we can write the lattice version of the Kähler-Dirac operator as

$$(K + m_0) \, \overline{\omega} = (\overline{d} - \overline{\delta} + m_0) \, \overline{\omega}, \tag{2.95}$$

where $\overline{\omega}$ represents the lattice differential forms. Note furthermore that the Laplacian

$$\Delta = \overline{KK}^{\dagger} = -(\overline{d\delta} + \overline{\delta d}), \tag{2.96}$$

is a block-diagonal matrix, consisting out of (d+1) blocks, one for each of the sub-simplices. We will show this explicitly in the following. In $d = 4$, the blocks containing the 0 -and 4-simplices correspond to the regular lattice Laplacians and carry information on which simplices are "neighbours". Here we use the term "neighbour" with caution, since two 4-simplices are considered to be neighbours when they share a 3-simplex, whereas two 0-simplices are dual-neighbours when they belong to the same 1-simplex, i.e., the 0-simplex Laplacian operates on the dual lattice. For the remaining sub-simplices there is an ambiguity, since they have both boundary as well as co-boundary simplices[16].

In practice all calculations are performed on a Euclidean, simplicial manifold with trivial topology, i.e., a 4-sphere. Orienting the lattice is a straightforward task for combinatorial lattices, since all simplices can be identified by a unique set of vertices. For reasons of computational power, we will be using degenerate lattices (see Chpt. 2.2.7, and it will be necessary to introduce additional labels for various sub-simplices in order to uniquely distinguish them. Assuming this has been done, one first orders the vertices of all 4-simplices in ascending order, such that when $j > i$ in Eq. (2.92) one necessarily has $v_j > v_i$ (since the vertices within a given simplex are distinct $v_j \neq v_i$ for any pair of vertices belonging to the same simplex). It should be noted that any ordering which can be consistently applied across the entire lattice is sufficient.

Once all 4-simplices have been ordered, we can start orienting the lattice. Starting out from any 4-simplex, we select one of its five 3-simplices (tetrahedra) and assign a (+) or (−) to it. This automatically fixes the orientation of the remaining four 3-simplices within the given 4-simplex and through repeated application of $\overline{\delta}$ the orientation of all other sub-simplices can be extracted as well. If we let $A = [a, b, c, d, e]$ denote this first 4-simplex, then we can orient the rest of the lattice as follows: Move along one of the tetrahedra of A to a neighbouring 4-simplex, B. Since A and B are neighbours, they share *at least* four vertices but, since the lattice is degenerate, they might share all five vertices. If they share all five vertices, then A and B may share up to four tetrahedra, but never five, since the lattice needs to remain connected if we wish to simulate a 4-sphere. In the case where they share only four vertices, one possibility is $B = [f, a, b, c, d]$, such that the common tetrahedra is $[a, b, c, d]$. If we apply the boundary operator to A, then we find that this 3-simplex has (+) parity. Acting on B with $\overline{\delta}$, we find a (+) parity as well. Since the parity of a shared 3-simplex needs to be opposite, we flip the parity of this 3-simplex in B to (−) and thereby automatically flip the parity of all other 3-simplices in B, schematically we let $B = -[f, a, b, c, d]$. Moving on to a neighbour of B which has not been visited yet (i.e., is not A), we assign a parity to the shared 3-simplex which is opposite to the parity it has in B and keep iterating this procedure until the entire lattice has been oriented. By only visiting lattice sites that have not been visited before, we build a so-called *minimal spanning tree*. A minimal spanning tree is a connected graph with N nodes (4-simplices) and $N - 1$ edges, such that each node is visited only once i.e., there are no cycles or disconnected pieces. Even though the spanning tree will in general not be unique, the orientation of the lattice is unique up to an overall sign.

[16] It should be noted that two d-simplices that are part of the same $(d + 1)$-simplex *necessarily* share a $(d - 1)$-simplex, e.g., the edges $E_0 = [1, 2]$ and $E_1 = [0, 2]$ both belong to $T = [0, 1, 2]$ and in addition share $v_2 = 2$.

After all 4-simplices have been visited and all 3-simplices oriented[17], we apply the boundary operator to obtain the orientation of all remaining sub-simplices and obtain the oriented lattice required for the inclusion of Kähler-Dirac fermions.

If we let N_d denote the total number of d-simplices then $\overline{d}_d$ is a $N_{d-1} \times N_d$ matrix holding the orientation of each d-simplex in terms of its $(d-1)$-simplices, such that each column of $\overline{d}_d$ contains an oriented list with $(d+1)$ entries (necessarily 1 or -1). For example, the column $\overline{d}_4$ holding A, will have entries $+1$ for the rows corresponding to the 3-simplices a, c, e and -1 for b, d. Since each 3-simplex can only belong to two distinct 4-simplices, each row of $\overline{d}_4$ should contain exactly one $+1$ and one -1 for an oriented lattice. Although it is true that also for the lower dimensional sub-simplices, each column contains exactly $d+1$ entries, the rows can contain an arbitrary number of entries due to the degeneracy of the lattice. Similarly, the boundary operator $\overline{\delta}_4 = \overline{d}_4^T$ is represented by a $N_4 \times N_3$ dimensional matrix, where the entries of a column indicate for which 4-simplices the given 3-simplex is a boundary element.

The full co-boundary matrix, $\overline{d}$, should provide a mapping from all sub-simplices to the corresponding oriented, higher-dimensional simplex and the opposite for $\overline{\delta}$. In $d = 4$ we may then write

$$\overline{d} = \begin{pmatrix} 0 & 0 & 0 & 0 & 0 \\ \overline{d}_4 & 0 & 0 & 0 & 0 \\ 0 & \overline{d}_3 & 0 & 0 & 0 \\ 0 & 0 & \overline{d}_2 & 0 & 0 \\ 0 & 0 & 0 & \overline{d}_1 & 0 \end{pmatrix}, \quad \overline{\delta} = \begin{pmatrix} 0 & \overline{\delta}_4 & 0 & 0 & 0 \\ 0 & 0 & \overline{\delta}_3 & 0 & 0 \\ 0 & 0 & 0 & \overline{\delta}_2 & 0 \\ 0 & 0 & 0 & 0 & \overline{\delta}_1 \\ 0 & 0 & 0 & 0 & 0 \end{pmatrix}, \tag{2.97}$$

where we emphasise that each element is again a matrix (e.g., a 0 in the first column of $\overline{d}$ is a $N_3 \times N_4$ dimensional matrix filled with zeros). Using the matrix representation above, we find for the square of the Kähler-Dirac operator in Eq. (2.96)

$$\begin{aligned} \overline{KK}^\dagger &= -(\overline{d\delta} + \overline{\delta d}) \\ &= -\begin{pmatrix} 0 & 0 & 0 & 0 & 0 \\ 0 & \overline{d}_4\overline{\delta}_4 & 0 & 0 & 0 \\ 0 & 0 & \overline{d}_3\overline{\delta}_3 & 0 & 0 \\ 0 & 0 & 0 & \overline{d}_2\overline{\delta}_2 & 0 \\ 0 & 0 & 0 & 0 & \overline{d}_1\overline{\delta}_1 \end{pmatrix} - \begin{pmatrix} \overline{\delta}_4\overline{d}_4 & 0 & 0 & 0 & 0 \\ 0 & \overline{\delta}_3\overline{d}_3 & 0 & 0 & 0 \\ 0 & 0 & \overline{\delta}_2\overline{d}_2 & 0 & 0 \\ 0 & 0 & 0 & \overline{\delta}_1\overline{d}_1 & 0 \\ 0 & 0 & 0 & 0 & 0 \end{pmatrix} \\ &= -\begin{pmatrix} \overline{\delta}_4\overline{d}_4 & 0 & 0 & 0 & 0 \\ 0 & \overline{d}_4\overline{\delta}_4 + \overline{\delta}_3\overline{d}_3 & 0 & 0 & 0 \\ 0 & 0 & \overline{d}_3\overline{\delta}_3 + \overline{\delta}_2\overline{d}_2 & 0 & 0 \\ 0 & 0 & 0 & \overline{d}_2\overline{\delta}_2 + \overline{\delta}_1\overline{d}_1 & 0 \\ 0 & 0 & 0 & 0 & \overline{d}_1\overline{\delta}_1 \end{pmatrix}. \end{aligned} \tag{2.98}$$

[17]Note that for d-dimensional simplicial manifolds with d even, we may think of the orientation of the lattice as assigning a parity to the d-simplices rather than the $(d-1)$-simplices. In $d = 4$, a 4-simplex with three parity $(+)$ 3-simplices is then positively oriented and the opposite for three 3-simplices with parity $(-)$. Since the vertices have been ordered, this uniquely fixes all signs. This does not work if d is uneven, since then the number of $(d-1)$-simplices with $(+)$ and $(-)$ is exactly even, such that the d-simplices would be "neutral".

We see then that indeed, with the exception of the 0 -and 4-component, we obtain a modified Laplacian type of operator for each d-simplex. Note that the dimensionality of the matrix $\overline{d}_4\overline{\delta}_4$ is $N_3 \times N_3$ since it is constructed by multiplying a $(N_3 \times N_4)$ matrix with a $(N_4 \times N_3)$ matrix. The added matrices are then of the correct dimensionality and the final matrix $\overline{KK}^\dagger$ is block-diagonal with dimensionality $N \times N$ where $N \equiv N_4 + N_3 + N_2 + N_1 + N_0$. Finally, since the mass m_0 is real, we have

$$\begin{aligned}(\overline{K} + \mathbb{1}m_0)(\overline{K} + \mathbb{1}m_0)^\dagger &= \overline{d\delta} + \overline{\delta d} + \mathbb{1}m_0^2 \\ &= \overline{KK}^\dagger + \mathbb{1}m_0^2,\end{aligned} \tag{2.99}$$

corresponding to the continuum expression $-\Box + m_0^2$.

In a first approximation, the construction above can be used to evaluate the effects of dynamical gravity on matter degrees of freedom, without taking into account the back-reaction of matter on the dynamical lattice itself. This is referred to as the *quenched* approximation and provides a significant computational simplification since one can re-use lattices which have already been generated and "place" the Kähler-Dirac fermions on the lattice. This approximation was used in [76] to verify explicitly that the Kähler-Dirac fermions satisfy several expected properties, such as the appearance of four degenerate Dirac fermions as one moves closer to the continuum limit and the presence of zero-modes in the chiral limit $m_0 \to 0$.

In the massless case, it can be shown that K anti-commutes with the operator Γ, which effectively sends any d-dimensional simplex to $(-1)^d$ times itself. That these operations anti-commute is easiest to understand by considering the action of $\overline{\Gamma}$ on Eq. (2.92)

$$\overline{\Gamma}\left(\overline{\delta}_d\left[v_0, ..., v_d\right]\right) = (-1)^{d-1}\sum_{i=0}^{d}(-1)^i[v_0, ..., v_d] \setminus [v_i], \tag{2.100}$$

whereas

$$\overline{\delta}_d\left(\overline{\Gamma}\left[v_0, ..., v_d\right]\right) = (-1)^{d}\sum_{i=0}^{d}(-1)^i[v_0, ..., v_d] \setminus [v_i], \tag{2.101}$$

and hence

$$\left(\overline{\Gamma\delta}_d + \overline{\delta}_d\overline{\Gamma}\right)\overline{\omega}_d = 0. \tag{2.102}$$

A similar construction holds for $\overline{d}$, such that also $\overline{K}$ will anti-commute with $\overline{\Gamma}$. This anti-commutation can be translated into a $U(1)$ symmetry of the Kähler-Dirac action. As was shown in [292], this symmetry will be anomalous on a lattice with non-vanishing Euler characteristic, χ. Since we are simulating a topological 4-sphere, the Euler characteristic is $\chi = 2$ and hence, we expect the anomaly to be broken. Alternatively, we can understand this by noticing that the $d = 0$ simplices do not have a boundary, and hence $\overline{\delta}\overline{\omega}_0 = 0$ such that Eq. (2.102) does not hold for the 0-simplices. Similarly, the $d = 4$ simplices do not have a co-boundary, resulting in $\overline{d}_4\overline{\omega}_4 = 0$. This then leads to zero-modes associated with the 0-simplices and 4-simplices in the limit where $m_0 \to 0$, i.e., in the chiral limit.

For the construction above to be observationally viable, this $U(1)$ chiral-like symmetry cannot be spontaneously broken since this would lead to the generation of bound states with Planckian-size

masses. The authors of [76] investigated this by constructing quartic operators, as for these the two mass factors will cancel the factors coming from the two zero-modes in the chiral limit [292, 293]. The simplest example is given by a construction of pion-like mesons in terms of two-fermion propagators

$$\begin{aligned}\langle \pi(x)\pi(y)\rangle &= (\overline{K}+m_0)^{-1}_{yx}((\overline{K}+m_0)^{-1}_{xy})^* \\ &= \langle \omega_y \overline{\omega}_x\rangle \, \langle (\omega_y \overline{\omega}_x)^\dagger\rangle.\end{aligned} \tag{2.103}$$

Where here x and y refer to two of the d-simplices on the lattice and the approximation was made that one can work with two flavours of the Kähler-Dirac field. One can then study the meson propagator between two d-simplices and calculate the associated mass. Specifically, from continuum considerations one expects

$$\langle \pi(x)\pi(y)\rangle \sim a e^{-m\,|x-y|}, \tag{2.104}$$

for lattices with relatively large lattice spacing. As one decreases the lattice spacing, i.e., moves closer to the line AB in Fig. 2.20, the simulations become more expensive and the physical volumes are smaller. Therefore, simulations on these lattices are expected to be sensitive to curvature effects and the modified form of the pion propagator becomes

$$\langle \pi(x)\pi(y)\rangle \sim a \frac{e^{-m\,|x-y|}}{|x-y|^b}, \tag{2.105}$$

with $a,\ b, m$ parameters used to fit the data. These studies have to be performed with care, since at short distances there will be discretisation effects and at distances that are too long, a contamination by finite-volume effects due to baby universes will spoil the results. The meson mass should then be extracted at intermediate distance scales, where the lattices show semi-classical properties that resemble Euclidean de Sitter spacetime.

The obtained results [76] signal that the masses of mesons associated with zero- and four-simplices have a mass which vanishes in the chiral limit, whereas the masses of the remaining three sub-simplices take on finite values. However, as one refines the lattice by taking the lattice spacing smaller, the squared masses of the remaining sub-simplices shrink linearly with the squared lattice spacing and can be extrapolated to zero. This provides evidence that in the continuum limit, there is no chiral symmetry breaking. It should be clear that more detailed studies are necessary to confirm these results. In particularly, at small distances there may be discretisation effects which seep into the results, whereas long distances should be probed with care to avoid finite-volume effects. This makes the region where one can extract physically meaningful information relatively narrow. The largest lattices used in the studies described here are relatively small, i.e., 16000 four-simplices, and it is thus important to repeat these studies at larger volumes to confirm that there is indeed no chiral symmetry breaking. Nevertheless, since there appears to be no spontaneous breaking of chiral symmetry within the numerical limits of the studies here, no bound-states with Planck-scale masses were generated. This cross-check is crucial if EDT is to provide a quantum-gravity theory consistent with observations.

2.2.6.2 Unquenched formulation

An important next step involves the unquenching of the procedure above, such that the generation of the dynamical lattice itself is sensitive to the matter content. In particular, this includes modifying the microscopic action by adding a matter contribution such that in the continuum

$$\begin{aligned} Z_E &= \int \mathcal{D}[g]\, e^{-S_{EH}[g]}\, Z_{KD}[\overline{\omega},\, \omega] \\ &= \int \mathcal{D}[g]\, \mathcal{D}[\overline{\omega}]\, \mathcal{D}[\omega]\, e^{-S_{EH}[g]\, -S_{KD}[\overline{\omega},\, \omega]}, \end{aligned} \tag{2.106}$$

where the continuum Kähler-Dirac action is

$$S_{KD}[\overline{\omega}, \omega] = \int d^4x \sqrt{g}\, \overline{\omega}\, (d - \delta + m_0)\, \omega. \tag{2.107}$$

Note that here $\overline{\omega} = \omega^\dagger \gamma^0$ refers to the *continuum* conjugate of ω. For the remainder of this discussion we will work in the discrete lattice setting unless indicated otherwise. To keep the notation clean, we will not introduce additional operators to distinguish between continuum and discrete quantities.

Since there is only a minimal coupling between the gravitational and matter sector, we can discretise the Einstein-Hilbert action in the usual way, i.e., Eq. (2.61) in $d = 4$ dimensions with a non-trivial measure term Eq. (2.83). As for the Kähler-Dirac part, we may use standard lattice methods and perform the Gaussian Grassman integral over $\overline{\omega}$ and ω. Specifically, we define

$$\omega'(\mathbf{n}) = \sum_{\mathbf{m}} (K + \mathbb{1} m_0)_{\mathbf{nm}}\, \omega(\mathbf{m}), \tag{2.108}$$

where $\mathbf{n}$ and $\mathbf{m}$ are lattice points. Taking the measure for the matter part to be trivial, such that $\mathcal{D}[\overline{\omega}] = \prod_{\mathbf{n}} d\overline{\omega}(\mathbf{n})$ and using that $d\omega(\mathbf{n}) = \det(K + m_0)\, d\omega'(\mathbf{n})$, then we find

$$\begin{aligned} Z_{KD} &= \det(K + m_0) \int \left[\prod_{\mathbf{n}} d\overline{\omega}(\mathbf{n})\, d\omega'(\mathbf{n}) \right] \, e^{-\sum_{\mathbf{n}} \overline{\omega}(\mathbf{n})\, \omega'(\mathbf{n})} \\ &= \det(K + m_0) \int \prod_{\mathbf{n}} d\overline{\omega}(\mathbf{n})\, d\omega'(\mathbf{n})\, e^{-\overline{\omega}(\mathbf{n})\, \omega'(\mathbf{n})} \\ &= \det(K + m_0), \end{aligned} \tag{2.109}$$

for the Kähler-Dirac term in the partition function (where m_0 now denotes a diagonal matrix). We redefine the Kähler-Dirac action on the lattice to $S_{KD} = -\ln(\det(K + m_0))$ such that the discretised version of Eq. (2.106) takes the form

$$Z_E = \sum_{\mathcal{T}} \frac{1}{C_{\mathcal{T}}} \left[\prod_{j=1}^{N_2} \mathcal{O}(t_j)^\beta \right] \, e^{-S_{ER}\, -S_{KD}}. \tag{2.110}$$

The partition function above can be readily evaluated on the lattice using Monte-Carlo methods. In practice, this means that after each update of the geometry i.e., after each Pachner move, we need to re-evaluate $\det(K + m_0)$. Since the inversion of a matrix is a computationally expensive process, one ideally tries to avoid performing a large number of explicit inversions. This holds especially when the matrices under consideration are *sparse*, i.e., matrices that contain relatively few non-zero entries. In general, diagonal matrices are computationally less expensive to invert than non-diagonal matrices and thus, one of the most straightforward simplifications we can do is to cast the Kähler-Dirac action in the form: $S_{KD} = -\ln\left(\det(K + m_0)\right) = -\frac{1}{2}\ln\left(\det(K + m_0)^2\right)$.

The update procedure implemented here can be described as a repetition of the following steps: Starting out from a triangulation, T_i, we perform a large number of attempted update moves to create a trial configuration T_j. To determine whether or not the trial configuration is accepted, we do a global Metropolis step (see Chpt. 2.2.7.1 for a description of the Metropolis algorithm). If the trial configuration is accepted, then T_j will be the next configuration in the Markov chain. If not, then we stay with T_i and redo the updating process.

The acceptance probability of a Metropolis step depends only on the entropic difference between the current and trial configuration, Eq. (2.126), hence, we are interested in the change of the determinant

$$\Delta_{\det}(T_i,\, T_j) \equiv \det(K + m_0)^2_{T_j} - \det(K + m_0)^2_{T_i}. \tag{2.111}$$

Moreover, since the square of the Kähler-Dirac matrix is a block-diagonal matrix, the determinant of the entire matrix simplifies to the sum of the determinant of the individual blocks. Using this property, the change of the total determinant becomes the change of the determinant of the blocks

$$\Delta_{\det}(T_i,\, T_j) = \sum_{n=0}^{4} \left[\det\left(K^{(n)}_{T_j}\right)^2 - \det\left(K^{(n)}_{T_i}\right)^2 \right], \tag{2.112}$$

where we defined $K^{(n)} \equiv K^{(n)} + m_0^{(n)}$ such that $K^{(n)}$ and $m_0^{(n)}$ refer to the $N_n \times N_n$ block in Eq. (2.98). In general, significant changes in the determinant of a matrix occur whenever the size of the matrix changes, i.e., whenever simplices are created or removed. From Fig. 2.21, we see that the $(1-5)$ and $(2-4)$ moves create new simplices, leading to the addition of rows and columns to K. The opposite is true for the $(5-1)$ and $(4-2)$ moves, which will delete simplices. The $(3-3)$ move leaves the size of K invariant and is thus expected to have little to no influence on the change of the determinant. Since each move always creates or deletes a fixed amount of simplices, the change in the determinant is expected to be roughly constant for each move. For example, the $(5-1)$ move always shrinks $K^{(4)}$ by deleting four rows and four columns, independent of the configuration on which it is evaluated. If we let $\Delta^{(n)}_{\det,\,1-5}$ denote the *fixed* change in the determinant of the n-simplices Laplacian, through the $(1-5)$ move then

$$\Delta_{\det,\,1-5} = \sum_{n=0}^{4} \Delta^{(n)}_{\det,\,1-5}. \tag{2.113}$$

To obtain the actual numbers $\Delta^{(n)}_{\det,\,1-5}$, we explicitly evaluate the determinant before and after the update move $1-5$ and verify that it is indeed approximately constant. Since each trial configuration

is obtained through a sequence of moves on the current configuration, we can write the estimated total change in the determinant as

$$\Delta^{\#}_{\mathrm{det}} = (\#_{1-5} - \#_{5-1})\,\Delta_{\mathrm{det},\,1-5} + \#_{3-3}\Delta_{\mathrm{det},\,3-3} + (\#_{2-4} - \#_{4-2})\,\Delta_{\mathrm{det},\,2-4}. \tag{2.114}$$

Here $\#_i$ indicates the total number of i-moves and we used that $\Delta_{\mathrm{det},\,5-1} \approx -\Delta_{\mathrm{det},\,1-5}$ and similarly for the $2-4$ move. After a certain number of moves, we explicitly evaluate the determinants, Δ_{det}, as in Eq. (2.112), and compare the exact change with the estimated change Eq. (2.114). To determine whether or not the new configuration should be accepted, we perform a global Metropolis step with probability

$$A_M(T_i \to T_j) = \min\left[1, e^{-\frac{n_f}{2}\left(\ln\Delta^{\#}_{\mathrm{det}} - \ln\Delta_{\mathrm{det}}\right)}\right], \tag{2.115}$$

where we included the number of Kähler-Dirac fermions, n_f, for completeness (throughout this work $n_f = 1$) and we abbreviated $\Delta_{\mathrm{det}}(T_i, T_j) = \Delta_{\mathrm{det}}$. By using the method described above, we can drastically reduce the number of matrix inversions that need to be performed and gain significant speed-ups. Nevertheless, the construction of the matrices and their determinants causes a significant slow-down in the generation of the dynamical lattices. For example, if the generation of a $N_4 = 4000$ lattice requires of the order $\mathcal{O}(10^5)$ trial configurations, and we evaluate the Kähler-Dirac matrix approximately $\mathcal{O}(10^4)$ times per trial configuration[18], then we need to perform around $\mathcal{O}(10^9)$ inversions. At the moment, each inversion takes roughly ~ 0.1 seconds, meaning that we would need to run the algorithm for roughly 30 months *plus* the time taken by the pure-gravity evaluation, to obtain a dynamical lattice.

Algorithmically there are still many angles left which should yield orders of magnitude in computation time. The largest speed-ups are expected to come from two modifications. Currently the matrices are constructed and inverted from scratch during each explicit evaluation. Since the update moves always affect a fixed number of simplices, the first improvement we can perform is updating the matrices rather than re-constructing them. To do so, we need to know exactly how the individual matrices change and how this affects the computation of $(K + m_0)^2$ (note that since the update moves are local, the orientation of the lattice only varies locally). Once this has been worked out, we can make use of pre-designed algorithms to update the determinant and hence, can avoid explicit inversions. Secondly, we can create speed-ups through the implementation of parallel algorithms. We are currently looking into both methods and once these are taken full advantage of, it should be possible to generate dynamical lattices with dynamical fermions in a reasonable time-frame.

The status of chiral symmetry breaking in chiral-fermion and asymptotically-safe gravity systems has been addressed through FRG methods as well [77, 172]. Since chiral-symmetry breaking in QCD occurs in the strong coupling regime, the analog in the gravitational setting was studied at strong gravitational coupling. The results obtained there are in line with the perseverance of chiral symmetry around the Planck scale and therefore match what was found in the work above.

[18] The more often we evaluate the determinants, the larger the acceptance probability will be. As matrix inversions go hand-in-hand with significant computational slow-down, one tries to find a minimal number of explicit evaluations such that the acceptance probability is still reasonable without slowing down the code too much.

Let us point out that there are calculations which can be performed on lattices as small as $N_4 = 500$. An example is the running of G and Λ as was evaluated in [282], Fig. 19. The generation of these lattices requires significantly smaller matrices, such that $\mathcal{O}(10^5)$ trial configurations is sufficient and the inversion of a single matrix takes roughly $\mathcal{O}(10^{-3})$ seconds, depending on how close to the phase-transition one simulates. This adds up to 1-2 days of computational time spend purely on the inversion of matrices. These time-scales are reasonable and simulations for different values of β, κ_2 are currently on the way.

In summary, the original Euclidean DT model was modified by the inclusion of a non-trivial, ultra-local measure term, motivated by the observation that the regulator breaks diffeomorphism invariance and additional tuning might be necessary in order to find a continuum phase transition. The additional parameter β in the EDT model, was found to enrich the phase-structure and in particular, evidence was found of a phase with Hausdorff dimension close to four and an expectation value of the summed-over geometries which resembles that of Euclidean de Sitter spacetime. This gives hope that EDT might lie in the same universality class as CDT which would imply that EDT is unitary [294]. Moreover, since a continuous phase transition signals scale invariance, its existence is crucial in the search for asymptotic safety. If EDT indeed proves to be a lattice formulation of asymptotic safety, then EDT and continuum asymptotic safety, as discussed in Chpt. 2.1, should lie in the same universality class as well. If all three theories (CDT, EDT and asymptotically safe quantum-gravity) are indeed connected by universality, then this implies that asymptotically safe quantum-gravity is unitary as well.

An interesting question is whether the phase diagram of EDT changes under the inclusion of matter degrees of freedom, i.e., is (Euclidean) spacetime sensitive to matter? Simulations involving scalars [287] and gauge fields [288, 278] have been performed in the past, but addition of fermions to the lattice has been difficult. In [76], the description of Kähler-Dirac fermions in terms of exterior derivatives was used to include fermions in EDT simulations. The results obtained there did not take into account the back-reaction of the fermions on the lattice, i.e., the fermions were quenched. To obtain results of the effects of matter on the lattice and study whether or not the phase diagram changes, it is crucial to include this back-reaction. New code accomplishing this has been developed but is currently not efficient enough to produce unquenched lattices within a reasonable time frame. We can, however, study the running of G and Λ as in [282], Fig. 19, and hope to report on this soon.

2.2.7 Lattice methods

Dynamical triangulations (in all its forms) admits a straightforward statistical interpretation due to its Euclidean nature[19]. This is particularly convenient for numerical evaluations utilising Monte Carlo methods. It can be shown that the moves are ergodic in $d \leq 4$ spacetime dimension, provided that for $d > 2$ the volume is allowed to fluctuate [295]. In practice this is implemented by adding a term $-\delta(N_d - \bar{N}_d)^2$ to the partition sum. Here $\bar{N}_d$ is the target volume and δ is chosen such

[19]CDT is in principle formulated as a Lorentzian path integral, but for all practical purposes the theory is analytically continued to Euclidean signature. The rotation back is assumed to be possible after the continuum limit has been taken.

that the fluctuations are small. Furthermore, as has been argued above, one would like to restrict the global topology of the summed-over triangulations on grounds of convergence of the partition function. As a direct consequence the *local* update moves need to be topology preserving.

In Fig. 2.21 we show the so-called Pachner moves [296, 297] in $d = 4$ dimensions. If we label the vertices corresponding to a 4-simplex as $\{0, 1, 2, 3, 4\}$ then we find for the $5 - 1$ move

$$
\begin{array}{l}
(\mathbf{5-1}): \\
\begin{array}{lll}
A = \{1,2,3,4,5\} & & a_1 = \{1,2,3,4\} \\
B = \{0,2,3,4,5\} & & b_1 = \{0,2,3,4\} \\
C = \{0,1,3,4,5\} & \Rightarrow F = \{0,1,2,3,4\} \quad \text{with:} & c_1 = \{0,1,3,4\}, \\
D = \{0,1,2,4,5\} & & d_1 = \{0,1,2,4\} \\
E = \{0,1,2,3,5\} & & e_1 = \{0,1,2,3\}
\end{array}
\end{array}
\tag{2.116}
$$

where a_1, b_1, c_1, d_1, e_1 correspond to the correspondingly labelled tetrahedra in Fig. 2.21. The created tetrahedra are determined uniquely from 4-simplices they share, for example the tetrahedra connecting A with B is given by $A \cap B = \{2, 3, 4, 5\}$.

The $4 - 2$ move:

$$
\begin{array}{l}
(\mathbf{4-2}): \\
\begin{array}{lll}
 & & a_1 = \{0,1,3,4\} \\
 & & a_2 = \{1,3,4,5\} \\
A = \{0,1,3,4,5\} & & b_1 = \{0,2,3,4\} \\
B = \{0,2,3,4,5\} & \Rightarrow \begin{array}{l} E = \{0,1,2,3,4\} \\ F = \{1,2,3,4,5\} \end{array} \quad \text{with:} & b_2 = \{2,3,4,5\} \\
C = \{0,1,2,3,5\} & & c_1 = \{0,1,2,3\}. \\
D = \{0,1,2,4,5\} & & c_2 = \{1,2,3,5\} \\
 & & d_1 = \{0,1,2,3\} \\
 & & d_2 = \{1,2,4,5\}
\end{array}
\end{array}
\tag{2.117}
$$

Here the vertex labelled as 5 is removed from A and B, and vertex 0 from C and D. The new 4-simplices E and F share the tetrahedra $E \cap F = \{1, 2, 3, 4\}$ and the external tetrahedra are then redistributed such that the labelling remains consistent.

Lastly, the $3 - 3$ move "flips" a triangle:

$$
\begin{array}{l}
(\mathbf{4-2}): \\
\begin{array}{lll}
 & & a_1 = \{1,2,3,4\} \\
 & & a_2 = \{0,2,3,4\} \\
 & & a_3 = \{0,1,3,4\} \\
A = \{0,1,2,3,4\} & D = \{1,2,3,4,5\} & b_1 = \{1,2,3,5\} \\
B = \{0,1,2,3,5\} & \Rightarrow E = \{0,2,3,4,5\} \quad \text{with:} & b_2 = \{0,2,3,5\}. \\
C = \{0,1,2,4,5\} & F = \{0,1,3,4,5\} & b_3 = \{0,1,3,5\} \\
 & & c_1 = \{1,2,4,5\} \\
 & & c_2 = \{0,2,4,5\} \\
 & & c_3 = \{0,1,4,5\}
\end{array}
\end{array}
\tag{2.118}
$$

The 4-simplices A, B, C share the triangle $\{0, 1, 2\}$. We remove this triangle and replace it by the only other triangle consistent with the labelling conventions. It can be formed through taking the pairwise complement $\{A \setminus C,\, C \setminus B,\, B \setminus A\} = \{3, 4, 5\}$. This last move leaves the total number of simplices unaltered and is for that reason often seen as an "identity" operation.

Note that in all cases the moves are local since they only affect those parts of the lattice shown in the illustrations Fig. 2.21, i.e., all new links (tetrahedra) created/deleted are local (grey, internal lines connecting 4-simplices A, B, C, ...), whereas links that connect to the rest of the lattice (red links labelled by a_1, b_1, ...) remain intact.

Despite these restrictions there is still some freedom left in the construction of a simplicial manifold. In particular, there are different ways of gluing simplices together which should lead to the same continuum physics but might differ on the level of the lattice. Originally the set of summed over triangulations were all combinatorial. In a combinatorial lattice one can uniquely identify a d-dimensional simplex by its $(d + 1)$ vertices, suggesting that two simplices can at most have one face in common, e.g., any two triangles in a combinatorial triangulations have either zero or one edge in common. This condition can be relaxed to different degrees. If two simplices are allowed to have the same set of vertices, but *within* a single simplex the vertices itself are distinct, then such a triangulation is called restricted degenerate. These type of triangulations occur when two simplices are allowed to be glued on top of one another. Taking the degeneracy one step further leads to triangulations where a simplex may be glued to itself and, hence, even within a single simplex the vertices are no longer unique. This last class of simplices is called maximally degenerate. In two dimensions it can be shown that all three types of triangulations lead to the same continuum theory. However, it turns out that relaxing the conditions placed on the triangulations results in a reduction of finite-size effects [298, 277]. This can be understood by observing that at a finite total volume, the ensemble of degenerate triangulations is larger than the set of combinatorial triangulations and hence, it becomes easier to accurately simulate the provided geometry [299]. Furthermore, the combinatorial lattices require additional checks during update moves, which cause significant slow downs.

For the rest of this work we will refer to the second case as "degenerate" unless otherwise indicated. Giving up on some of the combinatorial relations does have its downsides since we can no longer uniquely identify a simplex by its vertices. It could then happen that for three *distinct* 4-simplices $A = \{0, 1, 2, 3, 4\}$, $B = \{0, 1, 2, 3, 4\}$, $C = \{0, 1, 2, 3, 5\}$ we find that the set of nearest neighbours of A (i.e., those 4-simplices sharing a 3-simplex with A) is given by $A_{NN} = \{B,\, B,\, B,\, B,\, C\}$. Thus, A shares four of its tetrahedra with B and one with C. Note that it is not allowed for A and B to share all five tetrahedra since then it would become energetically favourable for the lattice to collapse into just two 4-simplices and this does not share any resemblance with our continuous universe.

2.2.7.1 Monte Carlo methods

Here we give a brief overview of the simulation techniques employed to generate the triangulated manifolds used, following [300, 301]. In general, whenever an analytic treatment of a given physical

system is not possible, it may still be possible to generate an ensemble of configurations from which thermodynamic (equilibrium) quantities can be extracted. To do so, the set of configurations needs to provide an "honest" representation of the full (possibly infinite) configuration space. In other words, we are in need of a sampling procedure which somehow respects the physical properties of the system under consideration, such that we may obtain statistical information reliably. A prominent example is so-called importance sampling, which selects the set of configurations with the highest contribution to statistical averages. This set can then be used to extract equilibrium properties of the system without having to simulate all possible states allowed by symmetries.

In practice, Monte Carlo simulations almost always have to satisfy two basic properties: Ergodicity and detailed balance. We say our simulations are ergodic if, given two configurations C_0 and C_1 with non-vanishing probability of being generated (i.e., their Boltzmann weight is non-zero), there exists a path of finitely many Monte Carlo moves which transforms C_0 into C_1. In other words, any configuration in the configuration space needs to be reachable from any other configuration space. Without this demand, it could happen that one artificially (i.e., without physical motivation) excludes part of the physical configuration space.

To specify the second condition (detailed balance), we first introduce the transition probability $W(C_i \to C_j)$ as the probability for the system to transition from a configuration C_i to a configuration C_j. This transition probability can be written as

$$W(C_i \to C_j) = T(C_i \to C_j) \times A(C_i \to C_j), \tag{2.119}$$

where $T(C_i \to C_j)$ is the trial proposition probability, i.e., given C_i, an initial configuration, $T(C_i \to C_j)$ gives the probability that the trial configuration C_j is proposed as the next "step". Whether the configuration then indeed transitions to this trial configuration depends on whether or not C_j is accepted, i.e., it depends on the acceptance probability $A(C_i \to C_j)$. The set of configurations that we end up with $C_0, ..., C_N$ is called a Markov chain. To have a well-defined probabilistic interpretation we must have $\forall i, j\, W(C_i \to C_j) \geq 0$ and $\sum_j W(C_i \to C_j) = 1$. Furthermore, let P_{C_i} and P_{C_j} denote the probability of finding the system in configuration C_i or C_j respectively, then detailed balance requires that for every pair of configurations, the ratio of the transition amplitude from one to the other is the same as the ratio between the probabilities of those configurations to occur in the first place

$$\frac{T(C_i \to C_j) \times A(C_i \to C_j)}{T(C_j \to C_i) \times A(C_j \to C_i)} = \frac{P_{C_j}}{P_{C_i}}. \tag{2.120}$$

If we now let $P_{C_i}(t)$ denote the probability of finding our system in configuration C_i after t time-steps (transitions), then the rate of change of $P_{C_i}(t)$ is given by

$$\frac{dP_{C_i}(t)}{dt} = \sum_{i \neq j} \left[P_{C_j}(t) W(C_j \to C_i) - P_{C_i}(t) W(C_i \to C_j) \right]. \tag{2.121}$$

We see then that the condition of detailed balance, Eq. (2.120), is exactly such that $\frac{dP_{C_i}(t)}{dt} = 0$ and thus, the probability for a given configuration to occur does not depend on the number of Monte Carlo time-steps that have passed. Note that if detailed balance is not satisfied, then the

probability to transition out of a configuration can be different from the probability to transition into it. This has the consequence that the simulation is not guaranteed to end up simulating the desired probability distribution, hence

$$P_{C_i} = \sum_j P_{C_j} W(C_j \to C_i), \tag{2.122}$$

is not necessarily an equilibrium of the dynamics. In particular, if our system can be described through the partition function

$$Z = \sum_{\mathcal{C}} e^{-\beta S(\mathcal{C})}, \tag{2.123}$$

with $\mathcal{C}$ the set of configurations, then we would like the probability for the system to equilibrate to a certain configuration, C_i, to be given by

$$P_{C_i} = \frac{e^{-\beta S(C_i)}}{Z}. \tag{2.124}$$

Whether or not this is indeed the case will depend on the set of update moves and the transition amplitudes between configurations.

A well-known algorithm which satisfies the condition of detailed balance above, is the Metropolis algorithm. Here the trial probability proposal between two configurations are chosen to be the same, i.e., $T(C_i \to C_j) = T(C_j \to C_i)$ (which is generically the case for update moves that are local). Detailed balance then reduces to the condition

$$\frac{A(C_i \to C_j)}{A(C_j \to C_i)} = \frac{P_{C_j}}{P_{C_i}} = e^{-\beta(S(C_j) - S(C_i))}, \tag{2.125}$$

where we explicitly plugged in the equilibrated probabilities in terms of the partition function. We are then free to scale up the acceptance probabilities by a common factor, such that the largest of the two is equal to 1 (this is by definition the largest value, since we are dealing with probabilities here). There is no profound reason for this scaling other than that it generates a speed up in the simulations. Since the ratio between the acceptance probabilities and the equilibrated probabilities needs to remain constant, we can write for the acceptance probability of a Metropolis step

$$A_M(C_i \to C_j) = \min\left[1,\, \frac{P_{C_j}}{P_{C_i}}\right] = \min\left[1,\, e^{-\beta(S(C_j) - S(C_i))}\right]. \tag{2.126}$$

Hence, configurations with $S(C_j) < S(C_i)$ are entropically favoured and result in an acceptance probability of 1.

For the generation of dynamical triangulations, the configurations C_i are the triangulated manifolds, weighted by the Regge action for pure (dynamical) gravity or by both the Regge action and an additional matter action, see Chpt. 2.2.6.

In addition, it can be shown that in $d = 4$ dimension, the Pachner moves are only ergodic if the total four-volume can fluctuate. To incorporate this, one can include a term $\delta\lambda|N_4^f - N_4|$ for small $\delta\lambda$, such that fluctuations around the target four-volume N_4^f are small and errors due to this term are found to be small (this can be tested by varying $\delta\lambda$) [282].

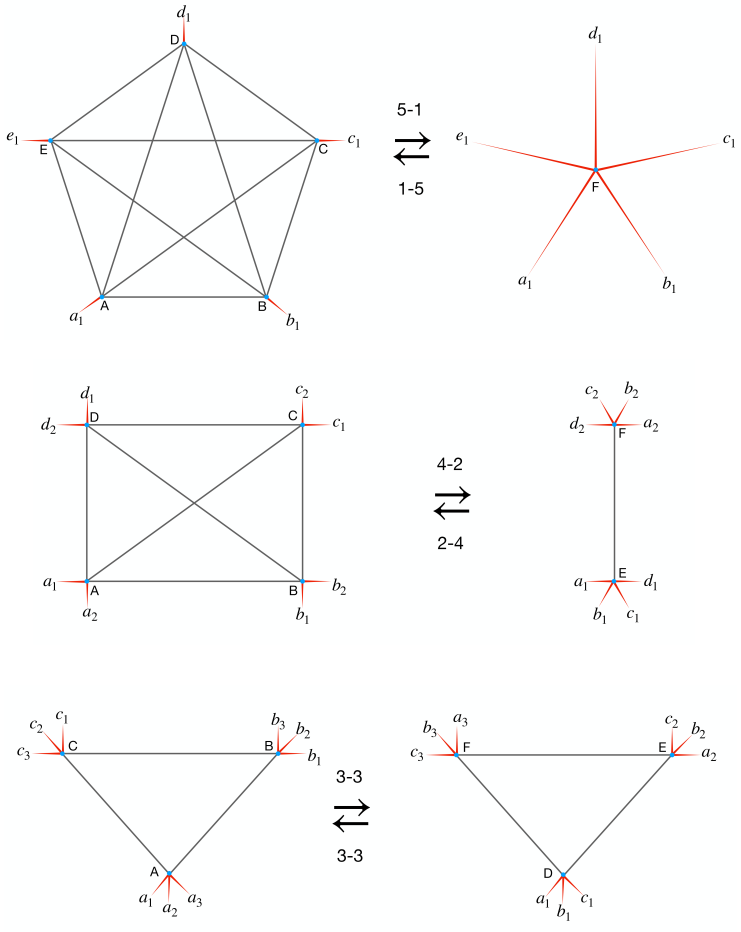

Figure 2.21: Pachner moves in 4 dimensions on the dual lattice. The vertices of the dual lattice correspond to the 4-simplices on the regular lattice and are labelled (A, B, C, ...) here. The 3-simplices (tetrahedra) are represented as links on the dual lattice (a_1, b_1, c_1, ...). Note that the external tetrahedra (red lines) remain intact under all moves.

Chapter 3

Causal Set Theory

Causal Set Theory (CST) [105] is in some sense the most minimalistic under the broad range of approaches to quantum gravity. It demands that a Planck-scale description of spacetime should above anything else respect causality and posits that in a finite region of spacetime only a finite number of events can occur. As a direct consequence of the latter, CST is a *fundamentally* discrete quantum-gravity model. By "fundamental", we mean that CST interprets the discreteness as a physical property of the short-distance description of spacetime, in contrast to approaches such as Causal/Euclidean Dynamical Triangulations, where the discretisation is used as a regularisation procedure and physics is expected to be recovered once the "right" continuum limit is taken. In CST, no continuum limit is taken and low-energy continuum spacetime is interpreted as a mere approximation to the fundamentally discrete setting. For reviews see [302, 303, 304, 305, 306, 307, 308].

Mathematically, a causal set, $\mathcal{C}$, is a locally finite and partially-ordered set (poset) of elements (spacetime events) where the ordering relation $\prec$ is given by the causal relations between different set elements, i.e., $x \prec y$ is translated to: the event x occurs to the causal past of the even y. Specifically, for any three events in a causal set, x, y, $z \in \mathcal{C}$, the following conditions have to be satisfied

$$\begin{aligned} &\text{i) Transitivity: } x \prec y \text{ and } y \prec z \Rightarrow x \prec z, \\ &\text{ii) Acyclicity: } x \prec y \text{ and } y \prec x \Rightarrow x = y, \end{aligned} \tag{3.1}$$

where the second condition ensures that no time-like loops can be formed, i.e., the acyclicity puts the "causal" in causal sets and equips them with a *partial* order relation. In addition to the conditions above, local finiteness is enforced by demanding that the *Alexandrov* interval between any two elements in $\mathcal{C}$ is finite, i.e., $\text{card}\{z \in \mathcal{C} \,|\, x \prec z \prec y\} < \infty$, cf. Fig. 3.1. This final condition bears resemblance to the compactness condition satisfied by globally-hyperbolic spacetimes which, heuristically, allows one to stitch together local properties of each spacetime point to extract global information. Note that it is exactly the compactness condition which in continuum settings protects spacetime from naked singularities.

The necessity of local finiteness in its current form is still a point of discussion. In particular, anti-de Sitter spacetime is not globally hyperbolic, but otherwise causally well-behaved, [309] With

the definition given above, discrete causally-ordered posets that are derived from anti-de Sitter do currently not classify as causal sets and are therefore not included in the causal-set configuration space. To be more precise, the causal-set path integral

$$Z_{CST}(\Omega) = \sum_{\mathcal{C}\in\Omega} e^{\frac{i}{\hbar}S_{CST}(\mathcal{C})}, \tag{3.2}$$

consists of the sum over *all* causal sets, $\mathcal{C}$, weighed by a discrete, fundamental action $S_{CST}(\mathcal{C})$. Note that in principle there could be a non-trivial measure term to account for any over-counting of configurations or/and breaking of symmetries.

Let us emphasise the fundamental difference between the lattice discretisation techniques discussed earlier and CST. First and foremost, the causality requirements, summarised in Eq. (3.1), give rise to a much broader class of configurations then a global time-foliation condition (as in CDT) does[1]. In fact, it allows for structures that do not bear any resemblance to continuum spacetime whatsoever, as we will discuss in more detail below. The configuration space, Ω, then contains all possible causal sets and there is no restriction on any emergent properties such as topology or dimension, or even whether any form of geometry can be extracted. A further consequence of the causality condition is that there is no sensible Euclidean version of the causal-ordering relation between spacetime events. Consequently, there is no causal set implementation of a Wick rotation, i.e., a continuation along the lines "$\prec \to \prec_E$" is not well-defined. CST aims then to provide a fundamentally (local) Lorentzian description of spacetime and with that distinguishes itself from other approaches to quantum gravity.

The properties listed above are all on the level of the kinematics of the theory, but do not provide any guidelines for the underlying microscopic dynamics which should ultimately reproduce the observable universe. Lattice theories such as (C/E)DT, Chpt. 2.2, treat the lattice discretisation merely as a tool, ultimately to be removed through a suitable continuum limit at a critical point in theory space. At this critical point, the theory becomes scale invariant and signals that macroscopic physics is independent of the microscopic details of the theory and hence, the exact regularisation method. In the case of CST, the discreteness is *fundamental*[2]. As a direct consequence there is no critical point which dictates what set of parameters defines the microscopic theory. Without such a guiding principle, the fundamental action, $S_{CST}(\mathcal{C})$, can be chosen in infinitely many different ways and hence, the theory has no predictive power. We emphasise that the existence of a critical point is just one particular way in which one can fix the dynamical properties of a theory. One way or another, if CST is to provide a fundamental description of spacetime, then there necessarily should be some principle through which one fixes the dynamics.

It should be noted that there is a CST version of the Einstein-Hilbert action, dubbed the *Benincasa-Dowker* action, S_{BD}, [312, 313, 314], see Chpt. 3.3.2. Even though there is *a priori* no reason to identify the fundamental action, S_{CST}, with S_{BD}, it is a natural choice from a continuum point of view and it is possible there exists a mechanism which naturally selects S_{BD} as the microscopic action.

[1] It can be shown that the demand of a well-defined partial causal ordering necessarily require a Lorentzian metric signature. In particular, a metric $(-,-,+,+)$ does not give rise to a well-defined partial causal order [310].

[2] There has been recent work proposing to use the causal set as a Lorentzian discretisation of spacetime [311].

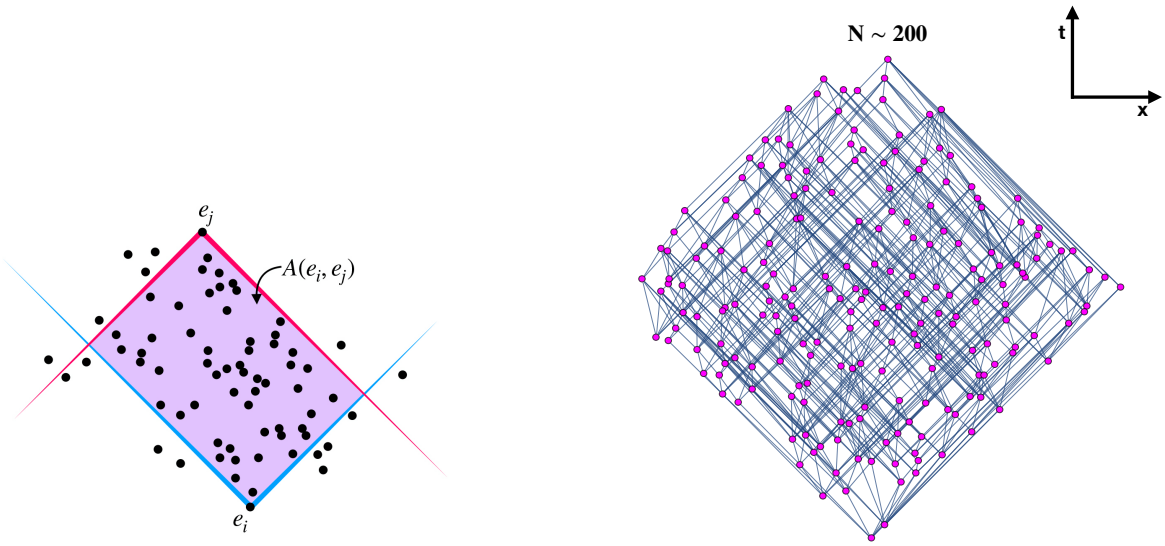

Figure 3.1: Left: The Alexandrov interval $A(e_i, e_j)$ between the elements e_i and e_j in $(1+1)$-dimensional Minkowski spacetime. Right: A causal set of approximately 200 elements obtained from a sprinkling into $(1+1)$-dimensional Minkowski spacetime is shown. Nearly all links (blue lines) between elements (pink dots) lie close to the light cone in the frame chosen above.

In the following sections we will motivate the causal-set approach in Chpt. 3.1 and discuss the consequences of the proposed fundamentally discrete, causal paradigm. Since the lack of a natural choice for the underlying dynamics is a clear weakness of the theory, we will discuss in detail some of the work that has been done in the direction of CST dynamics in Chpt. 3.2. Finally, we will give a detailed account on the formulation of specific geometric quantities. In particular, we will formulate a notion of spatial distances in Chpt. 3.3.3, which paves the way for the construction of two dimensional estimators: the Hausdorff dimension, Chpt. 3.3.4 and the spectral dimension, Chpt. 3.3.5.

3.1 Motivation

CST operates under the assumption that a theory of quantum gravity should describe geometry in the vicinity of the Planck scale, much like GR describes geometry at macroscopic scales. The large-scale description of geometry is entirely captured by the metric tensor and determines the motion of a particle through spacetime as well as the dynamics of spacetime itself. An interesting question is then how one could recover the metric degrees of freedom without relying on a mathematical framework such as differential geometry. To answer this, it is instructive to remember what physical information is carried by the metric. Naively, the metric gives a notion of spacetime volume and specifies the local light-cone structure at a given spacetime point. These notions were made exact in [315, 316], where it was shown that the causal-ordering relations endowed on spacetime are enough to extract the local light-cone structure of a continuous spacetime. Under certain assumptions, i.e., that of faithful embedding, this result can be shown to hold for causal sets as well [309]. The causal

ordering relations alone are then enough to extract a conformal metric, but give us no notion of length or volume. This is where discreteness comes in [105]. In a continuous spacetime there is no natural way to determine the conformal factor. A discrete spacetime, however, does not suffer from this problem since the spacetime volume of a certain region can be extracted from the number of elements within this region. For this reason, the CST program can be described by the slogan "Order + Number = Geometry" [310, 302].

We have argued that CST is a quantum-gravity candidate, founded in part on the assumption that spacetime is discrete close to the Planck scale, but so far it has not been made explicit at which point the Planckian nature enters exactly. The only notion of scale at hand is that of a spacetime volume, V, which is directly associated with the number of elements N as $V \equiv V_N \sim N V_1$. However, without specifying the unit volume, V_1, associated with a single element, it would only be possible to obtain information on the relative volume of a region. Since the unit volume carries information on the discreteness scale, ℓ, and causal-set quantum gravity was designed to describe spacetime at Planckian scales, the fundamental discreteness scale should be of Planckian order. Then $\ell \sim \ell_{Pl}$ and $V_1 = V_{Pl}$.

Despite the fact that very few assumptions go into the construction of causal-set quantum gravity, the approach is usually regarded as radically different from other approaches. Since this is largely due to the assumption of fundamental discreteness, it is instructive to motivate the discreteness condition.

3.1.1 Black-hole entropy

The original argument for fundamental discreteness comes from the so called Bekenstein-Hawking entropy of a black hole, which can be derived from the four laws of black hole thermodynamics [317].

The four laws were derived as an analogue to the laws of thermodynamics

$$\begin{aligned}
&\textbf{0}^{\textbf{th}}\ \textbf{law:} && \text{The temperature } T \text{ is constant throughout a system in equilibrium,}\\
&\textbf{1}^{\textbf{st}}\ \textbf{law:} && \text{Energy is conserved in an isolated system: } dE = T\,dS - p\,dV,\\
&\textbf{2}^{\textbf{nd}}\ \textbf{law:} && \text{Entropy cannot decrease: } dS \geq 0,\\
&\textbf{3}^{\textbf{rd}}\ \textbf{law:} && \text{The temperature } T \text{ cannot be reduced to absolute zero in a finite process.}
\end{aligned} \tag{3.3}$$

The original laws of black hole thermodynamics were formulated in terms of the surface gravity, κ, and the event horizon area, A. The most obvious analogue was noticed when Hawking showed that (classically) the area of the event horizon cannot decrease in any process [318], that is $dA \geq 0$, similar to the 2^{nd} law of thermodynamics. Hints towards a correspondence between κ and temperature were presented by the observation that κ is constant over the event horizon in an equilibrium setting, i.e., for a stationary black hole, and thus shares an important property with the temperature represented by the 0^{th} law. Additionally, as a consequence of the *no hair* theorem

[319] [3], the black hole horizon area A must be written as $A = A(M, Q, J)$ with M, Q, J the mass, charge and angular momentum of the black hole. The first law of black hole thermodynamics states then

$$dM = \frac{\kappa}{8\pi G}\, dA - \Omega\, dJ - \Phi\, dQ, \tag{3.4}$$

with Ω the angular velocity and Φ the electrostatic potential. The change in J and Q represent work done on the black hole by its environment, similar to the work done $p\, dV$ in the 1^{st} law of thermodynamics. Note that in the presence of stationary matter outside the black hole, the right-hand side of Eq. (3.4) may include more terms.

Comparing Eq. (3.4) to the first law of thermodynamics, it is hard to miss the similarities between the surface gravity, κ, and area, A, of the event horizon of the black hole with the temperature T and entropy S of a thermodynamic process. Bekenstein suggested that the apparent similarities were more than just that, and conjectured a one-to-one relationship between the area and surface gravity of a black hole with its entropy and temperature [320]. To do so, multiple issues needed to be resolved, arguably the most obvious one is that entropy is a dimensionless quantity whereas area is not. Additionally, in thermodynamics it is the total entropy which is non-decreasing, contrary to the area of the horizon which is independently non-decreasing. When Bekenstein tried to address these apparent inconsistencies, he was naturally led to the inclusion of quantum theory. Specifically, based on the notion that an increase in entropy can equivalently be viewed as an increase in information, Bekenstein suggested that entropy should be measured in terms of "bits of entropy" and hence, area increases in "bits of area". Associating the minimum increase of area with a minimum increase in entropy, one finds on dimensional grounds that a bit of information is inversely proportional to ℓ_P^2. Moreover, he wrote down a generalised second law which includes the entropy external to the black hole: $dS_{BH} + dS_{ext} \geq 0$ where $S_{BH} = \alpha\, \frac{k_B\, A}{4\pi\, \ell_P^2}$ and α a constant of proportionality.

The exact factor α was uniquely determined when Hawking showed that black holes radiate [321] with a temperature $T_{BH} = \frac{\kappa}{4\pi}$, leading to the famous Bekenstein-Hawking entropy

$$S_{BH} = \frac{k_B\, A}{4\ell_P^2}, \tag{3.5}$$

and the realisation that the horizon area can in fact decrease. In particular, if one tries to write down the area of the horizon in terms of the available black-hole microstates, then the idea that each Planck-sized patch of the horizon carries one "bit" of information comes naturally. Then the total number of microstate configurations is $N_m = 2^{\Omega}$ where $\Omega \sim A/\ell_{Pl}^2$ and hence, $S \sim k_B \ln \Omega \sim k_B A/\ell_{Pl}^2$, suggesting that the Planck-area (and consequently the Planck-length) sets a minimum area (length) scale in which area (length) should be measured. If the area of the horizon of a black hole is in fact discrete, then one necessarily concludes that spacetime itself is discrete. It should be noted that the argumentation above relies on semi-classical physics and, hence, holds under the assumption that quantum gravity does not induce additional contributions to Hawking radiation. However, even if close to the Planck scale a modified expression for S_{BH} holds, if the no

[3] A black hole can be completely described in terms of its mass, charge and angular momentum.

hair theorem still goes through then it is hard to imagine an entropy which is not proportional to the area and, hence, requires factors of ℓ_{Pl}^2 for dimensional reasons.

For completeness, the four laws of black hole thermodynamics can be summarised as

$$\begin{aligned}
&\textbf{0}^{\textbf{th}}\ \textbf{law:}\ \text{The temperature } T_{BH} \text{ is constant over the horizon of a stationary black hole,}\\
&\textbf{1}^{\textbf{st}}\ \textbf{law:}\ dM = T_{BH}\, dS_{BH} - \text{work},\\
&\textbf{2}^{\textbf{nd}}\ \textbf{law:}\ dS_{BH} + dS_{ext} \geq 0,\\
&\textbf{3}^{\textbf{rd}}\ \textbf{law:}\ \text{The temperature } T_{BH} \text{ cannot be reduced to absolute zero in a finite process.}
\end{aligned} \tag{3.6}$$

Here the 3$^{\text{rd}}$ law can be reinterpreted as the cosmic censorship conjecture, since a decrease in T_{BH} corresponds to decreasing κ and consequently the mass and radius of the black hole. If one was able to shrink the horizon of a black hole down to zero, then a naked singularity would present itself. Note that in the limit $\hbar \to 0$, the black-hole entropy diverges and the second law reduces again to its classical counter-part: $dA \geq 0$.

3.1.2 The causal consequences of Lorentz invariance

One of the cornerstones of causal-set theory is the preservation of (local) Lorentz invariance. This translation of Lorentz invariance at macroscopic scales into causality at the Planck scale directly leads to a notion of non-locality. The manifestation of this non-locality presents itself most clearly when one tries to associate a notion of nearest neighbours to a causal set element. On a regular d-dimensional lattice, the set of nearest neighbours of a lattice point is most straightforwardly defined as those points that lie at a *spatial* distance of one lattice spacing, a, from said point. In the case of CST the notion of a spatial distance is not readily available. For one possible construction see Chpt. 3.3.3. Staying in line with the concept of spacetime rather than that of space *and* time, we define the causal future and causal past of e as $J^+(e) \equiv \{c \in \mathcal{C} \,|\, e \prec c\}$ and $J^-(e) \equiv \{c \in \mathcal{C} \,|\, c \prec e\}$, respectively. An element n is then a nearest neighbour of e if $n \in J^+(e) \cup J^-(e)$ and the Alexandrov interval between them is empty: $\text{card}\{z \in \mathcal{C} \,|\, e \prec z \prec n \text{ or } n \prec z \prec e\} = 0$. In that case, we say that e and n share a *link*. Note that due to the transitivity of the causal ordering, the set of links yields the irreducible relations of the causal set.

In a more intuitive phrasing, two spacetime events, e_1 and e_2, are linked if one of them could have been influenced *directly* by the other one. When we say directly, we mean there does not exist any other event, e_3, which satisfies $e_1 \prec e_3 \prec e_2$, as this would indicate an indirect influence of the event e_1 on e_2 through e_3. Note that in such a setting where e_1 and e_3 are neighbours and e_3 and e_2 are neighbours one can think of e_1 and e_2 as being next-to-nearest neighbours.

Defining the set N_e of nearest neighbours of e as those elements that share a link with e, we still end up with a large and possibly infinite set of nearest neighbours. Specifically, for a finite causal set $\mathcal{C}$ approximated by d-dimensional Minkowski spacetime, the number of links grows as $\sim N^{\frac{d-2}{2}}$ [322] with N the number of elements in the causal set. Clearly this quantity diverges in the $N \to \infty$ limit. Now the non-locality will present itself in a two-fold way. First, when discretising a

continuum operator which extracts information based on nearest neighbour relations. An example would be the discrete d'Alembertian

$$D\Phi(n_i) = \sum_{n_{i+1}} \Phi(n_{i+1}) - \Phi(n_i), \tag{3.7}$$

where n_{i+1} corresponds to the set of nearest neighbours of n_i. On a causal set the number of nearest neighbours n_{i+1}, can be arbitrarily large and diverges in the $N \to \infty$ limit. A second, perhaps more intuitive, notion of non-locality, is that nearest neighbours of any element, e, lie almost exclusively close to the past and future light-cones of e in any given frame. Since these elements are near-null, the spatial separation between nearest neighbours can be arbitrarily large in any given frame.

Notice that we could employ a similar definition of spacetime-nearest neighbours on a regular lattice by choosing a more suitable lattice to reflect the properties of spacetime rather than just space. For instance, to simulate the light-cone structure of $\mathbb{M}^2$, the simplest construction would be a 2-dimensional lattice build up from isosceles, right triangles, i.e., triangles with internal angles $\pi/2, \pi/4, \pi/4$. Keeping in line with the definition of nearest neighbours via the links procedure, we find that every element still only has four nearest neighbours at fixed lattice spacing ${a_T}^4$. The key difference between such a lattice discretisation and a causal-set type of discretisation lies exactly in the random nature of the latter. Since Lorentz invariance dictates that there can not be a preferred frame of reference we must not impose a fixed background structure on the causal set. Consequently, we find that on average, the nearest neighbours of a causal set element do not lie exactly on the light-cone, but rather arbitrarily close to it, cf., Fig. 3.1. Thus, while the local nature of such a triangular lattice results in both intuitive and technical simplifications, the price to pay is the loss of local Lorentz invariance.

A natural question to ask at this point is whether or not such a minimalistic theory is actually able to capture continuum physics. More specifically, since the continuum manifold is thought of as an approximation to the more fundamental causal set, the question is whether one can indeed obtain a Lorentzian manifold by approximating a causal set. If answered in the affirmative, then such a causal set is called "manifold-like" and its properties are captured by the so called "Hauptvermutung" of causal sets, which states that a manifold-like causal set carries the same information as the continuum manifold up to the discreteness scale, ℓ. To check for manifold-likeness, we need to specify a procedure to relate a causal set to a continuum manifold. To this end it is convenient to introduce the notion of an embedding.

For (M, g) a Lorentzian, globally hyperbolic spacetime and $(C, \prec)$ a causal set, we can define a mapping, $f : C \to M$, which embeds C into M [5]. If C and M are to contain the same information, then we should be able to find an embedding which respects the causal ordering, i.e., for $\forall x, y \in C$ if $x \prec y$ then $f(x) \in J^-(f(y))$. Next to the causal ordering we also want to preserve the spacetime volume, meaning that the local volume element needs to be conserved under Lorentz transformations. This can be accomplished by randomly selecting spacetime points on M following

[4] Note that the lattice spacing a_T represents a spacetime distance. If one employs the Minkowski metric to calculate this spacetime distance then, strictly speaking, nearest neighbours lie at a distance $a_T = 0$ from one another.

[5] Note that we slightly abused notation by referring to the spacetime (M, g) and causal set $(C, \prec)$ as M and C respectively.

the Poisson distribution. Specifically, the probability of finding N points distributed with density $\rho = \frac{1}{\ell^d}$ in a spacetime volume V is given by the Poisson distribution

$$P(N) = \frac{(\rho V)^N}{N!} e^{-\rho V}. \tag{3.8}$$

The selection of elements from M according to the Poisson distribution is referred to as a *sprinkling* of the corresponding spacetime. It can be shown that individual causal sets obtained through a sprinkling of Minkowski spacetime are Lorentz invariant [323]. Lastly, since the fundamental length scale ℓ sets the discreteness scale, it should be much smaller than the characteristic length scale over which the continuum geometry of M varies, e.g., for a spacetime with a characteristic length scale given by a curvature radius R we need $R \gg \ell$ if we want C to capture these curvature effects. If the embedding f satisfies these three conditions, then we say that f is a *faithful embedding* and the causal set C is manifold-like.

Consequently, if a causal set C can be faithfully embedded in two spacetimes (M, g) and (M', g') at the same density, ρ, then there has to exist an approximate isometry between the two spacetimes (i.e., metric distances are preserved). This is exactly what the Hauptvermutung of CST conjectures and the causal set program hinges on. In contrast, if it were possible to find distinct features of (M, g) and (M', g') at scales significantly *larger* than the discreteness scale, then C alone would not be enough to sufficiently capture all continuum information contained in (M, g).

It is automatically clear that when one uses a Poisson process to select finitely many points of a globally hyperbolic spacetime at random, this will yield a causal set with the desired discreteness scale and Number$-$Volume $(N-V)$ correspondence. The causal relations are simply handed down from the spacetime to the causal set. It should be emphasised that the sprinkling procedure is by no means a physical process but rather a tool which allows the construction and study of manifold-like causal sets.

Now that we have defined a process which yields the desired Lorentzian nature of interest in CST, let us briefly revisit the idea of a fixed background structure. It is possible that the triangular lattice is just a poor choice and that there may very well exist a structure which preserves local Lorentz invariance and possesses appealing qualities such as finite valency. In [324] so called *Lorentzian lattices* were studied for exactly this reason. These lattices are by construction invariant under a discrete subgroup of the Lorentz group. Specifically, we represent a point of the d-dimensional lattice as $X = n^{(d)}\xi_{(d)}$, written in terms of the integers $n^{(d)}$ and the lattice generators $\xi_{(d)}$. If Λ is an element of the discrete Lorentz group then one demands that

$$\Lambda X = m^{(d)}\xi_{(d)} \equiv X', \tag{3.9}$$

is a point on the lattice as well, i.e., the lattice transforms into itself. In two dimensions we consider the generator Λ, corresponding to boosts and write the timelike and spacelike generators of the lattice as

$$\xi_0 = \epsilon(\cosh\phi, \sinh\phi) \quad \text{and} \quad \xi_1 = \delta(\sinh\theta, \cosh\theta), \tag{3.10}$$

with $\epsilon, \delta > 0$. By requiring that $\Lambda X = X'$, one obtains a set of relations between δ, ϵ, ϕ and θ that defines a set of Lorentzian lattices. The performance of these lattices can be tested by

using the invariance of the local volume element under Lorentz transformations as criteria. It turns out Lorentzian lattices perform better than Poisson sprinklings in preserving the volume-to-number correspondence in $\mathbb{M}^2$. However, the extension to higher dimensions introduces additional directions along which a boost may occur, which leads to a poor conservation of the spacetime volume. Additionally, such a lattice will not be invariant under the full continuum Lorentz group in any dimension, signalling a clear preference for sprinklings over these type of Lorentzian lattices.

Ideally, one would like to obtain a collection of properties derived from sprinkled spacetimes, such that for any given causal set the study of these properties is enough to conclude whether or not the causal set is manifold-like. However, this suggests that it is possible to uniquely distinguish between manifold-like and non-manifold-like causal sets using only the causal relations and volume as input. Clearly this is a non-trivial task but progress has been made in this direction, at least for certain sub-classes of causal sets, Chpt. 3.3 .

3.2 Dynamics

Irrespective of whether spacetime is discrete at the Planck scale, at larger scales the universe can be described as a continuous manifold. This suggests that from all the causal sets contributing to the path integral, only those that can be approximated by smooth, continuous 4-dimensional manifolds can make a significant contribution. It is thus crucial to know what the properties are of those causal sets dominating the path integral.

Ignoring the exact expression for the fundamental action for now, the configuration space Ω can be studied to obtain qualitative information on the different classes of causal sets that are included. Let us then naively propose that all causal sets contribute with equal weight. In this case, it can be shown that the class of causal sets which are *not* manifold-like, will dominate the path integral. More specifically, it was shown by Kleitman and Rothschild [325] that a partial order of N elements typically consists out of three "time steps" with approximately $N/4$ elements in the first and third layers and $N/2$ in the middle layer. Each element in the middle layer has probability $1/2$ to share a link with an element in the top and bottom layer, cf. Fig. 3.2. It can be shown that the number of KR orders grows as $\sim 2^{N^2/4}$ such that in the limit $N \to \infty$, the probability of finding a causal set which is not a KR order vanishes. This was dubbed the "entropy problem" in CST. Moreover, numerical studies have found that for causal sets as small as $N \approx 80$, the KR orders constitute approximately 90% of the configuration space [326]. In order for CST to be a viable quantum-gravity candidate, one thus necessarily needs a non-trivial action such that causal sets that are not manifold-like, e.g., KR orders, interfere destructively in the path integral. A first step in this direction was done in [327], where the authors showed that given the Benincasa-Dowker action, 2-layered causal sets (i.e., there are no $x, y, z \in \mathcal{C}$ such that $x \prec y \prec z$) are in fact suppressed.

As a toy-model, we may consider 2-dimensional spacetime to study the entropic behaviour of the path integral. Since in $d = 2$ the Ricci scalar becomes a topological invariant, one might hope that the entropy problem is easier to address on the corresponding causal sets. One would like to study a class of causal sets which contains both manifold-like as well as non-manifold-like causal sets. This introduces additional complications since the notion of dimension cannot be

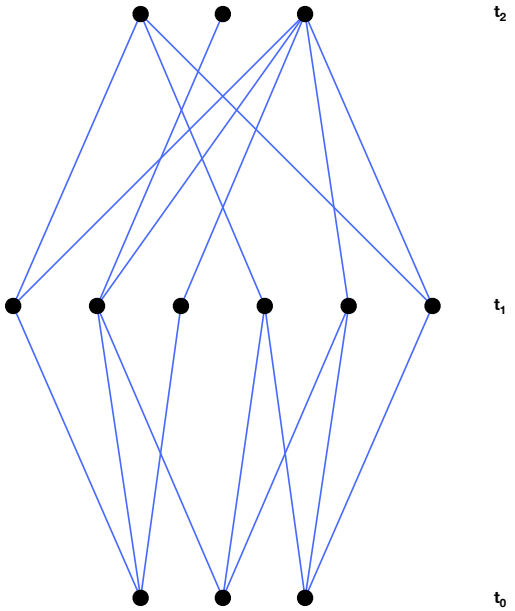

Figure 3.2: A causal set of $N = 12$ elements which falls in the class of KR orders. There are about $N/4$ elements in the bottom and top layer and $N/2$ in the middle layer. The bottom layer is linked to about half of the elements in the middle layer which is in turn linked to roughly half of the element sin the top layer.

derived from continuum considerations on non-manifold like causal sets. Instead, one can identify a subset of causal sets, dubbed "2D orders", which consists of manifold-like causal sets that imbed faithfully into conformally flat 2D intervals, but also contains non-manifold like causal sets [328]. This class is referred to as the 2D orders and it can be shown that they indeed exhibit a trivial spatial topology [328, 329]. A 2D order is a causal set which is constructed from the intersection of 2 linear orders, where a causal set, $\mathcal{C}$, is said to be a linear order when $\forall e_i, e_j \in \mathcal{C}$ either $e_i \prec e_j$ or $e_j \prec e_i$ (i.e., $\mathcal{C}$ admits a complete ordering). For example, for two causal sets $\mathcal{C}_1, \mathcal{C}_2$ with order relations $\{e_1 \prec e_2 \prec e_3 \prec e_4\}$ and $\{e_2 \prec e_3 \prec e_1 \prec e_4\}$, respectively, the intersection $\mathcal{C}_1 \cap \mathcal{C}_2 = \{e_2 \prec e_3 \prec e_4, e_1 \prec e_4\}$ is a 2D order (which itself does not need to be a linear order), cf. Fig. 3.3. Surprisingly, it was found that for this class the manifold-like causal sets grows as $N!/2$ and dominate over the non-manifold-like ones in the large-N limit. Of course this does not simply generalise to 4 dimensions, but it is nevertheless encouraging that two-dimensional Minkowski spacetime arises naturally.

The question remains whether one can obtain a mechanism through which the dynamics of CST can be obtained. Here we will concern ourselves with exactly that question, starting from the *classical* dynamics. In particular, we will first focus on how one "grows" a causal set through so called sequential growth models, Chpt. 3.2.1, proposed in [330]. In the original formulation, these models are classical (semi-classical at best) but nevertheless provide an intuition which might be useful for the more general quantum dynamics. At the very least one might argue that classical GR should be hiding in these classical growth models, under the (strong) assumption that the classical growth models appear as some low-energy limit of the currently unknown quantum dynamics.

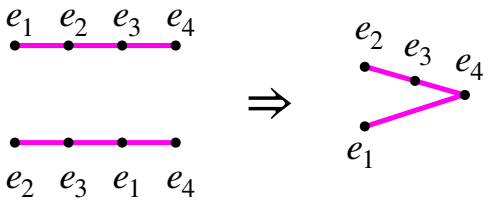

Figure 3.3: An example of a 2D order constructed out of two 1D orders. The solid, magenta, lines indicate a link and "time" can be taken to point from left to right, such that for both 1D orders, the element e_4 is to the future of all other elements.

Secondly, for a specific sub-class of sequential growth dynamics, named originary-percolation dynamics, the causal set goes through eras of expansion and contraction as it is grown, cf. Chpt. 3.2.2. As the causal set is thought of as spacetime itself, this type of behaviour hints towards a possible cosmological scenario and has been studied in exactly this context [331, 332, 333, 334].

Some work has been done into formulating a quantum version of these sequential growth models, Chpt. 3.2.3, which mainly focusses on generalising a stochastic measure theory to a quantum measure theory [335, 336, 337, 338]. Providing a physical interpretation turns out to be challenging on account of technical difficulties as well as the generalisation of classical concepts.

Lastly, the dynamical formulations listed above use a *bottom-up* type of approach, in the sense that one makes an *ansatz* for the dynamical generation in the deep UV and tries to match the resulting theory to observation at some experimentally accessible scale. Alternatively, one could handle the issue in a *top-down* manner, by assuming that the form of the microscopic action is the same as that of the macroscopic action, namely the Benincasa-Dowker (BD) action (the causal-set analogue of the Einstein-Hilbert action), cf. Chpt. 3.2.4. Given a form of the action, one can then attempt to evaluate the path-integral numerically via Monte Carlo methods. It should however be mentioned that there is *a priori* no reason to promote the BD action to a fundamental action. Especially, since CST does no attempt at taking a continuum limit, one cannot rely on universality arguments to motivate the specific form of the action.

3.2.1 Sequential growth models

To generate a consistent dynamics, sequential growth models introduced in the causal-set context [330, 331, 333, 334], are required to satisfy a set of three conditions. The first one demands an internally consistent time evolution, meaning that the dynamical evolution of a causal set needs to be future directed, such that the birth of a new element cannot in any way influence the past (hence, *sequential* growth). This condition essentially enforces the intuitive notion that present events will not change the past.

Secondly, the order in which one grows the causal set should not have any consequence for the probability of creating a specific N-element causal set. Basically, this boils down to the statement

that the physics is independent of the external time parameter through which the set was grown and can be thought of as a form of discrete diffeomorphism invariance.

Lastly, the probability of adding an element to the future of some sub-set (the ancestors), should not directly depend on the set of elements to which it is not related (the "spectator set"). This was called the (classical) Bell causality and it can be made explicit in the following way: let $P(C_N \to C_{N+1})$ denote the transition probability from a specific N-element causal set C_N to a specific $(N+1)$-element causal set C_{N+1} and let $P(C_N \to C'_{N+1})$ be the transition probability to some other $(N+1)$-element causal set. Since the transition probabilities should not depend on the spectators, we may write $P(\widetilde{C}_M \to \widetilde{C}_{M+1})$ and $P(\widetilde{C}_M \to \widetilde{C}'_{M+1})$ where now $\widetilde{C}_M$ represents the set C_N with all spectators removed and $M < N$. Then we find

$$\frac{P(C_N \to C_{N+1})}{P(C_N \to C'_{N+1})} = \frac{P(\widetilde{C}_M \to \widetilde{C}_{M+1})}{P(\widetilde{C}_M \to \widetilde{C}'_{M+1})}, \tag{3.11}$$

such that the likeliness of one transition over the other does indeed not depend on the spectator sets.

Arguably one of the simplest models to dynamically generate a causal set is that of transitive percolation. Here one starts with a set of N labeled elements and introduces a link between all $\frac{N(N-1)}{2}$ pairs with some probability $p \in [0,1]$. Transitivity is then enforced by demanding that if $i \prec j$ and $j \prec k$, then $i \prec k$. Obviously this procedure will not produce a single N-element causal set, but rather yield a distribution. The next step would be to assign a weight to each member of the distribution and this is where the difficulty lies. As discussed above, the KR-orders will dominate in the $N \to \infty$ limit, in particular, the number of KR-orders grows exponentially with $\sim 2^{N^2/4}$. To counteract this growth, one would necessarily need the dynamics to be such that the action grows (at least) quadratically with energy (this already rules out the use of a Boltzmann-type of distribution, as this would yield a linear growth with energy). Due to the inherently non-local nature of causal sets, it is certainly feasible that CST indeed features such an action. The generating process described above clearly does not in any way distinguish between elements, in the sense that the future and past of an element are assigned independently. Consequently, the resulting causal sets will be best approximated by maximally symmetric spacetimes, i.e., Minkowski or de Sitter[6]. The *growth* of an $(N+1)$-element causal set from N elements through transitive percolation can then be described as a Markov process: one adds a single element which is necessarily either unrelated or to the future of an existing element[7] cf. Fig. 3.4.

The transitive percolation model described above has been used to search for the existence of a continuum limit [331]. This line of thinking was motivated by the observation that while physics is (presumably) discrete at the Planck scale, one might expect there to be some limit in which classical gravity is recovered. In this case, the continuum limit corresponds to a critical point one needs to tune to in parameter space. For the transitive percolation model, there are two such parameters: the probability p and the number of elements, N. Similar to C/EDT, the continuum is expected

[6] Anti de Sitter falls within the class of maximally symmetric spacetimes as well but, as mentioned earlier, posets approximating AdS are not locally finite and therefore do not fall in the class of causal sets.

[7] If we would allow the addition of elements to the past of existing elements, then one could grow posets which are not locally finite in the $N \to \infty$ limit.

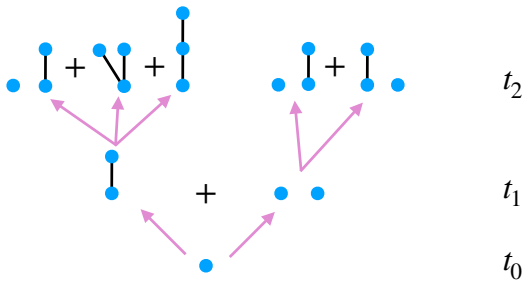

Figure 3.4: We illustrate three steps of a transitive percolation model. At each step the new element is either unrelated or born to the future of an existing element.

to be recovered in the infinite-volume limit, that is $N \to \infty$. The authors of [331] considered the critical point $p = 0$, $N \to \infty$, i.e., an infinitely large chain where none of the elements are related. Since moving away from this point noticeably changes the characteristics of the causal set, it can be argued that a phase-transition occurs at this point. The tuning of parameters to a critical point requires the introduction of concepts along the lines of a renormalisation flow and running couplings. In causal-set language, there is a natural way to give meaning to these concepts through the process of coarse graining.

In a causal-set context, the coarse graining of a manifold-like causal set, $\mathcal{C}$, can be performed by randomly selecting a sub-set of elements from $\mathcal{C}$. This sub-set, $\mathcal{C}'$ is a causal set itself with its causal relations inherited from $\mathcal{C}$. Since the coarse-graining procedure is random, there are many ways to coarse grain an N-element causal set down to an N'-element causal set (where $N' < N$) and hence, one obtains a distribution of causal sets with N' elements. The direct relation between volume and spacetime volume signals that a reduction of the number of elements as described above can be viewed as "zooming in" on the causal set. In particular, consider a continuous volume V which is held fixed in the limit $N \to \infty$. Then, coarse graining down to N' elements corresponds to obtaining an effective causal set at the volume scale $\frac{V}{N'}$ (or length scale $\left(\frac{V}{N'}\right)^{1/d}$). We may then think of this as a redefinition of the discreteness scale from $\rho = N/V$ in $\mathcal{C}$ to $\rho' = N'/V$ in $\mathcal{C}'$. See [339] for steps towards setting up a renormalisation group scheme for causal sets.

Now that there is a notion of coarse graining, the question becomes whether there exists a trajectory, $p(N)$, along which some quantity approaches a fixed-point value. Here, the only varying quantities one can consider are the distributions of N-element causal sets. These distributions are said to approach a fixed-point value if they asymptote to some fixed distribution for N in the limit $N \to \infty$. Evidence supports that there indeed exists such an asymptotic distribution which is non-trivial (i.e., p does not tend to either 0 or 1) [330, 331].

3.2.2 Causal set cosmology

For cosmological purposes, a sub-class of transitive percolation models, named originary percolation models, have been studied. The essence of these models is rooted in the idea that the universe "started" at some moment in time, by demanding that every causal set grown through transitive percolation has an origin (the 0^{th} element) to which all other elements are related. An element that is related to *all* other elements in the set is called a post. Enforcing this condition entails that if at step N of the growth process, the newly born element does not "choose" any of the existing elements to be related to, then one simply repeats the process until it is related to at least one other element. It should be clear this is necessary for the universe to have just a single beginning.

It was shown early on that the dynamics of transitive percolation is completely captured by the "coupling constants" t_N for each time-step N,

$$t_N = \sum_{k=0}^{N} (-1)^{N-k} \binom{N}{k} \frac{1}{q_k}, \tag{3.12}$$

where one adds a new element to the future of the k^{th} element in the causal set with probability $1 - q_k$. In such a case, there is a sequence of these couplings

$$t_0, t_1, t_2, \ldots t_i, \ldots, \tag{3.13}$$

comprising a countably infinite set of coupling constants. It was then proposed in [332] that cosmological evolution might be used to reduce this set of coupling constants, since each new element needs to be related to the "beginning". Earlier results from graph theory reported that random posets with these type of growth dynamics will go through endless cycles of expansion followed by contraction to a single element [340]. In a cosmological setting, these cycles can be interpreted as the causal-set version of a bouncing scenario, cf., Fig. 3.5, where expansion (contraction) corresponds to the usual notion of a growing (shrinking) spatial volume. Furthermore, it was observed that an expansion followed by a contraction of the causal set tended to "renormalise" [341] the parameters t_N. This type of bounce-renormalisation has been put forward as a mechanism for the creation of new universes after the singularity of a black hole [342].

To explain the concept of renormalisation in this context, we first associate a weight with each choice of ancestor-set. This weight is simply a relative probability

$$\omega(N_a, N_m) = \sum_{k=N_m}^{N_a} \binom{N_a - N_m}{k - N_m} t_k, \tag{3.14}$$

which depends only on the size of the set of ancestors, N_a, and the size of the set of immediate ancestors N_m (i.e., the set of elements which share a link with the newly born element). Let e_2^i denote an element in the second cycle, Cyc_2, and let N_2^i be the number of ancestors of e_1^i that lie within the second cycle, i.e., $N_2^i = \text{card}\{e_2^k \in \text{Cyc}_2 \,|\, e_2^k \prec e_2^i\}$ and the post e_2^0 is included in the second cycle, cf., Fig. 3.5. Since the dynamical evolution of the causal set before the second cycle

is captured by the post e_2^0, the effective dynamics of e_2^i can be completely described by the N_2^i ancestors within Cyc_2. In other words, the effective weights $\bar{\omega}(N_2^i, N_m)$ can be expressed as

$$\bar{\omega}(N_2^i, N_m) = \omega(N_2^i + N_2^0, N_m), \tag{3.15}$$

where N_2^0 denote the number of ancestors of the post e_2^0. This can be translated into a recursive transformation of the coupling t_N. For $N_2^0 = 1$, we have

$$\bar{t}_N = t_N + t_{N+1}, \tag{3.16}$$

and for $N_2^0 = j$ the above transformation is applied j times, such that

$$\bar{t}_N(N_2^0) = \sum_{k=0}^{N_2^0} \binom{N_2^0}{k} t_{N+k}. \tag{3.17}$$

Fixed points of this transformation are then exactly given by transitive percolation models for which

$$t_N = t^N = \left(\frac{1-q}{q}\right)^N. \tag{3.18}$$

As it turns out, through repeated application of the transformation Eq. (3.17) (i.e., after many cycles/bounces), most cases indeed converge to these fixed points [332].

Let us take a step back and recapitulate what the analysis above entails. For the special type of percolation models which force each element to be to the future of a single, initial element, we found that the t_N describing the dynamical evolution undergo a form of self-similarity transformations. Specifically, the occurrence of bounces, render the system "scale" invariant with respect to cosmological time evolution, i.e., the dynamical evolution in each cycle proceeds independently of the preceding cycles. In the large N limit, the dependence of the couplings t_N on N takes the specific form $t_N = t^N$, signalling that this is a "fixed point" of the dynamics. Rather than observing scale invariance of the couplings under "zooming-in" on spacetime, they take on fixed expressions as one "fast-forwards" through time.

Note that in this model the causal set contracts to a single element anti-chain with no links passing through, i.e., all elements in the set are by construction related to the posts. It is exactly this feature which renders the posts *true* Cauchy hypersurfaces, since, in principle, one can determine the evolution of an entire cycle by specifying the initial data on the post.

In [343] such a model was grown and interestingly it was found that the resulting sets seemed to go through a de-Sitter-type phase, i.e., a phase of exponential expansion. Moreover, the extraction of a numerical estimation of the dimension of spacetime was shown to be best fitted by $(3+1)$-dimensions curves. This in itself is, surprising since the spacetime dimension is not in any way forced upon the causal set throughout the growth process. However, in [344] it was found that the interval abundances[8] of this exponentially growing phase did not agree with what one would expect

[8] An "abundance of k-intervals" refers to the number of chains of length k present in the causal set, and can be used as an indicator for manifold-likeness.

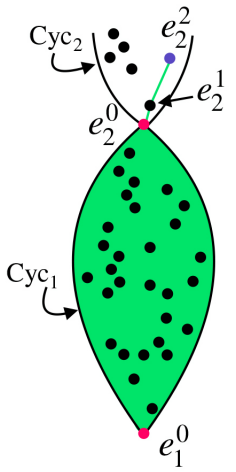

Figure 3.5: Illustration of an originary percolation model. Evolution starts at a post, e_1^0 (magenta dot), and expands as new elements are added, each of which is by construction related to the original element. After a finite amount of time has passed the universe contracts into a second post, e_2^0, ending the first cycle, Cyc_1 and starting the second, Cyc_2. The element e_2^2 has one immediate ancestor, e_2^1, through which it is linked to the post e_2^0 and, hence, all elements in the first cycle (green region). This scenario corresponds to the causal-set-analogue of a bounce, with the advantage that there is no singularity due to the discrete nature of spacetime.

from a de Sitter spacetime, suggesting that the observed de Sitter phase is not manifold-like. In addition, the $N \to \infty$ limit yields a non-manifold-like structure which carries no spatial information [345, 346]. It would be interesting to see whether the classical limit of a quantum growth model could lead to a modified dynamics with a manifold-like phase and dimension four in the $N \to \infty$ limit.

3.2.3 Quantum complex percolation

A possible extension of classical percolation to the quantum level goes under the name quantum percolation. The key idea is to generalise the classical stochastic dynamics (as in classical percolation) through Quantum Measure Theory [335, 336, 337, 338, 347]. To describe a quantum system, one defines a so-called quantum measure space as the triple (Ω, A, μ). Here, Ω is the space of all spacetime histories and the event algebra, A, consists of all possible events and can be thought of as representing our "knowledge" of the system. All dynamical properties are represented by the quantum measure (path integral), $\mu : A \to \mathbb{R}^+$, which assigns a probability to (sets of) events. Heuristically, if $\alpha_{BH} \in A$ represents the event "a Planck-size black hole is generated", then $\mu(\alpha_{BH})$ provides a notion of the likelihood with which this event takes place, based on all causal-set configurations included in Ω.

For three sets of events α, β, $\gamma \in A$, that are disjoint (i.e., no elements in common) this quantum

measure satisfies the quantum sum rule

$$\mu(\alpha \cup \beta \cup \gamma) = \mu(\alpha \cup \beta) + \mu(\alpha \cup \gamma) + \mu(\beta \cup \gamma) - \mu(\alpha) - \mu(\beta) - \mu(\gamma). \tag{3.19}$$

If μ were a classical measure, μ_{class}, then necessarily $\mu_{class}(\alpha \cup \beta) = \mu_{class}(\alpha) + \mu_{class}(\beta)$ for $\alpha \cap \beta = \emptyset$. Then the measure would have a probabilistic interpretation (i.e., $\mu_{class}(\alpha) = p$, the probability for the event(s) α to occur) and the set algebra A would be a σ-algebra (i.e., A only contains those events to which a probability can be assigned). Due to quantum interference, the quantum measure does not have to satisfy this condition, making it difficult to find a physical interpretation. Nevertheless, it has been advocated that the dynamics of CST is in fact a quantum measure space [306].

Some first steps using a measure as defined above were done in the context of complex percolation models, where the transition amplitude between events is allowed to be complex. The issue with these models is that not all observables can be captured by such a quantum measure, which in turn makes it difficult to formulate observables in a covariant manner as we will explain below. In particular, classical measures can be extended from finite-time events to infinite-time events due to their probabilistic interpretation. For quantum measures this extension is not straightforward (if it exists at all). For example, the event "a Planck-size black hole is generated *in this instant*" can be seen as a finite-time event, whereas "a Planck-size black hole is generated at some moment in time" clearly does not have a finite-time span.

For a causal set grown through (classical) transitive percolation, all elements can be distinguished by the order in which they were created. For example, for a 10-element causal set, element e_7 was born at step 7 of the growing process. Furthermore, since every newly born element cannot be to the past of a predecessor, the induced labelling is a natural one, in the sense that if element e_2 and e_7 are related, then automatically $e_2 \prec e_7$. Then let $\widetilde{\Omega}(N)$ contain all labelled causal sets of N elements. Since the labels themselves are artificial, we would like to construct $\Omega(N)$, the space of unlabelled causal-set histories (basically Ω contains equivalence classes within $\widetilde{\Omega}$) and extend the set algebra A accordingly [348]. This bears a similarity to diffeomorphisms in the continuum, for which one typically assumes relabelling invariance is a necessary, but not sufficient, condition. Intuitively, if Ω corresponds to the relabelling invariant space of histories, then we associate the algebra A with the relabelling invariant questions one can ask and the quantum measure μ should associate a well-defined probability[9] to the outcome of these questions. The crucial point is that the relabelling can in principle occur infinitely far into the future, meaning that no event is covariant, unless our algebra is extended to handle infinite events. Accordingly, we extend the set algebra to the full σ-algebra, which is closed under countable infinite set operations. This extended algebra does in general contain events which are not relabelling invariant, but we can identify those events which are covariant and only focus on those. The final step is then to define an "upgraded" measure, which can associate a well-defined probability to infinite time events of the full σ-algebra[10]. For a classical measure this can be done but a quantum measure does not share this feature and we cannot pass to a covariant description of the dynamics.

[9] By "well-defined" we mean that each probability is positive and the sum of all probabilities adds up to one.

[10] The extension can be done via the so-called Kolmogorov–Caratheodary–Hahn theorem.

Nevertheless, under certain conditions it is possible to extend the quantum pre-measure[11] to the full (covariant) σ-algebra [347], but it turns out that the complex percolation models do not satisfy the necessary conditions, unless one takes the probabilities to be real, in which case the classical and quantum covariant observables coincide[12]. It has been argued [349] that perhaps the mathematical conditions are too stringent and one should instead search for physically-motivated conditions. In other words, it might be possible to extend a pre-measure to a full measure given that we restrict ourselves to a certain class of "physical" questions. The extension is then not exact in the mathematical sense, but could possibly still be sufficient to obtain physical information from the system.

Despite the difficulties underlying a consistent definition of CST dynamics, the fact that such a simple (albeit classical) growth model does not generate causal sets which in any way resemble KR-orders, might give hope that the true quantum dynamics indeed give rise to causal sets which asymptotically reproduce the observed universe, i.e., exhibits a de-Sitter-like phase. Additionally, if the technical obstacles blocking us from formulating a quantum growth model can be overcome, then it would be worth-while to investigate the running of the parameters of the theory. In particular, it would be interesting to study whether or not a phase exists which shares features with classical percolation models.

3.2.4 Quantum partition functions

A more traditional approach comes from the formulation of a causal-set action. This action can be analytically continued to Euclidean signature, such that one obtains a statistical interpretation and, hence, standard computational tools such as Monte Carlo methods become available. It is not clear, however, why the (discretised) Einstein-Hilbert action should provide the full microscopic action. It might very well be that the dynamics are provided through a different mechanism and the Einstein-Hilbert action only appears on an effective level.

Assuming that the Einstein-Hilbert action does provide a realistic dynamics, we may identify S_{CST} in Eq. (3.2) with S_{BD} [312, 314] to obtain the quantum partition function

$$Z(\Omega) \equiv \sum_{\mathcal{C}\in\Omega} e^{\frac{i}{\hbar}S_{BD}(\mathcal{C})}. \tag{3.20}$$

Here Ω is the space of histories. As argued before, it is exactly the sample space Ω which gives rise to the entropy problem, since it is dominated by the KR-orders. The analytical results of [327], which show that a sub-class of the KR-orders is suppressed under certain conditions, become increasingly difficult to generalise to more general KR-orders. It is then important to evaluate Eq. (3.20) numerically and analyse which causal sets dominate the partition function.

Due to the Lorentzian nature of causal sets, there is no "natural" way of associating a statistical interpretation to the quantum partition function. In particular, one cannot Wick rotate the causal

[11] A pre-measure satisfies the same conditions as a measure, except that it does not need to be defined on a σ-algebra.

[12] Note that these quantum real percolation models are not the same as the classical percolation models since the quantum measure is non-additive.

relations, since they would lose their meaning in Euclidean settings. Nevertheless, in [350] a new parameter β was used to analytically continue the quantum partition function to a statistical one,

$$Z(\Omega,\,\beta) \equiv \sum_{\mathcal{C}\in\Omega} e^{\frac{i}{\hbar}\beta\, S_{BD}(\mathcal{C})}. \tag{3.21}$$

The definition above opened the door to employing numerical methods such as Markov Chain Monte Carlo methods (MCMC) [351, 352, 353, 326].

Already for relatively small causal sets the KR-orders dominate [326] and so the space of all histories, Σ, becomes very large, very quickly. In turn one needs a rather long Monte Carlo time for the simulations to thermalise, rendering the MCMC methods computationally expensive. It should be pointed out that increasingly more efficient algorithms have been developed in recent years [354]. It is then not unlikely that significant speed-ups in MCMC calculations will be achieved in the future as well.

A different route to making the computations feasible, is to choose Σ as some smaller space. In general this is not easy to accomplish consistently (i.e., without removing subsets of the sample space that are physically relevant), but one of the examples in which this works was already discussed above, namely the sub-class of 2D orders. Exhaustive studies in for example (E/C)DT in 2 dimensions exist and it would be interesting to compare with these. Since Liouville gravity requires a coupling to conformal matter, the inclusion of matter degrees of freedom in the simulations may shed light on whether or not the 2D orders reproduce Liouville quantum gravity. First steps in this direction have been taken in [352], where strong hints were found for a first-order phase transition. This discrepancy between CST and (E/C)DT could possibly be attributed to the inclusion of non-manifold like configurations in the former. It would then be interesting to see if a configuration space restricted to manifold-like causal sets yields a different phase diagram.

Furthermore, in [353] an Ising model was coupled to 2D orders. The simulations were performed in both quenched (fixed causal-set background) and unquenched (varying background) settings. A phase diagram in β and the Ising coupling j was constructed and various (possibly higher order) phase-transitions were found. Although further studies are required, there are at least indications that a coupling to matter degrees of freedom enriches the $2d$ causal set quantum gravity phase diagram.

3.3 Recovering continuum properties

One of the challenges in CST is the recovery of otherwise taken for granted geometric information on the continuum. As mentioned before, most causal sets will not embed into any kind of manifold and it is conjectured that the fundamental causal-set action is such that these type of causal sets will interfere destructively. Assuming this is indeed the case and only causal sets which can be faithfully embedded yield a significant contribution, then it remains a highly non-trivial task to extract information on topological and geometric properties from these manifold-like causal sets.

Procedures to reconstruct geometric information come for example in the form of spacetime dimensions [355, 356, 344], Chpt. 3.3.4 and Chpt. 3.3.5, timelike and spacelike distances [357], spatial distances [2], Chpt. 3.3.3, spatial topology [329, 358, 359], see Chpt. 3.3.1, the scalar d'Alembertian [360, 361, 314] and the scalar curvature [312, 313], Chpt. 3.3.2.

3.3.1 Spatial homology

Next to geometrical properties, the general conjecture is that the causal set carries topological information as well. If that is the case, then we would like to be able to extract information on topological invariants such as, e.g., the number of holes or connected components of a space. This information can be capture by the homology groups, H_k, of a space. Intuitively, H_k tells us whether or not the space has a k-dimensional hole, where a hole has dimension k if its boundary is k-dimensional. In that language, a hole with a 0-dimensional boundary, H_0, corresponds to a connected component. As a simple example, a circle (sphere in 1-dimension) is characterised by a single connected component $H_0(S^1) = \mathbb{Z}$ and a 1-dimensional hole $H_1(S^1) = \mathbb{Z}$ (i.e., the boundary of the hole is one dimensional) and all other homology groups vanish[13]. A two-sphere has a 2-dimensional hole, such that $H_0(S^2) = \mathbb{Z}$ and $H_2(S^2) = \mathbb{Z}$ and a disc (2-dimensional ball) has no holes such that only $H_0(B^2) = \mathbb{Z}$ is non-vanishing.

In [329, 358] the homology groups of *antichains* were found to give an indication of manifold-likeness. An antichain, $\mathcal{A}$ of a causal set, $\mathcal{C}$, is a subset of $\mathcal{C}$ such that $\forall x,\, y \in \mathcal{A}$, $x \not\prec y$ and $y \not\prec x$. This is the causal-set analogue of a spatial hypersurface. Note, however, that links can "pass through" the antichain, indicating that such a spatial hypersurface will not suffice as an initial data surface from which one can evolve the rest of the spacetime, see Fig. 3.6. We say an antichain is inextendible if all elements in $\mathcal{C} \setminus \mathcal{A}$ are related to at least one element in $\mathcal{A}$. This antichain has a discrete topology and to extract any information on the continuum topology, it needs to incorporate some structural information of the region close to $\mathcal{A}$. To this end a *thickened* antichain is defined as an inextendible antichian which includes elements to the immediate future of $\mathcal{A}$. The first "layer" to be included in the thickened antichain would be those elements that share a link with an element in $\mathcal{A}$. To be more precise, one can choose a "thickening" parameter, t, which dictates how many "layers" to include in the thickened antichain, $\mathcal{A}_t$. It turns out that for causal sets constructed through a sprinkling of continuum spacetimes which admit a compact Cauchy hypersurface (e.g., compact regions of globally hyperbolic spacetimes), it is possible to derive quantities from the thickened antichain which are homological to the continuum Cauchy hypersurface, i.e., their homology groups H_k match. This indicates that it is indeed possible to recover information on the spatial topology of the continuum from a causal set.

3.3.2 Benincasa-Dowker action

Due to the inherent non-locality discussed in Chpt. 3.1.2, an element can have an infinite number of nearest neighbours. As a consequence, it is not possible to define a local tangent space which

[13] When we write $H_k = \mathbb{Z}$, we mean that a single generator is sufficient to describe the k-dimensional hole.

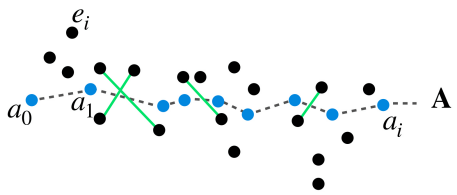

Figure 3.6: Illustration of an antichain $\mathcal{A} = a_0, a_1, ..., a_n$ (blue dots) with links passing through (green lines).

makes it difficult to add dynamical matter to the causal set. On the other hand, scalar quantities do not require a tangent space, making them the preferred candidate. One such a quantity is the d'Alembertian of a scalar field in a causal set approximated by two dimensional Minkowski spacetime [362, 305] which was later generalised to higher dimensions [312, 313]

$$B\,\phi(x) \equiv \frac{4}{\sqrt{6}}\left[-\phi(x) + \left(\sum_{y\in L_0(x)} -9 \sum_{y\in L_1(x)} +16 \sum_{y\in L_2(x)} -8 \sum_{y\in L_3(x)}\right)\phi(y)\right]. \tag{3.22}$$

Here ϕ is a real scalar field, living on the causal set $\mathcal{C}$ and x, $y \in \mathcal{C}$. The quantities $L_i(x)$ are subsets containing the i^{th} generation of ancestors of x. Specifically, $L_0(x)$ contains all elements $y \in \mathcal{C}$, such that $\text{card}\{z \in \mathcal{C} | y \prec z \prec x\} = 0$, hence, y is a *past* nearest neighbour (parent) of x, i.e., x and y are connected by a one-link path. Likewise, $L_1(x)$ contains the next-to-nearest past neighbours (grandparents), satisfying $\text{card}\{z \in \mathcal{C} | y \prec z \prec x\} = 1$, i.e., x and y are connected by a two-link path. The definition of $L_3(x)$, $L_4(x)$ follows this pattern. Note that $L_i(x)$ includes settings where the element x is connected to y through multiple i-link paths, e.g., the paths $x \prec z_1 \prec y$ and $x \prec z_2 \prec y$ are both included in $L_1(x)$.

At first sight this operator suffers from non-localities since the subsets $L_i(x)$ can count an infinite number of elements. Upon further inspection it actually seems that cancellations occur which render contributions from elements that lie far down the past lightcone insignificant, under certain conditions. These conditions can be derived by inspecting the expectation value of the random variable $\mathbf{B}\phi(x)$ at each point x in $\mathbb{M}^4$. This random variable can be generated by a sprinkling at density ρ and its expectation value is found to be

$$\begin{aligned}\frac{1}{\sqrt{\rho}}\,\langle \mathbf{B}\phi(x)\rangle &= -4\sqrt{\frac{\rho}{6}}\phi(x) \\ &+ \rho 4\sqrt{\frac{\rho}{6}}\int_{y\in J^-(x)} d^4y\,\sqrt{g}\,\phi(y)\,e^{-\rho V(x,y)}\left(1 - 9\,\rho\,V(x,y) + 8\,(\rho\,V(x,y))^2 - \frac{4}{3}\,(\rho\,V(x,y))^3\right).\end{aligned} \tag{3.23}$$

Here $V(x,y)$ is the volume of the spacetime interval between x and y and the Poisson distribution was used to determine the probability for the spacetime interval $V(x,y)$ to contain 0, 1, 2 or 3 elements (i.e., the probability that x and y are nearest neighbours, next-to-nearest neighbours, etc.). The expression above can be evaluated if ϕ varies slowly, such that an expansion around $\phi(x)$

can be performed (note that this is a frame-dependent statement). Furthermore, if one takes ϕ of compact support, then the region of integration can be well-defined. In the limit of infinite density the continuum d'Alembertian can then be recovered

$$\lim_{\rho\to\infty} \frac{1}{\rho} \langle \mathbf{B}\phi(x)\rangle = \Box\, \phi(x). \tag{3.24}$$

In this frame it would then seem that $\mathbf{B}\phi(x)$ is restricted to a local neighbourhood around x. Whether or not this operator leads to a stable evolution in 4 dimension has not been settled, since the operator defined here seems to contain complex poles [361]. Alternative operators have been proposed [361, 363] and while a final conclusion on stability has not been reached, it did inspire a proposal for a mechanism for dark-matter production[14].

In the analysis above, the construction of $\mathbf{B}\phi(x)$ was restricted to flat Minkowski spacetime. In the more general curved spacetime setting [312], an additional term proportional to the Ricci scalar, R, is recovered in the continuum limit

$$\lim_{\rho\to\infty} \frac{1}{\rho} \langle \mathbf{B}\phi(x)\rangle = \Box\, \phi(x) - \frac{1}{2}\mathcal{R}(x)\phi(x). \tag{3.25}$$

The expression above then provides the possibility to extract the discrete Ricci curvature

$$R(e) = \frac{4}{\sqrt{6}} \left[1 - N_0(e) + 9N_1(e) - 16N_2(e) + 8N_3(e)\right], \tag{3.26}$$

at an element $e \in \mathcal{C}$. Here $N_i(e)$ is the cardinality of the subset $L_i(e)$. If N_i refers to the total number of i-element intervals in $\mathcal{C}$, then the Benincasa-Dowker action in four dimensions can be written as

$$S(\mathcal{C}) = \sum_{e\in\mathcal{C}} R(e) = \frac{4}{\sqrt{6}} \left[n - N_0 + 9N_1 - 16N_2 + 8N_3\right], \tag{3.27}$$

where n is the total number of elements in the causal set, assumed to be finite here. It was shown explicitly [314] that the continuum approximation of the random variable $\mathbf{S}(\mathcal{C})$ generated through a sprinkling indeed reproduces the Einstein-Hilbert action

$$\lim_{\rho\to\infty} \hbar \frac{l^2}{l_{Pl}^2} \langle \mathbf{S}(\mathcal{C})\rangle = S_{EH}(g), \tag{3.28}$$

under the assumption that there are no significant contributions coming from regions that lie close to the light cone. This assumption can be shown to hold in regions which are approximately flat, but has not (yet) been generalised to higher dimensions.

It is important to stress that the result obtained above only contains information about the *mean* of the action and could be spoiled by fluctuations. Indeed, for a fixed continuum volume

[14]The core idea is to promote B to a frame independent operator, i.e., a Lorentz invariant operator. It turns out that for an interacting continuum theory, this new operator can be used to generate massive, non-interacting particles, which occur as a remnant of the fundamental discrete, underlying theory.

an increase in density results in growing fluctuations [362, 314]. Since the fluctuations grow with $\ell = \rho^{1/4}$, it was proposed in [362] to introduce an intermediate length scale (mesoscale) $\ell_k \geq \ell$ to suppress the fluctuations.Then Eq. (3.22) becomes

$$B_k\phi(x) \equiv \frac{4}{\sqrt{6}}\left[-\phi(x) + \epsilon \sum_{y \prec x} f(N(y,\, x),\, \epsilon)\phi(y)\right], \tag{3.29}$$

with $\epsilon \equiv \frac{\ell^4}{\ell_k^4} = \frac{\rho_k}{\rho}$ and $N(y,\, x)$ the number of elements in the spacetime volume between x and y. Note that ϵ can be thought of as a coupling and an interesting question is whether fixed points, $\epsilon*$, exist [350]. The above definition involves a sum over all ancestors y of x (rather than just those in the layers $L_i(x)$) and is in that sense more in the spirit of the continuum expression. The purpose of the function $f(N,\, \epsilon)$ is then to smear out the contributions over this new scale such that when $\ell_k \gg \ell$ ($\epsilon \ll 1$) large fluctuations are suppressed

$$f(N,\, \epsilon) = (1-\epsilon)^N \left[1 - 9\frac{\epsilon N}{1-\epsilon} + 8\frac{\epsilon^2 N\,(N-1)}{(1-\epsilon)^2} - 4\frac{\epsilon^3 N\,(N-1)(N-2)}{3(1-\epsilon)^3}\right]. \tag{3.30}$$

We see indeed that contributions coming from $N > 3$ are suppressed by factors $(1-\epsilon)^N$, where $\epsilon < 1$. With these definitions, B_k becomes a one-parameter family of d'Alembertian operators, limiting to Eq. (3.22) when $\epsilon = 1$ and yielding the desired expression for the mean Eq. (3.23) with ρ replaced by ρ_k.

An interesting question is that of the free parameters of the theory. More precisely, given that we can find a form of quantum dynamics, then what would the parameter space of causal sets correspond to? In particular, the definition of the BD action requires a non-locality scale ℓ_k which suppresses large fluctuations in the classical limit. This non-locality scale is chosen such that $\ell_{Pl} < \ell_k$ and in [350] the question was posed whether there are circumstances under which the non-locality scale becomes a prediction of the theory. It was then proposed that such a scenario might be possible if one can set up a form of renormalisation group flow and finds a fixed point for the ratio $\frac{\ell_{Pl}^2}{\ell_k^2} < 1$.

3.3.3 Spatial distances

Arguably, one of the most basic geometrical quantities one can think of is a notion of distance. Since we are trying to construct a theory of spacetime, there are several definitions of distances one might be interested in. Here we will focus on reproducing spatial distances, following [2].

The key constructions presented below are based on the intuitive idea of approximating the length of a smooth curve through a piecewise linearisation of the curve. To be more precise, given a 2-dimensional plane on a Riemannian geometry, we embed a smooth curve, γ, with end-points p and q in this plane. If we let $d_\gamma(p,\, q)$ denote the distance between p and q as measured along the curve γ, then we approximate the curve through a sequence of straight line segments, $\gamma_{i,i+1}$,

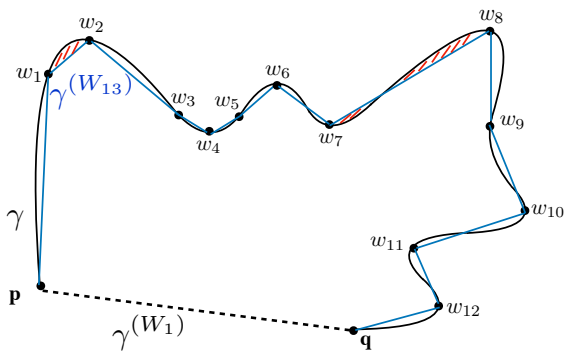

Figure 3.7: We show a curve, γ, embedded in $\mathbb{R}^2$ and two piecewise linear paths approximating the curve. The path γ^{W_1} (dashed, black line) gives a poor approximation whereas $\gamma^{(W_{13})}$ (blue, solid lines) approximates the curve more closely. We indicated two of the suspended areas, $A_{1,2}$ and $A_{7,8}$ (red, shaded areas) between $\gamma^{(W_{13})}$ and γ. Using the size of these areas to estimate the quality of the approximation, we see that the suspended area between $\gamma^{(W_1)}$ and γ is much larger than that for $\gamma^{(W_{13})}$ and γ.

and obtain an estimate for $d_\gamma(p,\, q)$ by summing over the sequence of straight line segments, as in Fig. 3.7

In other words, for a finite number of flat line segments, $\gamma_{i,i+1}$ between two points $w_i,\, w_{i+1} \in \gamma$, the piecewise linearisation is the pairwise union between these segments

$$\gamma^{(W_k)} \equiv \bigsqcup_{i=0}^{k-1} \gamma_{i,i+1}, \tag{3.31}$$

where $W_k \equiv w_0, \ldots, w_k$ and $w_0 = p,\ w_k = q$. The piecewise distance on $\gamma^{(W_k)}$ is then simply the sum of the length of each line segment

$$d_{W_k}(p, q) \equiv \sum_{i=0}^{k-1} d_{\mathbb{R}^2}(w_i, w_{i+1}). \tag{3.32}$$

Here $d_{\mathbb{R}^2}(w_i, w_{i+1})$ refers to the ambient distance in $\mathbb{R}^2$, i.e., the length of the (1-dimensional) line embedded in $\mathbb{R}^2$. It is intuitively straightforward to see that increasing the number of line segments k will lead to a more accurate approximation of the smooth curve, for a curve along which the curvature is constant. However, if some regions of γ exhibit larger curvature effects than others, then one would like to increase the number of line segments within this region specifically. One way of accomplishing this is by demanding that for any two consecutive points on the smooth curve, the error introduced by the linear approximation is bounded

$$|d_{\mathbb{R}^2}(w_i, w_{i+1}) - d_\gamma(w_i, w_{i+1})| < \epsilon. \tag{3.33}$$

This then ensures that strongly curved sections of γ are supplemented with a larger number of piecewise straight segments.

Since the continuous curve γ contains an infinite number of points, there is in principle an infinite number of discrete paths one could construct. We can then follow continuum intuition, where a distance function between two points is obtained through a minimisation over all possible paths, to select a unique distance function on γ. However, since we are using the ambient distance on $\mathbb{R}^2$ to construct distances, this procedure does not take into account any curvature effects along the curve. For the curve in Fig. 3.7, we would then obtain $\gamma^{(W_1)}$ as the minimal distance path between p and q. Ideally, we want to restrict each piecewise linear segment to be smaller than the local radius of curvature, as this would guarantee the discretisation only introduces a small error as in Eq. (3.33). The issue is that this construction implicitly uses continuum knowledge on the local curvature of γ. To avoid this, we instead require the suspended area between the straight line $\gamma(i, i+1)$ and the curve segment $\gamma(w_i, w_{i+1})$ to be sufficiently small. The discrete distance function on $\gamma(p, q)$ is then defined through a minimisation of all piecewise linear, discrete paths $\gamma^{(W_k)}$, such that for all consecutive elements in W_k, we have $A_{i,i+1} < \ell$, where ℓ functions as a mesoscale cutoff. Note that for a given piecewise linear path we always satisfy the triangle inequality exactly, since $d_{W_k}(w_i, w_{i+2}) = d_{W_k}(w_i, w_{i+1}) + d_{W_k}(w_{i+1}, w_{i+2})$. Furthermore, since the procedure described above varies over all discretisations of γ, we are guaranteed to satisfy the triangle inequality for all points on γ.

Applied to a Riemannian setting, the construction here will result in a path with the smallest value of k while still satisfying $A_{i,i+1} < \ell$, simply because the shortest distance between two points on $\mathbb{R}^2$ is a straight line. In the following, we will generalise this construction to Lorentzian geometries and we will find that the shortest path is not necessarily minimal in k. An advantage of globally hyperbolic spacetimes, is that, in any dimension, the suspended volume has a natural interpretation in terms of local light-cones, as will be demonstrated below. This interpretation is not restricted to $d = 2$ manifolds, unlike the Riemannian case, where already in $d = 3$ dimensions, there is no straightforward way to define the suspended area.

Starting from flat, d-dimensional Minkowski spacetime, we are interested in deriving a spatial distance function based solely on volume and local light-cone structures [2].

If we let Σ be the inertial Cauchy hypersurface we would like to define our distances on, then the backwards light-cone of a spacetime point x, to the future of Σ encloses a volume[15]

$$\begin{aligned} V(\Sigma, x) &\equiv J^+(\Sigma) \cap J^-(x) = \zeta_d \, T^d, \\ \zeta_d &= \frac{\pi^{(d-1)/2}}{d\,\Gamma\left(\frac{d+1}{2}\right)}, \end{aligned} \tag{3.34}$$

where T is the height of the cone, i.e., the proper time between Σ and x. The key point is that the height of the cone is directly related to the diameter, $\widetilde{d}$, of the base $2T = \widetilde{d}$. Then, since the distance between two maximally separated points, p, q, on the base of the cone is exactly the

[15] Note that the volume enclosed by a d-dimensional cone is related to the volume of a $(d-1)$-dimensional ball as $V^{(d)}_{cone}(R) = V^{(d-1)}_{ball}(R)R/d$.

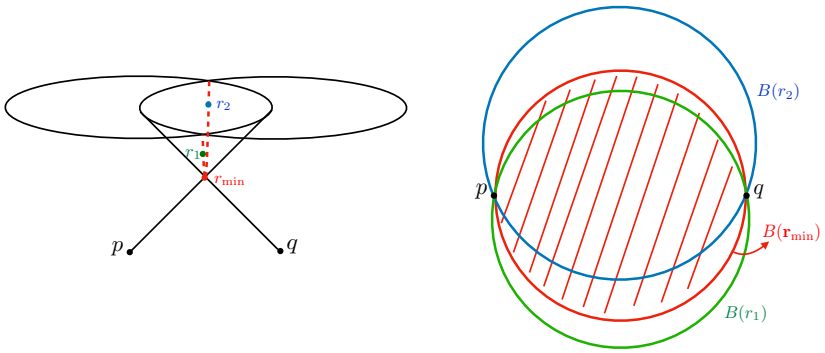

Figure 3.8: Left: The intersection between $\partial J^+(p)$ and $\partial J^+(q)$ in $d = 3$ dimensions yields a 1-dimensional hyperboloid $\mathcal{H}$. The points, r, on $\mathcal{H}$ may be used to calculate the suspended volume between r and Σ. Right: We show the base of the backward light-cones cast by the points r_1, r_2 r_{min}. The distance between the points p and q corresponds to the diameter of the base associated to r_{min}.

diameter, $\widetilde{d}$ of the base[16] we can extract a notion of distance from the spacetime volume

$$\widetilde{d}(p,q) = 2\left(\frac{V(\Sigma,x)}{\zeta_d}\right)^{\frac{1}{d}}, \tag{3.35}$$

see the left-hand panel of Fig. 3.9.

As a final step, we need to check that this construction indeed minimises the suspended volume. To do so, we introduce a d-dimensional Cartesian coordinate system and place the $(d-1)$ dimensional plane spanned by Σ at $t = 0$. Then for two points $p, q \in \Sigma$, located at the origin and $(0, x_q, 0, \ldots, 0)$, respectively, we define the set $\mathcal{H}(p,q) \equiv \partial J^+(p) \cap \partial J^+(q)$ to be the set of null-like events to the future of p and q (we can think of $\partial J^+(p)$ as the set of future directed light-rays send out from the point p). Then, with r any point to the future of Σ, we can write the sets

$$\begin{aligned}
\partial J^+(p) &= \left\{ r \mid -t^2(r) + \sum_{i=1}^{d-1} x_i^2(r) = 0 \right\}, \\
\partial J^+(q) &= \left\{ r \mid -t^2(r) + (x_1(r) - x_q)^2 + \sum_{i=2}^{d-1} x_i^2(r) = 0 \right\}.
\end{aligned} \tag{3.36}$$

The intersection between these sets forms a hyperboloid, as illustrated in Fig. 3.8

$$\mathcal{H}(p,q) = \left\{ r \mid x_1(r) = \frac{x_q}{2}, -t^2(r) + \left(\frac{x_q}{2}\right)^2 + \sum_{i=2}^{d-1} x_i^2(r) = 0 \right\}. \tag{3.37}$$

The suspended volume, $V(r) = \zeta_d t^d(r)$, grows as t^d and is thus minimal for the point $r \in \mathcal{H}$ minimising $t(r)$. From Eq. (3.37), we see that $t(r)$ is minimal at the point $r_{min} = \left(\frac{x_q}{2}, \frac{x_q}{2}, 0, \ldots, 0\right)$ and hence, the minimal volume is $V(r_{min})$. We have then obtained a well-defined distance function Eq. (3.35), which we will call the *predistance function*.

[16] In $\mathbb{M}^d$ the base is given by S^{d-2} and hence, for $d = 2$ the diameter of the base is the base itself, whereas in $d = 4$ the base is a 2-sphere.

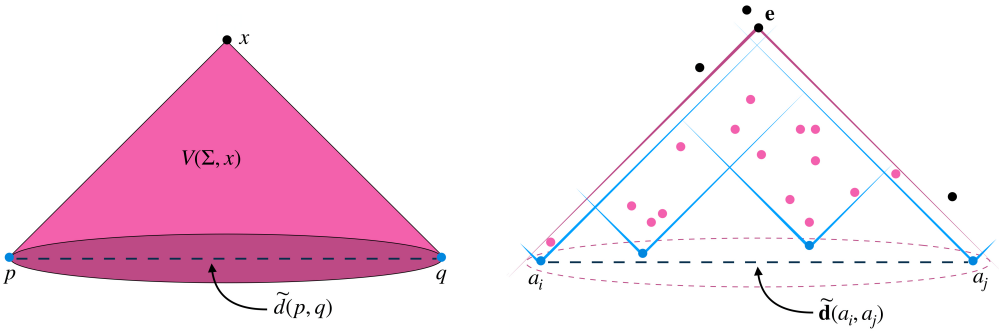

Figure 3.9: Left: In a continuous spacetime, the distance between two antipodal points p and q on the base of the backwards cone cast by the spacetime point x is given by the diameter $\widetilde{d}(p,q)$ of the base. Right: The discrete analogue of the figure on the left, where now the volume is given by the number of elements (pink dots) contained in the intersection of the antichain (blue dots) and e_k.

The causal set equivalent can then be constructed in a straightforward manner: Instead of a Cauchy hypersurface we construct the inextendible antichain $\mathcal{A}$, with causal future $J^+(\mathcal{A}) \equiv \bigcup_{i=0}^{n} J^+(a_i)$ for an $(n+1)$-element antichain. We then thicken the antichain as to define the suspended volume, similar to [329, 358], where the estimation of the spatial homology needed a thickening parameter (see Chpt. 3.3.1). The volume $V(\mathcal{A}, e_k)$ of the backwards light-cone cast by an element $e_k \in J^+(\mathcal{A})$ in the antichain is then simply the number of elements in the region $J^+(\mathcal{A}) \cap J^-(e_k)$, cf. right-hand panel Fig. 3.9. Analogously to the continuum setting where $J^+(p) \cap J^+(q)$ contains an infinite number of spacetime points, the common future of a_i and a_j is in general a large and possibly (countable) infinite set. The continuum definition $\widetilde{d}$ minimises over all these spacetime points by selecting the point, x, where the future lightcones of p and q intersect for the first time. Carrying this idea over to the discrete setting corresponds to finding the element $\mathbf{e}$ for which the intersection with $\mathcal{A}$ is minimised

$$\mathbf{V}(\mathbf{e}) \equiv \inf_{e \in \mathrm{Fut}(a_i, a_j)} \mathbf{V}(e), \tag{3.38}$$

where $\mathrm{Fut}(\mathrm{a_i}, \mathrm{a_j}) \equiv J^+(a_i) \cap J^+(a_j)$, the common future of a_i and a_j. Note that as a consequence of the discreteness, the element e_k does not lie *exactly* on the intersection of the continuum future lightcones cast by a_i and a_j, implying that in the discrete setting there is a "lag" in the transfer of information between two elements. This lag was coined *asymptotic silence* in [364]. As a consequence of asymptotic silence, the backwards light-cone cast by e_k will enclose a larger volume than its continuum analogue and, hence, will result in an overestimation of the spatial distance for elements that are (spatially) very close to one another. We associate the scale ℓ_{DAS} with the onset of the discrete asymptotic silence such that the validity of our construction only holds for scales larger than ℓ_{DAS}.

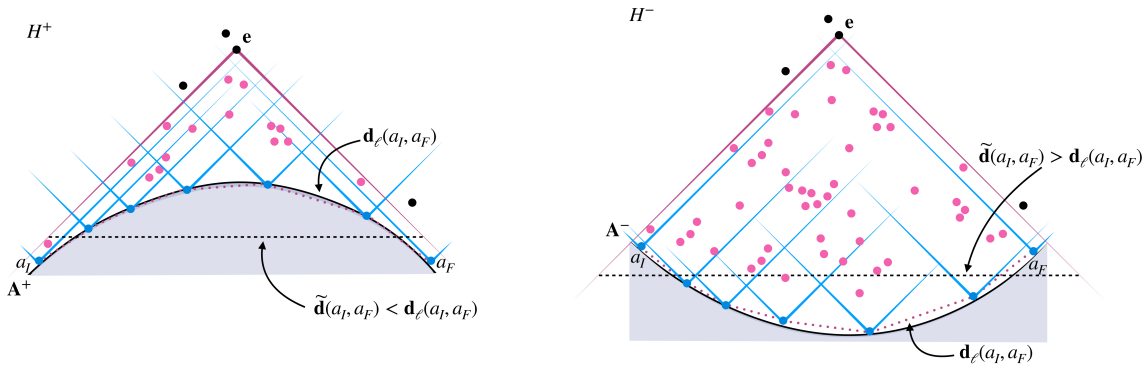

Figure 3.10: Left: For an initial boundary with positive, constant curvature, H^+, the predistance $\widetilde{\mathbf{d}}(a_I, a_F)$ (black, dashed path) underestimates the piecewise flat distance $\mathbf{d}_\ell(a_I, a_F)$ (dotted, dark magenta path). Right: In the negative curvature case H^-, predistance overestimates the distance. Note that the black, dashed path can be thought of as the effective, flat hypersurface with respect to which we attempt to calculate the distance when utilising $\widetilde{\mathbf{d}}$.

The discrete predistance function is then

$$\widetilde{\mathbf{d}}(a_i, a_j) \equiv 2\left(\frac{\mathbf{V}(\mathbf{e})}{\zeta_d}\right)^{\frac{1}{d}} \tag{3.39}$$

We tested the construction above extensively for causal sets obtained through sprinklings in $\mathbb{M}^2$ and $\mathbb{M}^3$ and find good agreement between the continuum distance $\widetilde{d}(p, q)$ and discrete distance $\widetilde{\mathbf{d}}(a_i, a_j)$ [2].

So far we have limited ourselves to flat Cauchy hypersurfaces in d-dimensional Minkowski spacetime, where the predistance coincides with the distance. To extend the discussion to extrinsically curved Cauchy surfaces, we need to account for any curvature effects that cause alterations of the volume contained in the past light-cone of $\mathbf{e}$, see Fig. 3.10. To compensate for these effects we introduce the mesoscale cut-off, ℓ, on the height of the cone (i.e., the thickness of the antichain) such that the probed distance is larger than ℓ_{DAS} but smaller than ℓ_K, the curvature radius, $\ell_{DAS} \ll \ell \ll \ell_K$. In this regime we can assume spacetime is approximately flat and, hence, the construction above is valid. To substantiate this claim, we now explicitly show its validity in the continuum.

The idea is to apply the construction above to a globally hyperbolic spacetime (M, g), with compact Cauchy hypersurface Σ. To do so, we need to be able to restrict to locally flat neighbourhoods around a point $p \in \Sigma$. Given such a region, M_p, and a second point $q \in M_p$, we define $\mathcal{H}(p, q) \equiv \partial J^+(p) \cap \partial J^+(q) \cap D(M_p)$ where $D(M_p)$ is the domain of dependence of M_p, i.e., all events in M for which all future directed or all past directed inextendible causal curves pass through M_p. By restricting $\mathcal{H}$ to lie within $D(M_p)$, we ensure that all $r \in \mathcal{H}(p, q)$ lie within a sufficiently small neighbourhood around M_p so that we may employ the flat construction detailed above. We then define

$$V(p, q) \equiv \inf_{r \in \mathcal{H}(p,q)} V(r). \tag{3.40}$$

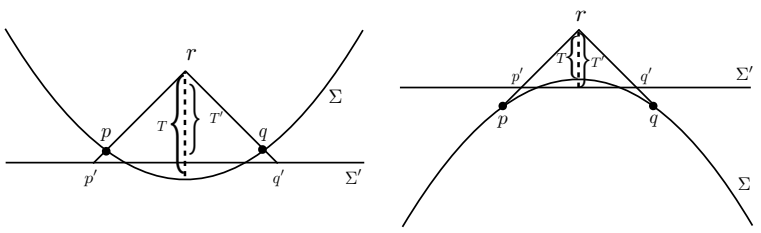

Figure 3.11: Due to the curvature of Σ, the predistance function effectively calculates the distance with respect to Σ'.

It can be shown that this function exists at some $r_{min} \in \mathcal{H}(p,q)$, such that $V(r_{min}) = V(p,q)$. We may then use the predistance function Eq. (3.35) within a sufficiently small neighbourhood M_p around p.

In terms of curvature components, it was shown in [365] that we can express $V(r)$ in terms of the Riemannian volume V_η as

$$V(r) = V_\eta(r)(1 + \frac{d}{2(d+1)}K(r_0)T) + \mathcal{O}(T^{d+2}), \tag{3.41}$$

where $r_0 \in \Sigma$ such that the proper time between r_0 and r_{min} is minimal and $K(r_0)$ the trace of the extrinsic curvature at the point r_0. The key point is that the leading order corrections come from constant $K(r_0)$ and we may thus focus on surfaces in flat spacetime which exhibit constant extrinsic curvature.

In the case of Minkowski spacetime, the simplest constant K cases we can consider are the d-dimensional hyperboloids $\mathcal{H}^+$, with $K > 0$ and $\mathcal{H}^-$, with $K < 0$, parametrised by the equation

$$t^2 - \sum_i^{d-1} x_i^2 = \tau^2, \tag{3.42}$$

where $t > 0$ ($t < 0$) for $\mathcal{H}^-$ ($\mathcal{H}^+$) and $K = -1/\tau$. The volume $V(r_{min})$ is then no longer given by the predistance $\widetilde{d}(p,q)$, see Fig. 3.11

The predistance function calculates the distance with respect to flat Cauchy surface Σ', such that

$$\widetilde{d}(p,q) = 2T' = 2T\left(1 + \frac{1}{2(d+1)}KT\right) + \mathcal{O}(T^3). \tag{3.43}$$

We see then that for $K > 0$, $\widetilde{d}$ will be larger than the flat spacetime distance $2T$ and for $K < 0$ it will be smaller. Additionally, we can calculate the distance between two points p and q on $\mathcal{H}^\pm$ through the induced, spatial metric on these surfaces. We then find that for small extrinsic curvature

$$d_{\mathcal{H}}(p,q) = 2T(1 + \frac{1}{2}KT + \mathcal{O}(T^2)), \tag{3.44}$$

which is expected to also hold in the more general case of non-constant K, as long as the neighbourhoods under consideration are sufficiently small. We then find that the error induced by employing the predistance is

$$\widetilde{d}(p,q) - d_h(p,q) \approx -\frac{d}{d+1} K T^2, \tag{3.45}$$

and, hence, $\widetilde{d}$ will underestimate the continuum distance when $K > 0$ and conversely for $K < 0$. Note that the error above can be reduced by choosing T sufficiently small, i.e., by restricting the points p and q to lie within a small neighbourhood of one-another.

The next step is to translate the construction above to the discrete setting. The distance between elements $(a_I,\, a_F)$ which are separated on scales similar to or larger than the radius of curvature, ℓ_K, can be constructed through a piecewise flat path $\gamma_n = (a_0,\, a_1,\, ...,\, a_n)$ where $a_0 = a_I$ and $a_n = a_F$, such that for each of the n consecutive steps $\widetilde{\mathbf{d}}_\ell(a_k, a_{k+1}) \ll \ell$. To each possible path from a_0 to a_n we can associate a path length

$$\widetilde{\mathbf{d}}_{\gamma_n,\,\ell}(a_I, a_F) \equiv \sum_{k=0}^{n-1} \widetilde{\mathbf{d}}_\ell(a_k, a_{k+1}). \tag{3.46}$$

Even with the restriction on the step-size, the number of elements, n, contained in the path is not fixed and hence, there exist a large number of paths constituting various path lengths between any two elements in the antichain. We then define the distance as the shortest path, given that each step-size is less than ℓ

$$\mathbf{d}_\ell(a_I, a_F) \equiv \inf_\gamma \widetilde{\mathbf{d}}_{\gamma,\,\ell}(a_I, a_F). \tag{3.47}$$

Note then that the difference between the continuum and discrete case is exactly the presence of asymptotic silence in the latter, since it places a lower-bound on the cutoff ℓ which is no there in the continuum. It is then exactly the discrete, random nature inherent to causal sets which induces this difference.

3.3.3.1 Numerical results

Now that we have a clear setup, we can test our proposed distance function through numerical simulations. The causal sets used here were obtained through a Poisson sprinkling into 2 -and 3-dimensional Minkowski spacetimes, with initial boundaries that can either be flat or exhibit extrinsic curvature. The distance function is then tested on these initial boundaries and compared to the induced continuum distance. Since one can only perform an approximate comparison between the discrete causal set and the continuum spacetime when the causal set is sufficiently large, we will need to have an overall large enough number of elements, N, as well as a large enough antichain. The size, N_A, of the antichain has direct consequences for the computational time it takes to minimise over all possible paths, since the number of paths grows factorially with the size of the paths. We can reduce the set of allowed paths between two elements a_I and a_F significantly by only allowing for paths that lie within the base of the cone cast by the minimising element e_k, see Fig. 3.9. This restriction is justified since any path that ventures outside of the base will always

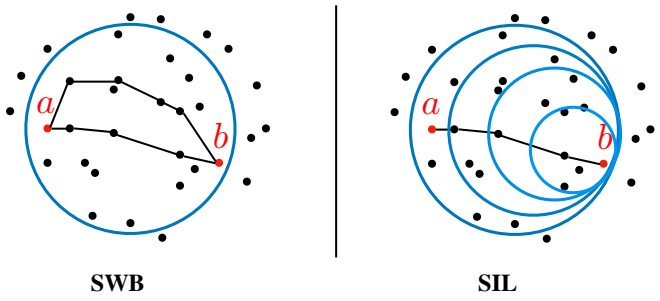

Figure 3.12: Left: The allowed set of paths considered by the SWB algorithm remain within the beam from a to b. Right: For the SIL algorithm, each intermediate step is forced to be within the respective beam between intermediate elements and the final element.

have a length that is larger than the diameter. This observation shrinks the set of considered paths significantly and ensures that the minimisation procedure converges to the correct distance faster. Since the base of the light-cone can be thought of as a "beam of light", $B_A(e)$ on the antichain A and cast by the minimising element e, we will refer to the algorithm following this line of though as "staying within the beam" (SWB). Furthermore, for any two elements a and b in the antichain, we can demand that at each intermediate step, a_i, the remaining part of the path connecting a_i to b should be within the beam of a_i and b, i.e., we keep "stepping into the light" (SIL), see Fig. 3.12

A benefit of the SWB algorithm is that for each element a_i in the beam $B_A(e(a,b))$, but not necessarily in the final path, the beam $B_A(e(a,a_i))$ lies approximately within the full beam $B_A(e(a,b))$, i.e., while calculating the distance $\mathbf{d}(a,b)$ we automatically calculate $\mathbf{d}(a,a_i)$. Note that this in general does not hold for the SIL algorithm, since here we reduce the set of possible paths at each intermediate step.

Rather than devising a new algorithm for the minimisation procedure, we would like to make use of algorithms developed in the context of graph theory. We mentioned before that causal sets can be thought of as directed, acyclic graphs with unbounded valency. However, once the predistances of all possible pairs of elements on A have been calculated, we may only concern ourselves with the antichian itself. The antichain itself can then be represented as an effective graph G, where the nodes correspond to the elements $a_i \in A$ and we draw a link between two nodes, a_i and a_j, whenever $\widetilde{\mathbf{d}}(a_i,a_j) < \ell$, i.e., there exists an approximately flat neighbourhood on A which contains a_i and a_j. Each link is then weighted by the predistance between the two nodes it connects. Moreover, for each pair of elements, we restrict the graph $G(a,b)$ to those elements that lie within the beam $B_A(e(a,b))$. Note that we then utilise the notion of "nearest neighbours" by considering two elements to be nearest neighbours whenever their predistance is smaller than ℓ. On this effective graph we employ the well-known Dijkstra algorithm [366] to find the shortest distance between two nodes.

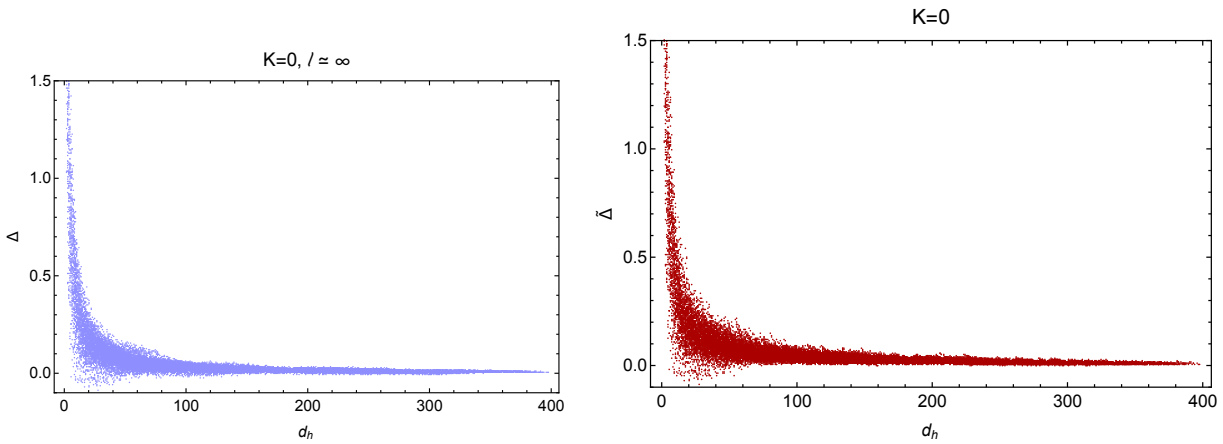

Figure 3.13: We show the error in the predistance (left) and distance (right) for a flat initial surface in $\mathbb{M}^2$.

To compare with the continuum distance, d_h, on the initial boundary, we define

$$\Delta(a,b) \equiv \frac{\mathbf{d}(a,b-d_h(a,b))}{d_h(a,b)}, \tag{3.48}$$

as the error on the distance function. The analogue for the predistance function is then

$$\widetilde{\Delta}(a,b) \equiv \frac{\widetilde{\mathbf{d}}(a,b-d_h(a,b))}{d_h(a,b)}. \tag{3.49}$$

At large continuum distances, d_h, we expect that the discrete distance will agree with the continuum version and hence, Δ will tend to zero. For small d_h, however, asymptotic silence will generate an overestimation of the distance such that $\Delta(a,b) \gg 0$.

K = 0

We first restrict ourselves to 2 -and 3-dimensional Minkowski spacetime with $K = 0$ initial boundaries and we set $\rho = 1$, i.e., the fundamental volume of the causal sets elements is of Planckian size. In flat spacetime the radius of curvature is infinite, $\ell_K \to \infty$, such that the predistance and distance function agree for any value of the cutoff, ℓ, cf. Fig. 3.13. We see indeed that at small d_h, asymptotic silence effects overestimate the distance. Consequently, if we make the cutoff so small that each individual step lies within the asymptotic silence regime ($\ell \sim \ell_{DAS}$), then we will overestimate the distance at each step and hence, overestimate the total path length as shown in the Fig. 3.14. Since we chose the initial boundary at $t = 0$, the continuum distance between two points is simply $d_h(p,q) = \sqrt{(x_p - x_q)^2}$ in two dimension and $d_h(p,q) = \sqrt{(x_p - x_q)^2 + (y_p - y_q)^2}$ in three dimensions.

K≠ 0

We performed a similar analyses for $K \neq 0$, where now the cutoff needs to be chosen such that $\ell_{DAS} \ll \ell \ll \ell_K$. As discussed above, constant K surfaces in Minkowski spacetime are parametrised by hyperbolae, and the predistance function will yield an underestimation or overestimation with

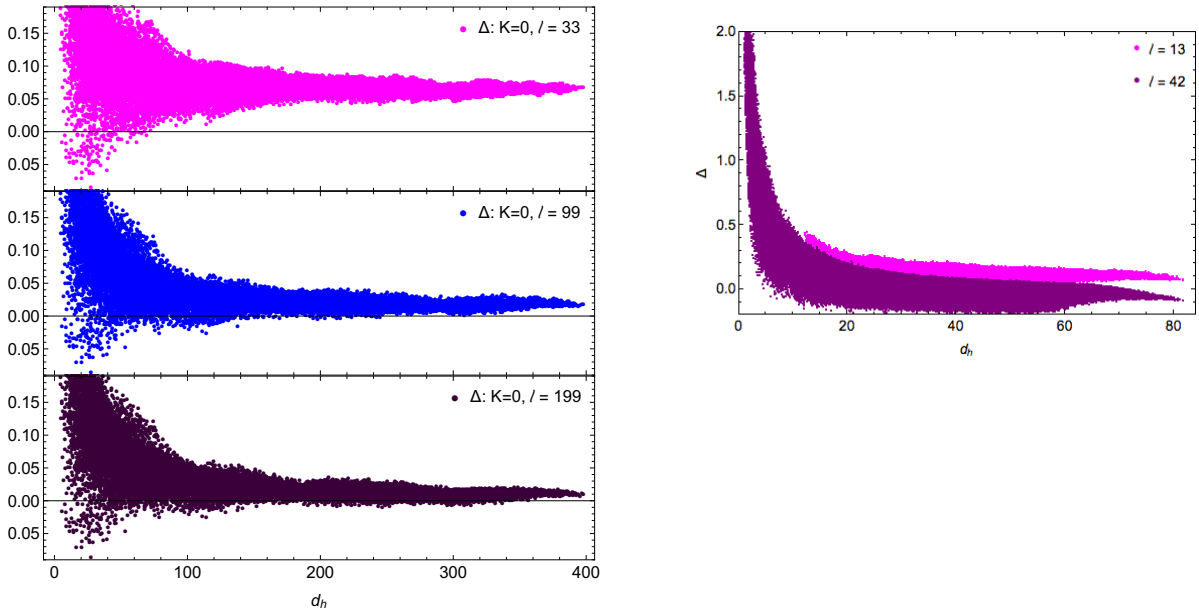

Figure 3.14: When $\ell \sim \ell_{DAS}$, the distance function in $d = 2$ (left) overestimates the continuum distance, even at larger d_h. The same is true in $d = 3$ dimensions, although we see that the asymptotic silence regime extends less far than the two-dimensional case.

respect to the continuum distance. The distance function is expected to reproduce the continuum distance at sufficiently large d_h if the separation of scales $\ell_{DAS} \ll \ell \ll \ell_K$ is achievable. The spacetime H_+ will refer to the case where the extrinsic curvature is positive with respect to the future directed normal of the initial boundary. H_- then refers to the opposite case. In App. B, we show an example of a sprinkling into these spacetimes, Fig. B.1 and provide the parametrisation employed here to calculate the continuum distance. Simulations of the predistance and distance function for $H_\pm$ and $\ell_K = 1000$ are shown in Fig. 3.15

For a radius of curvature $\ell_K = 1000$, we see indeed that the predistance on H_+ underestimates the continuum distance whereas it overestimates it on H_-. We then employ the distance function and vary ℓ to decrease the error between $\mathbf{d}$ and d_h. Note that for two values of the cutoff $\ell_1 < \ell_2$, all allowed paths with maximum step size ℓ_1 are automatically contained within the set of allowed paths with maximum step size ℓ_2. Since the distance function is obtained through a minimisation over paths, this means that if the ℓ_1 paths already contain the minimal path, the ℓ_2 paths will not minimise the distance further.

In the case of H_-, we see that the predistance overestimates the distance, whereas the minimi-

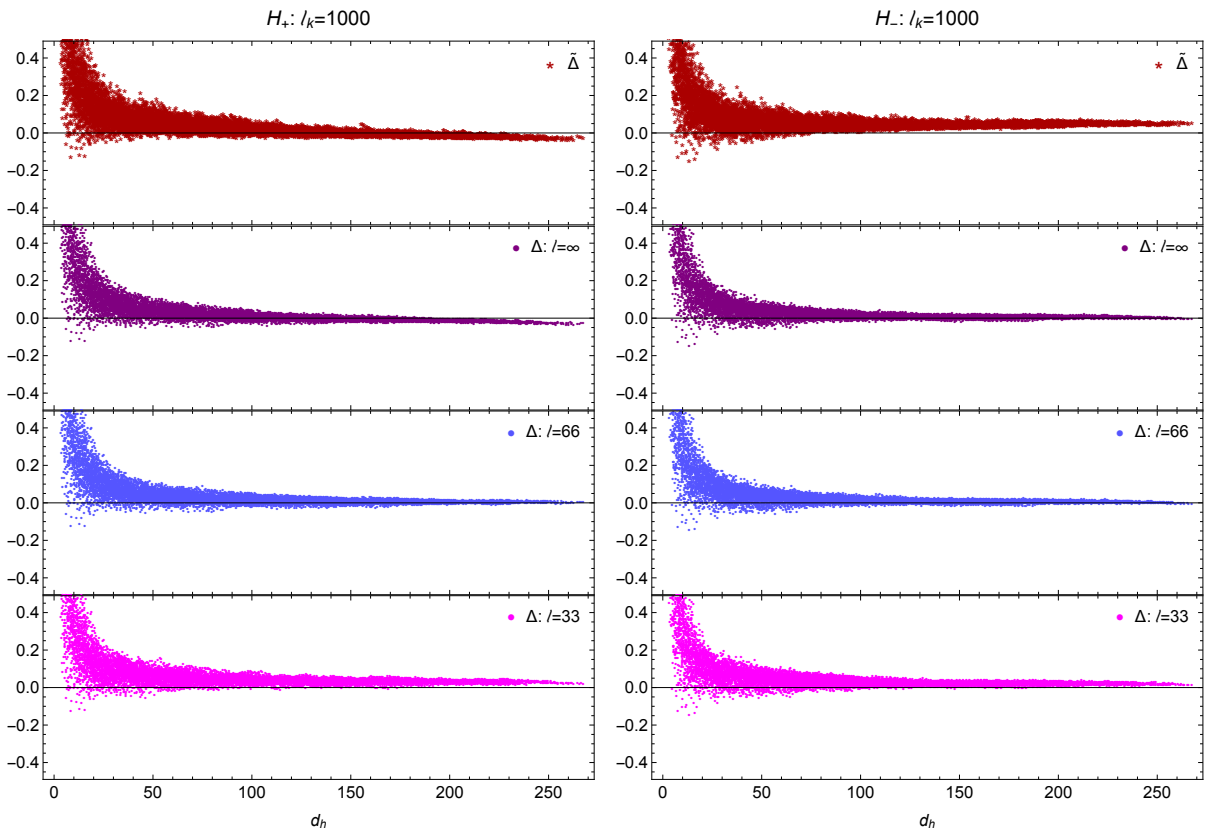

Figure 3.15: We show the error in the predistance function, $\widetilde{\Delta}$, (red) and the distance function, Δ, for various values of ℓ in the positive (H_+) and negative (H_-) curvature cases.

sation procedure of $\mathbf{d}$ already selects the minimum path at relatively small values of the cutoff and hence, increasing ℓ does not minimise the distance further. The asymptotic silence regime sets in around $\ell_{DAS} \approx 33$, but for $\ell > 66$ we get good agreement between $\mathbf{d}$ and d_h.

For H_+, the predistance, $\widetilde{d}$, underestimates the continuum distance, as does the distance, $\mathbf{d}$, in the infinite cutoff limit. By lowering the cutoff down to $\ell \approx 66$, we obtain agreement between $\mathbf{d}$ and the continuum distance. In this case, however, a further increase in ℓ, and consequently an increase in the number of allowed paths contributing to the minimisation procedure, results in an underestimation of the continuum distance (see the $\ell = \infty$ panel on the lef-hand side of Fig. 3.15).

In both cases, increasing the cutoff to $\ell \to \infty$, makes the construction of $\mathbf{d}$ sensitive to curvature effects. The difference between H_+ and H_- is then that for H_- the shortest path happens to be such that each individual step *does not* feel the curvature and thus we only need to tune ℓ outside of the asymptotic silence regime to obtain reliable results. For H_+, the shortest path is exactly one where each individual step *does* feel the curvature. Obtaining the correct distance then requires additional tuning of ℓ.

We saw above that when the curvature is sufficiently small, there is a large enough regime for ℓ where $\ell_{DAS} \ll \ell \ll \ell_K$ holds, such that we may obtain a distance function on $H_\pm$. Since ℓ_{DAS} is

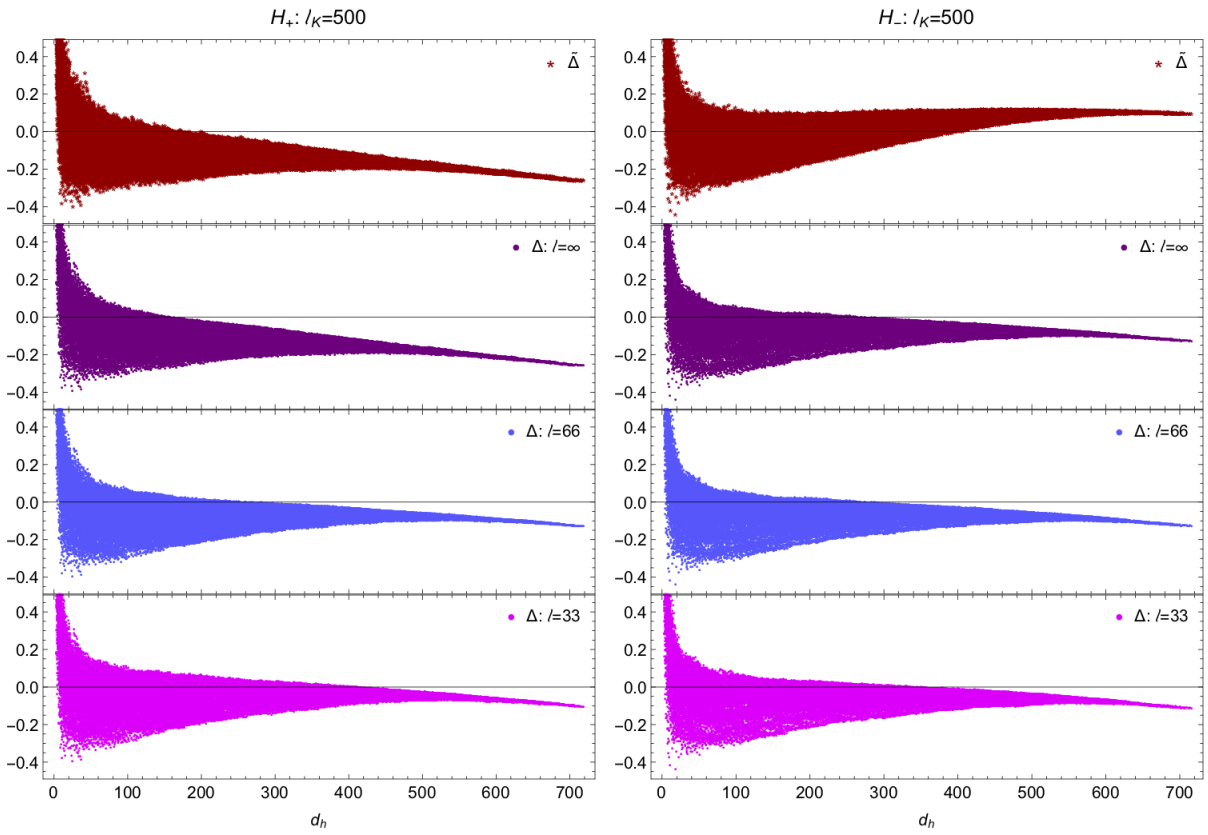

Figure 3.16: When curvature effects are too large, there is no value for ℓ for which $\mathbf{d}$ and d_h converge.

fixed by the dimensionality of spacetime, we can only decrease the range of the cutoff ℓ for which reliable distance estimation can be obtained by decreasing ℓ_K (increasing K). Let us then consider a case where it is no longer possible to obtain a sufficient separation of scales. For this purpose we choose a radius of curvature $\ell_K = 500$, and present the numerical results in Fig. 3.16.

For $\ell_K = 500$, the trend of $\widetilde{\Delta}$ and the various versions of Δ is in the same direction as for $\ell_K = 1000$ (see Fig. 3.15), but amplified to such extremes that we are no longer able the find a regime where $\mathbf{d}$ converges to the continuum distance. The question is then what the minimum value of ℓ_K is such that we still find convergence. Through direct simulations we find that $\ell_K = 580$ is the boundary value for which our construction manages to reproduce the continuum distance, see Fig. 3.17. This suggests that the critical value of ℓ_K for which our construction is still valid lies around $\ell/\ell_K \approx 0.12$. In addition, the setting above has been applied to a case where the curvature is not constant and the spatial hypersurface follows the shape of a circle section, see App. B.4.

If spacetime is indeed described by causal set theory in the deep UV, then continuum geometry needs to be encoded in terms of the causal relations and cardinality of the causal sets alone. It is then crucial to understand how to extract geometric properties. Here we set an important step by constructing a spatial distance function on an inertial spatial hypersurface Σ based on causal

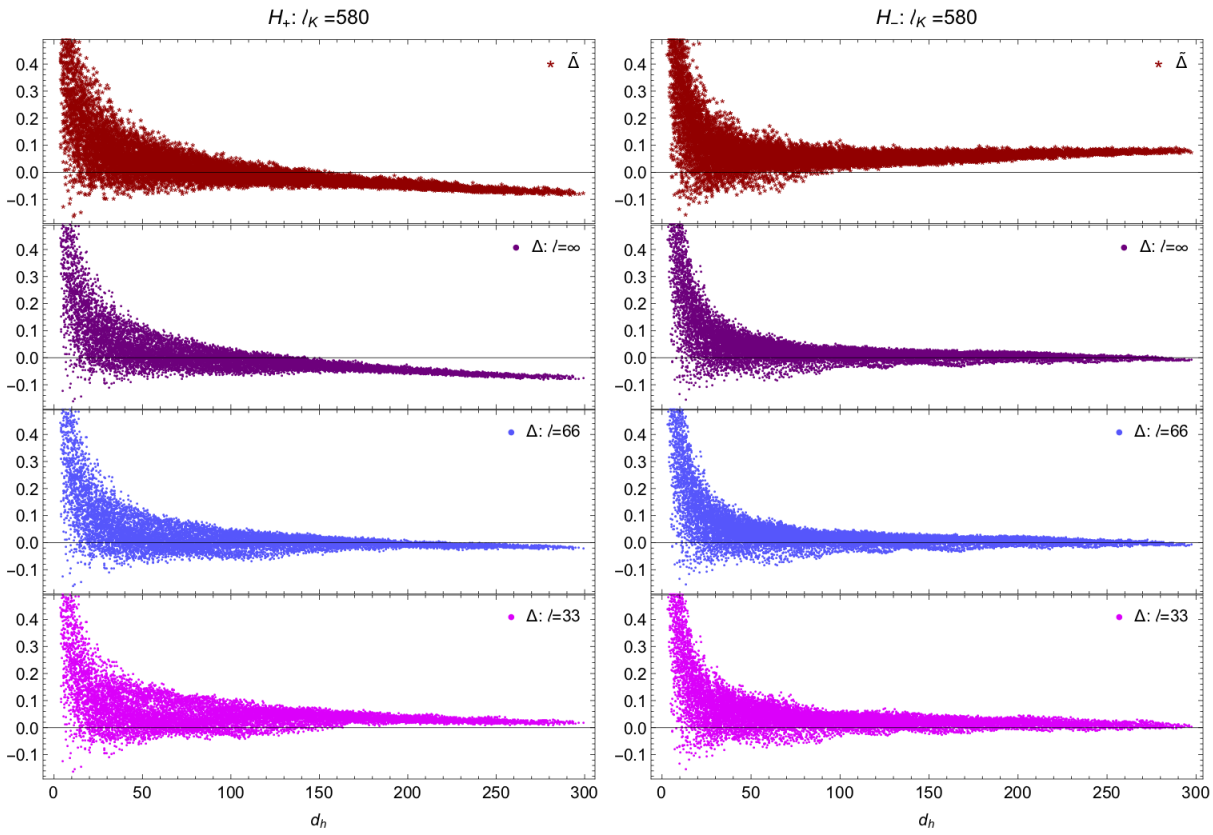

Figure 3.17: For $\ell_K = 580$ there is a regime for ℓ such that $\Delta \to 0$.

structure and volume alone. Such a construction is naturally translated to the discrete causal set and yields an intrinsic distance function on the antichain A of the causal set. We thicken the antichain by including causal information to the future of A (and past if A is not inertial/minimal), where ℓ functions as a cutoff on the number of "layers" included in the thickened antichain. In the flat spacetime setting, we saw that ℓ is bounded from below by ℓ_{DAS}, the scale associated to asymptotic silence. Within the asymptotic silence regime, the randomness of the causal set causes a significant overestimation of the continuum distance by the predistance in the regime where the continuum distance is small. Since the distance is calculated as a sum over predistances, these overestimations accumulate and cause an overestimation at all continuum distances. In the case where the inertial surface admits curvature, the cutoff scale ℓ is bounded from below by ℓ_{DAS} and from above by the radius of curvature ℓ_K. Through numerical simulations, we found that when $\ell/\ell_K < 0.12$ and $\ell > 33$, there exists a large enough range for which the distance function agrees with the continuum distance.

We will see in the following section that the construction above does not only yield a spatial distance function, but additionally provides an estimation of the dimension of spacetime. Furthermore, by associating a a graph with the antichain, A, we can set up a diffusion process and extract the *spectral dimension* of spacetime.

3.3.4 Dimensional estimator

The construction of the distance function, $\mathbf{d}$, can be used to extract the topological dimension of the inertial spatial hypersurface, Σ. On a Riemannian space, $\mathbb{R}^n$, one of the most straightforward constructions of the topological dimension, n, comes from the so-called *Hausdorff dimension*, d_H. In general, the Hausdorff dimension is obtained from the scaling relation between volume and radius $V(r) \propto r^{d_H}$, i.e., d_H encodes how the volume of a topological ball, $V(r)$, scales with its radius, r. Intuitively, this relation is easiest understood by considering an n-ball with radius r on $\mathbb{R}^n$. In a Riemannian setting, the volume scales with the radius as: $V(r) \propto r^n$ and hence, $d_H = n$, the topological dimension of $\mathbb{R}^n$.

Since the radius of a ball can be interpreted as a distance, we already possess one of the geometric properties needed to construct d_H. The other property we will need is that of a volume. On the causal set there is a direct correspondence between the volume and the number of elements, $V \sim N$, and we can thus obtain the volume by simply counting elements. Let us then choose an element $a \in A$ at random and associate a (spatial) volume $V_a(d_{crit})$ to a, by counting the number of elements that lie within a radius d_{crit} around a. The scaling behaviour $V_a(d_{crit}) \propto d_{crit}^{d_H}$ is shown in the top panels of Fig. 3.18 for $n = 2$ and $n = 3$ *spacetime* dimensions (i.e., 1 and 2 spatial dimensions, respectively).

We see that in 2 spacetime dimensions, the spatial volume scales as $V_a(d_{crit}) \propto d_{crit}$, suggesting $d_H = 1$, whereas in 3 spacetime dimensions $V_a(d_{crit}) \propto d_{crit}^2$, such that $d_H = 2$. We see then that when $K = 0$, the spatial distance can be used to recover the topological dimension of spacetime. Since d_H only agrees with the topological dimension in flat spacetime, we expect this analogy to break down whenever ℓ_K is too small, cf. Fig. 3.18 bottom panels.

3.3.5 Spectral dimension

The construction of the spatial distance on an inextendible antichain opens the door to the extraction of other geometrical properties. In the previous section we saw how to obtain an estimation of the topological dimension of spacetime. Here we will focus on a different notion of dimension, namely the *spectral* dimension.

The spectral dimension is one of the few geometrical quantities studied across different approaches to quantum gravity [270, 367, 368, 369, 370, 274, 371, 372, 373, 374, 282, 375]. The idea is to set a random walker loose on space(time) and extract a notion of dimension from the probability of the random walker to return to its starting point. This dimension is called the spectral dimension and reflects which dimension is "felt" by the random walker. Intuitively one can imagine that a random walker is more likely to cross a specific point twice if it is constraint to a line (one dimension) rather than a surface (the trivial example is zero dimensions, where the random walker is confined to its starting point and hence, the return probability is constant at all times). This is simply a consequence of the fact that for a walker in flat n-dimensional space, the total volume that can be reached after σ steps grows as $\sim \sigma^n$, such that there exist more paths that lead away

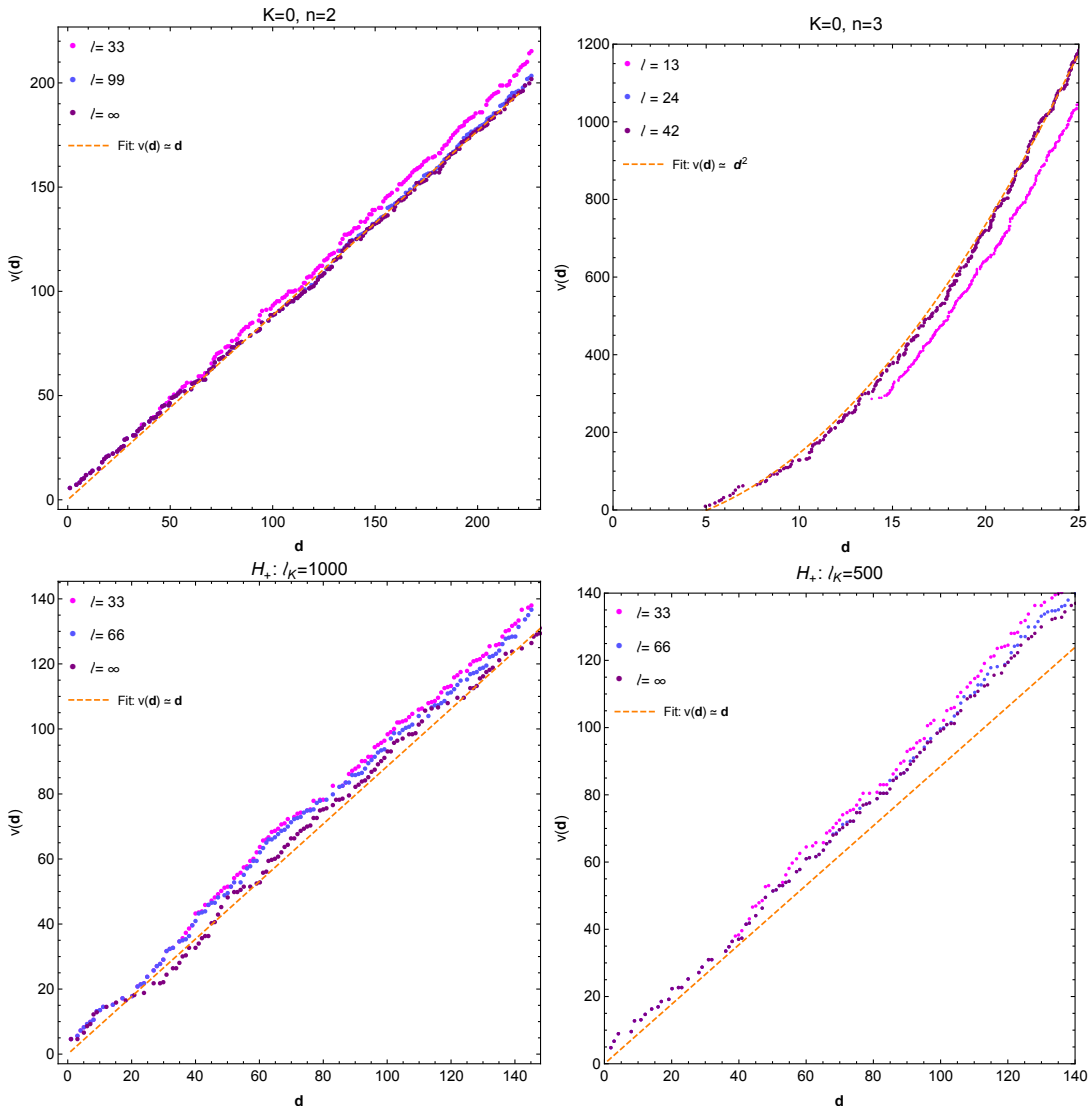

Figure 3.18: Top: We show the scaling of the spatial volume with the distance for different choices of the cutoff, ℓ. In both $n = 2$ (left) and $n = 3$ spacetime dimensions, the scaling behaviour agrees with the continuum fit when $\ell_{DAS} \ll \ell$. Bottom: For small curvature effects (left), the scaling between volume and radius reproduces the Hausdorff dimension for sufficiently large ℓ. When curvature effects become too strong (right), the scaling no longer yields the topological dimension.

from the origin in higher dimensions[17], see Fig. 3.19.

Mathematically, the probability for a random walker to transition from position x to x' is given by the solution to the so-called diffusion equation

$$(\partial_\sigma - \partial_x^2)P(x, x', \sigma) = 0. \tag{3.50}$$

[17]This only holds under the assumption that the random walker chooses its next position uniformly from a local neighbourhood around its current position.

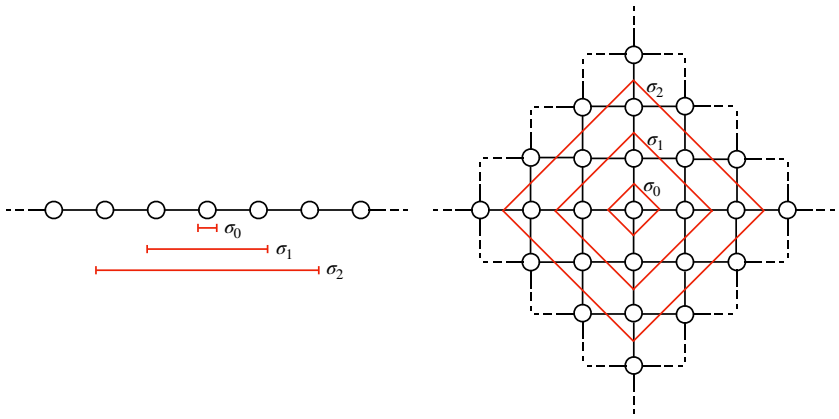

Figure 3.19: Illustration of the number of elements reachable after $\sigma = 0, 1, 2$ steps on a regular, square lattice where the step-size of the walker is restricted to the lattice spacing such that only the nearest neighbours of a current element are available at each step. Left: In one dimension, the volume (number of elements) grows linearly with each step. Right: In two dimension the volume (illustrated here by the elements that fall within the red lines, tracing out a diamond shape) grows quadratically with σ, leading to a lower return probability.

It is important to emphasise that here σ is an external "laboratory" time, completely independent of the internal properties of the spacetime. In flat spacetime, the equation above is solved by a Gaussian, peaked around x' and with standard deviation σ

$$P(x, x', \sigma) = \frac{1}{(4\pi\sigma)^{d/2}} e^{-\frac{(x-x')^2}{4\sigma}}. \tag{3.51}$$

The probability for a walker to return back to its origin x after some external time σ has passed is given by

$$P_r(\sigma) = \frac{1}{V} \int dV\, P(x, x, \sigma) = (4\pi\sigma)^{d/2}. \tag{3.52}$$

Using that in flat spacetime there is a particular scaling relation between the return probability and the external time σ, we define the spectral dimension to be this scaling dimension and extract it as

$$d_s(\sigma) = -2 \frac{d \ln P_r(\sigma)}{d \ln \sigma} \tag{3.53}$$

Such that $P_r(\sigma) \approx \sigma^{-\frac{d_s}{2}}$ and $d_s = d$ indeed holds in flat spacetime but can have a more complicated (σ dependent) form in general.

The general consensus for various quantum-gravity approaches seems to be that at low energies (IR) a random walker moves according to the topological dimension of spacetime, whereas quantum gravity effects at high energies (UV) modify the behaviour of the random walker as if it is moving in a lower-dimensional spacetime. In particular, in four dimensional flat space, the return probability in the UV scales as if the walker were moving in a two dimensional space [270, 367, 368, 369,

370, 274, 371, 372, 373, 374, 282], reviewed in [376, 377, 378]. Causal set quantum gravity has been the exception to the rule and registers a dimensional increase rather than a reduction [2]. The reason being the inherent non-locality of the causal set. As sketched in Fig. 3.19, the return probability is sensitive to the "cumulative volume" available at each step. If we confine the walker to only transition between nearest neighbours, then at each step on a regular lattice the walker stays within a region that is local to the current element. On a causal set these notions of locality are by construction lost. If we define two elements to be nearest neighbours whenever they share a link, then any element can have a large (possibly infinite) number of nearest neighbours. This suggests that the scaling of the total available volume at each step will grow much faster than $\sim \sigma^d$, and hence, the return probability gives rise to a spectral dimension much larger than the topological dimension at small σ. As σ grows, the walker rapidly moves away from its starting point (superdiffusion), resulting in the return probability quickly dropping down to zero and consequently $d_s \to 0$. Alternatively, one could modify the diffusion equation Eq. (3.50) by employing the causal set d'Alembertian [312, 360, 313, 361] or its continuum approximation [379, 380], where the non-locality scale, ℓ_k, (see Chpt. 3.3.2) is taken to be much larger than the discreteness scale. One can then find an analytic approximation to the spectral dimension and within certain regimes, this leads to dimensional reduction. Note that in this case the dynamics of the diffusion process is not the same as when one directly places a random walker on the causal set, since associating the non-locality scale with the discreteness scale leads to an ill-defined diffusion equation.

It is then clear that the large number of nearest neighbours prohibits us from setting up a random walk in the usual way and hence, define the desired spectral dimension estimator. In particular, we would like to find a notion of locality such that our walker is constrained to taking "small" steps in the sense of crossing small distances as well as having a relatively small subset of nearest elements. This was accomplished in [3] by implementing the spatial distance function defined in the previous section. We then set up a spatial diffusion process on an antichain, where we now define two elements to be nearest neighbours if they lie within a certain spatial distance $\mathbf{d}_c$ of one another. We would then expect that a random walk reproduces the topological dimension, if the scaling of the volume with the number of steps is $V \sim \sigma^n$, where $n = d - 1$ the number of spatial dimensions, cf., Fig. 3.20.

3.3.5.1 Numerical results

To be more specific, we consider sprinklings into $\mathbb{M}^3$, such that the inertial antichains approximate a flat spatial hypersurface. In total we will consider 10 such sprinklings, each with antichains of approximately 1600 elements and we select 30 starting points on each of the antichains, chosen to lie in the centre of the causal set to delay the onset of boundary effect. For each sprinkling, we calculate the spatial distance between all pairs of elements according the process described in Chpt. 3.3.3[18] Two elements are defined to be nearest neighbours when they lie within a distance of $\mathbf{d}_c$ of one another. This gives rise to an effective graph with connectivity between the nodes depending on the value of $\mathbf{d}_c$, see Fig. 3.22. We then place a diffuser on a starting element, e, and assign a uniform jump probability to any of the nearest neighbours of e. Specifically, the probability

[18] Note that since we are working in a flat setting, the distance and predistance functions coincide.

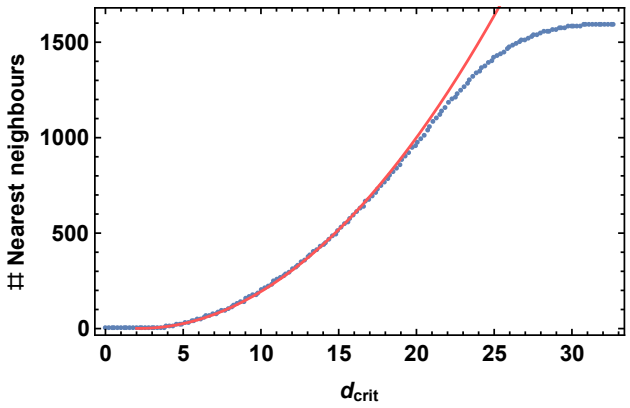

Figure 3.20: The number of nearest neighbours as a function of d_{crit} (blue, dashed line) shows similar scaling behaviour as the growth of the volume of a two dimensional ball with its radius (continuous, red line), $n = 1 + \pi(r - r_0)^2$ with $r_0 = 2.166$, the minimum distance above which an element has more than just one nearest neighbour.

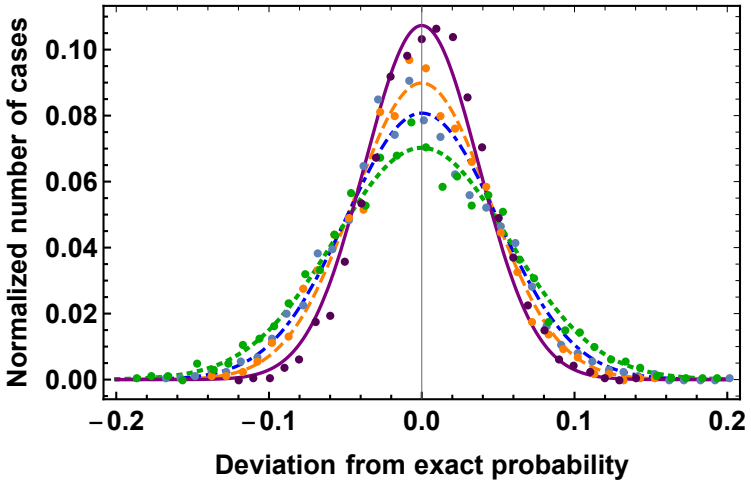

Figure 3.21: The deviation from the exact probability of the normalised number of cases and a Gaussian fit to the data are shown for $3\dot{1}0^4$ diffusion processes (green dots, green dotted line), $4\dot{1}0^4$ diffusion processes (blue dots, blue dashed-dotted line), $5\dot{1}0^4$ (orange dots, orange dashed line) and $7\dot{1}0^4$ (purple dots, purple solid line). We see then that an increase in the number of diffusion processes results in a more sharply peaked Gaussian.

for the diffuser to jump to any of the $n(e)$ neighbours of e is set to $1/n(e)$, where e is taken to be a neighbour of itself (i.e., the diffuser is allowed to stay on e). Depending on the value of $\mathbf{d}_c$, a large number of diffusion processes is initiated at each starting point.

The correctness of our code can be cross-checked by comparing the jump probability from an element e to any of its nearest neighbours, $1/n(e)$, with the number of times the diffuser actually jumps to that specific nearest neighbour. This will simultaneously allow us to determine an appropriate number of diffusion processes given a value for $\mathbf{d}_c$, since a small number of diffusion processes

$\mathbf{d}_c$	3.5	3.9	4.3	5.9	6.9	7.9	9.8	11.8
# diffusion processes	$3 \cdot 10^4$	$3 \cdot 10^4$	$3 \cdot 10^4$	$5 \cdot 10^4$	$5 \cdot 10^4$	$7 \cdot 10^4$	$7 \cdot 10^4$	$7 \cdot 10^4$

Table 3.1: For each value of $\mathbf{d}_c$ we start a large number of diffusion processes on each sprinkling and each starting point.

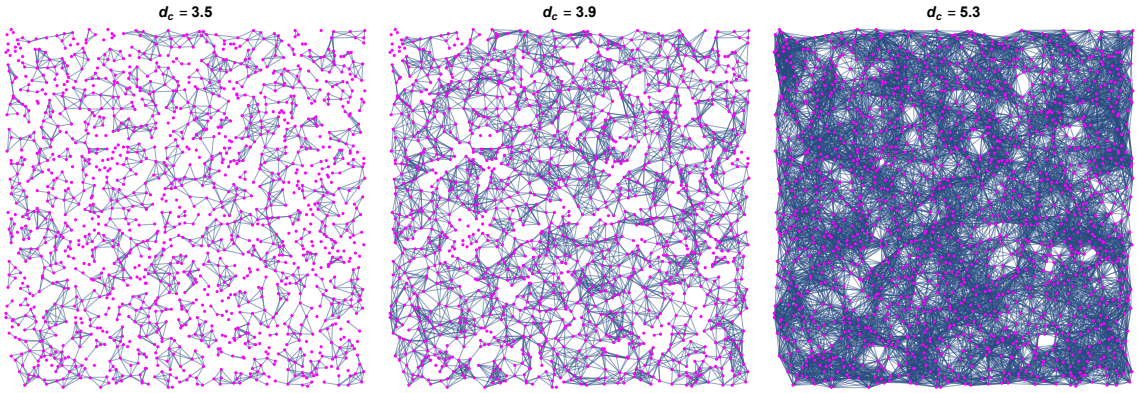

Figure 3.22: The effective graph depicting the connectivity between different elements (magenta dots) on an antichain obtained through a sprinkling in $\mathbb{M}^3$ is shown. We see that the connectivity (number of links) grows with $_c$. The coordinates of the nodes are derived from the embedding.

leads to a significant deviation from the exact probability. As shown in Fig. 3.21, increasing the number of diffusion processes decreases statistical errors. In Tab. 3.1 we summarise the number of diffusion processes for various values of $\mathbf{d}_c$.

From Fig. 3.22 we see that for small values of $\mathbf{d}_c$, each elements only has a small set of nearest neighbours and the connectivity across the graph will be limited. For example, when $\mathbf{d}_c = 3.5$, the graph consists of disconnected "islands" and hence, connectivity across the graph is lost. Even though the scaling between volume and radius already yields the Hausdorff dimension at small distances, cf. Fig. 3.20, the diffusion process will get stuck on the small islands if $\mathbf{d}_c$ is too small. Since a diffuser on one of those islands is "blind" to the elements that lie outside of its island, the diffusion process will be bounded to a small subset of the effective graph. As a result, boundary effects are expected to set in almost immediately and the spectral dimension will underestimate the topological dimension. The existence of these islands is a direct consequence of the inherent randomness of the causal set and hence, of asymptotic silence. On the other hand, when we choose $\mathbf{d}_c$ too large, the causal set will be well-connected but the diffuser will reach the boundary of the causal set in only a few steps and we expect that the spectral dimension will not exhibit a stable regime.

As the causal sets under consideration are small, we expect that already for relatively small values of σ the diffuser will reach the boundary. Let $\sigma_{bd}(\mathbf{d}_c)$ be the diffusion time where boundary effects set in for a given value of $\mathbf{d}_c$ and hence, the number of steps after which the diffusion process is halted. We then determine $\sigma_{bd}(\mathbf{d}_c)$ by studying the average number of nearest neighbours an element has. Elements that lie closer to the boundary of the causal set will on average have a smaller number of nearest numbers than elements in the centre of the causal set. We then associate

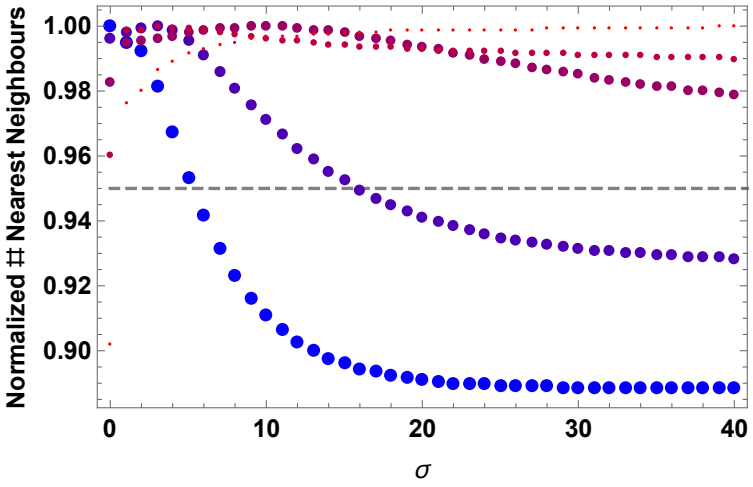

Figure 3.23: The normalised number of nearest neighbours decreases as σ increases with different rates for different values of $\mathbf{d}_c$. From top to bottom the values of $\mathbf{d}_c$ increase with the size of the dots and are $\mathbf{d}_c \approx 3.5, 4.3, 5.9, 7.9, 9.8$. Once the normalised number of nearest neighbours drops below 95% (grey, dashed line), we read off the value for $\sigma_{bd}(\mathbf{d}_c)$.

$\sigma_{bd}(\mathbf{d}_c)$ to the value of the diffusion time after which the number of nearest neighbours has fallen by approximately $\sim 5\%$, as illustrated in Fig. 3.23

Following the procedure described above, we start a large number of diffusion processes where we limit the diffusion time to $\sigma_{bd}(\mathbf{d}_c)$. The return probability at each step σ is then readily obtained as the average number of times a diffuser crosses the starting point at time-step σ. The average is taken over all sprinklings, starting points and number of initiated processes. We show the return probability $P_r(\sigma)$ in Fig. 3.24

We see that for all $\mathbf{d}_c$ the return probability drops rapidly and approaches a constant for large diffusion times. This suggests that the diffusion process equilibrates and is a direct consequence of the finite size of the antichain, i.e., the diffuser cannot "escape" infinitely far away. The spectral dimension is calculated as the logarithmic derivative of the return probability and hence, will drop to zero for large diffusion times since P_r becomes constant here. Note that $P_r(\sigma = 0) \approx P_r(\sigma = 1)$ in all cases. This is simply because the probability of staying at the origin at $\sigma = 0$ is $P_r(0) = 1/n(o)$ and the probability of being at the origin after one time step is $P_r(1) \approx P_r(0) \cdot 1/n(o) + (1 - P_r(0)) \cdot 1/n(o) = (P_r(0))^2 + (1 - P_r(0)) \cdot P_r(0) = P_r(0)$, where we made the approximation that all nearest neighbours of o have approximately $\sim n(o)$ neighbours. Note that this relation holds exactly a lattice of fixed valency.

Equipped with the return probability, the discrete spectral dimension can be calculated by means of a discrete derivative

$$d_{s,n} = -2\frac{\sigma_i}{P_r(\sigma_i)}\frac{P_r(\sigma_{i+n}) - P_r(\sigma_i)}{n}, \tag{3.54}$$

where fluctuations between intermediate steps of P_r are smeared out by increasing the value n.

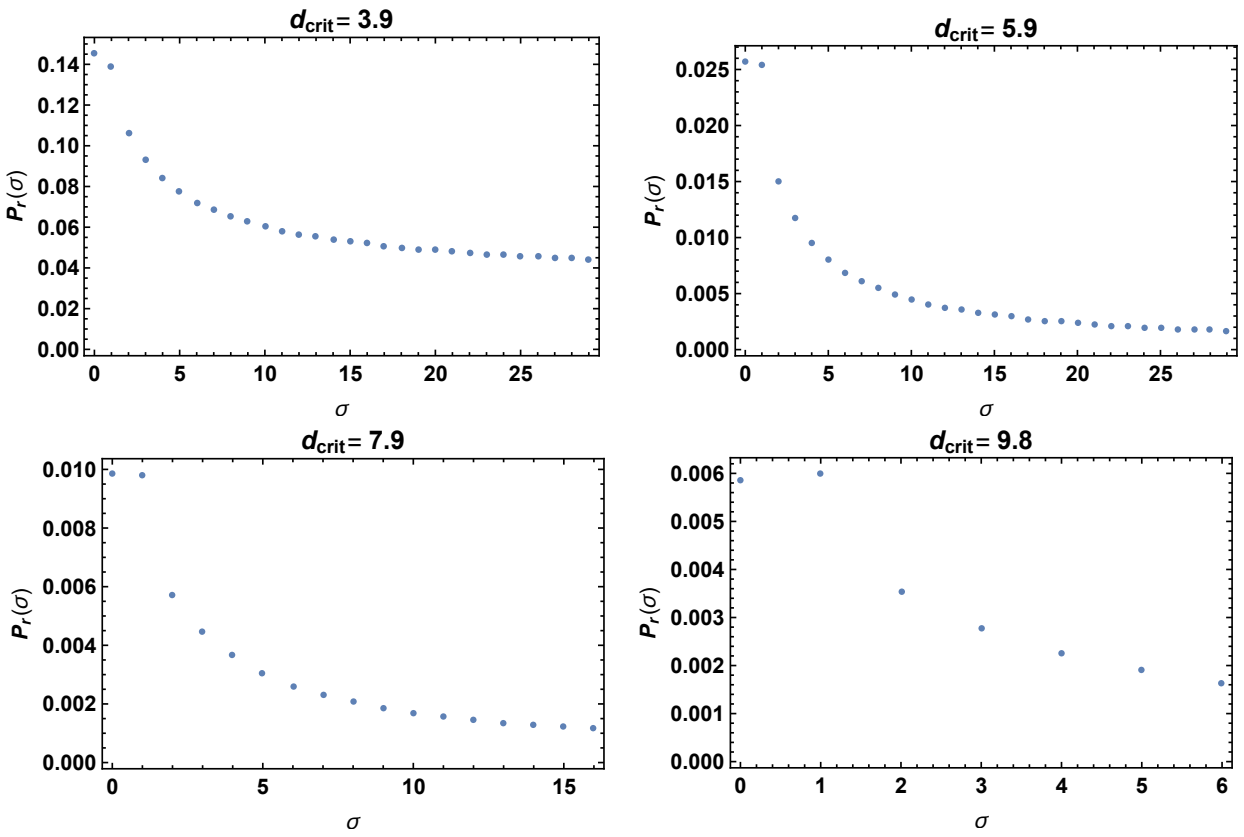

Figure 3.24: The return probability as a function of the diffusion time is shown for $\mathbf{d}_c = 3.9, 5.9, 7.9, 9.8$.

Here we will focus on $n = 2, 3$ and show the results for the spectral dimension in Fig. 3.25 and Fig. 3.26.

When $\mathbf{d}_c$ is too small, the spectral dimension drops quickly and no intermediate plateau is formed, as can be seen from the top panels of Fig. 3.25. Here the diffuser is confined to small islands resulting in an early onset of boundary effects, see the bottom panels of Fig. 3.25. The presence of a boundary equilibrates the diffusion process quickly, such that the return probability becomes approximately constant and hence, the spectral dimension drops to zero. We can interpret the underestimation of the topological dimension $d_s < d_H$ for small values $\mathbf{d}_c$ as a form of dimensional reduction, instantiated by asymptotic silence effects.

Increasing $\mathbf{d}_c$ to large enough values allows us to read off the spectral dimension from a plateau in d_s at intermediate values of σ, see Fig. 3.26. For $\mathbf{d}_c = 5.9, 7.9$ the connectivity is such that (almost) the entire antichain can be reached, meaning that we not only obtain continuum-like connectivity, but also push boundary effects to large enough values of σ such that a stable intermediate regime exists. We then find that the spectral dimension tends to the Hausdorff dimension.

An important difference between the causal set and a finite, regular, two-dimensional lattice is that the associate discreteness scale of the lattice, i.e., the lattice spacing a, gives the exact distance

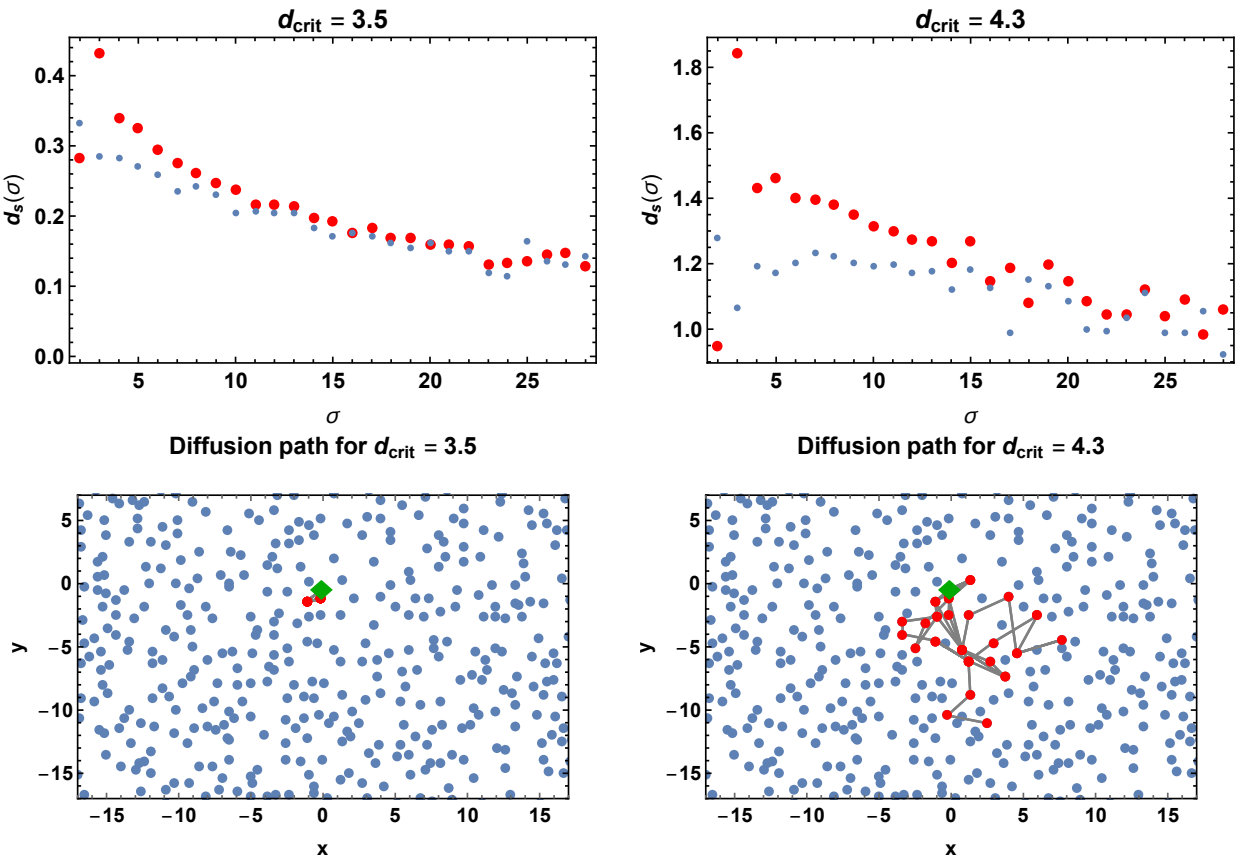

Figure 3.25: Top: The spectral dimension as a function of σ for $\mathbf{d}_c = 3.5$ (left) and $\mathbf{d}_c = 4.3$, where the smaller blue dots depict the choice $n = 2$ in Eq. (3.54) and the larger red dots $n = 3$. In both cases the diffusion process drops to zero quickly without equilibrating at intermediate values. Bottom: An example of a diffusion path (red dots) on the antichain (blue dots) where the starting point is represented by a green diamond. For $\mathbf{d}_c = 3.5$ (left), the diffuser is restricted to a small island of only three elements. Increasing to $\mathbf{d}_c = 4.3$ (right), enlarges the island but nevertheless traps the diffuser.

between any two nearest neighbours on the lattice. As a consequence, for any $\mathbf{d}_c < a$, the lattice is completely disconnected and consists of single-element islands, leading to a spectral dimension which vanishes at all scales. When we set $\mathbf{d}_c = a$, instant connectivity of the entire lattice is reached and we find $d_s = 2$, cf. Fig. 3.27

To summarise, we have used the discrete distance function detailed in the Chpt. 3.3.3 to assign a notion of nearest neighbours to an inertial antichain. This allowed us to set up a random walk on the antichain and extract the return probability and associated spectral dimension of the process. For small values of the diffusion time σ, we saw that the discreteness results in small values of d_s independent of the value of $\mathbf{d}_c$. However, when $\mathbf{d}_c$ is small, the process is restricted to small regions on the causal set and hence, probe UV physics. In these cases the spectral dimension remains small for all values of σ, which we interpret as a form of dimensional reduction, instantiated by

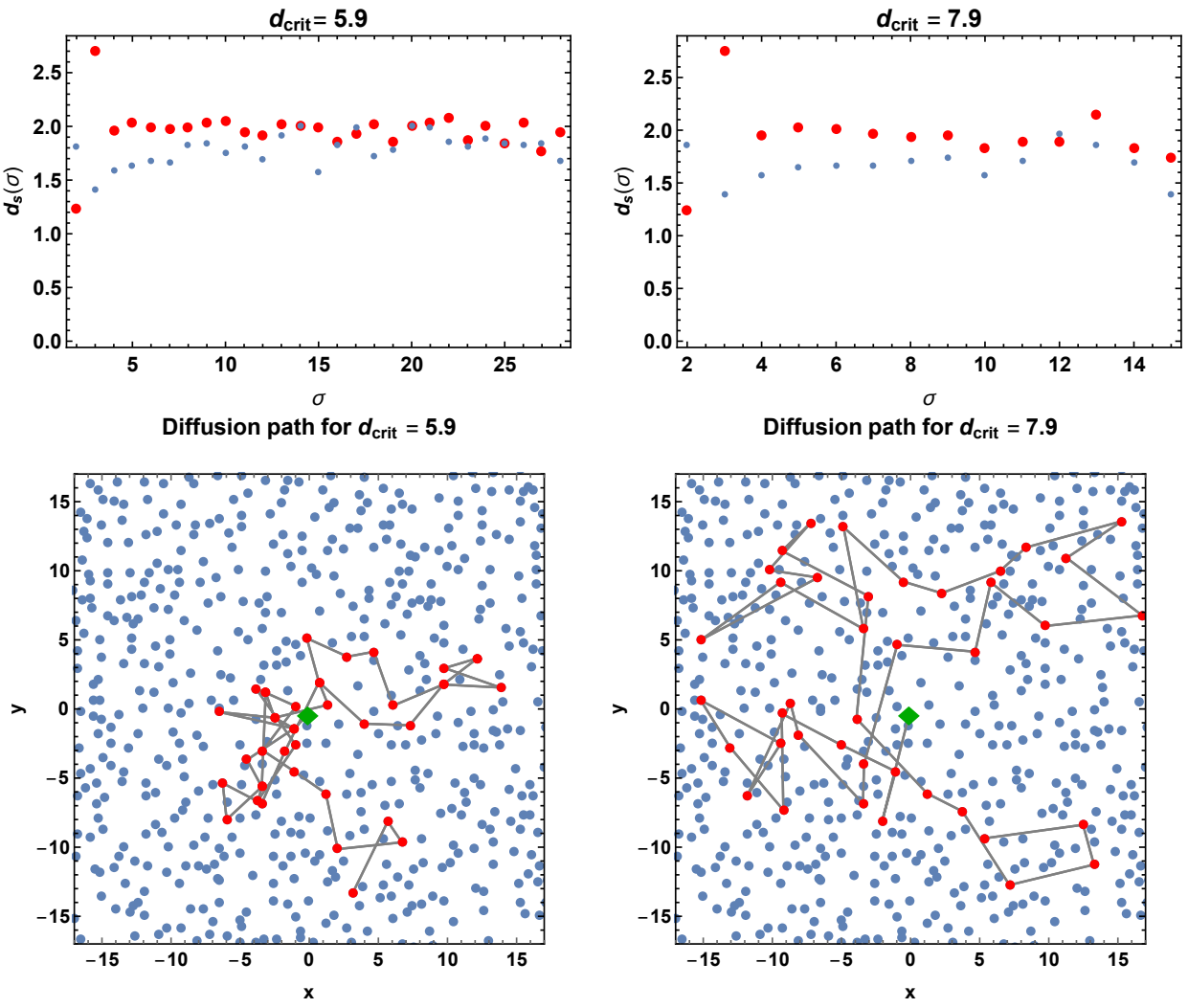

Figure 3.26: Top: In both cases there is a clear intermediate regime where we may read off the spectral dimension, calculated from Eq. (3.54). The case $n = 3$ (red dots) smooths out more of the fluctuations caused by the discrete nature of the causal set as compared to $n = 2$ (blue dots). Bottom: Examples of the diffusion paths associated with the diffusion processes in the top panels.

asymptotic silence. For larger values of $\mathbf{d}_c$, the diffuser explores the IR regime and the spectral dimension reproduces the Hausdorff dimension.

Let us point out that the dimensional reduction here is purely on the kinematical level, i.e., given a causal set, we employ a discrete random walk. In other quantum-gravity approaches this is not necessarily the case. For instance, in asymptotically safe quantum gravity, the dimensional reduction is directly related to the dynamics reaching scale invariance [162, 114, 371]. To study a dynamical form of dimensional reduction on the causal set, one would need to specify the dynamics. It would be interesting to see whether dimensional reduction persists on the dynamical level in future studies.

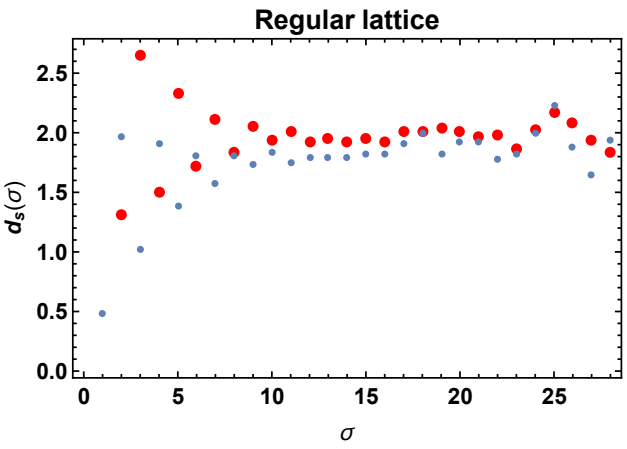

Figure 3.27: The spectral dimension for a regular two-dimensional lattice jumps sharply at small values of σ due to discretisation effects, before plateauing around the topological dimension $d_s = d_H = 2$.

Despite the minimalistic nature of CST, we have seen that the extraction of geometric information is indeed possible. In particular, the definition of a single geometric quantity, the spatial distance, allows us to find two dimensional estimators. The topological dimension, d_H, of spacetime can be found by comparing the scaling of volume with the radius $\mathbf{d}_c$ around an element on the antichain, A. Note that it is only possible to establish this relation due to the direct relation between volume and the number of elements in CST. In addition, we set up a diffusion process on an antichain and obtained the spectral dimension, which limits to the Hausdorff dimension in the IR regime and exhibits dimensional reduction in the UV on account of asymptotic silence. The definition of d_s allows us to directly compare with other approaches to quantum gravity and a compelling next step would be to extend the analyses performed here to higher dimensions. In particular, since most other approaches to quantum-gravity work in a 4-dimensional Euclidean setting, we would have to construct the spatial distance on an inertial spatial hypersurface in $\mathcal{M}^5$. The diffusion process would then take place on a 4-dimensional spatial slice and, based on results from other quantum-gravity approaches, it would be interesting to see if dimensional reduction gives an intermediate plateau around $d_s = 2$ in the UV. However, for now we are limited to 3-dimensional spacetime due to computational restrictions. Nevertheless, a more detailed study of the spectral dimension above might reveal the presence of a plateau at intermediate values of σ for some value of $\mathbf{d}_c$. Specifically, using the value of $\mathbf{d}_c$ for which connectivity across the antichain is reached for the first time, one might expect that the spectral dimension plateaus around $d_s = 1$. Further studies will have to confirm whether this is indeed the case.

Chapter 4

Conclusions

The formulation of a consistent theory of quantum gravity is without question a daunting task and has been a topic of interest for decades. As it is difficult to obtain an observational guiding principle against which specific models may be tested, it becomes useful to approach the problem from several directions simultaneoulsy and highlight different aspects of a possible theory of quantum gravity.

The asymptotic-safety scenario for gravity conjectures a symmetry enhancement at high energies, leading to a fixed point in theory space at which the microscopic theory can be defined. A coupling between (Standard Model) matter degrees of freedom and asymptotically safe gravity allows for the search of quantum-gravity imprints at observationally accessible scales and places the asymptotic-safety scenario in the unique position of potentially obtaining indirect experimental falsification. In particular, here we studied the renormalisation group flow of a gravity-matter system comprised of a minimal coupling between the Abelian hypercharge g_Y, and asymptotically safe gravity. As signalled by fixed points of the renormalisation-group flow, the system reaches scale invariance in the deep UV and enters a regime where the dimensionless couplings G, Λ and g_Y no longer change with scale. This fixed-point structure has particularly interesting consequences for the Abelian hypercharge g_Y, as it provides a UV completion and hence, renders g_Y to be well-defined up to arbitrarily high scales.

In addition, the pure-matter and the matter-gravity contribution come with opposite signs in the beta function of the hypercharge, i.e., the beta function is of the form

$$\beta_{g_Y} = \#_1 g_Y^3 - f_g g_Y, \tag{4.1}$$

where $f_g \sim G$ and $f_g > 0$ for the preferred gauge. The trivial fixed point at $g_Y = 0$ results in a UV completion where the coupling g_Y becomes non-interacting at high energies. Furthermore, g_Y corresponds to a relevant direction at the fixed point and as one follows the flow of the coupling to the IR, a range of low-energy values become available for g_Y. Crucially, the experimentally observed value falls within this range of IR values, providing a hint that the model studied here is consistent with experiment. This range of IR values is bounded from above by the interacting fixed point, g_Y^*, at which g_Y is an irrelevant direction. Since the Abelian coupling is IR attractive at the interacting fixed point, we obtain a *prediction* of the IR value for g_Y, which lies within

35% of the experimentally observed value. In [191], the systematic error in the fixed-point values of Λ and G, induced by the choice or regulator, was estimated to be up to 60%, indicating that the predictive, interacting fixed point studied here is viable within systematic errors. To test the stability of our results, we studied the sensitivity of the critical exponents to changes in η_h and found only a minor dependence. Since η_h can to some extent be used to parametrise the strength of the gravity contributions, the stability of our results were tested by studying the sensitivity of the critical exponents to changes in η_h. We found only minor dependencies, which is certainly encouraging but does not take away the necessity for extended studies. In particular, one could take into account the back-reaction of the matter degrees of freedom on gravity by studying a system where all three couplings G, Λ, g_Y are allowed to run. Extensions in the truncation can be done by including terms R^2, $(R^{\mu\nu})^2$ in the gravity sector or photon self-interactions F^4 in the pure matter sector. In addition, one might study a non-minimal coupling between gravity and matter of the form $\sim \sigma R^{\mu\nu} g^{\kappa\omega} F_{\mu\kappa} F_{\nu\omega}$. It is only by studying extended truncations that we may check for the robustness of our findings. Moreover, it will be interesting to see the fate of the IR prediction for g_Y in these scenarios.

We see then that in addition to providing a solution to the triviality problem, asymptotically safe gravity, within the truncation studied here, provides an enhancement of predictivity by eliminating a free parameter from the system. It is then the inclusion of matter degrees of freedom which provide the additional structure necessary to "bring quantum gravity down" to observationally accessible scales. Since one can argue that a theory of quantum gravity consistent with observations should be able to account for matter, it becomes of crucial importance that any viable approach to quantum gravity passes this test. The added predictivity of matter-gravity models is then a highly intriguing phenomenon which certainly deserves further study in the future.

Next to a functional analyses of asymptotically-safe gravity, one can regularise (Einstein-Hilbert) quantum gravity by utilising lattice techniques as a regularisation procedure. An advantage of the lattice methods employed in dynamical triangulations is that, in contrast to the continuum approach, a direct (numerical) evaluation of the microscopic dynamics becomes available so that one does not need to work in truncations. We add the disclaimer that one nevertheless makes an *ansatz* for the microscopic action and hence, the relevant parameters of the fundamental model.

Recently, Kähler-Dirac fermions were added to the dynamical lattice and their properties studied. There are indications that Kähler-Dirac fermions reduce to four copies of the ordinary Dirac fermions in the continuum and their representation in terms of exterior derivatives is naturally translated to lattice settings. The studies that were performed verified that the masses of mesons associated with zero- and four-simplices have a mass which vanishes in the chiral limit, whereas the masses of the remaining three sub-simplices take on finite values. However, as one refines the lattice by making the lattice spacing smaller, the squared masses of the remaining sub-simplices shrink linearly with the squared lattice spacing and can be extrapolated to zero. This provides strong hints that in the continuum limit, there is no chiral symmetry breaking. It should be clear that more detailed studies are necessary to confirm these results. In particularly, at small distances there may be discretisation effects which seep into the results, whereas long distances should be probed with care to avoid finite-volume effects. This makes the region where one can extract physically meaningful information relatively narrow. The largest lattices used in the studies described

here are relatively small, i.e., 16000 four-simplices, and it is thus important to repeat these studies at larger volumes to confirm that there is indeed no chiral symmetry breaking. Nevertheless, since there appears to be no spontaneous breaking of chiral symmetry within the numerical limits of the studies here, no bound-states with Planck-scale masses were generated. This cross-check is crucial if EDT is to provide a quantum-gravity theory consistent with observations.

Since the studies so far were restricted to a quenched setting, i.e., the back-reaction of the fermions on the lattice was not taken into account, an important next step is to unquench the calculations. Specifically, one adds the (discretised) Kähler-Dirac action to the microscopic action and studies the evolution of the dynamical lattice using such a modified partition function. These simulations become numerically very heavy, since the inclusion of the Kähler-Dirac fermions requires the repeated evaluation of the determinant of the Kähler-Dirac matrix. Since this matrix is *sparse*, i.e., a large fraction of the matrix entries are zero, the inversions are numerically expensive. Let us emphasise that with the techniques developed, the difficulties of adding fermions are all of numerical/algorithmic nature but pose no conceptual issue. Since algorithmic improvements are expected to improve the performance of the code, a treatment of fully dynamical fermions on dynamical triangulations is only a matter of time.

We note that chiral symmetry breaking induced through asymptotically-safe gravity has been addressed using FRG methods as well [77]. Here it was found that chiral symmetry remains intact around the Planck scale, irrespective of whether gravity becomes strongly interacting or not. It is exciting that this finding is in line with the quenched studies performed here and it would be highly interesting to investigate whether future endeavours with unquenched fermions support these results.

Since the algorithm performs well enough to simulate dynamical Kähler-Dirac fermions on small triangulations, we may extract the running of the renormalised cosmological constant, Λ, for constant values of β and as a function of the renormalised gravitational coupling $1/G$, which sets the lattice spacing. Simulations of this kind are currently underway and might provide important insights on the effects of matter on lattice gravity.

As one approaches the phase transition, simulations become more expensive such that one is limited to smaller physical volumes and finite-size effects in the form of baby universes might contaminate the results. Since these are the observationally relevant parts of the phase diagram (close to the conjectured continuum limit), it is of importance to check the robustness of the results on larger and finer lattices.

Whereas the concepts of asymptotically-safe quantum gravity work under the assumption that physics below and above the Planck scale can be described through a modification of known frameworks, the causal-set approach to quantum gravity separates itself from this idea. CST distinguishes itself from other approaches in two ways: First and foremost, CST is currently the *only* approach to quantum gravity which is truly Lorentzian and therefore potentially captures features of quantum-gravity which Euclidean theories miss. Secondly, CST proposes that spacetime is *fundamentally* discrete at scales of Planckian-order. Specifically, spacetime is conjectured to be a set of discrete elements with a causal ordering relation between them. A notion of volume can then be recovered by counting the number of elements. It is conjectured that the causal ordering relations and local

volume elements are enough to reconstruct all geometric and topological properties of a spacetime. Since the analytical proof of this conjecture in its full generality is unlikely to exist, it is of great importance to construct the procedures by which one may extract geometric and topological properties from a causal set. The key point is that these properties should be obtained without relying on any continuum information, i.e., one can only use the causal relations and number-to-volume correspondence to construct these procedures. Here we take several important steps in the direction of reconstructing topological and geometrical properties.

A spatial distance function on an antichain, the causal-set analogue of a Cauchy hypersurface, was constructed by "borrowing" causal information of the neighbourhood close to the antichain, i.e., one thickens the antichain. The predistance function then follows from the relation between the volume of a (hyper)cone and its diameter in flat spacetime. On a causal set approximating flat spacetime, the predistance and distance functions coincide. However, for an antichain approximated by an initial hypersurface with constant curvature K, the predistance function either underestimates ($K > 0$) or overestimates ($K < 0$) the continuum distance. The distance function was then defined as a minimisation over paths between elements, where each step is restricted to be smaller than the cutoff ℓ. By choosing ℓ much smaller than the radius of curvature but larger than the scale where asymptotic silence sets in, one can avoid the underestimation/overestimation and obtain a distance which approximates the continuum distance. This construction breaks down when the separation of scales $\ell_{DAS} \ll \ell \ll \ell_K$ is not sufficiently large. In particular, we found that the boundary value of ℓ for which the separation of scales is sufficiently large, is given by the relation $\ell/\ell_K < 0.12$ with $\ell > 33$ such that one is well out of the asymptotic silence regime. The restriction to small curvature effects is clearly a limitation of the construction here, and it would be interesting to see if a generalisation to initial hypersurfaces admitting strong curvature effects is possible.

The definition of a spatial distance function opened the door to the extraction of two dimensional estimators: the Hausdorff dimension and the spectral dimension. In the continuum, the Hausdorff dimension is extracted as the scaling of the volume of a ball with its radius. In the discrete causal-set setting, we can estimate the Hausdorff dimension by randomly choosing an element in the centre of the antichain and counting the number of elements that lie within a radius $\mathbf{d}_c$ from it. It was found that in $d = 1 + 1$ and $d = 2 + 1$ spacetime dimensions, the connectivity of the antichain is such that the Hausdorff dimension is well-approximated.

An additional dimensional estimator came from the spectral dimension, d_s, which is related to the return probability of a random walker as a function of the (external) diffusion time. The spectral dimension has been analysed in a large set of quantum-gravity approaches and in almost all cases a dimensional reduction from $d = 4$ in the IR to $d = 2$ in the UV was observed. Causal sets formed an exception and showed a dimensional increase towards the UV when one set up a diffusion process along the links. This was identified as a direct consequence of the non-locality of causal sets and it was suggested that a "correct" setup, i..e, mimicking a Euclidean/Riemannian diffusion process, should lead to dimensional reduction. Indeed, here we found that a diffusion process on a two-dimensional antichain reproduces the Hausdorff dimension if one chooses $\mathbf{d}_c$, the spatial distance between neighbouring elements, to be sufficiently large. For small values of $\mathbf{d}_c$, we found a form of dimensional reduction, generated by asymptotic silence. All simulations are currently restricted to relatively small causal sets due to the computational complexity of the distance function, which

is necessary to obtain a notion of nearest neighbours on the antichain, and it would be of interest to double-check whether on larger antichains, higher values of $\mathbf{d}_c$ provide a large enough region of intermediate values for σ such that a plateau around $d_s = 2$ is observed. More interesting is of course the implementation of a random walk on a higher dimensional hypersurface. In particular, if one is able to set up a diffusion process on an initial surface in $\mathbb{M}^5$, then the return probability could be calculated on a 4-dimensional spatial slice and one could study whether a dimensional reduction from $d_s = 4$ in the IR to $d_s = 2$ in the UV occurs.

Taking a bird's-eye view on this thesis, we have discussed three approaches to quantum gravity, each with their own unique features. Let us for completeness briefly recapitulate how they relate and differ from one another.

Clearly, the asymptotic-safety scenario and dynamical triangulations are based on the same concepts, i.e., scale invariance in the UV. In the asymptotic-safety scenario, one employs FRG methods to search for fixed points in the flow of couplings. At these fixed points one can remove the cutoff and obtain a theory which is valid up to arbitrarily high energies. Similarly, on the lattice, one searches for second-order phase transitions at which the continuum limit can be taken, i.e., $a \to 0$. On grounds of universality, physics should not depend on the microscopic details of the theory, i.e., whether we employ lattice or functional methods for the regularisation procedure should not change the physical properties of the theory. A clear advantage of both methods is the ability to bridge a large range of scales and connect microscopic properties to observable, macroscopic physics. The truncation of the infinite space of operators in the functional approach is a disadvantage and becomes unnecessary when one moves to the lattice. On the other hand, it is still necessary to make a choice for the fundamental dynamics of the theory. Once this choice has been made, the corresponding set of relevant parameters will completely fix physics at all scales. Moreover, the addition of dynamical matter to the lattice is computationally expensive and it is therefore more straightforward to perform these computations through the FRG. Nevertheless, the comparison between lattice and functional methods will potentially strengthen the viability of both approaches and could render the worries concerning approximations in the latter mute. In addition, FRG calculations involving matter-gravity models could provide a guide, prioritising the addition of specific matter terms to the lattice. For example, the addition of a scalar QED type of interaction to the lattice should yield second-order phase transitions where either the hypercharge coupling needs to be tuned (relevant) or becomes a prediction (irrelevant). As a first approximation, the back-reaction of matter on the lattice can be ignored and one can study the Abelian hypercharge in a quenched approximation on the lattice.

One of the crucial open questions in CST is how to obtain the dynamics of the theory. Since there is no continuum limit, one cannot use universality arguments to hold one type of dynamics over the other. An important guiding principle for CST dynamics could come from other approaches to quantum gravity. Of course any *ad hoc* choice of the CST dynamics will not be fundamentally motivated, but it might provide the inspiration needed to construct a mechanism which does provide the dynamics. The other way around, since it is not clear whether a Euclidean formulation of quantum gravity will correctly reflect the Lorentzian nature of quantum gravity, it might be possible to identify those properties of quantum gravity which are inherently Lorentzian through CST mechanisms. One could then ask whether or not a Euclidean analogue of those properties exists

and if answered in the affirmative, what they correspond to.

Let us note that CST and asymptotically safe gravity are not necessarily mutually exclusive. In particular, one could imagine a scenario where spacetime becomes fundamentally discrete in the deep ultraviolet and enters an asymptotically safe scaling regime at intermediate scales. In such a setting, the asymptotic-safety scenario becomes an effective, low-energy limit of CST. A similar scenario for string theory and asymptotic safety has been proposed [4] and it was argued that such a setting could potentially have beneficial consequences for both. We will provide some comments on this possibility in Chpt. 5

We have seen that together, the different approaches to quantum-gravity discussed here, highlight a large set of properties the fundamental theory of spacetime might possess. In addition to those discussed here, there exist a large number of approaches to quantum gravity, each with their own distinct properties, which were either mentioned briefly or not at all. Let us then end on the note that the existence of a broad range of quantum-gravity approaches should not be interpreted as a hindrance, but rather as a vital asset which provides us with the potential to tackle the quantum-gravity enigma from multiple directions.

Chapter 5

Outlook

Throughout the preceding sections of this thesis, multiple proposals for future research have been hinted at in passing by. Let us summarise a selection of those more concretely here.

Extensive studies of matter coupled to asymptotically safe quantum gravity have been performed in the continuum setting through FRG methods. A drawback of the FRG approach is the need to truncate the infinite space of operators that are consistent with the symmetries. On the lattice such a truncation is not necessary and the partition sum is evaluated directly through Monte Carlo methods. However, the *ansatz* for the microscopic action, and hence, the fundamental parameters of the theory remain a choice. It is nevertheless clear that functional and lattice methods could provide important cross-checks in both directions. Based on the work in Chpt. 2.1.4 involving the Abelian hypercharge coupling, it would be exciting to add such a contribution to the lattice and study the phase diagram. In particular, the work presented here suggests that the combined system should have a fixed point where the Abelian hypercharge is irrelevant and, hence, does not require tuning on the lattice, and a second relevant fixed point where one should find indications that the hypercharge has to be tuned to zero. Early studies adding Abelian couplings were performed in DT [284, 285] and found no significant contributions. However, these studies have not been repeated yet in the relatively new EDT setting where one includes a non-trivial measure [279, 281, 282]. Studies in EDT involving such a measure term are expected to be performed within the near future.

In addition, the recent availability of MCMC methods in CST [351, 352, 353, 326] allows for an explicit comparison with discrete approaches such as (C/E)DT. Since CDT explicitly implements a causality condition, it seems natural to search for common ground. It is striking that first explorations of the CST phase diagram for 2D orders did not yield a higher-order phase transition [352], especially since the action encoding the dynamics in these studies limits to the Einstein-Hilbert action [314]. Under the assumption that the fundamental dynamics encoded in S_{BD} and the Regge action Z_R, are qualitatively the same, we are led to the conclusion that either the configuration space or the measure must be where the comparison breaks down. It is not clear whether CST should employ a measure term [327], but it is clear that the configuration space of CST and CDT are fundamentally different. Already in the restricted setting of the 2D orders,

there are non-manifold like contributions to the path integral. It would be of interest to see what the CST phase diagram looks like when one only accounts for sprinklings of $\mathbb{M}^2$. A technical hurdle here is that one needs an evolution algorithm which "updates" the causal set in such a way that the manifold-likeness is not destroyed. Let us emphasise that even if such an algorithm can be developed, the space of all manifold-like configurations is still larger than the space of configurations which admit a global time-foliation. Perhaps a more striking result is that of [353], where hints towards the existence of a higher-order phase transition in a CST-Ising setting were found. If these results persist under extended studies, in particular if the inclusion of additional matter degrees of freedom yield a higher-order phase transition, whereas the pure-gravity setting does not, then this potentially provides further support for a fundamental gravity-matter theory over a pure-gravity theory.

Inspired by the work in [4], where a scenario incorporating both string theory and asymptotic safety was proposed, let us briefly comment on possible implications of a similar setting involving CST and asymptotic safety. The ideal setting would combine the strengths of both theories while simultaneously removing some of the drawbacks associated with each model. As has been advocated extensively throughout this thesis, a clear strength of asymptotically safe quantum gravity is the link between UV and IR physics through matter couplings. The ability to potentially link Planck-scale physics to the Standard Model is rooted in the universality of the theory at the fixed point, which in turn provides a mechanism establishing the dynamics of the theory. To realise the asymptotic safety scenario for gravity, a near-scaling regime for the couplings is necessary. Assuming that CST functions as the fundamental description of spacetime, characterised by the scale Λ_{CST} where we expect spacetime to resemble a causal set, then $\Lambda_{CST} \gg M_{Pl}$. As we lower the energy from Λ_{CST}, we must enter a scaling regime at some scale Λ_{ASQG} sufficiently far above M_{Pl}, where quantum gravity fluctuations switch off. If we have a sufficiently large separation of scales $M_{Pl} \ll \Lambda_{ASQG}$ (the separation $\Lambda_{ASQG} \leq \Lambda_{CST}$ depends on how fast the theory approaches scale invariance as one lowers the scale from Λ_{CST}), then at M_{Pl} any information on Λ_{CST} will presumably have been "washed away" by the flow and all the beneficial features of asymptotic safety automatically potentially carry over to CST. The converse, where imprints of the fundamental discreteness of CST mediate all the way through to the IR, could potentially provide an interesting scenario as well.

Moreover, such a scenario could possibly function as a guiding principle for the CST dynamics, as it suggests that the microscopic action should be such that lowering the scale yields an approximate scaling regime. In that case, the fundamental CST dynamics might not be dominated by a fixed point, but the low-energy limit (i.e., as one "zooms out") should reduce to an effective dynamics compatible with approximate scale invariance.

The other way around, since CST is fundamentally Lorentzian, one could argue that a connection between asymptotically safe gravity and CST can only occur if a suitable Lorentzian description of the asymptotic-safety scenario exists. This might provide hints on whether Euclidean and Lorentzian quantum gravity lie in the same universality class.

Acknowledgments:

I would like to thank my supervisor, Astrid Eichhorn, for her unwavering encouragement and enthusiasm both on academic as well as personal matters. I am truly amazed by the selflessness and energy with which you developed a group from essentially non-existent, to an inclusive and diverse, self-organising entity. Thank you for letting me be part of that experience.

It goes without saying that I am grateful to all current and past group members for providing a stimulating work environment and for being more than just colleagues. A special thanks goes to Aaron Held, Marc Schiffer, Alessia Platania, Johannes Lumma, Antônio Pereira, Martin Pauly and Gustavo de Brito, for patiently entertaining any questions and doubts I have had over the last months. I also want to thank you for all the fun activities and discussions over the last years.

I also thank Aaron, Marc and Gustavo for reading through parts of this thesis and providing me with crucial feedback which, undoubtedly, has greatly improved the quality.

I thank Sumati Surya for fuelling my curiosity in causal set theory and for sharing her vast knowledge and enthusiasm with me. Thank you for many insightful and pleasant meetings and in particular for always being willing to answer any question I had over the last years.

Part of the work presented here was developed during a research stay at Syracuse university and I would like to thank the high-energy physics group at SU for giving me a warm welcome and including me in their activities. A special thanks goes to Jack Laiho and Judah Unmuth-Yockey, for many fruitful and always entertaining discussions. I am also grateful to Jack for introducing me to lattice methods and for providing helpful comments on an earlier version of this thesis.

I would like to thank Gustavo Ramírez, for his unconditional love and support and for never failing to make me laugh when I feel least like it. Especially during the final weeks that went into this thesis, you have been a rock.

I am also grateful to my parents and my sister, for their continuous support throughout the last years and for helping me take a step back and put things in perspective every now and then.

Finally, I would like to thank my father, who taught me to pursue what I enjoy the most, and who's enthusiastic reply to my decision to study physics has always been a source of motivation to me.

Appendix A

Hypercharge technicalities

Here we detail some of the technicalities that were omitted in the main text.

To identify the TT-mode of the graviton, we employ the projector

$$P^{TT}_{\alpha\beta\mu\nu}(p) = \frac{1}{2}P_{\alpha\nu}\,P_{\beta\mu} + \frac{1}{2}P_{\alpha\mu}\,P_{\beta\nu} - \frac{1}{3}P_{\alpha\beta}\,P_{\mu\nu}, \tag{A.1}$$

where p is the internal loop momentum running through the graviton propagator and we use the transverse projector

$$P_{\alpha\beta}(p) = \left(\delta_{\alpha\beta} - \frac{p_\alpha\,p_\beta}{p^2}\right). \tag{A.2}$$

Furthermore, to project onto the couplings we choose the external momenta to be totally symmetric. For the three-point vertex we then find

$$q_1 = |q| \begin{pmatrix} \frac{1}{2} \\ \frac{\sqrt{3}}{2} \\ 0 \\ 0 \end{pmatrix} \quad , \quad q_2 = |q| \begin{pmatrix} 1 \\ 0 \\ 0 \\ 0 \end{pmatrix} \quad , \quad q_3 = |q| \begin{pmatrix} \frac{1}{2} \\ -\frac{\sqrt{3}}{2} \\ 0 \\ 0 \end{pmatrix}.$$

Equivalently, we find the symmetric external momentum configuration of the four-point vertex

$$q_1 = |q| \begin{pmatrix} 1 \\ 0 \\ 0 \\ 0 \end{pmatrix} \quad , \quad q_2 = |q| \begin{pmatrix} \frac{1}{3} \\ -2\frac{\sqrt{2}}{3} \\ 0 \\ 0 \end{pmatrix} \quad , \quad q_3 = |q| \begin{pmatrix} -\frac{1}{3} \\ -\frac{\sqrt{2}}{3} \\ -\sqrt{\frac{2}{3}} \\ 0 \end{pmatrix} \quad , \quad q_4 = |q| \begin{pmatrix} -\frac{1}{3} \\ -\frac{\sqrt{2}}{3} \\ \sqrt{\frac{2}{3}} \\ 0 \end{pmatrix}.$$

The full beta-functions as read off from the three -and four-point vertex given by Eq. (2.48),

are written in terms of parameters $A = A(\alpha, \beta, \Lambda)$ and $B = B(\alpha, \beta, \Lambda)$, which were found to be

$$\begin{aligned} A &= \frac{2(2\Lambda-1)\left(32\alpha^2\Lambda(2\Lambda-1)+\alpha\left(3\beta^2(6\Lambda+1)-6\beta(2\Lambda+3)-38\Lambda+31\right)-3(\beta-1)^2\right)}{(2\alpha\Lambda-1)\left(16\alpha\Lambda^2-4(2\alpha+3)\Lambda+\beta^2(4\Lambda+1)-6\beta+9\right)} \\ B &= \frac{2(\beta-1)(\alpha(\beta+8\Lambda-5)-4\beta\Lambda+\beta-4\Lambda+3)}{(2\alpha\Lambda-1)\left(16\alpha\Lambda^2-4(2\alpha+3)\Lambda+\beta^2(4\Lambda+1)-6\beta+9\right)}+\frac{6(\alpha-1)}{2\alpha\Lambda-1}+12. \end{aligned} \tag{A.3}$$

Finally, we present the explicit expression for the vertices for completeness. We let $\phi(x) = \int d^4p\,\tilde{\phi}(p)e^{i\,p\cdot x}$, and omit the tilde on $\tilde{\phi}$ from here onwards to keep our notation clean. Then the vertices can be derived as

$$\Gamma_k^{(2)} = \frac{\delta}{\delta\Phi(-p)}\frac{\delta}{\delta\Phi(q)}\Gamma_k, \tag{A.4}$$

where Φ captures all degrees of freedom and $\Phi(p) = (\phi(p), \phi^\dagger(-p), A_\mu(p), h_{\mu\nu}(p))$. Note that$\Gamma_k^{(2)}$ is a matrix in field space, and we use the fields as indices for the different matrix components, i.e., $\Gamma_{k\,\phi\,\phi^\dagger}(p,q) = \frac{\delta}{\delta\phi(-p)}\frac{\delta}{\delta\phi^\dagger(-q)}\Gamma_k$.

Then we may write for the pure matter vertices

$$\begin{aligned} \Gamma_{k\,\phi\,\phi^\dagger}(p,q) &= \rho A_\mu(p-q)\,(q+p)^\mu + \rho^2\int_r A_\mu(r)\,A^\mu(p-q-r), \\ \Gamma_{k\,\phi^\dagger\,\phi}(p,q) &= \Gamma_{k\,\phi\,\phi^\dagger}(-q,-p), \\ \Gamma_{k\,A_\mu\,\phi}(p,q) &= \rho\,(p-2q)^\mu\,\phi^\dagger(q-p) + 2\rho^2\int_r A^\mu(r+p-q)\,\phi^\dagger(r), \\ \Gamma_{k\,\phi\,A_\mu}(p,q) &= \Gamma_{k\,A_\mu\,\phi}(-q,-p), \\ \Gamma_{k\,A_\mu\,\phi^\dagger}(p,q) &= \rho\,(2q-p)^\mu\,\phi(p-q) + 2\rho^2\int_r A^\mu(-r+p-q)\,\phi(r), \\ \Gamma_{k\,\phi^\dagger\,A_\mu}(p,q) &= \Gamma_{k\,A_\mu\,\phi^\dagger}(-q,-p), \\ \Gamma_{k\,A_\mu\,A_\nu}(p,q) &= 2\rho^2\int_r \delta^{\mu\nu}\,\phi(r)\,\phi^\dagger(r+q-p). \end{aligned} \tag{A.5}$$

Similarly for the vertices receiving a graviton contribution

$$
\begin{aligned}
&\Gamma_{k\,h_{\gamma\kappa}\,\phi}(p,q)\\
&=\left[\frac{1}{2}\delta^{\gamma\kappa}\delta^{\mu\nu}-\delta^{\mu[\kappa}\,\delta^{\gamma]\nu}\right]\Big(\phi^{\dagger}(q-p)\,q_{\mu}(q-p)_{\nu}-\rho\int_{r}\phi^{\dagger}(r)\,(r+q)^{\gamma}\,A^{\kappa}(r+p-q)\\
&+\rho^{2}\int_{r\,m}\phi^{\dagger}(r)\,A^{\kappa}(m)\,A^{\gamma}(r+p-m-q)\Big),\\
&\Gamma_{k\,\phi\,h_{\gamma\kappa}}(p,q)=\Gamma_{k\,h_{\gamma\kappa}\,\phi}(-q,-p),\\
&\Gamma_{k\,\phi^{\dagger}\,h_{\gamma\kappa}}(p,q)\\
&=\left[\frac{1}{2}\delta^{\gamma\kappa}\delta^{\mu\nu}-\delta^{\mu[\kappa}\,\delta^{\gamma]\nu}\right]\Big(\phi(p-q)\,p_{\nu}\,(p-q)_{\mu}-\rho\int_{r}\phi(r)\,(r+p)^{\gamma}\,A^{\kappa}(p-r-q)\\
&+\rho^{2}\int_{r\,m}\phi^{\dagger}(r)\,A^{\kappa}(m)\,A^{\gamma}(p-m-r-q)\Big),\\
&\Gamma_{k\,h_{\gamma\kappa}\,\phi^{\dagger}}(p,q)=\Gamma_{k\,\phi^{\dagger}\,h_{\gamma\kappa}}(-q,-p),\\
&\Gamma_{k\,h_{\alpha\beta}\,h_{\gamma\kappa}}(p,q)=\frac{1}{2\alpha}\int_{l}\left(\delta^{\gamma(\alpha}\,\delta^{\beta)\kappa}-\frac{1}{2}\delta^{\alpha\beta}\,\delta^{\gamma\kappa}\right)\,l^{\mu}\,A_{\mu}(l)\,(p-q-l)^{\mu}\\
&+\frac{1}{2}\int_{s}\Big[\frac{1}{2}\delta^{\mu\nu}\,\delta^{\alpha\beta}\,\delta^{\gamma\kappa}-\delta^{\mu\nu}\,\delta^{\gamma(\alpha}\,\delta^{\beta)\kappa}+4\delta^{(\mu(\alpha}\,\delta^{\beta)(\gamma}\,\delta^{\kappa)\nu)}\;-\delta^{\alpha\beta}\,\delta^{\mu(\gamma}\,\delta^{\kappa)\nu}-\delta^{\gamma\kappa}\,\delta^{\mu(\alpha}\,\delta^{\beta)\nu}\Big]\\
&\quad\times\Big[(s+p-q)_{\mu}\,s_{\nu}\,\phi(s+p-q)\,\phi^{\dagger}(s)-\rho\int_{r}\Big((r+s)_{\mu}\,\phi(r)\,\phi^{\dagger}(s)\,A_{\nu}(s+p-q-r)\\
&\quad+\rho\int_{l}A_{\mu}(l)\,A_{\nu}(s+p-q-r-l)\Big)\Big]\\
&+\frac{1}{2}\Big[\delta^{\epsilon\lambda}\,\Big(\delta^{\mu\nu}\left(\frac{1}{2}\delta^{\alpha\beta}\,\delta^{\gamma\kappa}-\delta^{\alpha(\gamma}\,\delta^{\kappa)\beta}\right)+4\delta^{(\mu(\alpha}\,\delta^{\beta)(\gamma}\,\delta^{\kappa)\nu)}\;-\delta^{\alpha\beta}\,\delta^{\mu(\gamma}\,\delta^{\kappa)\nu)}-\delta^{\gamma\kappa}\,\delta^{\mu(\alpha}\,\delta^{\beta)\nu)}\Big)\\
&+\delta^{\mu\nu}\left(4\delta^{(\epsilon(\alpha}\,\delta^{\beta)(\gamma}\,\delta^{\kappa)\lambda)}-\delta^{\alpha\beta}\,\delta^{\epsilon(\gamma}\,\delta^{\kappa)\lambda)}-\delta^{\gamma\kappa}\,\delta^{\epsilon(\alpha}\,\delta^{\beta)\lambda)}\right)\\
&+2\delta^{\mu(\alpha}\,\delta^{\beta)\nu}\,\delta^{\epsilon(\gamma}\,\delta^{\kappa)\lambda}2\delta^{\mu(\gamma}\,\delta^{\kappa)\nu}\,\delta^{\epsilon(\alpha}\,\delta^{\beta)\lambda}\Big]\\
&\quad\times\int_{l}\left(2l_{(\mu}\,A_{\epsilon)}(l)\,(p-l-q)_{\lambda}\,A_{\nu}(p-l-q)-2l_{(\mu}\,A_{\epsilon)}(l)\,(p-l-q)_{\nu}\,A_{\lambda}(p-l-q)\right).
\end{aligned}
$$

Appendix B

Non-constant extrinsic curvature boundaries

We show the sprinklings into spacetimes exhibiting positive or negative extrinsic curvature initial boundaries, cf. Fig B.1. The hyperbolae are parametrised by the formula

$$\frac{(x-x_0)^2}{a^2} - \frac{(t-t_0)^2}{b^2} = -1, \tag{B.1}$$

where a and b are defined as in Fig. B.2. The extrinsic curvature $K_{ab} = \nabla_a N_b$ with N_b the tangent to the hyperbola and ∇_a the covariant derivative, yields a radius of curvature $\ell_K = 1/K = a^2/b$. In the case of constant curvature, one sets $c \equiv a = b$ and the induced distance between any two points on the hypersurface is simply

$$\Delta s = c\left(\arcsin\left(\frac{x_p}{c}\right) - \arcsin\left(\frac{x_1}{c}\right)\right). \tag{B.2}$$

In addition to the cases of hyperbolic boundaries with constant curvature, we examine boundaries which exhibit non-zero extrinsic curvature. Specifically, we will look at hyperbolae with non-constant curvature and circle segments, which have constant extrinsic curvature in Euclidean space, but not in a Lorentzian spacetime.

We see that curvature scale ℓ_K indeed affects the distance estimation. If one increases ℓ beyond a critical value, then Δ severely overestimates the continuum distance, as shown in Fig. B.3. In the specific setting here, where $a \sim 485$, $b \sim 97$, we can choose $\ell \sim 164$ to reduce the error Δ, in contrast to $\ell \approx 199$ whichesults in a visible deviation, cf. Fig. B.3.

Our first result highlights the fact that the predistance is no longer a useful distance estimator in this case, cf. Fig. B.4. As is obvious from the zoomed-in plot in the right panel of this figure, the error $\widetilde{\Delta}$ for the predistance goes to zero around $d_h \approx 180$. Yet, one immediately sees that this is not due to a convergence of $\widetilde{\Delta} \to 0$, since $\widetilde{\Delta}$ continues to decrease past this point becoming increasingly negative as $d_h \gtrsim 200$. In addition, the predistance does not fully converge to d_h even

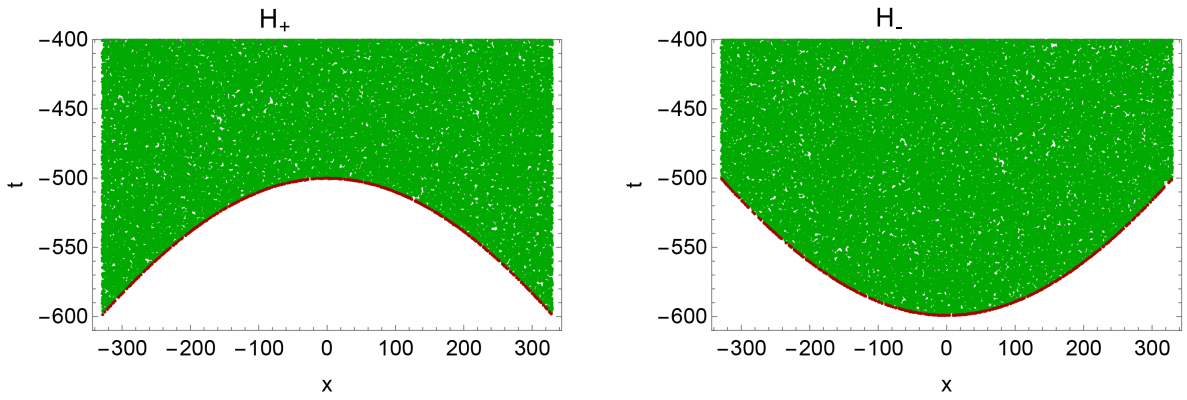

Figure B.1: We show sprinklings into regions of 2d Minkowski spacetime with positive and negative curvature initial boundaries for a radius of curvature $\ell_K = 500$. The antichian (red dots) lies close to the spacelike boundary. Note that for the simulations $-600 \leq t \leq 600$, here we only show part of the t-axis.

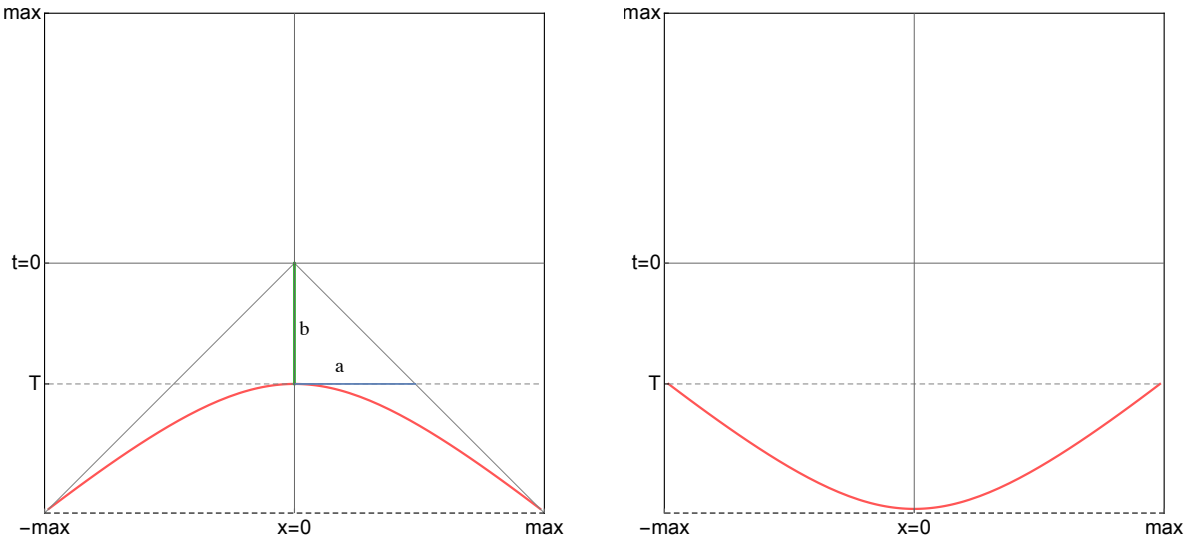

Figure B.2: The H_+ hypersurface is shown on the left and the H_- on the right..

at large d_h for C_- (negative non-constant extrinsic curvature), cf. Fig. B.4, right panel, leading to an overestimation in this case.

The predistance no longer converges to the correct result, see in cf. Fig. B.4. Rather, the error drops below zero around $d_h \approx 180$ and keeps decreasing further as $d_h \gtrsim 200$. Additionally, we see that for C_- (negative non-constant extrinsic curvature), the predistance does not fully converge to d_h for any value of d_h cf. Fig. B.4, right panel. These effects become more pronounced, the larger the curvature is chosen.

We see that if ℓ is too large, the error Δ grows with a similar trend as the predistance. For C_+, the distance function underestimates $\Delta < 0$ at large continuum distances(cf. Fig. B.4). The

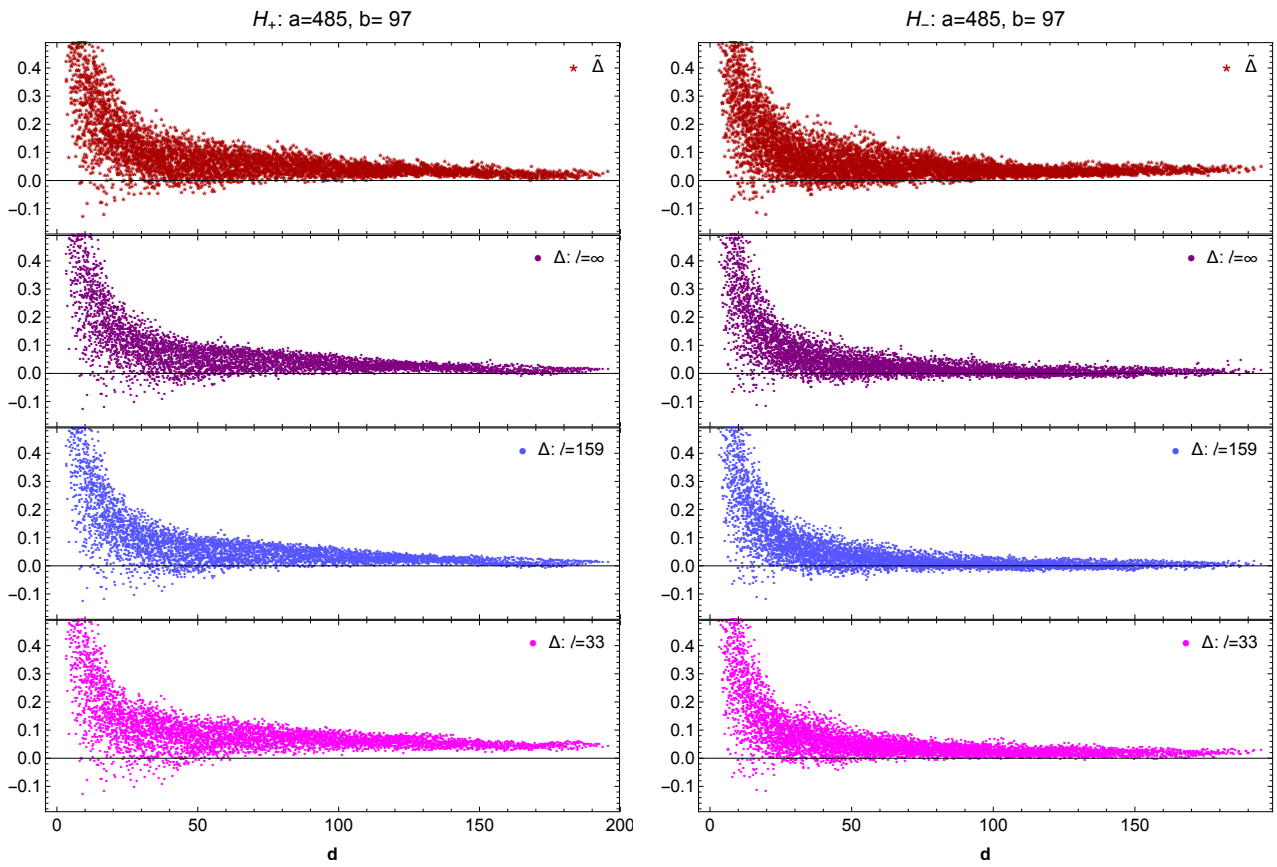

Figure B.3: $\widetilde{\Delta}$ (red stars) and Δ (magenta, blue and purple dots) for the H_+ (left) and H_- case (right) for the complete range of d_h (left panel).

opposite case, C_-, is not as sensitive to variations of ℓ as long as we do not drop down to ℓ_{DAS}.

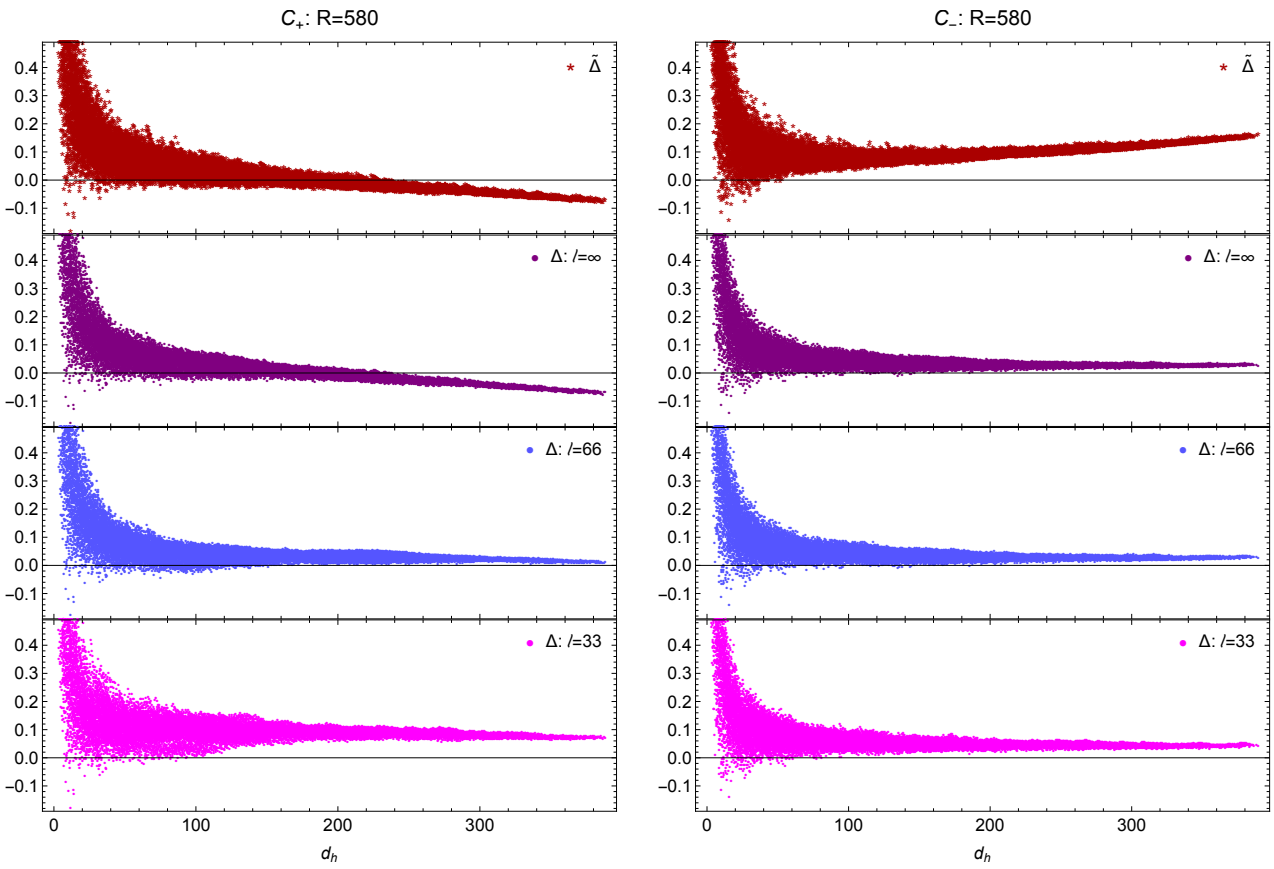

Figure B.4: The predistance (red asterisks) either underestimates ($\widetilde{\Delta} < 0$) or overestimates ($\widetilde{\Delta} > 0$) the distance at large values of d_h due to curvature effects. For large values of the cutoff ($\ell = \infty$, purple dots) for the C_+ case, Δ drops below zero as well.

I have collaborated on the following work, which has been included in this thesis.

- **Asymptotic safety, string theory and the weak gravity conjecture**
  Senarath de Alwis, Senarath, Astrid Eichhorn, Aaron Held,
  Jan M. Pawlowski, Marc Schiffer, Fleur Versteegen
  Submitted to: Phys.Lett. B
  e-Print: arXiv:1907.07894 (2019)

- **Spectral dimension on spatial hypersurfaces in causal set quantum gravity**
  Astrid Eichhorn, Sumati Surya, Fleur Versteegen
  Submitted to: Class. Quant. Grav.
  e-Print: arXiv:1905.13498

- **Induced Spatial Geometry from Causal Structure**
  Astrid Eichhorn, Sumati Surya, Fleur Versteegen
  Class. Quantum Grav. 36. 10 (2019), p. 105005
  e-Print: arXiv:1809.06192 (2018)

- **Upper bound on the Abelian gauge coupling from asymptotic safety**
  Astrid Eichhorn and Fleur Versteegen
  JHEP 01 10 (2018), p. 030
  e-Print: arXiv:1709.07252

The following publications were not used in this thesis

- **Quantum Gravity signatures in the Unruh effect**
  Natalia Alkofer, Giulio D'Odorico, Frank Saueressig, Fleur Versteegen
  Phys. Rev. D94 (2016), 10 p. 104055
  e-Print: arXiv:1605.08015

- **First- and second-order error estimates in Monte Carlo integration**
  R. Bakx, R. H. P. Kleiss, F. Versteegen
  Comput. Phys. Commun. 208 (2016), p. 29-34
  e-Print: arXiv:1507.05031

Bibliography

[1] Astrid Eichhorn and Fleur Versteegen. "Upper bound on the Abelian gauge coupling from asymptotic safety". In: *JHEP* 01 (2018), p. 030. DOI: 10.1007/JHEP01(2018)030. arXiv: 1709.07252 [hep-th].

[2] Astrid Eichhorn, Sumati Surya, and Fleur Versteegen. "Induced Spatial Geometry from Causal Structure". In: *Class. Quant. Grav.* 36.10 (2019), p. 105005. DOI: 10.1088/1361-6382/ab114b. arXiv: 1809.06192 [gr-qc].

[3] Astrid Eichhorn, Sumati Surya, and Fleur Versteegen. "Spectral dimension on spatial hypersurfaces in causal set quantum gravity". In: (2019). arXiv: 1905.13498 [gr-qc].

[4] Senarath de Alwis et al. "Asymptotic safety, string theory and the weak gravity conjecture". In: (2019). arXiv: 1907.07894 [hep-th].

[5] Sin-Itiro Tomonaga and J. R. Oppenheimer. "On Infinite Field Reactions in Quantum Field Theory". In: *Phys. Rev.* 74 (1948), pp. 224–225. DOI: 10.1103/PhysRev.74.224.

[6] R. P. Feynman. "Mathematical formulation of the quantum theory of electromagnetic interaction". In: *Phys. Rev.* 80 (1950). [,198(1950)], pp. 440–457. DOI: 10.1103/PhysRev.80.440.

[7] Julian S. Schwinger. "On gauge invariance and vacuum polarization". In: *Phys. Rev.* 82 (1951). [,116(1951)], pp. 664–679. DOI: 10.1103/PhysRev.82.664.

[8] S. L. Glashow. "Partial Symmetries of Weak Interactions". In: *Nucl. Phys.* 22 (1961), pp. 579–588. DOI: 10.1016/0029-5582(61)90469-2.

[9] Abdus Salam. "Weak and Electromagnetic Interactions". In: *Conf. Proc.* C680519 (1968), pp. 367–377.

[10] Steven Weinberg. "A Model of Leptons". In: *Phys. Rev. Lett.* 19 (1967), pp. 1264–1266. DOI: 10.1103/PhysRevLett.19.1264.

[11] F. Abe et al. "Observation of top quark production in $\bar{p}p$ collisions". In: *Phys. Rev. Lett.* 74 (1995), pp. 2626–2631. DOI: 10.1103/PhysRevLett.74.2626. arXiv: hep-ex/9503002 [hep-ex].

[12] Georges Aad et al. "Observation of a new particle in the search for the Standard Model Higgs boson with the ATLAS detector at the LHC". In: *Phys. Lett.* B716 (2012), pp. 1–29. DOI: 10.1016/j.physletb.2012.08.020. arXiv: 1207.7214 [hep-ex].

[13] Serguei Chatrchyan et al. "Observation of a New Boson at a Mass of 125 GeV with the CMS Experiment at the LHC". In: *Phys. Lett.* B716 (2012), pp. 30–61. DOI: 10.1016/j.physletb.2012.08.021. arXiv: 1207.7235 [hep-ex].

[14] Roel Aaij et al. "Observation of the resonant character of the $Z(4430)^-$ state". In: *Phys. Rev. Lett.* 112.22 (2014), p. 222002. DOI: 10.1103/PhysRevLett.112.222002. arXiv: 1404.1903 [hep-ex].

[15] M. Tanabashi et al. "Review of Particle Physics". In: *Phys. Rev.* D98.3 (2018), p. 030001. DOI: 10.1103/PhysRevD.98.030001.

[16] J. Beringer et al. "Review of Particle Physics (RPP)". In: *Phys. Rev.* D86 (2012), p. 010001. DOI: 10.1103/PhysRevD.86.010001.

[17] S. Perlmutter et al. "Discovery of a supernova explosion at half the age of the Universe and its cosmological implications". In: *Nature* 391 (1998), pp. 51–54. DOI: 10.1038/34124. arXiv: astro-ph/9712212 [astro-ph].

[18] S. Perlmutter et al. "Measurements of Ω and Λ from 42 high redshift supernovae". In: *Astrophys. J.* 517 (1999), pp. 565–586. DOI: 10.1086/307221. arXiv: astro-ph/9812133 [astro-ph].

[19] Brian P. Schmidt et al. "The High Z supernova search: Measuring cosmic deceleration and global curvature of the universe using type Ia supernovae". In: *Astrophys. J.* 507 (1998), pp. 46–63. DOI: 10.1086/306308. arXiv: astro-ph/9805200 [astro-ph].

[20] Adam G. Riess et al. "Observational evidence from supernovae for an accelerating universe and a cosmological constant". In: *Astron. J.* 116 (1998), pp. 1009–1038. DOI: 10.1086/300499. arXiv: astro-ph/9805201 [astro-ph].

[21] Gianfranco Bertone, Dan Hooper, and Joseph Silk. "Particle dark matter: Evidence, candidates and constraints". In: *Phys. Rept.* 405 (2005), pp. 279–390. DOI: 10.1016/j.physrep.2004.08.031. arXiv: hep-ph/0404175 [hep-ph].

[22] Albert Einstein. "The Foundation of the General Theory of Relativity". In: *Annalen Phys.* 49.7 (1916). [Annalen Phys.354,no.7,769(1916)], pp. 769–822. DOI: 10.1002/andp.200590044, 10.1002/andp.19163540702.

[23] B Riemann. "On the Hypotheses that Lie at the Bases of Geometry (1854)". In: *English Translation by WK Clifford, Nature* 8 (1873).

[24] N. Aghanim et al. "Planck 2018 results. VI. Cosmological parameters". In: (2018). arXiv: 1807.06209 [astro-ph.CO].

[25] Steven Weinberg. "The Cosmological Constant Problem". In: *Rev. Mod. Phys.* 61 (1989). [,569(1988)], pp. 1–23. DOI: 10.1103/RevModPhys.61.1.

[26] Karl Schwarzschild. "On the gravitational field of a mass point according to Einstein's theory". In: *Sitzungsber. Preuss. Akad. Wiss. Berlin (Math. Phys.)* 1916 (1916), pp. 189–196. arXiv: physics/9905030 [physics].

[27] Tessa Baker, Dimitrios Psaltis, and Constantinos Skordis. "Linking Tests of Gravity On All Scales: from the Strong-Field Regime to Cosmology". In: *Astrophys. J.* 802 (2015), p. 63. DOI: 10.1088/0004-637X/802/1/63. arXiv: 1412.3455 [astro-ph.CO].

[28] Tessa Baker et al. "Void Lensing as a Test of Gravity". In: *Phys. Rev.* D98.2 (2018), p. 023511. DOI: 10.1103/PhysRevD.98.023511. arXiv: 1803.07533 [astro-ph.CO].

[29] Clifford M. Will. "The Confrontation between General Relativity and Experiment". In: *Living Rev. Rel.* 17 (2014), p. 4. DOI: 10.12942/lrr-2014-4. arXiv: 1403.7377 [gr-qc].

[30] Lijing Shao and Norbert Wex. "New limits on the violation of local position invariance of gravity". In: *Class. Quant. Grav.* 30 (2013), p. 165020. DOI: 10.1088/0264-9381/30/16/165020. arXiv: 1307.2637 [gr-qc].

[31] Dimitrios Psaltis. "Probes and Tests of Strong-Field Gravity with Observations in the Electromagnetic Spectrum". In: *Living Rev. Rel.* 11 (2008), p. 9. DOI: 10.12942/lrr-2008-9. arXiv: 0806.1531 [astro-ph].

[32] Kenneth Nordtvedt. "Equivalence Principle for Massive Bodies. 2. Theory". In: *Phys. Rev.* 169 (1968), pp. 1017–1025. DOI: 10.1103/PhysRev.169.1017.

[33] Clifford M. Will. "Theoretical Frameworks for Testing Relativistic Gravity. 2. Parametrized Post-Newtonian Hydrodynamics, and the Nordtvedt Effect". In: *Astrophys. J.* 163 (1971), pp. 611–627. DOI: 10.1086/150804.

[34] Clifford M. Will and Kenneth Nordtvedt Jr. "Conservation Laws and Preferred Frames in Relativistic Gravity. I. Preferred-Frame Theories and an Extended PPN Formalism". In: *Astrophys. J.* 177 (1972), p. 757. DOI: 10.1086/151754.

[35] B. Bertotti, L. Iess, and P. Tortora. "A test of general relativity using radio links with the Cassini spacecraft". In: *Nature* 425 (2003), pp. 374–376. DOI: 10.1038/nature01997.

[36] B. P. Abbott et al. "Observation of Gravitational Waves from a Binary Black Hole Merger". In: *Phys. Rev. Lett.* 116.6 (2016), p. 061102. DOI: 10.1103/PhysRevLett.116.061102. arXiv: 1602.03837 [gr-qc].

[37] B. P. Abbott et al. "GWTC-1: A Gravitational-Wave Transient Catalog of Compact Binary Mergers Observed by LIGO and Virgo during the First and Second Observing Runs". In: (2018). arXiv: 1811.12907 [astro-ph.HE].

[38] B. P. Abbott et al. "Tests of General Relativity with the Binary Black Hole Signals from the LIGO-Virgo Catalog GWTC-1". In: (2019). arXiv: 1903.04467 [gr-qc].

[39] Event Horizon Telescope Collaboration. "First M87 Event Horizon Telescope Results. I. The Shadow of the Supermassive Black Hole". In: *Astrophys. J.* 875.1 (2019), p. L1. DOI: 10.3847/2041-8213/ab0ec7. arXiv: 1906.11238 [astro-ph.GA].

[40] Event Horizon Telescope Collaboration. "First M87 Event Horizon Telescope Results. II. Array and Instrumentation". In: *Astrophys. J.* 875.1 (2019), p. L2. DOI: 10.3847/2041-8213/ab0c96. arXiv: 1906.11239 [astro-ph.IM].

[41] Event Horizon Telescope Collaboration. "First M87 Event Horizon Telescope Results. III. Data Processing and Calibration". In: *Astrophys. J.* 875.1 (2019), p. L3. DOI: 10.3847/2041-8213/ab0c57. arXiv: 1906.11240 [astro-ph.GA].

[42] Event Horizon Telescope Collaboration. "First M87 Event Horizon Telescope Results. IV. Imaging the Central Supermassive Black Hole". In: *Astrophys. J.* 875.1 (2019), p. L4. DOI: 10.3847/2041-8213/ab0e85. arXiv: 1906.11241 [astro-ph.GA].

[43] Event Horizon Telescope Collaboration. "First M87 Event Horizon Telescope Results. V. Physical Origin of the Asymmetric Ring". In: *Astrophys. J.* 875.1 (2019), p. L5. DOI: 10.3847/2041-8213/ab0f43. arXiv: 1906.11242 [astro-ph.GA].

[44] Event Horizon Telescope Collaboration. "First M87 Event Horizon Telescope Results. VI. The Shadow and Mass of the Central Black Hole". In: *Astrophys. J.* 875.1 (2019), p. L6. DOI: 10.3847/2041-8213/ab1141. arXiv: 1906.11243 [astro-ph.GA].

[45] Matt Visser. "Acoustic black holes: Horizons, ergospheres, and Hawking radiation". In: *Class. Quant. Grav.* 15 (1998), pp. 1767–1791. DOI: 10.1088/0264-9381/15/6/024. arXiv: gr-qc/9712010 [gr-qc].

[46] R. Balbinot et al. "Hawking radiation from acoustic black holes, short distance and back-reaction effects". In: *Riv. Nuovo Cim.* 28.3 (2005), pp. 1–55. DOI: 10.1393/ncr/i2006-10001-9. arXiv: gr-qc/0601079 [gr-qc].

[47] Carlos Barcelo, Stefano Liberati, and Matt Visser. "Analogue gravity". In: *Living Rev. Rel.* 8 (2005). [Living Rev. Rel.14,3(2011)], p. 12. DOI: 10.12942/lrr-2005-12. arXiv: gr-qc/0505065 [gr-qc].

[48] Peter W. Higgs. "Broken Symmetries and the Masses of Gauge Bosons". In: *Phys. Rev. Lett.* 13 (1964). [,160(1964)], pp. 508–509. DOI: 10.1103/PhysRevLett.13.508.

[49] F. Englert and R. Brout. "Broken Symmetry and the Mass of Gauge Vector Mesons". In: *Phys. Rev. Lett.* 13 (1964). [,157(1964)], pp. 321–323. DOI: 10.1103/PhysRevLett.13.321.

[50] S. Schael et al. "Precision electroweak measurements on the Z resonance". In: *Phys. Rept.* 427 (2006), pp. 257–454. DOI: 10.1016/j.physrep.2005.12.006. arXiv: hep-ex/0509008 [hep-ex].

[51] Savely G. Karshenboim. "Precision physics of simple atoms: QED tests, nuclear structure and fundamental constants". In: *Phys. Rept.* 422 (2005), pp. 1–63. DOI: 10.1016/j.physrep.2005.08.008. arXiv: hep-ph/0509010 [hep-ph].

[52] J. Bailey et al. "The Anomalous Magnetic Moment of Positive and Negative Muons". In: *Phys. Lett.* 67B (1977). [Phys. Lett.68B,191(1977)], p. 225. DOI: 10.1016/0370-2693(77)90110-1,10.1016/0370-2693(77)90199-X.

[53] G. W. Bennett et al. "Final Report of the Muon E821 Anomalous Magnetic Moment Measurement at BNL". In: *Phys. Rev.* D73 (2006), p. 072003. DOI: 10.1103/PhysRevD.73.072003. arXiv: hep-ex/0602035 [hep-ex].

[54] G. Gabrielse et al. "New Determination of the Fine Structure Constant from the Electron g Value and QED". In: *Phys. Rev. Lett.* 97 (2006). [Erratum: Phys. Rev. Lett.99,039902(2007)], p. 030802. DOI: 10.1103/PhysRevLett.97.030802,10.1103/PhysRevLett.99.039902.

[55] Tatsumi Aoyama et al. "Tenth-Order QED Contribution to the Electron g-2 and an Improved Value of the Fine Structure Constant". In: *Phys. Rev. Lett.* 109 (2012), p. 111807. DOI: 10.1103/PhysRevLett.109.111807. arXiv: 1205.5368 [hep-ph].

[56] Fred Jegerlehner and Andreas Nyffeler. "The Muon g-2". In: *Phys. Rept.* 477 (2009), pp. 1–110. DOI: 10.1016/j.physrep.2009.04.003. arXiv: 0902.3360 [hep-ph].

[57] Murray Gell-Mann and F. E. Low. "Quantum electrodynamics at small distances". In: *Phys. Rev.* 95 (1954), pp. 1300–1312. DOI: 10.1103/PhysRev.95.1300.

[58] L. Maiani, G. Parisi, and R. Petronzio. "Bounds on the Number and Masses of Quarks and Leptons". In: *Nucl. Phys.* B136 (1978), pp. 115–124. DOI: 10.1016/0550-3213(78)90018-4.

[59] N. Cabibbo et al. "Bounds on the Fermions and Higgs Boson Masses in Grand Unified Theories". In: *Nucl. Phys.* B158 (1979), pp. 295–305. DOI: 10.1016/0550-3213(79)90167-6.

[60] Roger F. Dashen and Herbert Neuberger. "How to Get an Upper Bound on the Higgs Mass". In: *Phys. Rev. Lett.* 50 (1983), p. 1897. DOI: 10.1103/PhysRevLett.50.1897.

[61] David J. E. Callaway. "Nontriviality of Gauge Theories With Elementary Scalars and Upper Bounds on Higgs Masses". In: *Nucl. Phys.* B233 (1984), pp. 189–203. DOI: 10.1016/0550-3213(84)90410-3.

[62] M. A. B. Beg, C. Panagiotakopoulos, and A. Sirlin. "Mass of the Higgs Boson in the Canonical Realization of the Weinberg-Salam Theory". In: *Phys. Rev. Lett.* 52 (1984), p. 883. DOI: 10.1103/PhysRevLett.52.883.

[63] M. Lindner. "Implications of Triviality for the Standard Model". In: *Z. Phys.* C31 (1986), p. 295. DOI: 10.1007/BF01479540.

[64] Julius Kuti, Lee Lin, and Yue Shen. "Upper Bound on the Higgs Mass in the Standard Model". In: *Phys. Rev. Lett.* 61 (1988), p. 678. DOI: 10.1103/PhysRevLett.61.678.

[65] Thomas Hambye and Kurt Riesselmann. "Matching conditions and Higgs mass upper bounds revisited". In: *Phys. Rev.* D55 (1997), pp. 7255–7262. DOI: 10.1103/PhysRevD.55.7255. arXiv: hep-ph/9610272 [hep-ph].

[66] M. Gockeler et al. "Is there a Landau pole problem in QED?" In: *Phys. Rev. Lett.* 80 (1998), pp. 4119–4122. DOI: 10.1103/PhysRevLett.80.4119. arXiv: hep-th/9712244 [hep-th].

[67] M. Gockeler et al. "Resolution of the Landau pole problem in QED". In: *Nucl. Phys. Proc. Suppl.* 63 (1998). [,290(1997)], pp. 694–696. DOI: 10.1016/S0920-5632(97)00875-X. arXiv: hep-lat/9801004 [hep-lat].

[68] J. Frohlich. "On the Triviality of Lambda (phi**4) in D-Dimensions Theories and the Approach to the Critical Point in D ¿= Four-Dimensions". In: *Nucl. Phys.* B200 (1982), pp. 281–296. DOI: 10.1016/0550-3213(82)90088-8.

[69] David J. E. Callaway. "Triviality Pursuit: Can Elementary Scalar Particles Exist?" In: *Phys. Rept.* 167 (1988), p. 241. DOI: 10.1016/0370-1573(88)90008-7.

[70] Holger Gies and Joerg Jaeckel. "Renormalization flow of QED". In: *Phys. Rev. Lett.* 93 (2004), p. 110405. DOI: 10.1103/PhysRevLett.93.110405. arXiv: hep-ph/0405183 [hep-ph].

[71] M. Baig et al. "On the Logarithmic triviality of scalar quantum electrodynamics". In: *Phys. Rev.* D48 (1993), R2385–R2388. DOI: 10.1103/PhysRevD.48.R2385. arXiv: hep-lat/9305008 [hep-lat].

[72] Aaron Held and René Sondenheimer. "Higgs stability-bound and fermionic dark matter". In: *JHEP* 02 (2019), p. 166. DOI: 10.1007/JHEP02(2019)166. arXiv: 1811.07898 [hep-ph].

[73] Antoine Tilloy. "Does gravity have to be quantized? Lessons from non-relativistic toy models". In: *9th International Conference: Spacetime - Matter - Quantum Mechanics: From discrete structures and dynamics to top-down causation (DICE2018) Castiglioncello , Tuscany , Italy, September 17-21, 2018*. 2019. arXiv: 1903.01823 [quant-ph].

[74] D. Espriu et al. "The Doubling Problem on a Random Lattice". In: *Nucl. Phys.* B275 (1986), pp. 39–76. DOI: 10.1016/0550-3213(86)90588-2.

[75] S. M. Catterall and J. F. Wheater. "PARITY VIOLATING VACUUM CURRENTS ON THE RANDOM LATTICE". In: *Phys. Lett.* B213 (1988), pp. 186–190. DOI: 10.1016/0370-2693(88)91023-4.

[76] Simon Catterall, Jack Laiho, and Judah Unmuth-Yockey. "Kähler-Dirac fermions on Euclidean dynamical triangulations". In: *Phys. Rev.* D98.11 (2018), p. 114503. DOI: 10.1103/PhysRevD.98.114503. arXiv: 1810.10626 [hep-lat].

[77] Astrid Eichhorn and Holger Gies. "Light fermions in quantum gravity". In: *New J. Phys.* 13 (2011), p. 125012. DOI: 10.1088/1367-2630/13/12/125012. arXiv: 1104.5366 [hep-th].

[78] Jan Meibohm and Jan M. Pawlowski. "Chiral fermions in asymptotically safe quantum gravity". In: *Eur. Phys. J.* C76.5 (2016), p. 285. DOI: 10.1140/epjc/s10052-016-4132-7. arXiv: 1601.04597 [hep-th].

[79] Astrid Eichhorn and Aaron Held. "Viability of quantum-gravity induced ultraviolet completions for matter". In: *Phys. Rev.* D96.8 (2017), p. 086025. DOI: 10.1103/PhysRevD.96.086025. arXiv: 1705.02342 [gr-qc].

[80] Astrid Eichhorn. "An asymptotically safe guide to quantum gravity and matter". In: *Front. Astron. Space Sci.* 5 (2019), p. 47. DOI: 10.3389/fspas.2018.00047. arXiv: 1810.07615 [hep-th].

[81] N. Klitgaard and R. Loll. "Introducing Quantum Ricci Curvature". In: *Phys. Rev.* D97.4 (2018), p. 046008. DOI: 10.1103/PhysRevD.97.046008. arXiv: 1712.08847 [hep-th].

[82] N. Klitgaard and R. Loll. "Implementing quantum Ricci curvature". In: *Phys. Rev.* D97.10 (2018), p. 106017. DOI: 10.1103/PhysRevD.97.106017. arXiv: 1802.10524 [hep-th].

[83] Benjamin Bahr and Sebastian Steinhaus. "Numerical evidence for a phase transition in 4d spin foam quantum gravity". In: *Phys. Rev. Lett.* 117.14 (2016), p. 141302. DOI: 10.1103/PhysRevLett.117.141302. arXiv: 1605.07649 [gr-qc].

[84] Bianca Dittrich. "The continuum limit of loop quantum gravity - a framework for solving the theory". In: *Loop Quantum Gravity: The First 30 Years*. Ed. by Abhay Ashtekar and Jorge Pullin. 2017, pp. 153–179. DOI: 10.1142/9789813220003_0006. arXiv: 1409.1450 [gr-qc].

[85] Sylvain Carrozza. "Flowing in Group Field Theory Space: a Review". In: *SIGMA* 12 (2016), p. 070. DOI: 10.3842/SIGMA.2016.070. arXiv: 1603.01902 [gr-qc].

[86] Razvan Gurau. "The 1/N expansion of colored tensor models". In: *Annales Henri Poincare* 12 (2011), pp. 829–847. DOI: 10.1007/s00023-011-0101-8. arXiv: 1011.2726 [gr-qc].

[87] Razvan Gurau. "Invitation to Random Tensors". In: *SIGMA* 12 (2016), p. 094. DOI: 10.3842/SIGMA.2016.094. arXiv: 1609.06439 [hep-th].

[88] Astrid Eichhorn and Tim Koslowski. "Flowing to the continuum in discrete tensor models for quantum gravity". In: *Ann. Inst. H. Poincare Comb. Phys. Interact.* 5.2 (2018), pp. 173–210. DOI: 10.4171/AIHPD/52. arXiv: 1701.03029 [gr-qc].

[89] Astrid Eichhorn, Tim Koslowski, and Antonio D. Pereira. "Status of background-independent coarse-graining in tensor models for quantum gravity". In: *Universe* 5.2 (2019), p. 53. DOI: 10.3390/universe5020053. arXiv: 1811.12909 [gr-qc].

[90] Daniele Oriti. *Approaches to quantum gravity: Toward a new understanding of space, time and matter*. Cambridge University Press, 2009. ISBN: 9780521860451, 9780511512407. URL: http://www.cambridge.org/catalogue/catalogue.asp?isbn=9780521860451.

[91] Claus Kiefer. "Quantum gravity: General introduction and recent developments". In: *Annalen Phys.* 15 (2005). [Annalen Phys.518,129(2006)], pp. 129–148. DOI: 10.1002/andp.200510175. arXiv: gr-qc/0508120 [gr-qc].

[92] Roberto Percacci. *An Introduction to Covariant Quantum Gravity and Asymptotic Safety*. Vol. 3. 100 Years of General Relativity. World Scientific, 2017. ISBN: 9789813207172, 9789813207196, 9789813207172, 9789813207196. DOI: 10.1142/10369.

[93] Gerard 't Hooft and M. J. G. Veltman. "One loop divergencies in the theory of gravitation". In: *Ann. Inst. H. Poincare Phys. Theor.* A20 (1974), pp. 69–94.

[94] Stanley Deser and P. Van Nieuwenhuizen. "Nonrenormalizability of quantized fermion-gravitation interactions". In: *Lett. Nuovo Cim.* 11S2 (1974). [Lett. Nuovo Cim.11,218(1974)], pp. 218–220.

[95] S. Deser and P. van Nieuwenhuizen. "Nonrenormalizability of the Quantized Einstein-Maxwell System". In: *Phys. Rev. Lett.* 32 (1974), pp. 245–247. DOI: 10.1103/PhysRevLett.32.245.

[96] Marc H. Goroff and Augusto Sagnotti. "The Ultraviolet Behavior of Einstein Gravity". In: *Nucl. Phys.* B266 (1986), pp. 709–736. DOI: 10.1016/0550-3213(86)90193-8.

[97] A. E. M. van de Ven. "Two loop quantum gravity". In: *Nucl. Phys.* B378 (1992), pp. 309–366. DOI: 10.1016/0550-3213(92)90011-Y.

[98] K. S. Stelle. "Renormalization of Higher Derivative Quantum Gravity". In: *Phys. Rev.* D16 (1977), pp. 953–969. DOI: 10.1103/PhysRevD.16.953.

[99] B. L. Voronov and I. V. Tyutin. "ON RENORMALIZATION OF R**2 GRAVITATION. (IN RUSSIAN)". In: *Yad. Fiz.* 39 (1984), pp. 998–1010.

[100] John F. Donoghue. "The effective field theory treatment of quantum gravity". In: *AIP Conf. Proc.* 1483.1 (2012), pp. 73–94. DOI: 10.1063/1.4756964. arXiv: 1209.3511 [gr-qc].

[101] John F. Donoghue. "General relativity as an effective field theory: The leading quantum corrections". In: *Phys. Rev.* D50 (1994), pp. 3874–3888. DOI: 10.1103/PhysRevD.50.3874. arXiv: gr-qc/9405057 [gr-qc].

[102] John F. Donoghue. "Leading quantum correction to the Newtonian potential". In: *Phys. Rev. Lett.* 72 (1994), pp. 2996–2999. DOI: 10.1103/PhysRevLett.72.2996. arXiv: gr-qc/9310024 [gr-qc].

[103] Carlo Rovelli. "Loop quantum gravity". In: *Living Rev. Rel.* 1 (1998), p. 1. DOI: 10.12942/lrr-1998-1. arXiv: gr-qc/9710008 [gr-qc].

[104] Abhay Ashtekar and Jerzy Lewandowski. "Background independent quantum gravity: A Status report". In: *Class. Quant. Grav.* 21 (2004), R53. DOI: 10.1088/0264-9381/21/15/R01. arXiv: gr-qc/0404018 [gr-qc].

[105] Luca Bombelli et al. "Space-Time as a Causal Set". In: *Phys. Rev. Lett.* 59 (1987), pp. 521–524. DOI: 10.1103/PhysRevLett.59.521.

[106] J. Polchinski. *String theory. Vol. 1: An introduction to the bosonic string*. Cambridge Monographs on Mathematical Physics. Cambridge University Press, 2007. ISBN: 9780511252273, 9780521672276, 9780521633031. DOI: 10.1017/CBO9780511816079.

[107] J. Polchinski. *String theory. Vol. 2: Superstring theory and beyond*. Cambridge Monographs on Mathematical Physics. Cambridge University Press, 2007. ISBN: 9780511252280, 9780521633048, 9780521672283. DOI: 10.1017/CBO9780511618123.

[108] K. Becker, M. Becker, and J. H. Schwarz. *String theory and M-theory: A modern introduction*. Cambridge University Press, 2006. ISBN: 9780511254864, 9780521860697.

[109] Matt Visser. "How to Wick rotate generic curved spacetime". In: (2017). arXiv: 1702.05572 [gr-qc].

[110] Alessio Baldazzi, Roberto Percacci, and Vedran Skrinjar. "Wicked metrics". In: *Class. Quant. Grav.* 36.10 (2019), p. 105008. DOI: 10.1088/1361-6382/ab187d. arXiv: 1811.03369 [gr-qc].

[111] "5. Riemannian and Lorentz Geometry". In: ed. by Barrett O'Neill. Vol. 103. Pure and Applied Mathematics. Elsevier, 1983, pp. 126 –157. DOI: https://doi.org/10.1016/S0079-8169(08)60040-9. URL: http://www.sciencedirect.com/science/article/pii/S0079816908600409.

[112] Steven Weinberg. "ULTRAVIOLET DIVERGENCES IN QUANTUM THEORIES OF GRAVITATION". In: *General Relativity: An Einstein Centenary Survey*. 1980, pp. 790–831.

[113] Max Niedermaier and Martin Reuter. "The Asymptotic Safety Scenario in Quantum Gravity". In: *Living Rev. Rel.* 9 (2006), pp. 5–173. DOI: 10.12942/lrr-2006-5.

[114] M. Niedermaier. "The Asymptotic safety scenario in quantum gravity: An Introduction". In: *Class. Quant. Grav.* 24 (2007), R171–230. DOI: 10.1088/0264-9381/24/18/R01. arXiv: gr-qc/0610018 [gr-qc].

[115] Daniel F. Litim. "Fixed Points of Quantum Gravity and the Renormalisation Group". In: (2008). [PoSQG-Ph,024(2007)]. DOI: 10.22323/1.043.0024. arXiv: 0810.3675 [hep-th].

[116] Roberto Percacci. "A Short introduction to asymptotic safety". In: *Time and Matter: Proceedings, 3rd International Conference, TAM2010, Budva, Montenegro, 4-8 October, 2010*. 2011, pp. 123–142. arXiv: 1110.6389 [hep-th].

[117] Martin Reuter and Frank Saueressig. "Quantum Einstein Gravity". In: *New J. Phys.* 14 (2012), p. 055022. DOI: 10.1088/1367-2630/14/5/055022. arXiv: 1202.2274 [hep-th].

[118] Astrid Eichhorn. "Status of the asymptotic safety paradigm for quantum gravity and matter". In: *Found. Phys.* 48.10 (2018), pp. 1407–1429. DOI: 10.1007/s10701-018-0196-6. arXiv: 1709.03696 [gr-qc].

[119] Martin Reuter and Frank Saueressig. *Quantum Gravity and the Functional Renormalization Group*. Cambridge University Press, 2019. ISBN: 9781107107328, 9781108670746. URL: https://www.cambridge.org/academic/subjects/physics/theoretical-physics-and-mathematical-physics/quantum-gravity-and-functional-renormalization-group-road-towards-asymptotic-safety?format=HB&isbn=9781107107328.

[120] C. Wetterich. "Quantum scale symmetry". In: (2019). arXiv: 1901.04741 [hep-th].

[121] Astrid Eichhorn et al. "How perturbative is quantum gravity?" In: *Phys. Lett.* B792 (2019), pp. 310–314. DOI: 10.1016/j.physletb.2019.01.071. arXiv: 1810.02828 [hep-th].

[122] Kenneth G. Wilson. "Renormalization group and critical phenomena. 1. Renormalization group and the Kadanoff scaling picture". In: *Phys. Rev.* B4 (1971), pp. 3174–3183. DOI: 10.1103/PhysRevB.4.3174.

[123] Kenneth G. Wilson. "Renormalization group and critical phenomena. 2. Phase space cell analysis of critical behavior". In: *Phys. Rev.* B4 (1971), pp. 3184–3205. DOI: 10.1103/PhysRevB.4.3184.

[124] Kenneth G. Wilson. "The Renormalization Group: Critical Phenomena and the Kondo Problem". In: *Rev. Mod. Phys.* 47 (1975), p. 773. DOI: 10.1103/RevModPhys.47.773.

[125] K. G. Wilson. "The renormalization group and critical phenomena". In: *Rev. Mod. Phys.* 55 (1983), pp. 583–600. DOI: 10.1103/RevModPhys.55.583.

[126] Steven Weinberg. *The quantum theory of fields. Vol. 2: Modern applications*. Cambridge University Press, 2013. ISBN: 9781139632478, 9780521670548, 9780521550024.

[127] Michael E. Peskin and Daniel V. Schroeder. *An Introduction to quantum field theory*. Reading, USA: Addison-Wesley, 1995. ISBN: 9780201503975, 0201503972. URL: http://www.slac.stanford.edu/~mpeskin/QFT.html.

[128] Jean Zinn-Justin. "Quantum field theory and critical phenomena". In: *Int. Ser. Monogr. Phys.* 113 (2002), pp. 1–1054.

[129] M. Srednicki. *Quantum field theory*. Cambridge University Press, 2007. ISBN: 9780521864497, 9780511267208.

[130] Christof Wetterich. "Exact evolution equation for the effective potential". In: *Phys. Lett.* B301 (1993), pp. 90–94. DOI: 10.1016/0370-2693(93)90726-X. arXiv: 1710.05815 [hep-th].

[131] Tim R. Morris. "The Exact renormalization group and approximate solutions". In: *Int. J. Mod. Phys.* A9 (1994), pp. 2411–2450. DOI: 10.1142/S0217751X94000972. arXiv: hep-ph/9308265 [hep-ph].

[132] Ulrich Ellwanger, Manfred Hirsch, and Axel Weber. "Flow equations for the relevant part of the pure Yang-Mills action". In: *Z. Phys.* C69 (1996), pp. 687–698. DOI: 10.1007/s002880050073. arXiv: hep-th/9506019 [hep-th].

[133] Juergen Berges, Nikolaos Tetradis, and Christof Wetterich. "Nonperturbative renormalization flow in quantum field theory and statistical physics". In: *Phys. Rept.* 363 (2002), pp. 223–386. DOI: 10.1016/S0370-1573(01)00098-9. arXiv: hep-ph/0005122 [hep-ph].

[134] K. Aoki. "Introduction to the nonperturbative renormalization group and its recent applications". In: *Int. J. Mod. Phys.* B14 (2000), pp. 1249–1326. DOI: 10.1016/S0217-9792(00)00092-3.

[135] Janos Polonyi. "Lectures on the functional renormalization group method". In: *Central Eur. J. Phys.* 1 (2003), pp. 1–71. DOI: 10.2478/BF02475552. arXiv: hep-th/0110026 [hep-th].

[136] Jan M. Pawlowski. "Aspects of the functional renormalisation group". In: *Annals Phys.* 322 (2007), pp. 2831–2915. DOI: 10.1016/j.aop.2007.01.007. arXiv: hep-th/0512261 [hep-th].

[137] Holger Gies. "Introduction to the functional RG and applications to gauge theories". In: *Lect. Notes Phys.* 852 (2012), pp. 287–348. DOI: 10.1007/978-3-642-27320-9_6. arXiv: hep-ph/0611146 [hep-ph].

[138] Bertrand Delamotte. "An Introduction to the nonperturbative renormalization group". In: *Lect. Notes Phys.* 852 (2012), pp. 49–132. DOI: 10.1007/978-3-642-27320-9_2. arXiv: cond-mat/0702365 [cond-mat.stat-mech].

[139] Oliver J. Rosten. "Fundamentals of the Exact Renormalization Group". In: *Phys. Rept.* 511 (2012), pp. 177–272. DOI: 10.1016/j.physrep.2011.12.003. arXiv: 1003.1366 [hep-th].

[140] Daniel F. Litim. "Optimization of the exact renormalization group". In: *Phys. Lett.* B486 (2000), pp. 92–99. DOI: 10.1016/S0370-2693(00)00748-6. arXiv: hep-th/0005245 [hep-th].

[141] Daniel F. Litim. "Optimized renormalization group flows". In: *Phys. Rev.* D64 (2001), p. 105007. DOI: 10.1103/PhysRevD.64.105007. arXiv: hep-th/0103195 [hep-th].

[142] M. Reuter and C. Wetterich. "Effective average action for gauge theories and exact evolution equations". In: *Nucl. Phys.* B417 (1994), pp. 181–214. DOI: 10.1016/0550-3213(94)90543-6.

[143] Marco D'Attanasio and Tim R. Morris. "Gauge invariance, the quantum action principle, and the renormalization group". In: *Phys. Lett.* B378 (1996), pp. 213–221. DOI: 10.1016/0370-2693(96)00411-X. arXiv: hep-th/9602156 [hep-th].

[144] M. Reuter and C. Wetterich. "Gluon condensation in nonperturbative flow equations". In: *Phys. Rev.* D56 (1997), pp. 7893–7916. DOI: 10.1103/PhysRevD.56.7893. arXiv: hep-th/9708051 [hep-th].

[145] Daniel F. Litim and Jan M. Pawlowski. "Flow equations for Yang-Mills theories in general axial gauges". In: *Phys. Lett.* B435 (1998), pp. 181–188. DOI: 10.1016/S0370-2693(98)00761-8. arXiv: hep-th/9802064 [hep-th].

[146] Filipe Freire, Daniel F. Litim, and Jan M. Pawlowski. "Gauge invariance and background field formalism in the exact renormalization group". In: *Phys. Lett.* B495 (2000), pp. 256–262. DOI: 10.1016/S0370-2693(00)01231-4. arXiv: hep-th/0009110 [hep-th].

[147] Holger Gies and Michael M. Scherer. "Asymptotic safety of simple Yukawa systems". In: *Eur. Phys. J.* C66 (2010), pp. 387–402. DOI: 10.1140/epjc/s10052-010-1256-z. arXiv: 0901.2459 [hep-th].

[148] Holger Gies. "Renormalizability of gauge theories in extra dimensions". In: *Phys. Rev.* D68 (2003), p. 085015. DOI: 10.1103/PhysRevD.68.085015. arXiv: hep-th/0305208 [hep-th].

[149] Daniel F. Litim and Francesco Sannino. "Asymptotic safety guaranteed". In: *JHEP* 12 (2014), p. 178. DOI: 10.1007/JHEP12(2014)178. arXiv: 1406.2337 [hep-th].

[150] Kenneth Intriligator and Francesco Sannino. "Supersymmetric asymptotic safety is not guaranteed". In: *JHEP* 11 (2015), p. 023. DOI: 10.1007/JHEP11(2015)023. arXiv: 1508.07411 [hep-th].

[151] Nicolai Christiansen, Astrid Eichhorn, and Aaron Held. "Is scale-invariance in gauge-Yukawa systems compatible with the graviton?" In: *Phys. Rev.* D96.8 (2017), p. 084021. DOI: 10.1103/PhysRevD.96.084021. arXiv: 1705.01858 [hep-th].

[152] Kenneth G. Wilson and Michael E. Fisher. "Critical exponents in 3.99 dimensions". In: *Phys. Rev. Lett.* 28 (1972), pp. 240–243. DOI: 10.1103/PhysRevLett.28.240.

[153] Leonie Canet et al. "Nonperturbative renormalization group approach to the Ising model: A Derivative expansion at order partial**4". In: *Phys. Rev.* B68 (2003), p. 064421. DOI: 10.1103/PhysRevB.68.064421. arXiv: hep-th/0302227 [hep-th].

[154] Daniel F. Litim and Dario Zappala. "Ising exponents from the functional renormalisation group". In: *Phys. Rev.* D83 (2011), p. 085009. DOI: 10.1103/PhysRevD.83.085009. arXiv: 1009.1948 [hep-th].

[155] Ivan Balog et al. "Convergence of Non-Perturbative Approximations to the Renormalization Group". In: (2019). arXiv: 1907.01829 [cond-mat.stat-mech].

[156] Kiyoshi Higashijima and Etsuko Itou. "Three-dimensional nonlinear sigma models in the Wilsonian renormalization method". In: *Prog. Theor. Phys.* 110 (2003), pp. 563–578. DOI: 10.1143/PTP.110.563. arXiv: hep-th/0304194 [hep-th].

[157] Alessandro Codello and Roberto Percacci. "Fixed Points of Nonlinear Sigma Models in d¿2". In: *Phys. Lett.* B672 (2009), pp. 280–283. DOI: 10.1016/j.physletb.2009.01.032. arXiv: 0810.0715 [hep-th].

[158] M. Fabbrichesi et al. "Asymptotic safety and the gauged SU(N) nonlinear σ-model". In: *Phys. Rev.* D83 (2011), p. 025016. DOI: 10.1103/PhysRevD.83.025016. arXiv: 1010.0912 [hep-ph].

[159] Jens Braun, Holger Gies, and Daniel D. Scherer. "Asymptotic safety: a simple example". In: *Phys. Rev.* D83 (2011), p. 085012. DOI: 10.1103/PhysRevD.83.085012. arXiv: 1011.1456 [hep-th].

[160] M. Reuter. "Nonperturbative evolution equation for quantum gravity". In: *Phys. Rev.* D57 (1998), pp. 971–985. DOI: 10.1103/PhysRevD.57.971. arXiv: hep-th/9605030 [hep-th].

[161] M. Reuter and Frank Saueressig. "Renormalization group flow of quantum gravity in the Einstein-Hilbert truncation". In: *Phys. Rev.* D65 (2002), p. 065016. DOI: 10.1103/PhysRevD.65.065016. arXiv: hep-th/0110054 [hep-th].

[162] O. Lauscher and M. Reuter. "Ultraviolet fixed point and generalized flow equation of quantum gravity". In: *Phys. Rev.* D65 (2002), p. 025013. DOI: 10.1103/PhysRevD.65.025013. arXiv: hep-th/0108040 [hep-th].

[163] Daniel F. Litim. "Fixed points of quantum gravity". In: *Phys. Rev. Lett.* 92 (2004), p. 201301. DOI: 10.1103/PhysRevLett.92.201301. arXiv: hep-th/0312114 [hep-th].

[164] O. Lauscher and M. Reuter. "Flow equation of quantum Einstein gravity in a higher derivative truncation". In: *Phys. Rev.* D66 (2002), p. 025026. DOI: 10.1103/PhysRevD.66.025026. arXiv: hep-th/0205062 [hep-th].

[165] Pedro F. Machado and Frank Saueressig. "On the renormalization group flow of f(R)-gravity". In: *Phys. Rev.* D77 (2008), p. 124045. DOI: 10.1103/PhysRevD.77.124045. arXiv: 0712.0445 [hep-th].

[166] Alessandro Codello, Roberto Percacci, and Christoph Rahmede. "Investigating the Ultraviolet Properties of Gravity with a Wilsonian Renormalization Group Equation". In: *Annals Phys.* 324 (2009), pp. 414–469. DOI: 10.1016/j.aop.2008.08.008. arXiv: 0805.2909 [hep-th].

[167] K. Falls et al. "A bootstrap towards asymptotic safety". In: (2013). arXiv: 1301.4191 [hep-th].

[168] Dario Benedetti, Pedro F. Machado, and Frank Saueressig. "Asymptotic safety in higher-derivative gravity". In: *Mod. Phys. Lett.* A24 (2009), pp. 2233–2241. DOI: 10.1142/S0217732309031521. arXiv: 0901.2984 [hep-th].

[169] Holger Gies et al. "Gravitational Two-Loop Counterterm Is Asymptotically Safe". In: *Phys. Rev. Lett.* 116.21 (2016), p. 211302. DOI: 10.1103/PhysRevLett.116.211302. arXiv: 1601.01800 [hep-th].

[170] Nicolai Christiansen et al. "Fixed points and infrared completion of quantum gravity". In: *Phys. Lett.* B728 (2014), pp. 114–117. DOI: 10.1016/j.physletb.2013.11.025. arXiv: 1209.4038 [hep-th].

[171] Nicolai Christiansen et al. "Global Flows in Quantum Gravity". In: *Phys. Rev.* D93.4 (2016), p. 044036. DOI: 10.1103/PhysRevD.93.044036. arXiv: 1403.1232 [hep-th].

[172] Nicolai Christiansen et al. "Local Quantum Gravity". In: *Phys. Rev.* D92.12 (2015), p. 121501. DOI: 10.1103/PhysRevD.92.121501. arXiv: 1506.07016 [hep-th].

[173] Tobias Denz, Jan M. Pawlowski, and Manuel Reichert. "Towards apparent convergence in asymptotically safe quantum gravity". In: *Eur. Phys. J.* C78.4 (2018), p. 336. DOI: 10.1140/epjc/s10052-018-5806-0. arXiv: 1612.07315 [hep-th].

[174] Elisa Manrique and Martin Reuter. "Bimetric Truncations for Quantum Einstein Gravity and Asymptotic Safety". In: *Annals Phys.* 325 (2010), pp. 785–815. DOI: 10.1016/j.aop.2009.11.009. arXiv: 0907.2617 [gr-qc].

[175] Elisa Manrique, Martin Reuter, and Frank Saueressig. "Matter Induced Bimetric Actions for Gravity". In: *Annals Phys.* 326 (2011), pp. 440–462. DOI: 10.1016/j.aop.2010.11.003. arXiv: 1003.5129 [hep-th].

[176] Elisa Manrique, Martin Reuter, and Frank Saueressig. "Bimetric Renormalization Group Flows in Quantum Einstein Gravity". In: *Annals Phys.* 326 (2011), pp. 463–485. DOI: 10.1016/j.aop.2010.11.006. arXiv: 1006.0099 [hep-th].

[177] Daniel Becker and Martin Reuter. "En route to Background Independence: Broken split-symmetry, and how to restore it with bi-metric average actions". In: *Annals Phys.* 350 (2014), pp. 225–301. DOI: 10.1016/j.aop.2014.07.023. arXiv: 1404.4537 [hep-th].

[178] Astrid Eichhorn and Aaron Held. "Top mass from asymptotic safety". In: *Phys. Lett.* B777 (2018), pp. 217–221. DOI: 10.1016/j.physletb.2017.12.040. arXiv: 1707.01107 [hep-th].

[179] Astrid Eichhorn and Stefan Lippoldt. "Quantum gravity and Standard-Model-like fermions". In: *Phys. Lett.* B767 (2017), pp. 142–146. DOI: 10.1016/j.physletb.2017.01.064. arXiv: 1611.05878 [gr-qc].

[180] U. Harst and M. Reuter. "QED coupled to QEG". In: *JHEP* 05 (2011), p. 119. DOI: 10.1007/JHEP05(2011)119. arXiv: 1101.6007 [hep-th].

[181] Nicolai Christiansen and Astrid Eichhorn. "An asymptotically safe solution to the U(1) triviality problem". In: *Phys. Lett.* B770 (2017), pp. 154–160. DOI: 10.1016/j.physletb.2017.04.047. arXiv: 1702.07724 [hep-th].

[182] Gaurav Narain and Roberto Percacci. "Renormalization Group Flow in Scalar-Tensor Theories. I". In: *Class. Quant. Grav.* 27 (2010), p. 075001. DOI: 10.1088/0264-9381/27/7/075001. arXiv: 0911.0386 [hep-th].

[183] O. Zanusso et al. "Gravitational corrections to Yukawa systems". In: *Phys. Lett.* B689 (2010), pp. 90–94. DOI: 10.1016/j.physletb.2010.04.043. arXiv: 0904.0938 [hep-th].

[184] Jan-Eric Daum, Ulrich Harst, and Martin Reuter. "Running Gauge Coupling in Asymptotically Safe Quantum Gravity". In: *JHEP* 01 (2010), p. 084. DOI: 10.1007/JHEP01(2010)084. arXiv: 0910.4938 [hep-th].

[185] G. P. Vacca and O. Zanusso. "Asymptotic Safety in Einstein Gravity and Scalar-Fermion Matter". In: *Phys. Rev. Lett.* 105 (2010), p. 231601. DOI: 10.1103/PhysRevLett.105.231601. arXiv: 1009.1735 [hep-th].

[186] Sarah Folkerts, Daniel F. Litim, and Jan M. Pawlowski. "Asymptotic freedom of Yang-Mills theory with gravity". In: *Phys. Lett.* B709 (2012), pp. 234–241. DOI: 10.1016/j.physletb.2012.02.002. arXiv: 1101.5552 [hep-th].

[187] Astrid Eichhorn. "Quantum-gravity-induced matter self-interactions in the asymptotic-safety scenario". In: *Phys. Rev.* D86 (2012), p. 105021. DOI: 10.1103/PhysRevD.86.105021. arXiv: 1204.0965 [gr-qc].

[188] Kin-ya Oda and Masatoshi Yamada. "Non-minimal coupling in Higgs–Yukawa model with asymptotically safe gravity". In: *Class. Quant. Grav.* 33.12 (2016), p. 125011. DOI: 10.1088/0264-9381/33/12/125011. arXiv: 1510.03734 [hep-th].

[189] Astrid Eichhorn, Aaron Held, and Jan M. Pawlowski. "Quantum-gravity effects on a Higgs-Yukawa model". In: *Phys. Rev.* D94.10 (2016), p. 104027. DOI: 10.1103/PhysRevD.94.104027. arXiv: 1604.02041 [hep-th].

[190] Yuta Hamada and Masatoshi Yamada. "Asymptotic safety of higher derivative quantum gravity non-minimally coupled with a matter system". In: *JHEP* 08 (2017), p. 070. DOI: 10.1007/JHEP08(2017)070. arXiv: 1703.09033 [hep-th].

[191] Pietro Donà, Astrid Eichhorn, and Roberto Percacci. "Matter matters in asymptotically safe quantum gravity". In: *Phys. Rev.* D89.8 (2014), p. 084035. DOI: 10.1103/PhysRevD.89.084035. arXiv: 1311.2898 [hep-th].

[192] Finn Larsen and Frank Wilczek. "Renormalization of black hole entropy and of the gravitational coupling constant". In: *Nucl. Phys.* B458 (1996), pp. 249–266. DOI: 10.1016/0550-3213(95)00548-X. arXiv: hep-th/9506066 [hep-th].

[193] Jan Meibohm, Jan M. Pawlowski, and Manuel Reichert. "Asymptotic safety of gravity-matter systems". In: *Phys. Rev.* D93.8 (2016), p. 084035. DOI: 10.1103/PhysRevD.93.084035. arXiv: 1510.07018 [hep-th].

[194] Roberto Percacci and Gian Paolo Vacca. "Search of scaling solutions in scalar-tensor gravity". In: *Eur. Phys. J.* C75.5 (2015), p. 188. DOI: 10.1140/epjc/s10052-015-3410-0. arXiv: 1501.00888 [hep-th].

[195] Pietro Donà et al. "Asymptotic safety in an interacting system of gravity and scalar matter". In: *Phys. Rev.* D93.4 (2016). [Erratum: Phys. Rev.D93,no.12,129904(2016)], p. 044049. DOI: 10.1103/PhysRevD.93.129904,10.1103/PhysRevD.93.044049. arXiv: 1512.01589 [gr-qc].

[196] Jorn Biemans, Alessia Platania, and Frank Saueressig. "Renormalization group fixed points of foliated gravity-matter systems". In: *JHEP* 05 (2017), p. 093. DOI: 10.1007/JHEP05(2017)093. arXiv: 1702.06539 [hep-th].

[197] Natália Alkofer and Frank Saueressig. "Asymptotically safe $f(R)$-gravity coupled to matter I: the polynomial case". In: *Annals Phys.* 396 (2018), pp. 173–201. DOI: 10.1016/j.aop.2018.07.017. arXiv: 1802.00498 [hep-th].

[198] Astrid Eichhorn et al. "Effective universality in quantum gravity". In: *SciPost Phys.* 5.4 (2018), p. 031. DOI: 10.21468/SciPostPhys.5.4.031. arXiv: 1804.00012 [hep-th].

[199] Nicolai Christiansen et al. "Asymptotic safety of gravity with matter". In: *Phys. Rev.* D97.10 (2018), p. 106012. DOI: 10.1103/PhysRevD.97.106012. arXiv: 1710.04669 [hep-th].

[200] Holger Gies, Benjamin Knorr, and Stefan Lippoldt. "Generalized Parametrization Dependence in Quantum Gravity". In: *Phys. Rev.* D92.8 (2015), p. 084020. DOI: 10.1103/PhysRevD.92.084020. arXiv: 1507.08859 [hep-th].

[201] Astrid Eichhorn, Stefan Lippoldt, and Vedran Skrinjar. "Nonminimal hints for asymptotic safety". In: *Phys. Rev.* D97.2 (2018), p. 026002. DOI: 10.1103/PhysRevD.97.026002. arXiv: 1710.03005 [hep-th].

[202] Astrid Eichhorn, Stefan Lippoldt, and Marc Schiffer. "Zooming in on fermions and quantum gravity". In: *Phys. Rev.* D99.8 (2019), p. 086002. DOI: 10.1103/PhysRevD.99.086002. arXiv: 1812.08782 [hep-th].

[203] Astrid Eichhorn, Aaron Held, and Christof Wetterich. "Quantum-gravity predictions for the fine-structure constant". In: *Phys. Lett.* B782 (2018), pp. 198–201. DOI: 10.1016/j.physletb.2018.05.016. arXiv: 1711.02949 [hep-th].

[204] S. Aoki et al. "Review of lattice results concerning low-energy particle physics". In: *Eur. Phys. J.* C77.2 (2017), p. 112. DOI: 10.1140/epjc/s10052-016-4509-7. arXiv: 1607.00299 [hep-lat].

[205] Lee Smolin. "QUANTUM GRAVITY ON A LATTICE". In: *Nucl. Phys.* B148 (1979), pp. 333–372. DOI: 10.1016/0550-3213(79)90140-8.

[206] Jan Ambjorn and Jerzy Jurkiewicz. "Four-dimensional simplicial quantum gravity". In: *Phys. Lett.* B278 (1992), pp. 42–50. DOI: 10.1016/0370-2693(92)90709-D.

[207] M. E. Agishtein and Alexander A. Migdal. "Simulations of four-dimensional simplicial quantum gravity". In: *Mod. Phys. Lett.* A7 (1992), pp. 1039–1062. DOI: 10.1142/S0217732392000938.

[208] Jan Ambjørn, Bergfinnur Durhuus, and Thordur Jonsson. *Quantum Geometry: A Statistical Field Theory Approach*. Cambridge Monographs on Mathematical Physics. Cambridge University Press, 1997. DOI: 10.1017/CBO9780511524417.

[209] S. Catterall. "Lattice quantum gravity: review and recent developments". In: *Nucl. Phys. Proc. Suppl.* 47 (1996), p. 59. DOI: 10.1016/0920-5632(96)00032-1. arXiv: hep-lat/9510008 [hep-lat].

[210] T. Regge. "GENERAL RELATIVITY WITHOUT COORDINATES". In: *Nuovo Cim.* 19 (1961), pp. 558–571. DOI: 10.1007/BF02733251.

[211] Edwin E. Moise. "Affine Structures in 3-Manifolds: V. The Triangulation Theorem and Hauptvermutung". In: *Annals of Mathematics* 56.1 (1952), pp. 96–114. ISSN: 0003486X. URL: http://www.jstor.org/stable/1969769.

[212] Michael Hartley Freedman. "The topology of four-dimensional manifolds". In: *J. Differential Geom.* 17.3 (1982), pp. 357–453. DOI: 10.4310/jdg/1214437136. URL: https://doi.org/10.4310/jdg/1214437136.

[213] F. David. "Planar Diagrams, Two-Dimensional Lattice Gravity and Surface Models". In: *Nucl. Phys.* B257 (1985). [,45(1984)], p. 45. DOI: 10.1016/0550-3213(85)90335-9.

[214] F. David. "A Model of Random Surfaces with Nontrivial Critical Behavior". In: *Nucl. Phys.* B257 (1985), pp. 543–576. DOI: 10.1016/0550-3213(85)90363-3.

[215] Jan Ambjorn, B. Durhuus, and J. Frohlich. "Diseases of Triangulated Random Surface Models, and Possible Cures". In: *Nucl. Phys.* B257 (1985), pp. 433–449. DOI: 10.1016/0550-3213(85)90356-6.

[216] V. A. Kazakov, Alexander A. Migdal, and I. K. Kostov. "Critical Properties of Randomly Triangulated Planar Random Surfaces". In: *Phys. Lett.* 157B (1985), pp. 295–300. DOI: 10.1016/0370-2693(85)90669-0.

[217] Martin Rocek and Ruth M. Williams. "INTRODUCTION TO QUANTUM REGGE CALCULUS". In: *Nuffield Workshop on Quantum Structure of Space and Time London, England, August 3-21, 1981*. 1981, pp. 105–116.

[218] M. Rocek and Ruth M. Williams. "QUANTUM REGGE CALCULUS". In: *Phys. Lett.* 104B (1981), p. 31. DOI: 10.1016/0370-2693(81)90848-0.

[219] John W. Barrett, Daniele Oriti, and Ruth M. Williams. "Tullio Regge's legacy: Regge calculus and discrete gravity". In: 2018. arXiv: 1812.06193 [gr-qc].

[220] Adrian P. Gentle. "A cosmological solution of Regge calculus". In: *Class. Quant. Grav.* 30 (2013), p. 085004. DOI: 10.1088/0264-9381/30/8/085004. arXiv: 1208.1502 [gr-qc].

[221] Rex G. Liu and Ruth M. Williams. "Regge calculus models of the closed vacuum Λ-FLRW universe". In: *Phys. Rev.* D93 (2016), p. 024032. DOI: 10.1103/PhysRevD.93.024032. arXiv: 1501.07614 [gr-qc].

[222] Rex G. Liu and Ruth M. Williams. "Regge calculus models of closed lattice universes". In: *Phys. Rev.* D93.2 (2016), p. 023502. DOI: 10.1103/PhysRevD.93.023502. arXiv: 1502.03000 [gr-qc].

[223] Rex G. Liu and Ruth M. Williams. "Cosmological modelling with Regge calculus". In: 2015. arXiv: 1510.05771 [gr-qc].

[224] Jeff Cheeger, Werner Müller, and Robert Schrader. "On the curvature of piecewise flat spaces". In: *Comm. Math. Phys.* 92.3 (1984), pp. 405–454. URL: https://projecteuclid.org:443/euclid.cmp/1103940867.

[225] Herbert W. Hamber. "Phases of simplicial quantum gravity". In: *Nucl. Phys. Proc. Suppl.* 25A (1992), pp. 150–175. DOI: 10.1016/S0920-5632(05)80016-7.

[226] Herbert W. Hamber. "Quantum Gravity on the Lattice". In: *Gen. Rel. Grav.* 41 (2009), pp. 817–876. DOI: 10.1007/s10714-009-0769-y. arXiv: 0901.0964 [gr-qc].

[227] Herbert W. Hamber. "Scaling Exponents for Lattice Quantum Gravity in Four Dimensions". In: *Phys. Rev.* D92.6 (2015), p. 064017. DOI: 10.1103/PhysRevD.92.064017. arXiv: 1506.07795 [hep-th].

[228] Pietro Menotti and Pier Paolo Peirano. "Functional integration for Regge gravity". In: *Nucl. Phys. Proc. Suppl.* 57 (1997). [,82(1996)], pp. 82–90. DOI: 10.1016/S0920-5632(97)00356-3. arXiv: gr-qc/9702020 [gr-qc].

[229] Dario Benedetti. "Quantum Gravity from Simplices: Analytical Investigations of Causal Dynamical Triangulations". PhD thesis. Utrecht U., 2007. arXiv: 0707.3070 [gr-qc].

[230] W. T. Tutte. "A Census of Planar Triangulations". In: *Canadian Journal of Mathematics* 14 (1962), 21–38. DOI: 10.4153/CJM-1962-002-9.

[231] Jan Ambjorn and Steen Varsted. "Entropy estimate in three-dimensional simplicial quantum gravity". In: *Phys. Lett.* B266 (1991), pp. 285–290. DOI: 10.1016/0370-2693(91)91041-S.

[232] Jan Ambjorn and J. Jurkiewicz. "On the exponential bound in four-dimensional simplicial gravity". In: *Phys. Lett.* B335 (1994), pp. 355–358. DOI: 10.1016/0370-2693(94)90363-8. arXiv: hep-lat/9405010 [hep-lat].

[233] Jan Ambjorn. "Barriers in quantum gravity". In: *Workshop on String Theory, Gauge Theory and Quantum Gravity Trieste, Italy, April 28-29, 1993*. 1993, pp. 0228–242. DOI: 10.1142/9789814447072_0007. arXiv: hep-th/9408129 [hep-th].

[234] Jan Ambjorn et al. "Observing 4-d baby universes in quantum gravity". In: *Phys. Lett.* B305 (1993), pp. 208–213. DOI: 10.1016/0370-2693(93)90109-U. arXiv: hep-th/9303041 [hep-th].

[235] J. Jurkiewicz, A. Krzywicki, and B. Petersson. "A Numerical Study of Discrete Euclidean Polyakov Surfaces". In: *Phys. Lett.* 168B (1986), pp. 273–278. DOI: 10.1016/0370-2693(86)90978-0.

[236] J. Jurkiewicz, A. Krzywicki, and B. Petersson. "A Grand Canonical Ensemble of Randomly Triangulated Surfaces". In: *Phys. Lett.* B177 (1986), pp. 89–92. DOI: 10.1016/0370-2693(86)90021-3.

[237] Jan Ambjorn et al. "The Appearance of Critical Dimensions in Regulated String Theories". In: *Nucl. Phys.* B270 (1986), pp. 457–482. DOI: 10.1016/0550-3213(86)90563-8.

[238] Jan Ambjorn, B. Durhuus, and J. Frohlich. "The Appearance of Critical Dimensions in Regulated String Theories. 2." In: *Nucl. Phys.* B275 (1986), pp. 161–184. DOI: 10.1016/0550-3213(86)90594-8.

[239] P. Di Francesco, Paul H. Ginsparg, and Jean Zinn-Justin. "2-D Gravity and random matrices". In: *Phys. Rept.* 254 (1995), pp. 1–133. DOI: 10.1016/0370-1573(94)00084-G. arXiv: hep-th/9306153 [hep-th].

[240] E. Brézin et al. "Planar diagrams". In: *Comm. Math. Phys.* 59.1 (1978), pp. 35–51. URL: https://projecteuclid.org:443/euclid.cmp/1103901558.

[241] Simeon Warner and Simon Catterall. "Phase diagram of four-dimensional dynamical triangulations with a boundary". In: *Phys. Lett.* B493 (2000), pp. 389–394. DOI: 10.1016/S0370-2693(00)01154-0. arXiv: hep-lat/0008015 [hep-lat].

[242] Bas V. de Bakker and Jan Smit. "Curvature and scaling in 4-d dynamical triangulation". In: *Nucl. Phys.* B439 (1995), pp. 239–258. DOI: 10.1016/0550-3213(95)00026-O. arXiv: hep-lat/9407014 [hep-lat].

[243] Jan Ambjorn and J. Jurkiewicz. "Scaling in four-dimensional quantum gravity". In: *Nucl. Phys.* B451 (1995), pp. 643–676. DOI: 10.1016/0550-3213(95)00303-A. arXiv: hep-th/9503006 [hep-th].

[244] H. S. Egawa et al. "Scaling behavior in 4-D simplicial quantum gravity". In: *Prog. Theor. Phys.* 97 (1997), pp. 539–552. DOI: 10.1143/PTP.97.539. arXiv: hep-lat/9611028 [hep-lat].

[245] P. Bialas et al. "Focusing on the fixed point of 4-D simplicial gravity". In: *Nucl. Phys.* B472 (1996), pp. 293–308. DOI: 10.1016/0550-3213(96)00214-3. arXiv: hep-lat/9601024 [hep-lat].

[246] S. Catterall, R. Renken, and John B. Kogut. "Singular structure in 4-D simplicial gravity". In: *Phys. Lett.* B416 (1998), pp. 274–280. DOI: 10.1016/S0370-2693(97)01349-X. arXiv: hep-lat/9709007 [hep-lat].

[247] Jan Ambjorn, J. Jurkiewicz, and R. Loll. "Nonperturbative 3-D Lorentzian quantum gravity". In: *Phys. Rev.* D64 (2001), p. 044011. DOI: 10.1103/PhysRevD.64.044011. arXiv: hep-th/0011276 [hep-th].

[248] S. Catterall et al. "Baby universes in 4-D dynamical triangulation". In: *Phys. Lett.* B366 (1996), pp. 72–76. DOI: 10.1016/0370-2693(95)01372-5. arXiv: hep-lat/9509004 [hep-lat].

[249] Jacques Distler and Hikaru Kawai. "Conformal Field Theory and 2D Quantum Gravity". In: *Nucl. Phys.* B321 (1989), pp. 509–527. DOI: 10.1016/0550-3213(89)90354-4.

[250] Alexander M. Polyakov. "Quantum Geometry of Bosonic Strings". In: *Phys. Lett.* B103 (1981). [,598(1981)], pp. 207–210. DOI: 10.1016/0370-2693(81)90743-7.

[251] Jan Ambjorn and R. Loll. "Nonperturbative Lorentzian quantum gravity, causality and topology change". In: *Nucl. Phys.* B536 (1998), pp. 407–434. DOI: 10.1016/S0550-3213(98)00692-0. arXiv: hep-th/9805108 [hep-th].

[252] Jan Ambjørn, J. Jurkiewicz, and R. Loll. "Lorentzian and Euclidean Quantum Gravity — Analytical and Numerical Results". In: *NATO Sci. Ser. C* 556 (2000), pp. 381–450. DOI: 10.1007/978-94-011-4303-5_9. arXiv: hep-th/0001124 [hep-th].

[253] Jan Ambjorn, J. Jurkiewicz, and R. Loll. "Dynamically triangulating Lorentzian quantum gravity". In: *Nucl. Phys.* B610 (2001), pp. 347–382. DOI: 10.1016/S0550-3213(01)00297-8. arXiv: hep-th/0105267 [hep-th].

[254] Jan Ambjorn, J. Jurkiewicz, and Y. Watabiki. "Dynamical triangulations, a gateway to quantum gravity?" In: *J. Math. Phys.* 36 (1995), pp. 6299–6339. DOI: 10.1063/1.531246. arXiv: hep-th/9503108 [hep-th].

[255] S. Zohren. "Analytic Results in 2D Causal Dynamical Triangulations: A Review". PhD thesis. Utrecht U., 2006. arXiv: hep-th/0609177 [hep-th].

[256] J. Ambjorn et al. "Nonperturbative Quantum Gravity". In: *Phys. Rept.* 519 (2012), pp. 127–210. DOI: 10.1016/j.physrep.2012.03.007. arXiv: 1203.3591 [hep-th].

[257] R. Loll. "Quantum Gravity from Causal Dynamical Triangulations: A Review". In: (2019). arXiv: 1905.08669 [hep-th].

[258] Ryuichi Nakayama. "2-D quantum gravity in the proper time gauge". In: *Phys. Lett.* B325 (1994), pp. 347–353. DOI: 10.1016/0370-2693(94)90023-X. arXiv: hep-th/9312158 [hep-th].

[259] Claudio Teitelboim. "Causality Versus Gauge Invariance in Quantum Gravity and Supergravity". In: *Phys. Rev. Lett.* 50 (10 1983), pp. 705–708. DOI: 10.1103/PhysRevLett.50.705. URL: https://link.aps.org/doi/10.1103/PhysRevLett.50.705.

[260] Tom Banks and Leonard Susskind. "Canonical Quantization of (1+1)-dimensional Gravity". In: *Int. J. Theor. Phys.* 23 (1984), p. 475. DOI: 10.1007/BF02083740.

[261] A. Carlini and J. Greensite. "Fundamental constants and the problem of time". In: *Phys. Rev.* D52 (1995), pp. 936–960. DOI: 10.1103/PhysRevD.52.936. arXiv: gr-qc/9406044 [gr-qc].

[262] A. Carlini and J. Greensite. "Square root actions, metric signature, and the path integral of quantum gravity". In: *Phys. Rev.* D52 (1995), pp. 6947–6964. DOI: 10.1103/PhysRevD.52.6947. arXiv: gr-qc/9502023 [gr-qc].

[263] J. Ambjorn, J. Jurkiewicz, and R. Loll. "Emergence of a 4-D world from causal quantum gravity". In: *Phys. Rev. Lett.* 93 (2004), p. 131301. DOI: 10.1103/PhysRevLett.93.131301. arXiv: hep-th/0404156 [hep-th].

[264] J. Ambjorn, J. Jurkiewicz, and R. Loll. "Reconstructing the universe". In: *Phys. Rev.* D72 (2005), p. 064014. DOI: 10.1103/PhysRevD.72.064014. arXiv: hep-th/0505154 [hep-th].

[265] J. Ambjorn et al. "CDT meets Horava-Lifshitz gravity". In: *Phys. Lett.* B690 (2010), pp. 413–419. DOI: 10.1016/j.physletb.2010.05.054. arXiv: 1002.3298 [hep-th].

[266] J. Ambjorn et al. "A Second-order phase transition in CDT". In: *Phys. Rev. Lett.* 107 (2011), p. 211303. DOI: 10.1103/PhysRevLett.107.211303. arXiv: 1108.3932 [hep-th].

[267] Jan Ambjorn et al. "Second- and First-Order Phase Transitions in CDT". In: *Phys. Rev.* D85 (2012), p. 124044. DOI: 10.1103/PhysRevD.85.124044. arXiv: 1205.1229 [hep-th].

[268] J. Ambjørn et al. "Characteristics of the new phase in CDT". In: *Eur. Phys. J.* C77.3 (2017), p. 152. DOI: 10.1140/epjc/s10052-017-4710-3. arXiv: 1610.05245 [hep-th].

[269] J. Ambjorn et al. "New higher-order transition in causal dynamical triangulations". In: *Phys. Rev.* D95.12 (2017), p. 124029. DOI: 10.1103/PhysRevD.95.124029. arXiv: 1704.04373 [hep-lat].

[270] J. Ambjorn, J. Jurkiewicz, and R. Loll. "Spectral dimension of the universe". In: *Phys. Rev. Lett.* 95 (2005), p. 171301. DOI: 10.1103/PhysRevLett.95.171301. arXiv: hep-th/0505113 [hep-th].

[271] D. N. Coumbe and J. Jurkiewicz. "Evidence for Asymptotic Safety from Dimensional Reduction in Causal Dynamical Triangulations". In: *JHEP* 03 (2015), p. 151. DOI: 10.1007/JHEP03(2015)151. arXiv: 1411.7712 [hep-th].

[272] Petr Horava. "Membranes at Quantum Criticality". In: *JHEP* 03 (2009), p. 020. DOI: 10.1088/1126-6708/2009/03/020. arXiv: 0812.4287 [hep-th].

[273] Petr Horava. "Quantum Gravity at a Lifshitz Point". In: *Phys. Rev.* D79 (2009), p. 084008. DOI: 10.1103/PhysRevD.79.084008. arXiv: 0901.3775 [hep-th].

[274] Christian Anderson et al. "Quantizing Horava-Lifshitz Gravity via Causal Dynamical Triangulations". In: *Phys. Rev.* D85 (2012), p. 044027. DOI: 10.1103/PhysRevD.85.044027, 10.1103/PhysRevD.85.049904. arXiv: 1111.6634 [hep-th].

[275] S. Jordan and R. Loll. "Causal Dynamical Triangulations without Preferred Foliation". In: *Phys. Lett.* B724 (2013), pp. 155–159. DOI: 10.1016/j.physletb.2013.06.007. arXiv: 1305.4582 [hep-th].

[276] S. Jordan and R. Loll. "De Sitter Universe from Causal Dynamical Triangulations without Preferred Foliation". In: *Phys. Rev.* D88 (2013), p. 044055. DOI: 10.1103/PhysRevD.88.044055. arXiv: 1307.5469 [hep-th].

[277] Bernd Bruegmann and Enzo Marinari. "4-d simplicial quantum gravity with a nontrivial measure". In: *Phys. Rev. Lett.* 70 (1993), pp. 1908–1911. DOI: 10.1103/PhysRevLett.70.1908. arXiv: hep-lat/9210002 [hep-lat].

[278] S. Bilke et al. "4-D simplicial quantum gravity: Matter fields and the corresponding effective action". In: *Phys. Lett.* B432 (1998), pp. 279–286. DOI: 10.1016/S0370-2693(98)00675-3. arXiv: hep-lat/9804011 [hep-lat].

[279] J. Laiho and D. Coumbe. "Evidence for Asymptotic Safety from Lattice Quantum Gravity". In: *Phys. Rev. Lett.* 107 (2011), p. 161301. DOI: 10.1103/PhysRevLett.107.161301. arXiv: 1104.5505 [hep-lat].

[280] J. Ambjorn et al. "Euclidian 4d quantum gravity with a non-trivial measure term". In: *JHEP* 10 (2013), p. 100. DOI: 10.1007/JHEP10(2013)100. arXiv: 1307.2270 [hep-lat].

[281] Daniel Coumbe and John Laiho. "Exploring Euclidean Dynamical Triangulations with a Non-trivial Measure Term". In: *JHEP* 04 (2015), p. 028. DOI: 10.1007/JHEP04(2015)028. arXiv: 1401.3299 [hep-th].

[282] J. Laiho et al. "Lattice Quantum Gravity and Asymptotic Safety". In: *Phys. Rev.* D96.6 (2017), p. 064015. DOI: 10.1103/PhysRevD.96.064015. arXiv: 1604.02745 [hep-th].

[283] Vladimir A. Kazakov, Matthias Staudacher, and Thomas Wynter. "Exact solution of discrete two-dimensional R**2 gravity". In: *Nucl. Phys.* B471 (1996), pp. 309–333. DOI: 10.1016/0550-3213(96)00184-8. arXiv: hep-th/9601069 [hep-th].

[284] S. Bilke et al. "4-D simplicial quantum gravity interacting with gauge matter fields". In: *Phys. Lett.* B418 (1998), pp. 266–272. DOI: 10.1016/S0370-2693(97)01409-3. arXiv: hep-lat/9710077 [hep-lat].

[285] Jan Ambjorn, K. N. Anagnostopoulos, and J. Jurkiewicz. "Abelian gauge fields coupled to simplicial quantum gravity". In: *JHEP* 08 (1999), p. 016. DOI: 10.1088/1126-6708/1999/08/016. arXiv: hep-lat/9907027 [hep-lat].

[286] Jan Ambjorn, Jerzy Jurkiewicz, and Charlotte F. Kristjansen. "Quantum gravity, dynamical triangulations and higher derivative regularization". In: *Nucl. Phys.* B393 (1993), pp. 601–632. DOI: 10.1016/0550-3213(93)90075-Z. arXiv: hep-th/9208032 [hep-th].

[287] Jan Ambjorn et al. "4-d quantum gravity coupled to matter". In: *Phys. Rev.* D48 (1993), pp. 3695–3703. DOI: 10.1103/PhysRevD.48.3695. arXiv: hep-th/9303042 [hep-th].

[288] Jan Ambjorn et al. "Z(2) gauge matter coupled to 4-D simplicial quantum gravity". In: *Mod. Phys. Lett.* A9 (1994), pp. 2527–2542. DOI: 10.1142/S0217732394002392.

[289] I. Montvay and G. Munster. *Quantum fields on a lattice*. Cambridge Monographs on Mathematical Physics. Cambridge University Press, 1997. ISBN: 9780521599177, 9780511879197. DOI: 10.1017/CBO9780511470783. URL: http://www.cambridge.org/uk/catalogue/catalogue.asp?isbn=0521404320.

[290] Jeffrey M. Rabin. "Homology Theory of Lattice Fermion Doubling". In: *Nucl. Phys.* B201 (1982), pp. 315–332. DOI: 10.1016/0550-3213(82)90434-5.

[291] Tom Banks, Y. Dothan, and D. Horn. "GEOMETRIC FERMIONS". In: *Phys. Lett.* 117B (1982), pp. 413–417. DOI: 10.1016/0370-2693(82)90571-8.

[292] Simon Catterall, Jack Laiho, and Judah Unmuth-Yockey. "Topological fermion condensates from anomalies". In: *JHEP* 10 (2018), p. 013. DOI: 10.1007/JHEP10(2018)013. arXiv: 1806.07845 [hep-lat].

[293] Michael Creutz. "The 't Hooft vertex revisited". In: *Annals Phys.* 323 (2008), pp. 2349–2365. DOI: 10.1016/j.aop.2007.12.008. arXiv: 0711.2640 [hep-ph].

[294] Jan Ambjorn, J. Jurkiewicz, and R. Loll. "A Nonperturbative Lorentzian path integral for gravity". In: *Phys. Rev. Lett.* 85 (2000), pp. 924–927. DOI: 10.1103/PhysRevLett.85.924. arXiv: hep-th/0002050 [hep-th].

[295] Mark Gross and Steen Varsted. "Elementary moves and ergodicity in D-dimensional simplicial quantum gravity". In: *Nucl. Phys.* B378 (1992), pp. 367–380. DOI: 10.1016/0550-3213(92)90012-Z.

[296] ME Agishtein and Alexander A Migdal. "Simulations of four-dimensional simplicial quantum gravity as dynamical triangulation". In: *Modern Physics Letters A* 7.12 (1992), pp. 1039–1061.

[297] M.E. Agishtein and A.A. Migdal. "Critical behavior of dynamically triangulated quantum gravity in four dimensions". In: *Nuclear Physics B* 385.1 (1992), pp. 395 –412. ISSN: 0550-3213. DOI: https://doi.org/10.1016/0550-3213(92)90106-L.

[298] Bernd Bruegmann. "Nonuniform measure in four-dimensional simplicial quantum gravity". In: *Phys. Rev.* D47 (1993), pp. 3330–3338. DOI: 10.1103/PhysRevD.47.3330. arXiv: hep-lat/9210001 [hep-lat].

[299] Gudmar Thorleifsson. "Lattice gravity and random surfaces". In: *Nucl. Phys. Proc. Suppl.* 73 (1999). [,133(1998)], pp. 133–145. DOI: 10.1016/S0920-5632(99)85013-0. arXiv: hep-lat/9809131 [hep-lat].

[300] J. C. Walter and G. T. Barkema. "An introduction to Monte Carlo methods". In: *Physica A Statistical Mechanics and its Applications* 418 (2015), pp. 78–87. DOI: 10.1016/j.physa.2014.06.014. arXiv: 1404.0209 [cond-mat.stat-mech].

[301] M.E.J. Newman and G.T. Barkema. *Monte Carlo Methods in Statistical Physics*. Clarendon Press, 1999. ISBN: 9780198517979. URL: https://books.google.de/books?id=J5aLdDN4uFwC.

[302] Rafael D. Sorkin. "Causal sets: Discrete gravity". In: *Lectures on quantum gravity. Proceedings, School of Quantum Gravity, Valdivia, Chile, January 4-14, 2002*. 2003, pp. 305–327. DOI: 10.1007/0-387-24992-3_7. arXiv: gr-qc/0309009 [gr-qc].

[303] Fay Dowker. "Causal sets and the deep structure of spacetime". In: *100 Years Of Relativity: space-time structure: Einstein and beyond*. Ed. by Abhay Ashtekar. 2005, pp. 445–464. DOI: 10.1142/9789812700988_0016. arXiv: gr-qc/0508109 [gr-qc].

[304] Joe Henson. "The Causal set approach to quantum gravity". In: (2006), pp. 393–413. arXiv: gr-qc/0601121 [gr-qc].

[305] Joe Henson. "Discovering the Discrete Universe". In: *Proceedings, Foundations of Space and Time: Reflections on Quantum Gravity: Cape Town, South Africa*. 2010. arXiv: 1003.5890 [gr-qc].

[306] Sumati Surya. "Directions in Causal Set Quantum Gravity". In: (2011). arXiv: 1103.6272 [gr-qc].

[307] Fay Dowker. "Introduction to causal sets and their phenomenology". In: *Gen. Rel. Grav.* 45.9 (2013), pp. 1651–1667. DOI: 10.1007/s10714-013-1569-y.

[308] Sumati Surya. "The causal set approach to quantum gravity". In: (2019). arXiv: 1903.11544 [gr-qc].

[309] Sumati Surya. "Causal set topology". In: *Theor. Comput. Sci.* 405 (2008), pp. 188–197. DOI: 10.1016/j.tcs.2008.06.033. arXiv: 0712.1648 [gr-qc].

[310] Rafael D. Sorkin. "Forks in the road, on the way to quantum gravity". In: *Int. J. Theor. Phys.* 36 (1997), pp. 2759–2781. DOI: 10.1007/BF02435709. arXiv: gr-qc/9706002 [gr-qc].

[311] Astrid Eichhorn. "Steps towards Lorentzian quantum gravity with causal sets". In: *9th International Conference: Spacetime - Matter - Quantum Mechanics: From discrete structures and dynamics to top-down causation (DICE2018) Castiglioncello , Tuscany , Italy, September 17-21, 2018*. 2019. arXiv: 1902.00391 [gr-qc].

[312] Dionigi M. T. Benincasa and Fay Dowker. "The Scalar Curvature of a Causal Set". In: *Phys. Rev. Lett.* 104 (2010), p. 181301. DOI: 10.1103/PhysRevLett.104.181301. arXiv: 1001.2725 [gr-qc].

[313] Fay Dowker and Lisa Glaser. "Causal set d'Alembertians for various dimensions". In: *Class. Quant. Grav.* 30 (2013), p. 195016. DOI: 10.1088/0264-9381/30/19/195016. arXiv: 1305.2588 [gr-qc].

[314] Alessio Belenchia, Dionigi M. T. Benincasa, and Fay Dowker. "The continuum limit of a 4-dimensional causal set scalar d'Alembertian". In: *Class. Quant. Grav.* 33.24 (2016), p. 245018. DOI: 10.1088/0264-9381/33/24/245018. arXiv: 1510.04656 [gr-qc].

[315] S. W. Hawking, A. R. King, and P. J. Mccarthy. "A New Topology for Curved Space-Time Which Incorporates the Causal, Differential, and Conformal Structures". In: *J. Math. Phys.* 17 (1976), pp. 174–181. DOI: 10.1063/1.522874.

[316] David B. Malament. "The class of continuous timelike curves determines the topology of spacetime". In: *Journal of Mathematical Physics* 18.7 (1977), pp. 1399–1404. DOI: 10.1063/1.523436. eprint: https://doi.org/10.1063/1.523436. URL: https://doi.org/10.1063/1.523436.

[317] James M. Bardeen, B. Carter, and S. W. Hawking. "The Four laws of black hole mechanics". In: *Commun. Math. Phys.* 31 (1973), pp. 161–170. DOI: 10.1007/BF01645742.

[318] S. W. Hawking. "Gravitational radiation from colliding black holes". In: *Phys. Rev. Lett.* 26 (1971), pp. 1344–1346. DOI: 10.1103/PhysRevLett.26.1344.

[319] Elizabeth Winstanley. "Classical Yang-Mills black hole hair in anti-de Sitter space". In: *Lect. Notes Phys.* 769 (2009), pp. 49–87. DOI: 10.1007/978-3-540-88460-6_2. arXiv: 0801.0527 [gr-qc].

[320] Jacob D. Bekenstein. "Black holes and entropy". In: *Phys. Rev.* D7 (1973), pp. 2333–2346. DOI: 10.1103/PhysRevD.7.2333.

[321] S. W. Hawking. "Particle Creation by Black Holes". In: *Commun. Math. Phys.* 43 (1975). [,167(1975)], pp. 199–220. DOI: 10.1007/BF02345020,10.1007/BF01608497.

[322] Luca Bombelli et al. "Bombelli et al reply to Comment on "Space-time as a causal set"". In: *Phys. Rev. Lett.* 60 (1988), p. 656. DOI: 10.1103/PhysRevLett.60.656.

[323] Luca Bombelli, Joe Henson, and Rafael D. Sorkin. "Discreteness without symmetry breaking: A Theorem". In: *Mod. Phys. Lett.* A24 (2009), pp. 2579–2587. DOI: 10.1142/S0217732309031958. arXiv: gr-qc/0605006 [gr-qc].

[324] Mehdi Saravani and Siavash Aslanbeigi. "On the Causal Set-Continuum Correspondence". In: *Class. Quant. Grav.* 31.20 (2014), p. 205013. DOI: 10.1088/0264-9381/31/20/205013. arXiv: 1403.6429 [hep-th].

[325] D. J. Kleitman and B. L. Rothschild. "Asymptotic Enumeration of Partial Orders on a Finite Set". In: *Transactions of the American Mathematical Society* 205 (1975), pp. 205–220. ISSN: 00029947.

[326] Joe Henson et al. "Onset of the Asymptotic Regime for Finite Orders". In: (2015). arXiv: 1504.05902 [math.CO].

[327] S. P. Loomis and S. Carlip. "Suppression of non-manifold-like sets in the causal set path integral". In: *Class. Quant. Grav.* 35.2 (2018), p. 024002. DOI: 10.1088/1361-6382/aa980b. arXiv: 1709.00064 [gr-qc].

[328] Graham Brightwell, Joe Henson, and Sumati Surya. "A 2D model of causal set quantum gravity: The Emergence of the continuum". In: *Class. Quant. Grav.* 25 (2008), p. 105025. DOI: 10.1088/0264-9381/25/10/105025. arXiv: 0706.0375 [gr-qc].

[329] Seth Major, David Rideout, and Sumati Surya. "On Recovering continuum topology from a causal set". In: *J. Math. Phys.* 48 (2007), p. 032501. DOI: 10.1063/1.2435599. arXiv: gr-qc/0604124 [gr-qc].

[330] D. P. Rideout and R. D. Sorkin. "A Classical sequential growth dynamics for causal sets". In: *Phys. Rev.* D61 (2000), p. 024002. DOI: 10.1103/PhysRevD.61.024002. arXiv: gr-qc/9904062 [gr-qc].

[331] D. P. Rideout and R. D. Sorkin. "Evidence for a continuum limit in causal set dynamics". In: *Phys. Rev.* D63 (2001), p. 104011. DOI: 10.1103/PhysRevD.63.104011. arXiv: gr-qc/0003117 [gr-qc].

[332] Xavier Martin et al. "On the 'renormalization' transformations induced by cycles of expansion and contraction in causal set cosmology". In: *Phys. Rev.* D63 (2001), p. 084026. DOI: 10.1103/PhysRevD.63.084026. arXiv: gr-qc/0009063 [gr-qc].

[333] David P Rideout. "Dynamics of causal sets". PhD thesis. Syracuse U., 2001. arXiv: gr-qc/0212064 [gr-qc].

[334] Madhavan Varadarajan and David Rideout. "A General solution for classical sequential growth dynamics of causal sets". In: *Phys. Rev.* D73 (2006), p. 104021. DOI: 10.1103/PhysRevD.73.104021. arXiv: gr-qc/0504066 [gr-qc].

[335] Rafael D. Sorkin. "Quantum mechanics as quantum measure theory". In: *Mod. Phys. Lett.* A9 (1994), pp. 3119–3128. DOI: 10.1142/S021773239400294X. arXiv: gr-qc/9401003 [gr-qc].

[336] Rafael D. Sorkin. "Quantum measure theory and its interpretation". In: *Physics and experiments with linear colliders. Proceedings, 3rd Workshop, Morioka-Appi, Japan, September 8-12, 1995. Vol. 1, 2.* 1995. arXiv: gr-qc/9507057 [gr-qc].

[337] Roberto B. Salgado. "Some identities for the quantum measure and its generalizations". In: *Mod. Phys. Lett.* A17 (2002), pp. 711–728. DOI: 10.1142/S0217732302007041. arXiv: gr-qc/9903015 [gr-qc].

[338] Rafael D. Sorkin. "Quantum dynamics without the wave function". In: *J. Phys.* A40 (2007), pp. 3207–3222. DOI: 10.1088/1751-8113/40/12/S20. arXiv: quant-ph/0610204 [quant-ph].

[339] Astrid Eichhorn. "Towards coarse graining of discrete Lorentzian quantum gravity". In: *Class. Quant. Grav.* 35.4 (2018), p. 044001. DOI: 10.1088/1361-6382/aaa0a3. arXiv: 1709.10419 [gr-qc].

[340] Noga Alon et al. "Linear Extensions of a Random Partial Order". In: *Ann. Appl. Probab.* 4.1 (Feb. 1994), pp. 108–123. DOI: 10.1214/aoap/1177005202. URL: https://doi.org/10.1214/aoap/1177005202.

[341] Rafael D. Sorkin. "Indications of causal set cosmology". In: *Int. J. Theor. Phys.* 39 (2000), pp. 1731–1736. DOI: 10.1023/A:1003629312096. arXiv: gr-qc/0003043 [gr-qc].

[342] Fay Dowker and Stav Zalel. "Evolution of Universes in Causal Set Cosmology". In: *Comptes Rendus Physique* 18 (2017), pp. 246–253. DOI: 10.1016/j.crhy.2017.03.002. arXiv: 1703.07556 [gr-qc].

[343] Maqbool Ahmed and David Rideout. "Indications of de Sitter Spacetime from Classical Sequential Growth Dynamics of Causal Sets". In: *Phys. Rev.* D81 (2010), p. 083528. DOI: 10.1103/PhysRevD.81.083528. arXiv: 0909.4771 [gr-qc].

[344] Lisa Glaser and Sumati Surya. "Towards a Definition of Locality in a Manifoldlike Causal Set". In: *Phys. Rev.* D88.12 (2013), p. 124026. DOI: 10.1103/PhysRevD.88.124026. arXiv: 1309.3403 [gr-qc].

[345] Graham Brightwell and Malwina Luczak. "The mathematics of causal sets". In: (2015). arXiv: 1510.05612 [math.CO].

[346] Graham Brightwell and Nicholas Georgiou. "Continuum limits for classical sequential growth models". In: *Random Structures & Algorithms* 36.2 (2010), pp. 218–250. DOI: 10.1002/rsa.20278.

[347] Fay Dowker, Steven Johnston, and Sumati Surya. "On extending the Quantum Measure". In: *J. Phys.* A43 (2010), p. 505305. DOI: 10.1088/1751-8113/43/50/505305. arXiv: 1007.2725 [gr-qc].

[348] Graham Brightwell et al. "General covariance and the 'Problem of time' in a discrete cosmology". In: *Alternative Natural Philosophy Association Meeting Cambridge, England, August 16-21, 2001*. 2002. arXiv: gr-qc/0202097 [gr-qc].

[349] Rafael D. Sorkin. "Toward a 'fundamental theorem of quantal measure theory'". In: (2011). arXiv: 1104.0997 [hep-th].

[350] Sumati Surya. "Evidence for a Phase Transition in 2D Causal Set Quantum Gravity". In: *Class. Quant. Grav.* 29 (2012), p. 132001. DOI: 10.1088/0264-9381/29/13/132001. arXiv: 1110.6244 [gr-qc].

[351] Lisa Glaser and Sumati Surya. "The Hartle–Hawking wave function in 2D causal set quantum gravity". In: *Class. Quant. Grav.* 33.6 (2016), p. 065003. DOI: 10.1088/0264-9381/33/6/065003. arXiv: 1410.8775 [gr-qc].

[352] Lisa Glaser, Denjoe O'Connor, and Sumati Surya. "Finite Size Scaling in 2d Causal Set Quantum Gravity". In: *Class. Quant. Grav.* 35.4 (2018), p. 045006. DOI: 10.1088/1361-6382/aa9540. arXiv: 1706.06432 [gr-qc].

[353] Lisa Glaser. "The Ising model coupled to 2d orders". In: *Class. Quant. Grav.* 35.8 (2018), p. 084001. DOI: 10.1088/1361-6382/aab139. arXiv: 1802.02519 [gr-qc].

[354] William J. Cunningham and Dmitri Krioukov. "Causal Set Generator and Action Computer". In: *Comput. Phys. Commun.* 233 (2018), pp. 123–133. DOI: 10.1016/j.cpc.2018.06.008. arXiv: 1709.03013 [gr-qc].

[355] J. Myrheim. "STATISTICAL GEOMETRY". In: (1978).

[356] David D. Reid. "The Manifold dimension of a causal set: Tests in conformally flat spacetimes". In: *Phys. Rev.* D67 (2003), p. 024034. DOI: 10.1103/PhysRevD.67.024034. arXiv: gr-qc/0207103 [gr-qc].

[357] David Rideout and Petros Wallden. "Spacelike distance from discrete causal order". In: *Class. Quant. Grav.* 26 (2009), p. 155013. DOI: 10.1088/0264-9381/26/15/155013. arXiv: 0810.1768 [gr-qc].

[358] Seth Major, David Rideout, and Sumati Surya. "Stable Homology as an Indicator of Manifoldlikeness in Causal Set Theory". In: *Class. Quant. Grav.* 26 (2009), p. 175008. DOI: 10.1088/0264-9381/26/17/175008. arXiv: 0902.0434 [gr-qc].

[359] Rafael D. Sorkin, Yasaman K. Yazdi, and Nosiphiwo Zwane. "Manifold-Topology from K-Causal Order". In: *Class. Quant. Grav.* 36.9 (2019), p. 095006. DOI: 10.1088/1361-6382/ab1166. arXiv: 1811.09765 [gr-qc].

[360] Dionigi M. T. Benincasa, Fay Dowker, and Bernhard Schmitzer. "The Random Discrete Action for 2-Dimensional Spacetime". In: *Class. Quant. Grav.* 28 (2011), p. 105018. DOI: 10.1088/0264-9381/28/10/105018. arXiv: 1011.5191 [gr-qc].

[361] Siavash Aslanbeigi, Mehdi Saravani, and Rafael D. Sorkin. "Generalized causal set d'Alembertians". In: *JHEP* 06 (2014), p. 024. DOI: 10.1007/JHEP06(2014)024. arXiv: 1403.1622 [hep-th].

[362] Rafael D. Sorkin. "Does locality fail at intermediate length-scales". In: (2007), pp. 26–43. arXiv: gr-qc/0703099 [GR-QC].

[363] Mehdi Saravani and Siavash Aslanbeigi. "Dark Matter From Spacetime Nonlocality". In: *Phys. Rev.* D92.10 (2015), p. 103504. DOI: 10.1103/PhysRevD.92.103504. arXiv: 1502.01655 [hep-th].

[364] Astrid Eichhorn, Sebastian Mizera, and Sumati Surya. "Echoes of Asymptotic Silence in Causal Set Quantum Gravity". In: *Class. Quant. Grav.* 34.16 (2017), 16LT01. DOI: 10.1088/1361-6382/aa7d1b. arXiv: 1703.08454 [gr-qc].

[365] Michel Buck et al. "Boundary Terms for Causal Sets". In: *Class. Quant. Grav.* 32.20 (2015), p. 205004. DOI: 10.1088/0264-9381/32/20/205004. arXiv: 1502.05388 [gr-qc].

[366] E. W. Dijkstra. "A Note on Two Problems in Connexion with Graphs". In: *Numer. Math.* 1.1 (Dec. 1959), pp. 269–271. ISSN: 0029-599X. DOI: 10.1007/BF01386390. URL: http://dx.doi.org/10.1007/BF01386390.

[367] O. Lauscher and M. Reuter. "Fractal spacetime structure in asymptotically safe gravity". In: *JHEP* 10 (2005), p. 050. DOI: 10.1088/1126-6708/2005/10/050. arXiv: hep-th/0508202 [hep-th].

[368] Petr Horava. "Spectral Dimension of the Universe in Quantum Gravity at a Lifshitz Point". In: *Phys. Rev. Lett.* 102 (2009), p. 161301. DOI: 10.1103/PhysRevLett.102.161301. arXiv: 0902.3657 [hep-th].

[369] Dario Benedetti. "Fractal properties of quantum spacetime". In: *Phys. Rev. Lett.* 102 (2009), p. 111303. DOI: 10.1103/PhysRevLett.102.111303. arXiv: 0811.1396 [hep-th].

[370] Dario Benedetti and Joe Henson. "Spectral geometry as a probe of quantum spacetime". In: *Phys. Rev.* D80 (2009), p. 124036. DOI: 10.1103/PhysRevD.80.124036. arXiv: 0911.0401 [hep-th].

[371] Martin Reuter and Frank Saueressig. "Fractal space-times under the microscope: A Renormalization Group view on Monte Carlo data". In: *JHEP* 12 (2011), p. 012. DOI: 10.1007/JHEP12(2011)012. arXiv: 1110.5224 [hep-th].

[372] Stefan Rechenberger and Frank Saueressig. "The R^2 phase-diagram of QEG and its spectral dimension". In: *Phys. Rev.* D86 (2012), p. 024018. DOI: 10.1103/PhysRevD.86.024018. arXiv: 1206.0657 [hep-th].

[373] Gianluca Calcagni, Astrid Eichhorn, and Frank Saueressig. "Probing the quantum nature of spacetime by diffusion". In: *Phys. Rev.* D87.12 (2013), p. 124028. DOI: 10.1103/PhysRevD.87.124028. arXiv: 1304.7247 [hep-th].

[374] Gianluca Calcagni, Daniele Oriti, and Johannes Thürigen. "Dimensional flow in discrete quantum geometries". In: *Phys. Rev.* D91.8 (2015), p. 084047. DOI: 10.1103/PhysRevD.91.084047. arXiv: 1412.8390 [hep-th].

[375] Astrid Eichhorn and Sebastian Mizera. "Spectral dimension in causal set quantum gravity". In: *Class. Quant. Grav.* 31 (2014), p. 125007. DOI: 10.1088/0264-9381/31/12/125007. arXiv: 1311.2530 [gr-qc].

[376] Steven Carlip. "Spontaneous Dimensional Reduction in Short-Distance Quantum Gravity?" In: *AIP Conf. Proc.* 1196.1 (2009), p. 72. DOI: 10.1063/1.3284402. arXiv: 0909.3329 [gr-qc].

[377] S. Carlip. "Dimension and Dimensional Reduction in Quantum Gravity". In: *Class. Quant. Grav.* 34.19 (2017), p. 193001. DOI: 10.1088/1361-6382/aa8535. arXiv: 1705.05417 [gr-qc].

[378] S. Carlip. "Dimension and Dimensional Reduction in Quantum Gravity". In: *Universe* 5 (2019), p. 83. DOI: 10.3390/universe5030083. arXiv: 1904.04379 [gr-qc].

[379] Alessio Belenchia et al. "Spectral Dimension from Nonlocal Dynamics on Causal Sets". In: *Phys. Rev.* D93.4 (2016), p. 044017. DOI: 10.1103/PhysRevD.93.044017. arXiv: 1507.00330 [gr-qc].

[380] S. Carlip. "Dimensional reduction in causal set gravity". In: *Class. Quant. Grav.* 32.23 (2015), p. 232001. DOI: 10.1088/0264-9381/32/23/232001. arXiv: 1506.08775 [gr-qc].